IMPLEMENTATION OF A PHASED ARRAY ANTENNA USING DIGITAL BEAMFORMING

by

Juan A. Torres-Rosario

A thesis submitted in partial fulfillment of the requirements for the degree of

MASTER OF SCIENCES.
in
ELECTRICAL ENGINEERING

UNIVERSITY OF PUERTO RICO
MAYAGÜEZ CAMPUS
2005

Approved by:

Jose G. Colom-Ustáriz, Ph. D. Member, Graduate Committee	Date
Rafael A. Rodríguez-Solís, Ph. D. Member, Graduate Committee	Date
Shawn Hunt, Ph. D. President, Graduate Committee	Date
Pedro Vazquez, Ph. D. Representative of Graduate Studies	Date
Isidoro Couvertier, Ph. D. Chairperson of the Department	Date

ABSTRACT

This work presents the design of a transmitter/receiver Digital Beamformer (DBF) based on the mathematical model of a far-field plane wave incident on a sensor array. Simulations of a DBF transmitter and receiver are performed to control the power pattern of a 4-element linear array, a 16-element linear array and a 16-element rectangular array. For each sensor array, two spatial filters were constructed with different pattern requirements to demonstrate the operation of the DBF. An implementation of a DBF transmitter was performed using a digital processing board containing a Virtex-II XC2V6000 FPGA to control the radiation pattern of a Phased Array Antenna transmitter. A 16-element patch antenna array and the RF front end were fabricated and its radiation pattern was measured in an anechoic chamber to test the performance of the DBF transmitter giving an error of less than 5 degrees in each angular direction of the main beam's angle-of-transmission.

RESUMEN

Este trabajo presenta el diseño de un “digital beamformer" (DBF) transmisor y receptor basados en el modelo matemático de una onda plana que incide en un arreglo de sensores. Simulaciones del DBF transmisor y receptor fueron realizadas para controlar el patrón de radiación de tres arreglos con geometrías diferentes. Para cada arreglo de sensores, dos filtros espaciales fueron construidos con requisitos específicos con el propósito de demostrar el funcionamiento del DBF y comparar sus resultados con los resultados obtenidos al calcular el patrón teóricamente. Una implementación del DBF tipo transmisor fue realizada utilizando una tarjeta de procesamiento de datos con un Virtex-II XC2V6000 FPGA para controlar el patrón de radiación de un arreglo de antenas transmisor. Para implementar los componentes RF del arreglo de antenas se diseñaron y construyeron un arreglo de parches con 16 elementos, una etapa de distribución para la señal del oscilador local, y una etapa de mezclado y amplificación de potencia. Finalmente, el patrón de radiación del arreglo de antenas fue medido utilizando una cámara anecoica con el fin de mostrar el funcionamiento del DBF transmisor donde se obtuvo patrones con menos de 5 grados de error en el ángulo de transmisión de su lóbulo principal.

ACKNOWLEDGEMENTS

This section is written to recognize those who have helped me during my life to work hard, and finish my work. To my God, my utmost thanks for giving me the courage and strength to follow my dreams and achieve my goals. To my Family and Friends, thanks for your unconditional love and support through all these years. Thanks to my advisor Prof. Shawn Hunt and my research professor Prof. Rafael Rodriguez for giving me the opportunity to research under your supervision and give me guidance through these years as a graduate student. Also, a special thanks to other Prof. Jose Colom, Prof. Manuel Jimenez and Prof. Domingo Rodriguez for your help during the course of my investigation.

NSF CASA ERC, 0313747 and NSF ECS-0093650 provided the funding and the resources for the development of this research.

"*El principio de la sabiduría es el temor de Jehová…*", Proverbios 1:7

Table of Contents

Table List

Figure List

1 INTRODUCTION

Phased array antennas are known for their capability to steer the beam pattern electronically with high effectiveness, managing to get minimal side-lobe levels and narrow beamwidths. Implementations beginning during the 1950s depended largely on microwave circuitry components such as phase shifters, and variable amplifiers. To achieve performance specifications such as narrow beamwidth or considerable scanning range with high angle resolution, a large number of antenna elements were needed to construct the array. The use of these microwave components in large quantities pose numerous obstacles to good performance and complicate the maintenance process of the phased array antenna.

Phase shifters, which are used in great quantities in a phased array antenna, have high power consumption. This might be perceived as a decrease in the gain of the phased antenna array. Another problem with phase shifters and their intrinsic tolerance of a phase shift value. The progressive phase shift between each phase shifter needs to be equal for all phase shifters in order to achieve a defined beam to fulfill antenna specifications. In order to achieve constant phase progression between phase shifters, every phase shifter in a phased array antenna needs to be calibrated. The calibration process is done after the array has been fabricated to ensure the correction of all the effects of phase and amplitude errors in the excitation. This calibration process tends to complicate the integration process of a communication system using a large phased array antenna. Also, since the phase shifter has inherent variations in its operation due to temperature, time, mechanical vibrations, etc., repetition of this calibration process may be needed over time.

An alternative approach in the design of a phased array antenna is to use digital beamforming. Digital beamforming consists of the spatial filtering of a signal where the phase shifting, amplitude scaling, and adding are implemented digitally. The idea is to use a computational and programmable environment which processes a signal in the digital domain to control the progressive phase shift between each antenna element in the array. Digital beamforming has many of the advantages a digital computational environment has over its analog counterpart. In most cases, less power is needed to perform the beam steering of the phased array antenna. Another advantage is the reduction of variations associated with time, temperature, and other environmental changes found in analog devices. The phased array antenna will still contain analog components such as Low Noise Amplifiers (LNAs) and Power Amplifiers (PA) found in the RF stages, but the number of analog components in general can be greatly reduced for large antenna arrays. Finally, an important reason which favors the use of a digital beamformer on a phased array antenna is its versatility. Digital beamformers can accomplish minimization of side-lobe levels, interference canceling and multiple beam operation without changing the physical architecture of the phased array antenna. Every mode of operation of the digital beamformer is created and controlled by means of code written on a programmable device of the digital beamformer.

In the beginning of the 1980s, advancement in digital circuitry technology made possible and feasible the idea of implementing the beamforming networks through digital signal processing. Digital Beamforming (DBF) offers advantages in terms of power consumption, flexibility, and accuracy. In general, digital systems tend to consume less power in computation operations and have programmable interface adding versatility to the system. Steyskal stated advantages in DBF implementation such as improved adaptive pattern nulling, superresolution, array element pattern correction, self calibration, and radar power and time management [*Steyskal*, 1988]. Experimental DBF systems have been built since then to improve the antenna performance for system-level environments. In the 1998, Simonangeli developed a testbed of a C band 32-element dipole DBF array [*Simonangeli*, 1988]. At the same time, the study of efficient beamforming algorithms paved the way for flexible and versatility in DBF designs [*Mucci*, 1984].

Phased array antenna designs based on DBF implementation are currently being devised for radar applications. Currently, the Netherlands Foundation for Research in Astronomy (NFRA) is working on the creation of a radio telescope based on the phased array antenna principle [*Hiemstra*, 2000]. The project is called the Square Kilometer Array (SKA). The radio telescope will consist of 32 array antennas stations. It will cover an area of a square kilometer with a frequency range from 200 MHz to 2 GHz. A series of four feasibility stages of four different array antennas are been developed for research and development purposes. In the two final array antennas, DBF will be implemented with a multi-processor computational environment. The DBF will consist of a processing board containing FPGAs and a DSP. For the third array antenna called Thousand Element Array (THEA), a group of six FPGAs will be used to process the signal. The DSP will be used to implement an adaptive algorithm based on Minimum Variance (MV) to calculate the beamformer's weigth coefficients [*Alliot*, 2000]. The signal will have a bandwidth of 20 MHz.

Finally, phased array antennas have been used largely in communication systems. Their capability to change radiation pattern electronically, multi-beam capacity and high spatial resolution has made them attractive for mobile communication applications. Miura [*Miura*, 1997] worked with a DBF Multibeam Antenna for mobile satellite communication. The DBF consisted on a 4 x 4 ring patch array which received a signal with a carrier frequency of 1542.5 MHz and a bandwidth of 11 kHz. The spatial filtering was performed using a DSP board of ten FPGAs. An adaptive beamforming algorithm called constant modulus algorithm (CMA) was used to perform the satellite tracking. To achieve multibeam operation, an FFT beamformer was implemented in conjunction with Multibeam selector, which decides the beam with the strongest receiving power to receive the arriving signal. Dreher [*Dreher*, 1999, 2003] worked with a planar DBF for satellite navigation. The antenna array, a 5 x 5 aperture coupled patch array, was designed to receive a signal with a carrier frequency of 5.15 GHz and a bandwidth of 16 MHz. The RF-signal is processed through an Intermediate Frequency (IF) network, digitized using a sub-sampling mechanism with a 40 Msps 10-bit ADC converters, modulated to baseband with DDC, and the actual beamforming is performed by a PC. The data transfer between the IF networks and the PC was done via the IEEE 488 standard bus. The calculation of the weights of the spatial filter was made using Schelkunnoff's method, where the radiation patterns' nulls are located at detected interfering signals.

In the next chapter of this thesis, a theoretical background of array signal processing is presented. The chapter describes the mathematical model of the DBF receiver and transmitter based on the behavior of a far-field plane wave traveling along a homogeneous medium and incident on an array of sensor. Detailed designs of the DBF receiver and transmitter are then derived, based on their mathematical model, with the goal of reducing the mathematical operational complexity of each DBF stage. In chapter 3, different spatial filters are designed as examples to satisfy certain requirements in the beam pattern of three different antenna arrays. A digital computational environment was programmed to corroborate the simplified DBF transmitter design presented in this thesis. Also, the rectangular patch antenna and two microwave circuits were simulated and tested to verify their performance on a 16-element rectangular PAA. Finally, the last chapter presents concluding remarks about the results obtained in each stage of the PAA and recommendations are suggested to improve the performance and decrease the complexity of a PAA.

2 THEORETICAL BACKGROUND

2.1 Array Processing Theory

2.1.1 Frequency-wavenumber Response and Beam Patterns

An array of sensors can be organized in any form in space, where the position of each sensor can be described by a coordinate $\boldsymbol{p} = (p_x, p_y, p_z)$. If a plane wave signal $f(t,\boldsymbol{p})$ is arriving at a particular point in space, and the position each sensor in space is different, the signal received by each sensor will be the same original signal with a time-delay, depending on the position of the sensor. The following vector can be used to describe the signal received by each sensor:

$$\overline{f(t,\boldsymbol{p})} = \begin{bmatrix} f_{p_0}(t) \\ f_{p_1}(t) \\ \vdots \\ f_{p_{N-1}}(t) \end{bmatrix} = \begin{bmatrix} f(t-\tau_0) \\ f(t-\tau_1) \\ \vdots \\ f(t-\tau_{N-1}) \end{bmatrix}, \qquad \textbf{2.1}$$

where N is the number of elements in the array and τ_i is a time-delay associated with the position of the element. Figure 1 shows an arbitrary N-element sensor array.

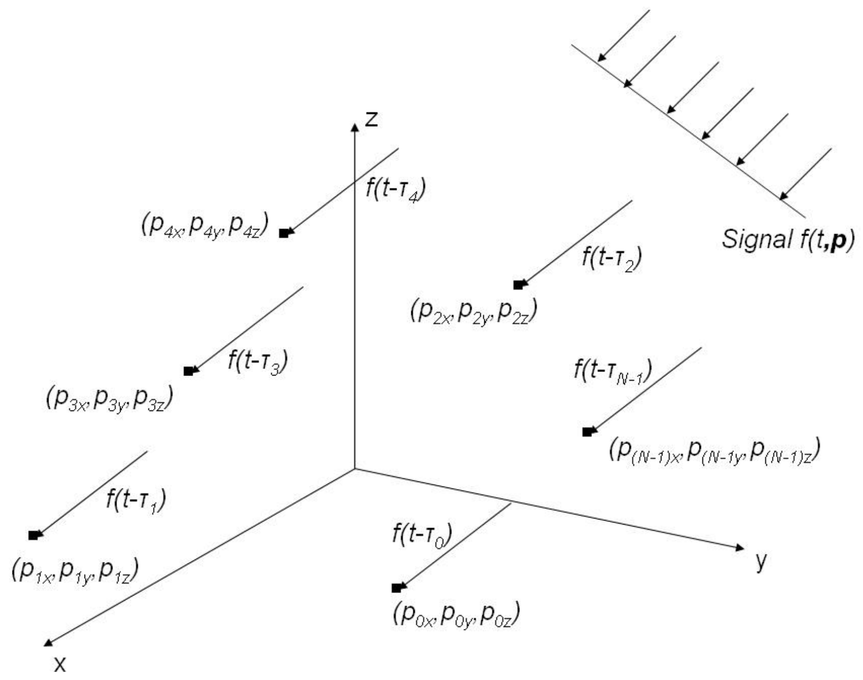

Figure 2.1 Diagram of an *N*-element sensor array receiving a plane wave signal *f(t,p)* coming from the far-field

If the signal *f(t,**p**)* generated in space is a far-field planar wave, the equation to describe each signal in the sensor array reduces to:

$$\overline{f\left(t,\overline{p_n}\right)}=\begin{bmatrix} f(t)e^{j\left(wt-\overline{k^T}\,\overline{p_0}\right)} \\ f(t)e^{j\left(wt-\overline{k^T}\,\overline{p_1}\right)} \\ \vdots \\ f(t)e^{j\left(wt-\overline{k^T}\,\overline{p_{N-1}}\right)} \end{bmatrix}, \qquad \textbf{2.2}$$

where *k* represents the wavenumber, *w* is the frequency of the plane wave, *t* is a variable representing the time, and *j* is $\sqrt{-1}$. The wavenumber *k* and the position of each sensor $\overline{p}$ can be represented in the following form:

$$\overline{k} = {}^{2\pi}\!/_{\lambda} \begin{bmatrix} \sin\theta\cos\phi \\ \sin\theta\sin\phi \\ \cos\theta \end{bmatrix}, \qquad \overline{p} = \begin{bmatrix} p_x \\ p_y \\ p_z \end{bmatrix}, \qquad \textbf{2.3}$$

where *λ* represents the wavelength, and *θ* and *φ* represent the angle of arrival of the incoming wave. If the Fourier Transform is applied to the incoming signal in each sensor, the signal in the spectral domain can be represented as:

$$\overline{F\left(w,\overline{p_n}\right)} = \int \overline{f\left(t,\overline{p_n}\right)} e^{-jwt} dt = \begin{bmatrix} \int f(t) e^{j\left(wt - \overline{k}^T \overline{p_0}\right)} e^{-jwt} dt \\ \int f(t) e^{j\left(wt - \overline{k}^T \overline{p_1}\right)} e^{-jwt} dt \\ \vdots \\ \int f(t) e^{j\left(wt - \overline{k}^T \overline{p_{N-1}}\right)} e^{-jwt} dt \end{bmatrix} = F(w) \begin{bmatrix} e^{-j\overline{k}^T \overline{p}_0} \\ e^{-j\overline{k}^T \overline{p}_1} \\ \vdots \\ e^{-j\overline{k}^T \overline{p}_{N-1}} \end{bmatrix} = F(w)\overline{v(\overline{k})}. \qquad \textbf{2.4}$$

The resulting vector *v(k)* is usually described in literature as the array manifold vector [*Van Trees*, 2002] and it gives a representation of the position of each sensor with respect to the incidence angle of an incoming plane wave. The incoming signal can be acquired if each sensor is considered a discrete sample in space. The resulting signal can be considered a superposition of all the sensor signals:

$$B\left(\overline{k}\right) = \sum_{l=0}^{N-1} v_l\left(\overline{k}\right). \qquad \textbf{2.5}$$

If a series of weights are applied to the output of each sensor and superposition is applied to acquire the incoming plane wave coming from the far-field, the equation for *B(k)* then reduces to:

$$B(\bar{k}) = \sum_{l=0}^{N-1} w_l^* v_l(\bar{k}) = \begin{bmatrix} w_0^* & w_1^* & \cdots & w_{N-1}^* \end{bmatrix} \begin{bmatrix} v_0(\bar{k}) \\ v_1(\bar{k}) \\ \vdots \\ v_{N-1}(\bar{k}) \end{bmatrix} = \overline{w^H}\,\overline{v(\bar{k})}. \qquad \mathbf{2.6}$$

B(k) is the value of the beam pattern at a particular position in space. Frequently, in Antenna Theory, it is easier to visualize the pattern in terms of angle of incidence between the source of the signal and a point in space. Thus, the following change of variables can be made to show *B(k)* in terms of the angle of incidence:

$$B(\theta,\phi) = B(\bar{k})\Big|_{\bar{k}=2\pi/\lambda\left[\sin\theta\cos\phi \quad \sin\theta\sin\phi \quad \cos\theta\right]^T}. \qquad \mathbf{2.7}$$

If the geometry of the sensors can be described using a mathematical equation for the variables of the position, the array manifold vector equation can be simplified. In this thesis, two antenna array geometries will be presented: a uniform linear antenna array and a uniform rectangular antenna array. For a uniform linear array, which is a linear array were the space between elements of the array is the same throughout the array, the position of each sensor can be described in the following form:

$$\overline{p_n} = \begin{bmatrix} 0 \\ 0 \\ p_{zn} \end{bmatrix} = \begin{bmatrix} 0 \\ 0 \\ \left(n - \frac{N-1}{2}\right)\Delta z \end{bmatrix}, \qquad \textbf{2.8}$$

where *Δz* is the spacing between the sensors in the z axis. For a uniform rectangular array, the position of each sensor can be described in the following form:

$$\overline{p_n} = \begin{bmatrix} p_{xn} \\ p_{yn} \\ 0 \end{bmatrix} = \begin{bmatrix} \left(l - \frac{L-1}{2}\right)\Delta x \\ \left(m - \frac{M-1}{2}\right)\Delta y \\ 0 \end{bmatrix}, \qquad \textbf{2.9}$$

where *L* and *M* are the number of elements in the x and y axis respectively and *Δx* and *Δy* are the spacing between the sensors in the x and y axis respectively. The number of elements *N* in a rectangular array is given by *L*M*. The mathematical description of the position of each sensor in the previous arrays has been developed to satisfy center of gravity at the origin:

$$\sum_{n=0}^{N-1} p_n = 0. \qquad \textbf{2.10}$$

The inter-element spacing in each axis of any array is adjusted to avoid a phenomenon known in antenna literature as grating lobe, which is the aliasing of a wavenumber occurring from the under sampling in space of a time-space signal. All the arrays described in this work will have inter-element spacing of 0.5λ in each axis, where λ is the wavelength of the carrier wave received by the array.

2.1.2 Delay-and-Sum Beamformer

If each sensor in the array receives a signal *f(t)* with a particular time-delay *τ*, recovery of the signal can be performed by means of linear processing. In this case, the filter for each channel *n* would be a time-delay τ_n associated with the channel. After all the space samples are aligned in time, they can be added to recover *f(t)*. It is important to consider that a scaling by *1/N* has to be applied to the resulting signal since adding the output of each processed channel would give a result of *N*f(t)*. Figure 2 shows a system illustration of the Delay-and-Sum Beamformer.

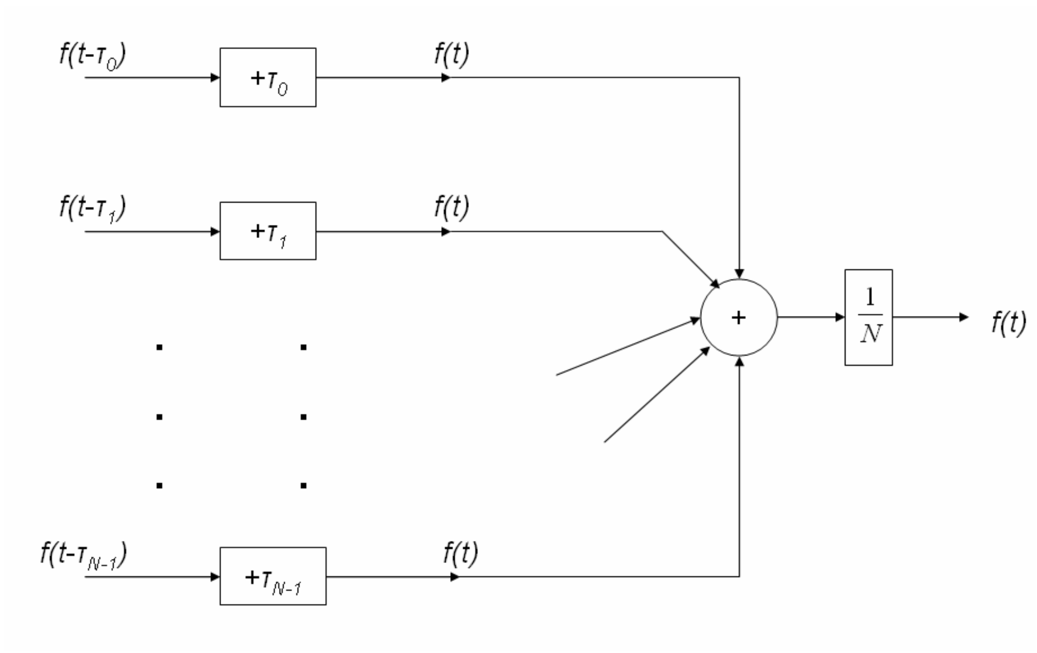

Figure 2.2 Diagram of a Delay-and-Sum Beamformer

2.1.3 Narrowband Beamformer

A general characterization of the signal *f(t,**p**)*, where a bandpass signal is used to transmit information, can be described in the following form:

$$f(t,\boldsymbol{p}_n) = \sqrt{2}\,\mathrm{Re}\left\{ \tilde{f}\left(t,\boldsymbol{p}_n\right) e^{jw_c t} \right\}, \quad n = 0,\ldots,N-1, \qquad \textbf{2.11}$$

where w_c is the carrier frequency and $\tilde{f}\left(t,\boldsymbol{p}_n\right)$ is the complex envelope [Van Trees]. If the signal *f(t,**p**)* is a plane-wave, the equation (2.11) can be simplified to:

$$f(t,\boldsymbol{p}_n) = \sqrt{2}\,\mathrm{Re}\left\{ \tilde{f}\left(t-\tau_n\right) e^{jw_c(t-\tau_n)} \right\}, \quad n = 0,\ldots,N-1, \qquad \textbf{2.12}$$

where τ_n is given by:

$$\tau_n = \frac{\overline{k}^T \cdot \overline{p}_n}{w_c}. \qquad \textbf{2.13}$$

An important parameter in the design of an array is ΔT_{max}, which is the maximum travel time of a plane wave between any two elements of the array. If the mathematical description of the position of the elements of the array satisfies (2.10) then:

$$\tau_n \le \Delta T_{max}, \quad n = 0,\ldots,N-1. \qquad \textbf{2.14}$$

A signal *f(t,**p**)*, which has a complex envelope $\tilde{f}\left(t,\boldsymbol{p}_n\right)$ with a bandwidth B_s, received by an array with a ΔT_{max} is defined as a narrowband signal if the following condition is satisfied:

$$\Delta T_{max} \cdot B_s \ll 1. \qquad \textbf{2.15}$$

When the signal *f(t,**p**)* is considered a narrowband signal, a suitable and convenient approximation can be used on the complex envelope:

$$\tilde{f}\left(t-\tau_n\right) \simeq \tilde{f}\left(t\right), \quad n = 0,\ldots,N-1. \qquad \textbf{2.16}$$

This approximation modifies the mathematical representation of *f(t,**p**)* into:

$$\begin{aligned} f\left(t,\boldsymbol{p}_n\right) &= \sqrt{2}\,\mathrm{Re}\left\{\tilde{f}\left(t\right)e^{jw_c\left(t-\tau_n\right)}\right\}, \quad n = 0,\ldots,N-1 \\ &= \sqrt{2}\,\mathrm{Re}\left\{\tilde{f}\left(t\right)e^{jw_c t}e^{-jw_c\tau_n}\right\}. \end{aligned} \qquad \textbf{2.17}$$

From this simplification, it can be seen that the delay lines associated with τ_n can be replaced with a phase shift $e^{-jw_c\tau_n}$. An array which uses phase shifts to approximate the delay lines to process a narrowband space-time signal is known as a phased array. For a uniform array, a progressive phase shift can be used to steer the main response axis (MRA), which is the direction where the beam pattern has its maximum absolute value, to any desired value. If additional requirements are imposed on the beam pattern of an array, such as a particular sidelobe level, minimum half-power beamwidth, and null placement, the amplitude of each sensor in the array needs to be adjusted. This leads to a beamformer configuration where the resulting signal becomes a linear combination of the received or transmitted signals and each sensor signal has a complex weight w^*_n, described in (2.6), which controls the MRA and the beam pattern characteristics of the array. A diagram of the narrowband beamformer model is shown in Figure 2.3.

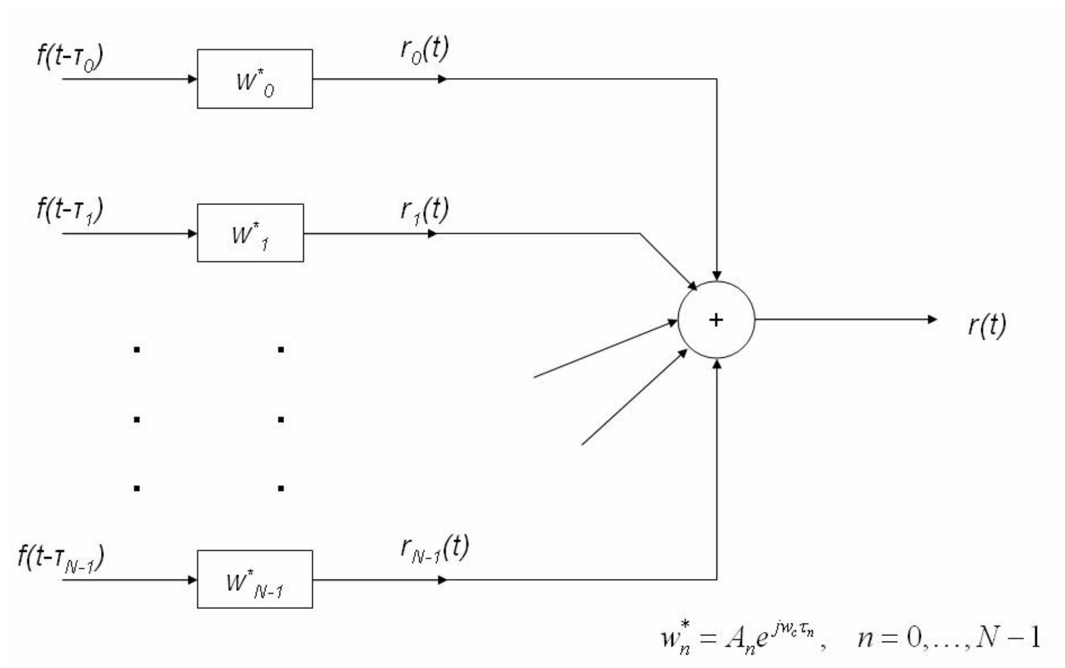

Figure 2.3 Diagram of Narrowband Beamformer

2.1.4 *Spatial Filter Design*

The beam pattern response of a sensor array is the inner product of the array manifold vector and the weights associated with each sensor. If the structure of the beam pattern response calculation is analyzed, it can be seen that the beam pattern response is a spatial filter. A spatial filter discriminates between planes waves coming from different locations in space, where the angle of incidence of the plane wave is related to a spatial frequency. Thus, for a particular sensor geometrical distribution, the weight vector characterizes the radiation pattern response of the sensor array. Such characterization is made by defining design constraints such as beamwidth of the MRA, sidelobe level behavior, null pattern placement, null-to-null beamwidth, etc. the same way a filter in the time domain characterizes a frequency response. For example, the beamwidth of the MRA defines the half-power angular difference near the maximum radiation intensity point in the beam pattern, similar to the passband frequency difference found in time series analysis. As for sidelobe level behavior, the sidelobe level defines the power level of the sidelobes with respect to the main lobe, analogous to the passband to stopband power difference found in the spectral representation of a time series. Although filter design is important in the radation pattern response of an antenna array, array geometry may impose limitations on some desirable beam pattern response characteristics. Analogous to choosing an appropriate sampling frequency in the time domain, spatial sampling selection, which is determined by the geometrical distribution and size of the array, determines some beam pattern response characteristics.

The process of obtaining a geometrical distribution and the coefficients for the weight vector for a beam pattern response is called beam pattern synthesis. In Antenna Theory, the radiation pattern response is constructed based on a realization of an analytical or desired model by an antenna model [*Balanis*, 1997]. The classification of beam pattern synthesis techniques are based on three beam pattern design constraints: null placement, beam shaping, and beamwidth-sidelobe behavior. Null placement synthesis consists of determining the coefficients of the weight vector based on the position of nulls in the radiation pattern response of the sensor array. A popular null placement synthesis technique is the Schelkunoff polynomial method. This method derives the weight coefficients of the array based on the root placement of a complex polynomial, which is derived form the beam pattern response equation (Eq. 2.6). In beam shaping synthesis, the weight vector is calculated based on a specified beam pattern response sampled at discrete wavenumber values. Classic antenna pattern synthesis methods included in this category are the Woodward-Lawson method, the Fourier Transform method and the z-transform method.

The last category of beam pattern synthesis based on spatial response design constraints is the beamwidth-sidelobe behavior. In these techniques, the weight vector coefficients are determined based on the desired behavior of the MRA's beamwidth and sidelobe level. A common synthesis technique used in the spectral analysis of time series in signal processing is the Spectral Weighting technique [*Van Trees*, 2002]. This technique defines a set of weights based on a windowing function, which simplifies the weight calculation procedure. The Uniform window, Cosine window, Hamming window, Hann window, etc. are just a few of the windowing functions available to control the response of a sensor array. Each window function provides a constant weight vector which defines a fixed beam pattern response. Through performance analysis of each windowing function, a tradeoff can be found between minimizing the MRA's beamwidth, reducing the sidelobe level, and increasing the directivity of the radiation pattern response. Other beamwidth-sidelobe behavior methods include Taylor distrimution method, Villanueava distribution and Dolph-Chevyshev method where the beamwidth of the radiation pattern's MRA is minimized for a particular sidelobe level value. Beam pattern synthesis can also be obtained through adaptive array processing. By changing the weights of each sensor adaptively, design goals such as minimizing the noise variance of the signal, minimizing the square error between the beamformer output and a reference signal, or maximize the signal-to-noise ratio of the receiver [*Haynes*] can be satisfied. Antennas using adaptive beamforming are, often referred as, "Smart Antennas" in communication literature.

Another method of synthesizing a beam pattern is beamspace processing. In this approach, a set of beams created at an introductory step are processed instead of the signals arriving at each sensor element [*Van Trees*, 2002]. The latter method of pattern synthesis is known as "element-space processing." Beamspace processing is typically used in applications where the number of elements in the array is very large and the received signals need to be reduced to simplify further processing. Three types of beamspace processing methods are full-dimension beamspace, reduced-dimension beamspace and multiple-beam beamspace. In full-dimension beamspace, the signals of the *N* sensor in the array are processed to deliver an output of *N* orthogonal beams. In the case of reduced-dimension beamspace, only a set of beams covering a particular wavenumber region are calculated. As for multiple-beam beamspace, multiple beams are created to span specific regions of the space. An example of a beamspace beamformer is the FFT beamformer (often called the conventional beamformer). In FFT beamforming, the Discrete Fourier Transform is used to process samples separated in distance to produce multiple beams separated in the space domain. All the generated beams in the FFT beamformer are orthogonal, fixed and equally spaced. The FFT beamformer depends largely on the spatial resolution of the array antenna. This beamformer performs a “spatial FFT” [*Haynes*] where input samples are separated by space and outputs samples are separated by direction-of-arrival. One disadvantage of FFT beamformers is its fixed beam performance. Alliot [*Alliot*, 2000] comments on beamforming interpolation techniques for FFT beamformers. Beamforming interpolation consists of the creation of a beam by adding of various beams generated by the FFT beamformer multiplied by real weights corresponding to a particular coordinate. The combination of multiple beam radiation pattern and versatility in direction of observation are the main advantages of beamforming interpolation.

In spatial filter design, alternative filter structures have been presented to solve the problem of narrow bandwidth in phased array antennas (PAA), such as the use of a filter-and-sum beamformer [*Kajala*, 1999, 2001]. The filter-and-sum beamforming operates on the amplitude and the phase of the digitized antenna element current signal. Each antenna element has its filter and the output of each filter is added in a summing network to acquire the desired spatial beam pattern. Various methods have been proposed to implement filter-and-sum beamformers. For example, Kajala implements spatial filtering through an optimized polynomial FIR filter. The polynomial FIR filters's coefficients are chosen to minimize the mean square error (MSE) between the desired and the actual response of the beamformer.

2.2 Phased Array Antenna Implementations

The PAA is composed of a group of similar antennas, each with its power feed network, phase shifter, variable amplifiers and a summing network which gives a resulting signal representing a beam on an expected location. Figure 2.4 shows a diagram of the transmitter and receiver stages of a phased array antenna. The complex weight w^*_n associated with each antenna element is implemented by means of a variable amplifier and a phase shifter. Analog components such as Low Noise Amplifiers (LNAs) and Power Amplifiers (PA) found in the RF stages are needed in order to condition the signal to be transmitted or received by the antenna array.

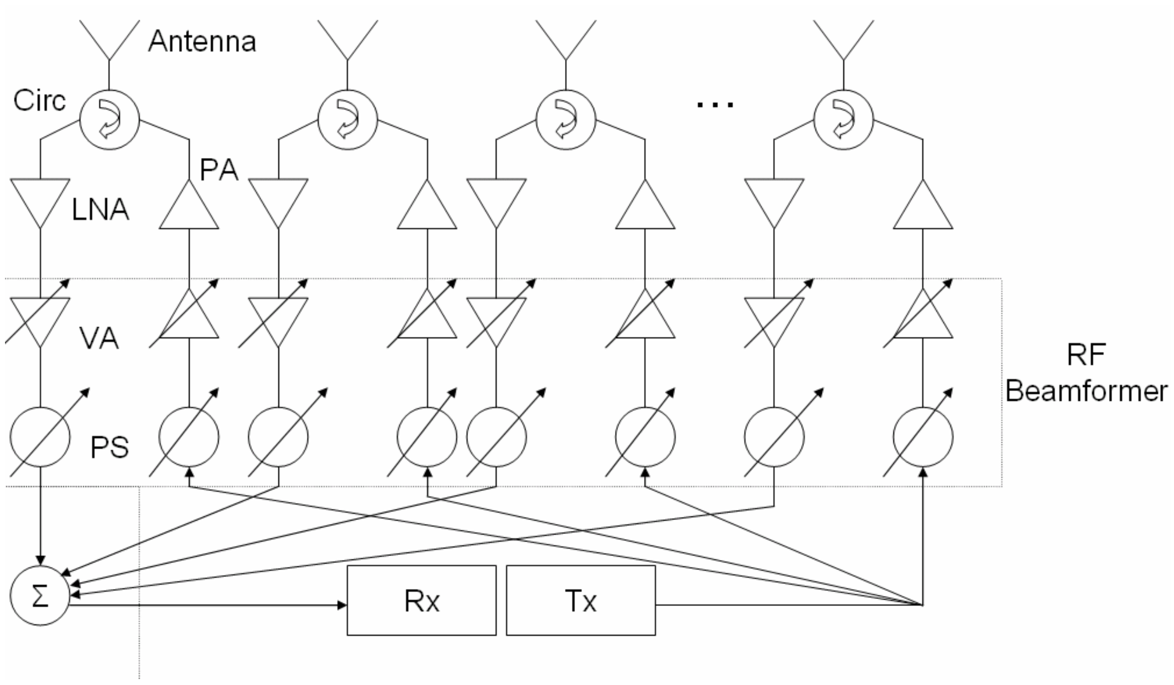

Figure 2.4 Diagram of PAA using an RF Beamformer

An alternative approach for implementing a beamformer is by means of quadrature modulation theory. In this approach, a signal is decomposed into its quadrature components which are processed separately in the baseband region using the complex weights w^*_n to achieve a desired beam pattern response. One way to implement quadrature modulation/demodulation is through digital beamforming. Digital beamforming (DBF) consists of the spatial filtering of a signal where the phase shifting, amplitude scaling, and adding are implemented digitally. Analog-to-Digital Converters (ADCs) and the Digital-to-Analog Converters (DACs) are required to make the necessary transformations of the signal between the IF analog domain and the digital domain. Figure 2.5 shows the architecture of a PAA using a DBF. A design example of a DBF was shown by Chang [*Chang*, 1988]. Chang created a DBF for a circularly polarized phased array antenna with resonant frequency of 2.95 GHz. The amplitude and phase of the current in the elements of the array were controlled by a weight vector applied to the In-phase (IC) and Quadrature (QC) channel of the element. The amplitude scaling, phase shifting and summing operation were performed digitally.

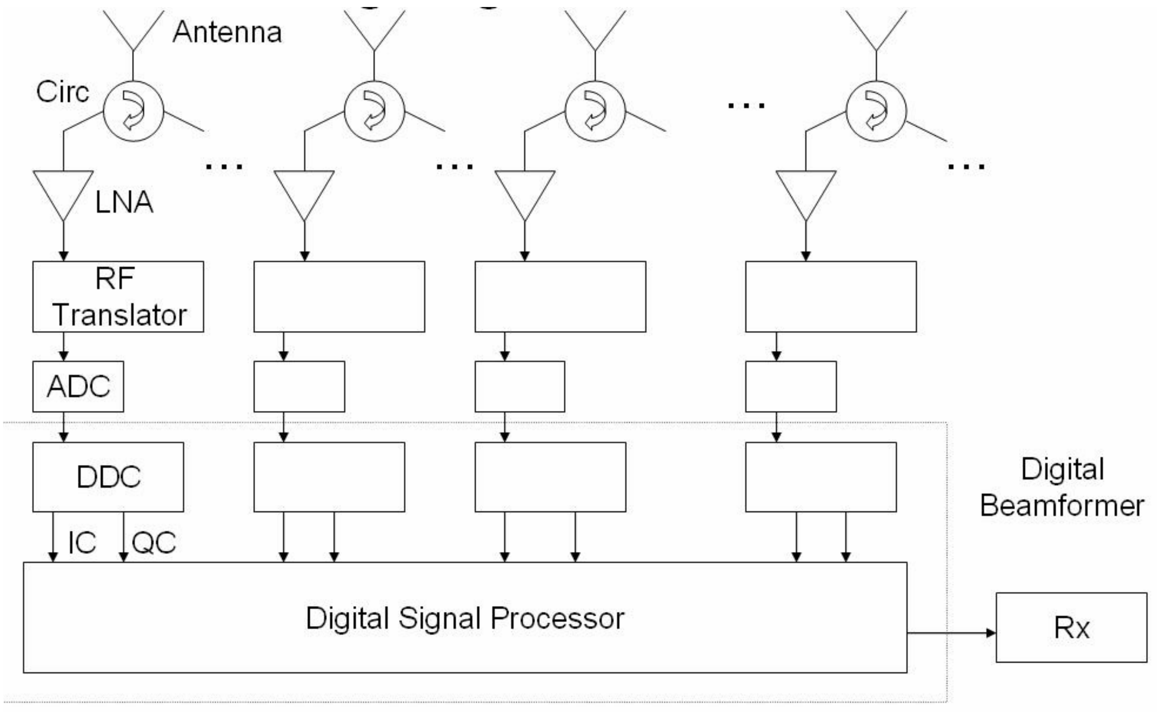

Figure 2.5 Diagram of a PAA using a Digital Beamformer

2.3 DBF Receiver

2.3.1 Mathematical Model of DBF Receiver

The incident plane wave on an antenna array's receiver can be modeled by the following equation:

$$
\begin{aligned}
f(t, \boldsymbol{p}_n) = c_n(t) = x(t-\tau_n)\cos\left(w_{RF}\,(t-\tau_n)\right), \quad n = 0,\ldots,N-1 \\
\approx x(t)\cos\left(w_{RF}t - \theta_n\right),
\end{aligned} \qquad \textbf{2.18}
$$

where θ_n is given by:

$$\theta_n = w_{RF}\tau_n. \qquad \textbf{2.19}$$

After the incident plane wave has been received by the antennas of the PAA, the incoming signal arrives at the RF Modulation Stage. This stage is often required because the incoming signal's frequency components are high compared to the speed of the ADCs and analog signal modulation is needed to shift the signal's frequency components into a lower frequency band. If the RF Modulation Stage has a Local Oscillator (LO) with a frequency of w_{LO}, then the signal modulation operation can be described in the following form:

$$g_n^{'}(t) = x(t)\cos\left(w_{RF}t - \theta_n\right)\cos\left(w_{LO}t\right). \qquad \textbf{2.20}$$

Using trigonometric identities, the signal $g'_n(t)$ can be represented as a sum of two cosines:

$$g_n^{'}(t) = \frac{x(t)}{2}\left[\cos\left(w_{IF}t - \theta_n\right) + \cos\left(w_{IM}t - \theta_n\right)\right], \qquad \textbf{2.21}$$

where:

$$w_{IF} \triangleq w_{RF} - w_{LO}, \quad w_{IM} \triangleq w_{RF} + w_{LO}, \qquad \textbf{2.22}$$

If a passband filter with gain *G=2* is used centered at the signal's component with w_{IF} as its center frequency, the output signal obtained is:

$$g_n(t) = x(t)\cos\left(w_{IF}t - \theta_n\right). \qquad \textbf{2.23}$$

The angular displacement, which represents the time delay of the incoming plane wave between the antennas of the array, is left unchanged in a modulation operation. After the incoming signal in an antenna channel has been modulated into an intermediate frequency and the signal higher frequency is at least half as small as the sampling frequency, the ADCs with a sampling rate T_S can be used to transform the signal into a digital representation:

$$g_n[m] = g_n(t)\Big|_{t=mT_s} = x[mT_s]\cos\left[w_{IF}mT_s - \theta_n\right], \qquad \textbf{2.24}$$

To simplify the mathematical representation of the signal $g_n[m]$, the constant T_S in the signal $x[mT_s]$ will be omitted and the variable $\omega_{IF} = w_{IF}T_S$ will be used to distinguish the cosine component in the digital signal representation from its analog representation. After making such simplifications, the digital signal observed in each DBF receiver channel *n* of the PAA is:

$$g_n[m] = x[m]\cos\left[\omega_{IF}m - \theta_n\right]. \qquad \textbf{2.25}$$

It is important to observe that the digital representation of the DBF receiver signal contains the phase delay θ_n associated with the time delay found in each *n* element of the PAA.

After the antenna signal has been successfully sampled into the digital domain, the signal needs to be processed by the first stage of the DBF receiver, which is the Digital Down-Converter (DDC). The Digital Down-Conversion is performed by multiplying the digital signal with a sinusoidal signal and a 90º phase-shifted version of the sinusoidal signal, both generated by digital local oscillator. Both mathematical operations can be represented in the following form:

$$\begin{aligned} i'_n[m] &= g_n[m]\cos[\omega_{DLO} m] \\ &= x[m]\cos[\omega_{IF} m - \theta_n]\cos[\omega_{DLO} m], \end{aligned} \qquad \textbf{2.26}$$

$$\begin{aligned} q'_n[m] &= g_n[m]\sin[\omega_{DLO} m] \\ &= x[m]\cos[\omega_{IF} m - \theta_n]\sin[\omega_{DLO} m]. \end{aligned} \qquad \textbf{2.27}$$

If the digital local oscillator frequency $\omega_{DLO} = \omega_{IF}$, the digital signals $i'_n[m]$ and $q'_n[m]$ for each DBF receiver channel can be represented in the following form:

$$i'_n[m] = \frac{x[m]}{2}\left(\cos[2\omega_{IF} m] + \cos[\theta_n]\right), \qquad \textbf{2.28}$$

$$q'_n[m] = \frac{x[m]}{2}\left(\sin[2\omega_{IF} m] + \sin[\theta_n]\right). \qquad \textbf{2.29}$$

The final step in the DDC stage of the DBF receiver is the filtering of the frequency component centered at the digital frequency $2\omega_{IF}$ for both digital signals (image frequencies). If a lowpass filter with a gain G=2 is used to process the signals $i_n'[m]$ and $q_n'[m]$, the output signals found in each filter are:

$$i_n[m] = x[m]\cos[\theta_n] \qquad \textbf{2.30}$$

$$q_n[m] = x[m]\sin[\theta_n] \qquad \textbf{2.31}$$

It can be seen that the DDC stage of the DBF receiver transforms a digital bandpass signal with the time-delay τ_n into two digital baseband signals where the phase information of the bandpass signal is represented in the amplitude of both baseband signals. The previous transformation of the signal into its quadrature components is necessary in order to apply the next filtering phase as a double-input, double-output lowpass filter operation, which is equivalent to a single-input, single-output bandpass filter operation [*Franks*, 1969]. Figure 2.6 shows a block diagram of the RF modulator and the DDC stage of each antenna channel in the PAA with the mathematical equations derived previously.

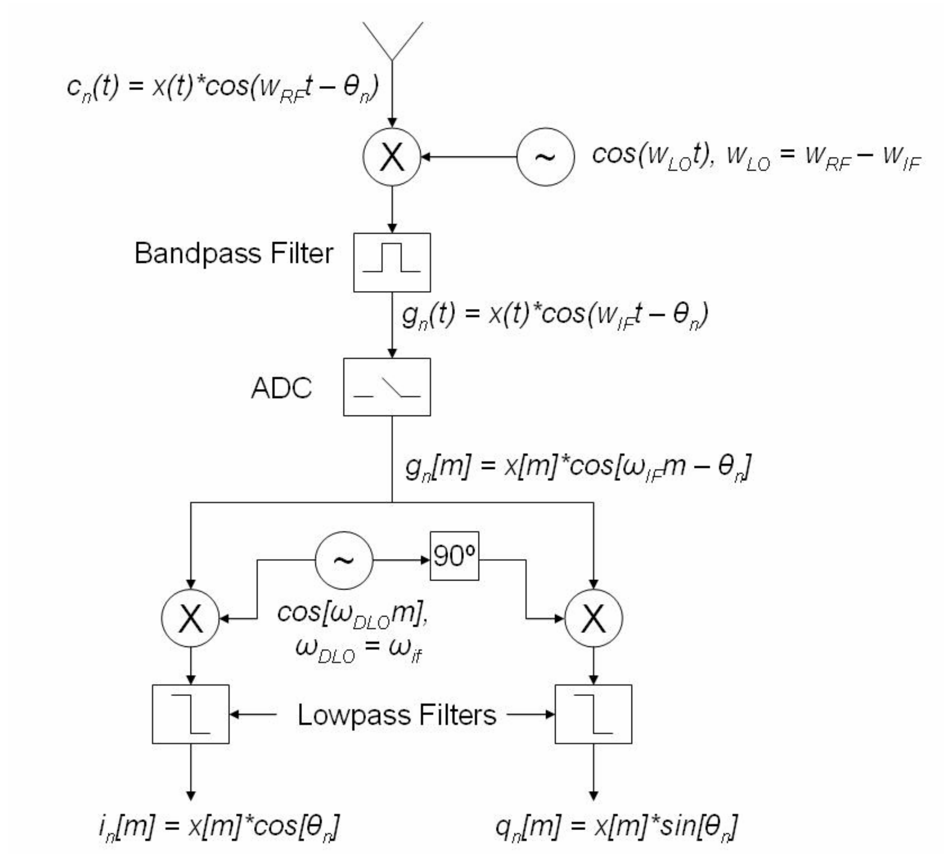
$c_n(t) = x(t)*\cos(w_{RF}t - \theta_n)$
$\cos(w_{LO}t),\ w_{LO} = w_{RF} - w_{IF}$
Bandpass Filter
$g_n(t) = x(t)*\cos(w_{IF}t - \theta_n)$
ADC
$g_n[m] = x[m]*\cos[\omega_{IF}m - \theta_n]$
90º
$\cos[\omega_{DLO}m]$, $\omega_{DLO} = \omega_{if}$
Lowpass Filters
$i_n[m] = x[m]*\cos[\theta_n]$
$q_n[m] = x[m]*\sin[\theta_n]$

Figure 2.6 Block diagram (including equations) of RF Modulator and DDC

The second stage of the DBF receiver is the Complex Weight Multiplication (CWM) stage. In this stage, the complex weight w^*_n associated with each antenna channel in the PAA is multiplied by the digital baseband signals $i_n[m]$ and $q_n[m]$. To represent this complex multiplication operation, a signal $b_n[m]$ will be defined which is composed of the signals $i_n[m]$ and $q_n[m]$:

$$\begin{aligned} b_n[m] &= i_n[m] - jq_n[m] \\ &= x[m]\left(\cos[\theta_n] - j\sin[\theta_n]\right) \\ &= x[m]e^{-j\theta_n}. \end{aligned} \qquad \textbf{2.32}$$

It can be seen that the defined signal $b_n[m]$ is basically the signal $x[m]$ multiplied by a complex constant with an associated phase θ_n. To recover $x[m]$, the complex signal $b_n[m]$ has to be multiplied by the complex conjugate of the complex constant. In other words, if the complex weight $w*_n = e^{j\theta_n}$, then the product of the complex signal $b_n[m]$ and the complex weight is equal to the signal $x[m]$:

$$\begin{aligned} y_n[m] &= w*_n\, b_n[m] \\ &= e^{j\theta_n} x[m] e^{-j\theta_n} \\ &= x[m]. \end{aligned} \qquad \textbf{2.33}$$

It is important to emphasize that the application of the previous $w*_n$ assures phase coherency only with signals coming from space with a phase delay θ_n associated to its carrier signal. If the incoming signal is coming from another direction in space, the multiplication of the complex weight and the complex coefficient will not equal 1, thus making $y_n[m] \neq x[m]$.

The CWM stage of the DBF receiver (shown in Figure 3.7) is applied by means of multiplication and addition of real-value variables. To make such operations possible, it is necessary to express the complex weight $w*_n$ in rectangular form:

$$w*_n = \mathrm{Re}\{w*_n\} + j\,\mathrm{Im}\{w*_n\}. \qquad \textbf{2.34}$$

Once $w*_n$ has been represented in rectangular form, the resulting signal $y_n[m]$ can be obtained by applying the following mathematical operations:

$$\begin{aligned} y_n[m] &= w^*{}_n\, b_n[m] \\ &= \left(\mathrm{Re}\{w^*{}_n\} + j\,\mathrm{Im}\{w^*{}_n\}\right)\left(i_n[m] - jq_n[m]\right) \\ &= r_n[m] + js_n[m], \end{aligned} \qquad \textbf{2.35}$$

where:

$$r_n[m] = i_n[m]\,\mathrm{Re}\{w^*{}_n\} + \left(-q_n[m]\right)\left(-\mathrm{Im}\{w^*{}_n\}\right), \qquad \textbf{2.36}$$

$$s_n[m] = i_n[m]\,\mathrm{Im}\{w^*{}_n\} + \left(-q_n[m]\right)\left(\mathrm{Re}\{w^*{}_n\}\right). \qquad \textbf{2.37}$$

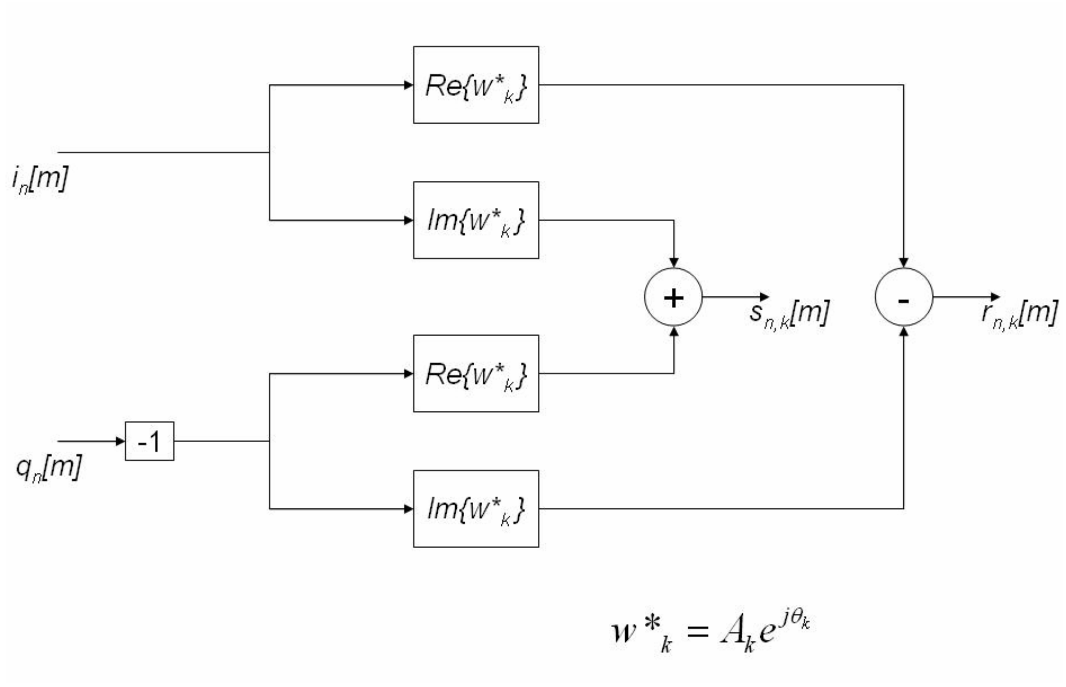

Figure 2.7 Block diagram of CWM phase

The last stage of the DBF receiver involves the addition of all the resulting signals *$y_n[m]$*:

$$\begin{aligned} y[m] &= \frac{1}{N}\sum_{n=0}^{N-1} y_n[m] = \frac{1}{N}\sum_{n=0}^{N-1} r_n[m] + j\frac{1}{N}\sum_{n=0}^{N-1} s_n[m] \\ &= r[m] + js[m] \end{aligned} \qquad \textbf{2.38}$$

An amplitude scaling by a factor of *N* is needed to recover *x[m]* without gain. If desired, the amplitude scaling factor can be included in the complex weight coefficient and omitted in the last phase of the DBF receiver. The signals *r[m]* and *s[m]*, which are the output of the DBF receiver, are the quadrature components of the resulting signal *y[m]*. Post-processing of this quadrature signals, which is done by other components of the system where the PAA is used, is needed for proper retrieval and analysis of the information signal *x[m]*.

2.3.2 DBF Receiver Design

The physical design of a DBF Receiver is based on the mathematical model described in the previous section. The design of the DBF Receiver considers how the mathematical model can be implemented using real components and takes into account limitations found in the physical implementation of the PAA system. The design of the DBF Receiver can be divided into four main components: RF Modulation Stage, Digital-Down Conversion stage, Complex Weight Multiplication stage, and the Summation stage. It is important to remember that the RF Modulation Stage is not implemented digitally (technically, it is not part of the Digital Beamformer), but it is essential in the implementation of the PAA and thus, its design will be also explained in this section.

The first stage in the implementation of an antenna channel in a PAA system is the RF Modulation Stage (also called RF Translator [*Haynes*]). The RF Modulator is implemented using an RF Mixer. RF Mixers are available as Integrated Circuits (ICs) component packages and can be bought in commercial microwave components stores. RF Mixers need to receive sufficient signal power in its input ports in order to work properly. In PAA systems, the power of the signal found at the output port of each antenna in the array is very low. Since the first stage of a receiver has a major effect on the noise performance of the system [*Pozar*, 1998], it is necessary to include Low Noise Amplifiers at the RF Modulator Stage. The LNAs help to reduce the Noise Figure in a microwave circuit and increase the Signal-to-Noise Ratio (SNR) of the PAA system. Therefore, the RF Modulator Stage of each antenna channel has one LNA and one RF mixer. Also, the lines that connect each component of this stage need to be designed to work in a 50Ω system at the desired RF carrier frequency of the antenna array.

An intermediate stage found in the antenna receiver channel of a PAA implemented using DBF is the ADC. The ADC transforms the analog signal found in the output of the RF Translator into a digital representation for further processing by the DBF. ADCs implement the operations of sampling, quantizing, and encoding of the analog signal [*Garret*, 1981]. Different ADC techniques can be used to perform the signal acquisition such as successive-approximation conversion technique, sigma-delta conversion technique, dual-slope conversion technique, voltage-comparison tracking conversion technique and charge balance conversion technique. Two important ADC parameters are the bit resolution and the sampling frequency per channel. The bit resolution parameter determines the quantization error found in the analog-to-digital transformation. This quantization error can be represented as noise power, which affects the SNR of the antenna channel’s signal. The sampling rate parameter determines the analog frequency band which can be represented in the digital domain, which extends from DC to the folding frequency (one half of the sampling frequency). These two parameters are set depending on the desired frequency of operation and SNR level of the PAA design. ADCs are available as IC component packages. In the implementation of a PAA, it is important to use a single clock to digitize all the channels in the antenna array to assure proper synchronization.

The first stage of the DBF Receiver (the second stage in antenna channel) is the Digital-Down Conversion Stage. The DDC receives an incoming digital IF signal (usually from an ADC), and modulates the signal into baseband and produces an in-phase signal and a quadrature signal as outputs. The design of the DDC can be implemented using FPGAs or dedicated ICs. The quadrature modulation is performed by the multiplication of the IF signal with a digital oscillator, as mentioned in the previous section. The implementation of the digital oscillator is accomplished using a direct digital synthesizer (DDS). Direct digital synthesis is a technique by which a sinusoidal signal is created by the generation of digital numbers which controls the input of a sinusoidal look-up table [*Manassewitsch*, 1980]. The digital numbers are generated by a phase accumulator, which receives a binary instruction representing a specific frequency of oscillation. The frequency of this digital oscillator is proportional to the phase increment created in the phase accumulator. Since the signal is produced by a look-up table, phase synchronization between the digital local oscillator and its 90º phase-shifted version can be achieved easier than an equivalent analog implementation counterpart. A single DDS must be used for all the channels in the DBF receiver in order to assure proper synchronization between the signals of each antenna channel. After the in-phase and quadrature signals have been produced, a lowpass filter is used to remove image frequency components located on both signals.

Some DDC designs may also include a multirate filter component. The multirate filter is a filter that alters the data rates [*Harris*, 1987]. In PAA applications, the received RF signals are centered at a high carrier frequency, which imposes the need for fast ADCs and DDCs with high sample rate frequencies. On the other hand, cost limitations and simplicity may motivate the need to use Digital Signal Processors (DSPs) working at low sample rate frequencies in the final stages of the DBF. The multirate filter, thus, allows the interconnection between fast DDCs and DSPs operating at different sample rate frequencies. In the case of a DBF receiver, a decimation filter is used to down-sample the output signal of the DDC. A typical decimation filter implementation is composed of a lowpass filtering stage and a subsampling stage. The design of both stages is related to the decrease ratio between the high input sample rate frequency and the low output sample rate frequency. An interesting approach to simplifying the DBF receiver design is the use of one single lowpass filter per antenna channel in the implementation of a DDC. The lowpass filter would accomplish two important tasks: removing image frequencies after modulation (DDC standard stage) and removing higher frequency components before subsampling (multirate filter stage).

If a multirate filter system is needed in the DBF Receiver, such a filter can be implemented using a Cascaded Integrator-Comb (CIC) filter. The CIC is a linear phase FIR filter implemented without the use of multiplication operations operating as a multirate filter to connect two signal processing system components operating at different sampling frequencies. Its name is derived from its structure, which consists of an integrator section operating at a high sampling rate combined with a comb section operating at a low sampling rate [*Hogenauer*, 1981]. CIC filters can be used to implement decimation and interpolation filters. Figure 2.8 shows the architecture of a CIC decimation filter. The CIC filter design parameters are the rate change factor of the multirate filter (*R*), the number of tap delays in each comb stage (*M*), and the number of stages in the integrator and comb section of the filter (*N*). The transfer function of the CIC filter referenced to the high sampling rate is a result of the multiplication of the transfer function of the integrator section and transfer function of the comb section:

$$H(z) = H_I^N(z)\,H_C^N(z) = \frac{\left(1 - z^{-RM}\right)^N}{\left(1 - z^{-1}\right)^N}$$

$$= \left[\sum_{k=0}^{RM-1} z^{-k} \right]^{N}, \qquad \textbf{2.39}$$

where:

$$H_C(z) = 1 - z^{-RM}, \quad H_I(z) = \frac{1}{1 - z^{-1}}, \quad z \in \mathbb{C}. \qquad \textbf{2.40}$$

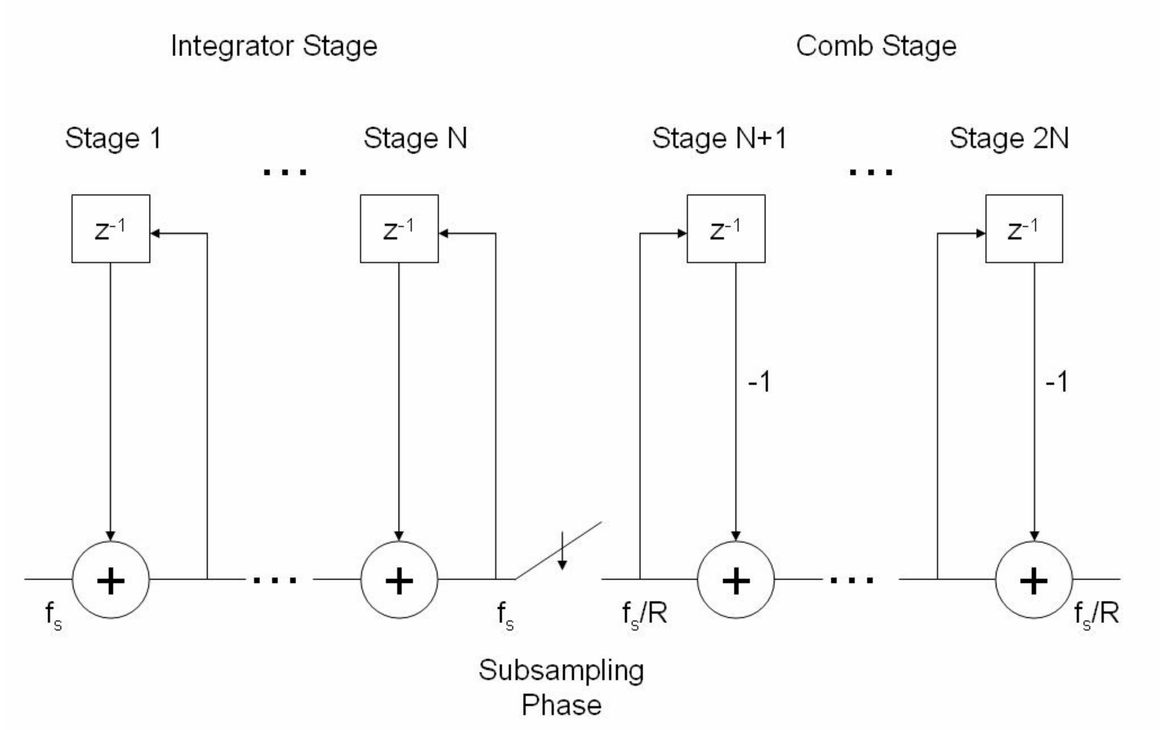

Figure 2.8 Architecture of CIC Decimation Filter

The power frequency response (shown graphically in Figure 2.9) of the CIC filter relative to the low sampling rate is given by the following equation:

$$P(f) = \left[\frac{\sin(\pi M f)}{\sin\left(\frac{\pi f}{R}\right)} \right]^{2N} . \qquad \textbf{2.41}$$

The power response of the CIC filter (decimator and interpolator) contains nulls at multiples of f = *1/M* (relative to the low sampling rate frequency). Since the imaging/aliasing bands in multirate filters appear at multiples of the rate change factor, the CIC filter can be designed to suppress these bands. Information about passband attenuation, stopband attenuation, aliasing attenuation (for CIC decimators), and imaging attenuation (for CIC interpolators) as a function of the CIC filter parameters can be found in Hogenauer's journal paper [*Hogenauer*, 1981] on CIC filters.

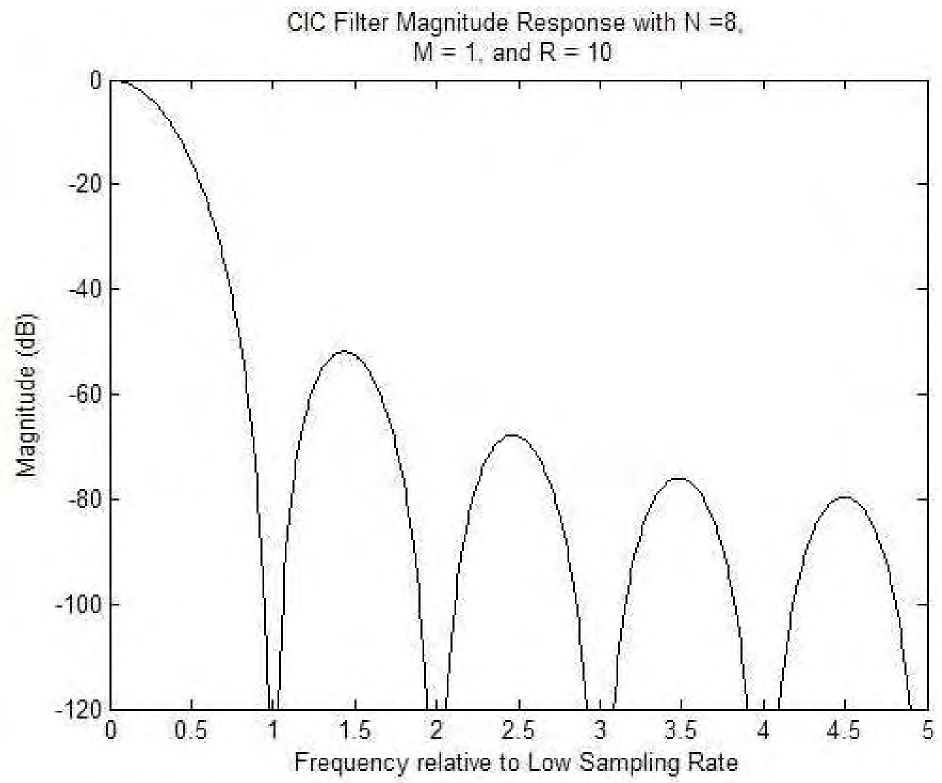

Figure 2.9 Power Response of a CIC Filter with the following parameters: N = 8, M = 1, R = 10

Each comb stage of the CIC filter is a subtraction operation of the current sample by a sample with an *M* delay. In the case of the integrator stage, each integrator has a unity feedback coefficient. When CIC decimation filters are employed, register overflow occurs in all integrator stages. To avoid consequences in the output of the filter, two requirements must be fulfilled: 1) the implementation of filter arithmetic must be based on a number system which allows “wrap-around” between the most positive and most negative number (like the two’s complement arithmetic) and 2) the range of the number system must be greater than or equal to the maximum magnitude expected at the output of the filter [*Hogenauer,* 1981]. Figure 2.10 shows the design of the DDC with the multirate filter (CIC implementation). An additional scale block is included at the output of the CIC filter to increase the gain of the signal by a factor of 2. Since digital circuits are implemented using binary arithmetic, the scale block by a factor of 2 can be easily implemented using a “shift right” operation on the sample’s binary point.

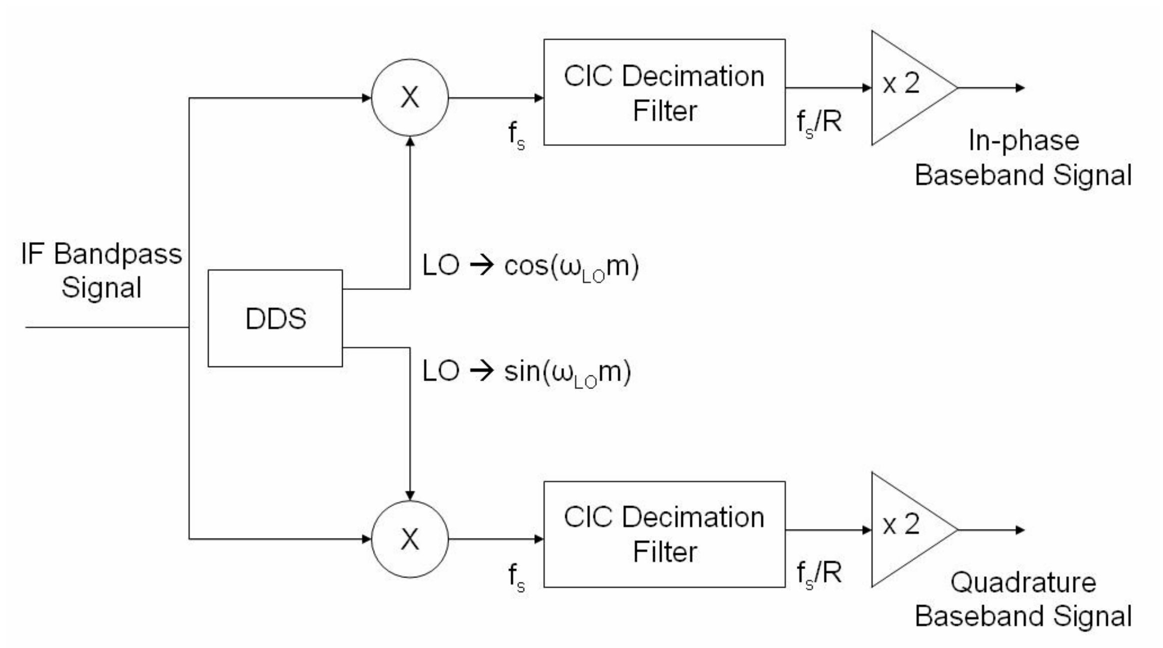

Figure 2.10 Design of a DDC for a DBF Receiver

The second stage in the DBF receiver (third stage in antenna channel) is the CWM stage. The CWM receives the in-phase baseband signal, the quadrature baseband signal, the magnitude of the complex weight and the phase of the complex weight as inputs. Figure 2.11 shows the design of the CWM phase. The CWM phase can be implemented using 7 multiplication operations and 2 addition operations per channel. The first 3 multiplication operations are the product of the complex weight's amplitude with the sine, the negative sine, and the cosine of the complex weight's phase which gives the real, imaginary, and negative imaginary part of the complex weight respectively. The other 4 multiplication operations are the product of the real and imaginary parts of the complex weight with the in-phase and quadrature baseband signals. Finally, the 2 addition operations add the resulting in-phase baseband result and the resulting quadrature baseband result in each channel. Also, 2 negation operators are needed to calculate the negative value of the quadrature baseband signal and the negative sine function and a sine look-up table is necessary to evaluate the sine and cosine function of the complex weight’s phase.

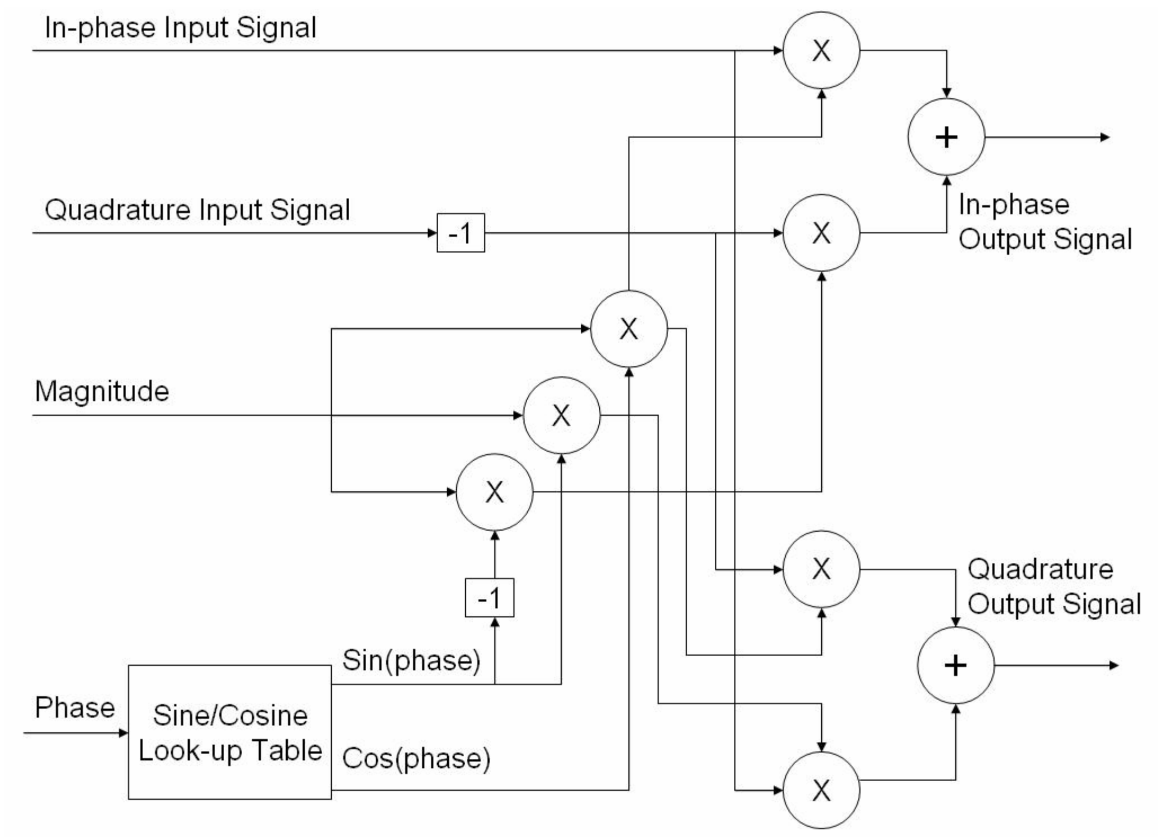

Figure 2.11 Design of CWM for a DBF Receiver

The CWM stage can be implemented using an FPGA or a DSP. The advantage of implementing the CWM in one of the previous devices mentioned strives in the tradeoff between speed of algorithm and cost of implementation. If a DSP is used, a single Multiply-accumulate (MAC) unit can be used to perform the addition and multiplication operations and a single look-up table can be used to evaluate the sine, negative sine and cosine of the complex weight's phase for all the antenna channels. If an FPGA is used, a parallel approach can be pursue, where each DBF channel has its 7 multipliers, 2 adders, and 2 sine look-up tables to process each in-phase and quadrature baseband signal. Also, multiple DSPs can be used to pursue a parallel approach implementation.

The final stage in the DBF Receiver is the Summation Stage. In this stage, the in-phase baseband signals and the quadrature baseband signals of all the antenna channels are added to give a final in-phase baseband signal and quadrature baseband signal as ouputs of the DBF receiver. The number of addition operations in this stage depends on the number of antenna channels in the PAA. The two resulting signals can be used in subsequent stages to process and analyze the data received in the information signal by the PAA.

2.4 DBF Transmitter

2.4.1 Mathematical Model of DBF Transmitter

An information signal *x[m]* represents data which needs to be transmitted into a particular region in space using a PAA. To achieve a specific MRA, the phase delay θ_n between each antenna *n* in the array (which contains *N* antenna elements) must be precisely controlled. The relationship between a complex weight w^*_n and the phase delay θ_n of each antenna are presented by the following equation:

$$w*_n = e^{j\theta_n} = \cos(\theta_n) + j\sin(\theta_n), \quad n = 0,1,\ldots,N-1. \qquad \textbf{2.42}$$

The complex weight's magnitude A_n for each antenna channel can have a particular value (different from one) if different beam pattern characteristics (change sidelobe level behavior, increase beamwidth, null placement, etc.) are required. The first stage of the DBF transmitter is the CWM stage, which consists in the multiplication of the information signal with the real part and the imaginary part of the complex weight. Two resulting signals $i_n[m]$ and $q_n[m]$ are obtained for each antenna channel:

$$i_n[m] = x[m]\,\mathrm{Re}\{w*_n\}, \qquad \textbf{2.43}$$

$$q_n[m] = x[m]\,\mathrm{Im}\{w*_n\}, \qquad \textbf{2.44}$$

where:

$$\mathrm{Re}\{w*_n\} = A_n\cos[\theta_n], \quad \mathrm{Im}\{w*_n\} = A_n\sin[\theta_n]. \qquad \textbf{2.45}$$

The second stage of the DBF transmitter is the Digital-Up Conversion stage. In this stage, the signals $i_n[m]$ and $q_n[m]$ are multiplied by a sinusoidal signal and its 90º phase-shifted version generated by a digital local oscillator with a sinosiodal frequency ω_{IF}. The output of the product the signals $i_n[m]$ and $q_n[m]$ and the digital local oscillator are:

$$fi_n[m] = i_n[m]\cos[\omega_{IF}m] = A_n \cdot x[m]\cos[\theta_n]\cos[\omega_{IF}m], \qquad \textbf{2.46}$$

$$fq_n[m] = i_n[m]\sin[\omega_{IF}m] = A_n \cdot x[m]\sin[\theta_n]\sin[\omega_{IF}m]. \qquad \textbf{2.47}$$

Using trigonometric identities, the signals $fi_n[m]$ and $fq_n[m]$ can be represented in the following form:

$$fi_n[m] = \frac{A_n \cdot x[m]}{2}\left(\cos\left[\omega_{IF} m + \theta_n\right] + \cos\left[\omega_{IF} m - \theta_n\right]\right), \quad \mathbf{2.48}$$

$$fq_n[m] = \frac{A_n \cdot x[m]}{2}\left(\cos\left[\omega_{IF} m - \theta_n\right] - \cos\left[\omega_{IF} m + \theta_n\right]\right). \quad \mathbf{2.49}$$

Then, the signals *fi*$_n$*[m]* and *fq*$_n$*[m]* are added in order to generate a bandpass signal *f[m]* with the desired phase delay θ_n:

$$f_n[m] = fi_n[m] + fq_n[m] = A_n \cdot x[m]\cos\left[\omega_{IF} m - \theta_n\right]. \quad \mathbf{2.50}$$

The last stage in the DBF transmitter consists of the transformation of the digital signal into the analog domain. If a Digital-to-Analog Converter (DAC) with a sampling frequency of f_s is used to transform the digital signal, the output of the DAC can be represented in the following form:

$$f_n(t) = f[m]\Big|_{m=tf_s} = A_n \cdot x(tf_s)\cos\left(\omega_{IF} f_s t - \theta_n\right). \quad \mathbf{2.51}$$

To simplify the mathematical representation of the signal $f_n(t)$, the constant f_S in the signal $x(tf_s)$ will be omitted and the variable $w_{IF} = \omega_{IF} f_S$ will be used to distinguish the cosine component in the analog domain from its digital representation. After making such simplifications, the analog signal observed at the output of each DBF transmitter *n* of the PAA is:

$$f_n(t) = A_n \cdot x(t)\cos\left(w_{IF} t - \theta_n\right). \quad \mathbf{2.52}$$

From the previous equation, it can be seen that the output of the DBF transmitter contains the phase delay θ_n and the magnitude A_n, necessary to construct the desired beam pattern for the PAA. Figure 2.12 shows a block diagram of the DBF transmitter's mathematical model (CWM and Digital-Up Conversion stages).

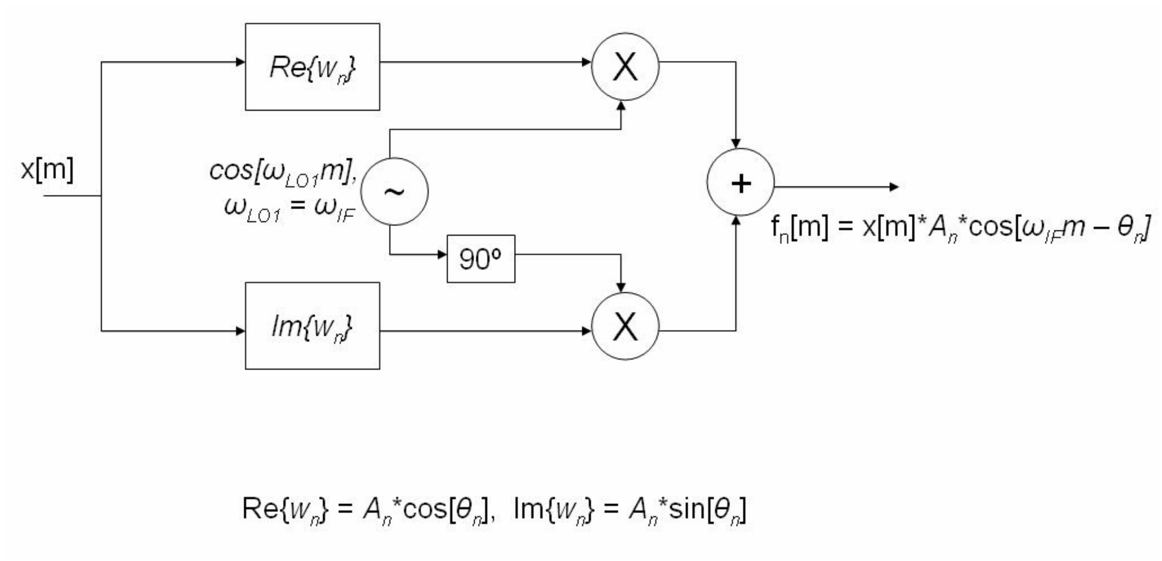
x[m]
Re{w_n}
Im{w_n}
cos[$\omega_{LO1}m$],
$\omega_{LO1} = \omega_{IF}$
~
90º
X
X
+
$f_n[m] = x[m]*A_n*\cos[\omega_{IF}m - \theta_n]$
Re{w_n} = A_n*cos[θ_n], Im{w_n} = A_n*sin[θ_n]

Figure 2.12 Block Diagram (with equations) of CWM and DUC for a DBF Transmitter

Often, engineering applications may emerge where the speed of DACs and cost reduction in DBF transmitter's design may limit the operating frequency of the carrier wave at the output of the DBF transmitter. If $f_n(t)$ needs to be transmitted at a higher frequency carrier, it is necessary to use an RF Modulator in the output of the DBF transmitter of the antenna channel. The RF Modulator Stage translates the output signal of the DBF transmitter into a higher frequency region, making the signal suitable for an antenna transmitting in the microwave frequency range. This operation can be represented by the product of the microwave local oscillator with frequency w_{LO} and the output of the DBF transmitter in each antenna channel:

$$c_n^{'}(t) = A_n \cdot x(t)\cos\left(w_{IF}t - \theta_n\right)\cos\left(w_{LO}t\right). \qquad \textbf{2.53}$$

Using trigonometric identities, the signal *c'ₙ(t)* can be represented as a sum of two cosines:

$$c^{'}_{n}(t) = \frac{A_n \cdot x(t)}{2}\left[\cos\left(w_{RF}t - \theta_n\right) + \cos\left(w_{IM}t - \theta_n\right)\right], \qquad \textbf{2.54}$$

where:

$$w_{RF} \triangleq w_{LO} - w_{IF}, \quad w_{IM} \triangleq w_{LO} + w_{IF}. \qquad \textbf{2.55}$$

If a passband filter with gain *G=2* is centered at the signal's component with w_{RF} as its center frequency, the output signal obtained is:

$$c_n(t) = A_n \cdot x(t)\cos\left(w_{RF}t - \theta_n\right). \qquad \textbf{2.56}$$

The signal $c_n(t)$ has a higher frequency carrier than the output signal of the DBF transmitter and the phase delay θ_n and the magnitude A_n for each antenna channel has been left unchanged during the mixing operation. If the bandwidth of the signal is small compared to the carrier's frequency (see Eq. 2.15), then $c_n(t)$ is considered a narrowband signal (in array processing theory context) and the following approximation is satisfied:

$$\begin{aligned} c_n(t) &= A_n \cdot x(t)\cos\left(w_{RF}t - \theta_n\right) \\ &= A_n \cdot x(t)\cos\left(w_{RF}\left(t - \tau_n\right)\right) \\ &\approx A_n \cdot x(t-\tau_n)\cos\left(w_{RF}\left(t - \tau_n\right)\right) = f(t, \boldsymbol{p}_n), \end{aligned} \qquad \textbf{2.57}$$

where τ_n is the necessary time-delay experienced between each antenna's irradiated plane wave in the PAA. Finally, the signal $c_n(t)$ satisfies the necessary conditions in order to direct the MRA of the beam pattern into a particular region in space and fulfill specific beam pattern requirements.

2.4.2 DBF Transmitter Design

The physical design of a DBF transmitter is based on the mathematical model described in the previous section. The design of the DBF transmitter can be divided into three main stages: the CWM stage, the Digital-Up Converter (DUC) stage, and the RF Modulation Stage. As it was explained in section 2.3.2, the RF Modulation is not part of the Digital Beamformer, but it is important in the implementation of the PAA, and thus, its role will be discussed in the DBF transmitter.

The first stage in the DBF transmitter is the CWM stage. Its function in the DBF transmitter is quite similar to its equivalent in the DBF receiver; it controls the amplitude of the in-phase and quadrature signals prior to the Digital-Up Conversion. The CWM stage receives the information signal as input, multiplies the signal by the real part and imaginary part of the complex weight assign to the channel, and outputs an in-phase signal and a quadrature signal. A simple CWM architecture consists of 4 multiplication operations per channel. The first 2 multiplication operations are used to evaluate the product of the complex weight's amplitude with the sine, and the cosine of the complex weight's phase which gives the real, and imaginary part of the complex weight respectively. The other 2 multiplication operations are used to evaluate the product of the real and imaginary parts of the complex weight with the information signal. In addition, as in the CWM for the DBF receiver, a sine look-up table is necessary to evaluate the sine and cosine function of the complex weight's phase. Figure 2.13 shows the design of the CWM stage for the DBF transmitter.

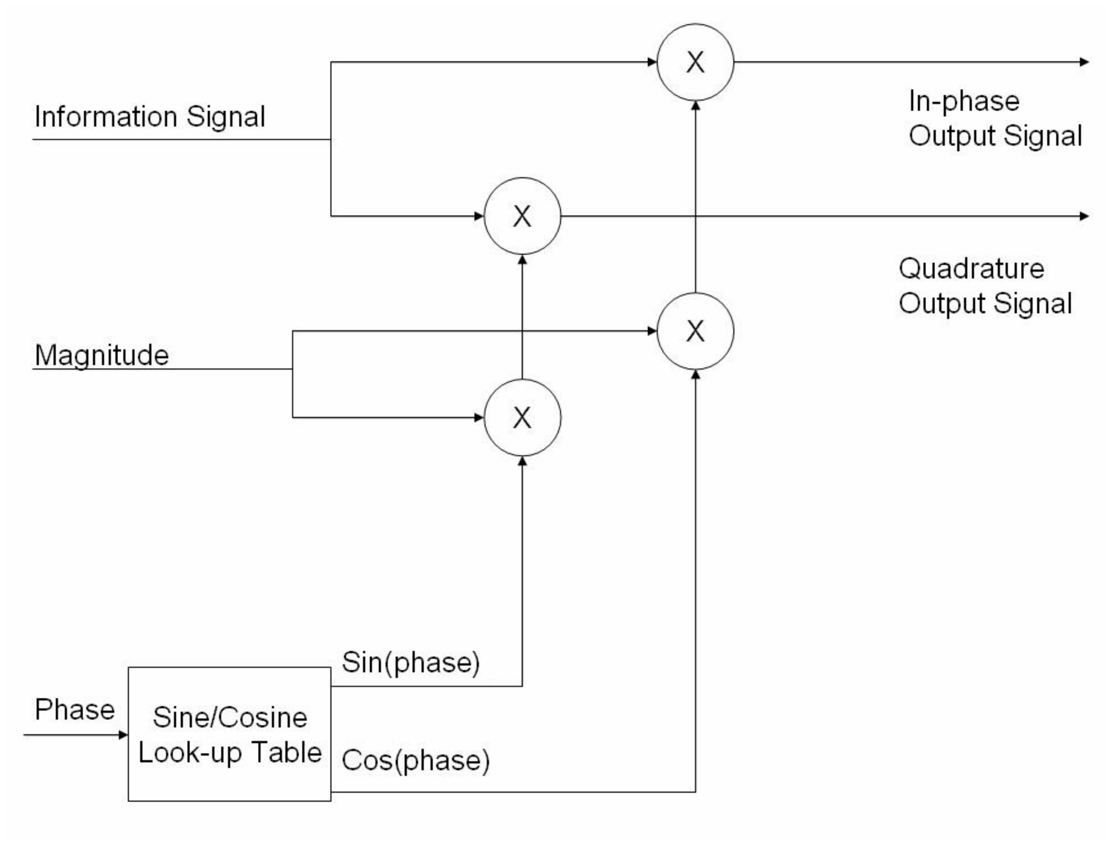

Figure 2.13 Design of CWM for a DBF Transmitter

As in the DBF receiver, the CWM stage in the DBF transmitter can be implemented using an FPGA or a DSP, depending on the importance given to the speed performance and/or the design cost. If the CWM is implemented using a DSP, a single Multiply-accumulate (MAC) unit can be used to execute the multiplication operations and a single look-up table can be used to evaluate the sine, and cosine of the complex weight's phase for all the antenna channels. On the other hand, an FPGA implementation gives the designer the flexibility for a parallel processing strategy where each multiplication operation and sine/cosine table in each antenna channel has separate dedicated hardware to process the information signal.

When the implementation of the DBF transmitter includes functions (software) or components (hardware) operating at different sampling frequencies, a multirate filter must be employed prior the DUC. For the DBF transmitter, a CIC interpolation filter should be used since it provides excellent results with low computational load. A standard interpolation filter implementation is composed of a zero-insertion phase and a lowpass filter phase. The design of both stages is related to the increase ratio between the input (low sample rate frequency) and the output (high sample rate frequency) of the filter. The CIC interpolation filter implements both phases using a unique design approach (shown in Figure 2.14). The low sampling comb stage followed by the high sampling integrator stage employs a lowpass linear phase FIR filter. The zero-insertion substage is performed between the two CIC interpolation filter stages. The nulls found at multiples of the frequency *1/M* (where *M* is the differential delay) relative to the low sampling rate are able to suppress the imaging bands found in the spectrum after the multirate filter's zero-insertion substage. As mentioned in Section 2.3.2, the frequency response characteristics of the filter (passband and stopband attenuation, number of nulls, etc.) are determined entirely by the CIC filter parameters (number of tap delays, CIC filter stages, and rate change factor).

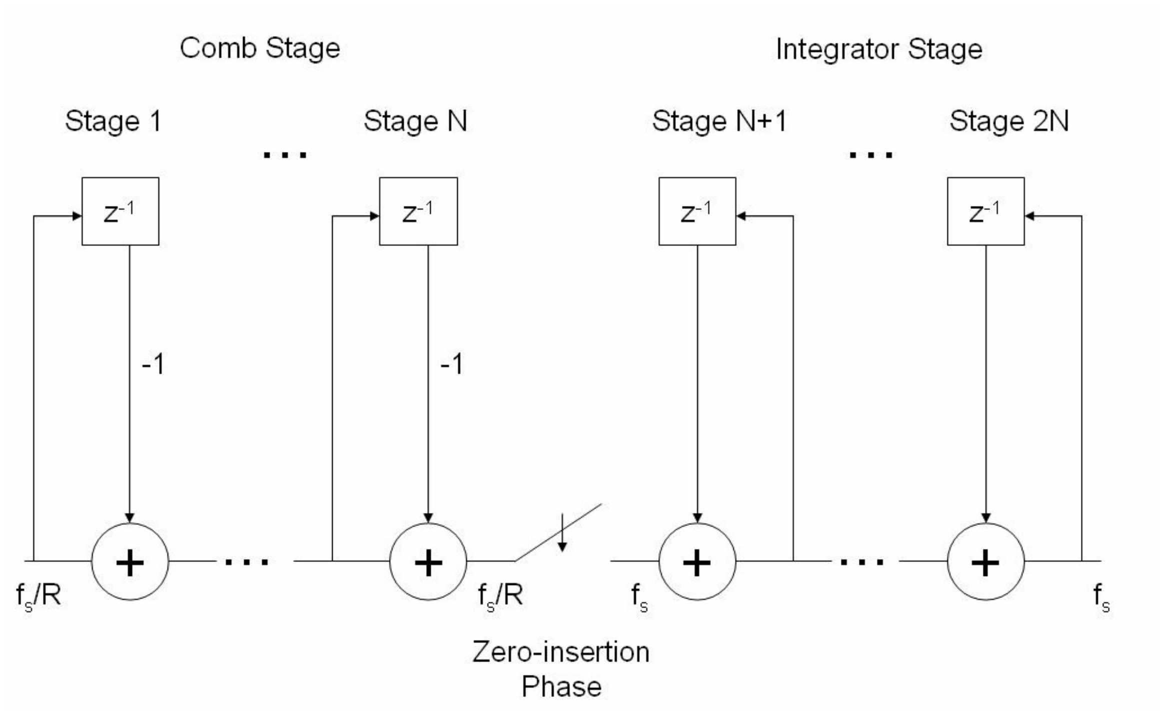

Figure 2.14 Architecture of CIC Interpolation Filter

The second stage in the DBF transmitter is the Digital-Up Conversion stage. The DUC receives two baseband signals (in-phase and quadrature lowpass signals) and modulates these signals into a single real bandpass signal. The design of the DUC can be implemented using FPGAs or dedicated ICs. The quadrature demodulation is performed by the multiplication of the in-phase and quadrature signal with the digital local oscillator and its 90º phase-shifted version respectively. The addition of these two resulting signals gives a real bandpass signal centered on the digital local oscilator's frequency with an amplitude and phase offset associated with the complex weight assigned to that specific channel. As in the DBF receiver, a DDS is used to implement the digital local oscillator. The use of a single DDS in all the DBF transmitters of the antenna array is crucial in guaranteeing proper synchronization between the signals of each antenna channel. Figure 2.15 shows the design of the DUC with the multirate filter (CIC implementation).

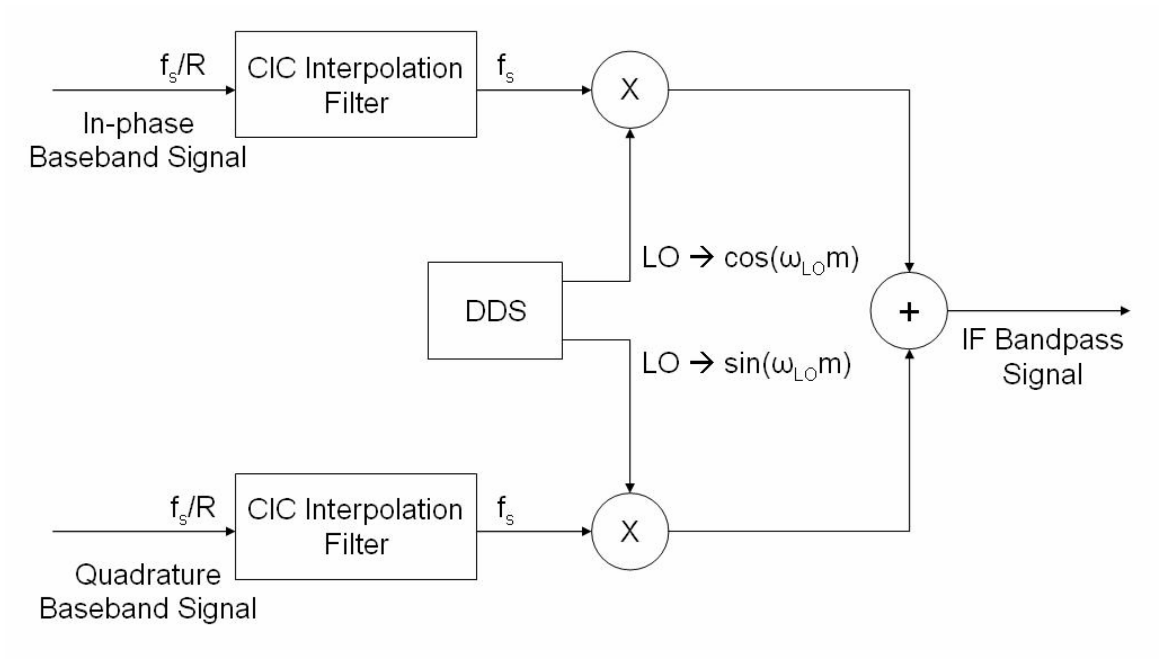

Figure 2.15 Design of DUC for a DBF Transmitter

The gateway between the output of the DBF, which is a digital signal, and the input of the RF Translator (which is an analog signal) is the DAC. The DAC transforms a digital signal into an analog representation. A DAC can be considered a digitally controlled potentiometer that provides an output current or voltage normalized to its full-scale [*Garret*, 1981]. The DAC has the same parameters as the ADC, which is its equivalent in a DBF receiver. In the implementation of a PAA, it is important to use a single clock for all the DACs to assure proper synchronization between each channel in the DBF transmitter.

The last stage in the antenna channel is the RF Translator. The RF Translator in the antenna's transmitter modulates an input signal, found in an intermediate frequency band, to a higher frequency band where it can be use as input to the PAA's antennas. Analogous to the DBF receiver's RF Translator, the RF Translator in the DBF transmitter is implemented using an RF Mixer per antenna channel. Typically, the level of signal power found at the output of the RF Mixer might not be high enough to excite the antenna ports of the PAA. In a typical microwave communication system, a power amplifier (PA) is used after the RF Mixer to amplify the microwave signal, which is then radiated by each antenna of the array [*Pozar*, 1998]. Finally, the lines that connect each component in this stage need to be designed to work on a 50Ω system at the desired RF carrier frequency of the PAA.

3 SIMULATION AND IMPLEMENTATION RESULTS

In this chapter, one DBF receiver and two DBF transmitter design prototypes will be presented. The difference between each design prototype consists in the number of elements and the geometrical distribution of the PAA where the DBF is used. The DBF receiver model shown in this chapter is designed for a 4-element linear PAA. As for DBF transmitters, models shown in this chapter are designed for a 16-element linear PAA and a 16-element 4x4 rectangular PAA. Two spatial filters will be applied to each design prototype and the resulting beam pattern on the simulations will be compared with the ideal beam pattern calculated using array processing theory. The computation of the ideal beam pattern is performed on MATLAB using the beam pattern equation (Eq. 2.6). All beam pattern plots shown in this chapter have been normalize with reference to the beam pattern's maximum value. Each DBF prototype has been designed in order to be implemented on an FPGA device using fixed-point two's complement arithmetic. The simulation of each DBF receiver and transmitter is performed on MATLAB's Simulink environment using the FPGA functional blocks provided by the Xilinx's System Generator Blockset. Finally, a 16-element 4x4 rectangular PAA will be constructed and a DBF transmitter, implemented on a commercial digital signal processing system, will be used to control the beam pattern of the PAA.

3.1 4-element linear PAA Receiver Prototype

The 4-element linear PAA Receiver Prototype consists of 4 isotropic radiating antennas arranged in a linear distribution and uniformly spaced by half-wavelength. The operating carrier frequency of the PAA is 5.85 GHz. The intermediate carrier frequency (where the ADCs sample the incoming signal) of the DBF is 3 MHz. The incoming signal's bandwidth specification is 2 MHz. Since the Narrowband Factor ($B_S \cdot \Delta T_{max}$) is extremely small compared to one, a narrowband beamformer can be used to control the beam pattern of the array. Table 3.1 summarizes the specifications of this linear PAA Receiver Prototype.

TABLE 3.1 4-element linear PAA parameters

Parameter	**Value**
RF Carrier Frequency	f_{RF} = 5.85 GHz
IF Frequency	f_{IF} = 3 MHz
Signal Bandwidth	B_S = 2 MHz
Number of Elements	N = 4
Inter-element Spacing	$\Delta z = \lambda_c/2$
Maximum Travel Time	$\Delta T_{max} = 3/2f_{RF}$
Narrowband Factor	$B_S \cdot \Delta T_{max}$ = 0.000513

The implementation of the DBF receiver for this PAA is based on the design described in Section 2.3.2. Figure 3.1 shows a diagram of the DBF receiver implementation for a 4-element linear PAA using MATLAB's Simulink and Xilinx's

System Generator Blockset. The blue blocks on the diagram are the components of the DBF receiver, where each block represents FPGA code which implements the mathematical or logical operator/operation performed by the block. The bit resolution of all the multipliers in the DBF receiver is 18 bits with 16 bits of decimal precision and a latency of 3 clock cycles. As for the addition operators, each operation has no latency giving an output sample with a resolution of 14 bits with 12 bits of decimal precision. The two big white blocks in the figure are two stages of the DBF receiver: the DDC and the CWM stage. The blue blocks at the left side of the CWM are the amplitude and phase of the weight coefficient of that DBF receiver channel. The addition blocks at the right side of the CWM stage implement the summation stage of the DBF receiver. A single DDS Block has been used as the local digital oscillator for the 4 DBF channels. The DDS outputs a sinusoidal signal and its 90º phase-shifted version at a frequency of 3 MHz, where each sample has a sample frequency of 200 MHz. The yellow blocks at the left side of the figure represent the ADCs of the DBF, which sample the incoming signal at 200 MHz per channel at a resolution of 14 bits with 12 bits of decimal precision. The yellow blocks at the right side of the figure represent the interface between the DBF Receiver output and the input of the data processing stage of the communication system where the PAA is used. The other white blocks in the diagram are Simulink blocks representing the incoming signal in each channel (left side of figure), and the post-processing stage receiving the data processed by the DBF receiver (right side of figure).

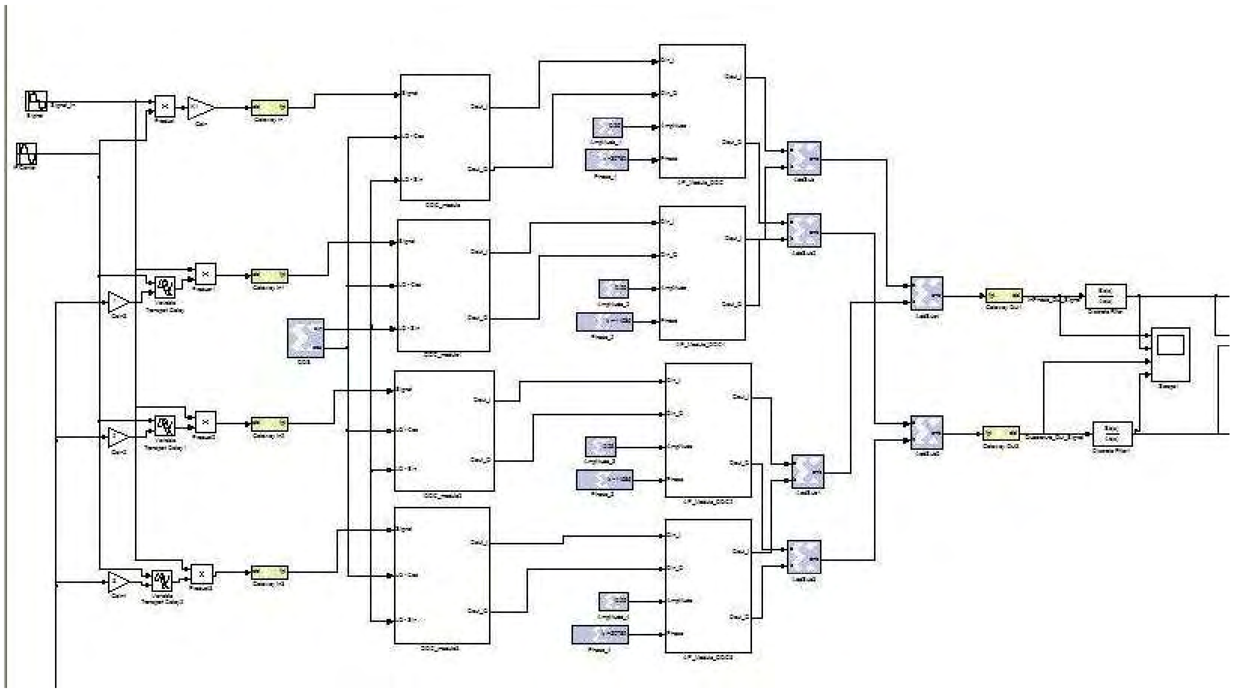

Figure 3.1 Diagram of a simulated 4-element DBF receiver

Figure 3.2 shows diagrams of the DDC and the CWM stage (components inside each stage). The DDC (Figure 3.2a) operates at the sampling frequency of the ADC, which is 200 MHz. Each DDC contains two CIC filters (one for each quadrature channel) with 8 stages (N = 8), a differential delay of 2 samples (M = 2), a rate change factor of 4 (R = 4) and a latency of 8 clock cycles. The two other blue blocks at the right of the CIC filter (“force” block and “cast” block) quantizes the output of the filter to samples with a bit resolution of 18 bits with 16 bits of decimal precision. The CWM (Figure 3.2b) operates at a sampling frequency of 50 MHz, which is the sampling frequency at the output of the CIC decimation filter. The resolution of the weight coefficient’s amplitude is 16 bits with 14 bits of decimal precision and the weight coefficient’s phase is 8 bits with no decimal precision. The output of the sine/cosine table in the CWM gives a bit resolution of 8 bits with 7 bits of decimal precision. As for the output of DBF receiver, each output quadrature channel has a bit resolution of 14 bits with 12 bits of decimal precision at a sampling frequency of 50 MHz. The measurement SNR of a typical anechoic chamber (used to measure the beam pattern of an antenna array) ranges around 40 dB, thus a resolution of more than 6 bits would satisfy the bit resolution requirement for each signal processing operation. Table 3.2 summarizes the parameters of the DBF receiver's components.

a)

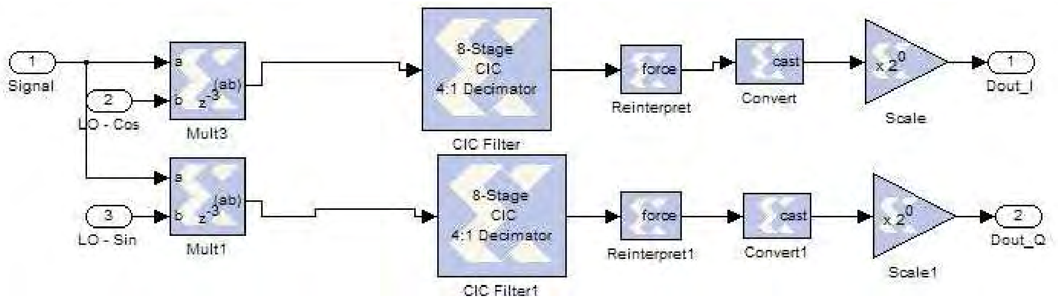

b)

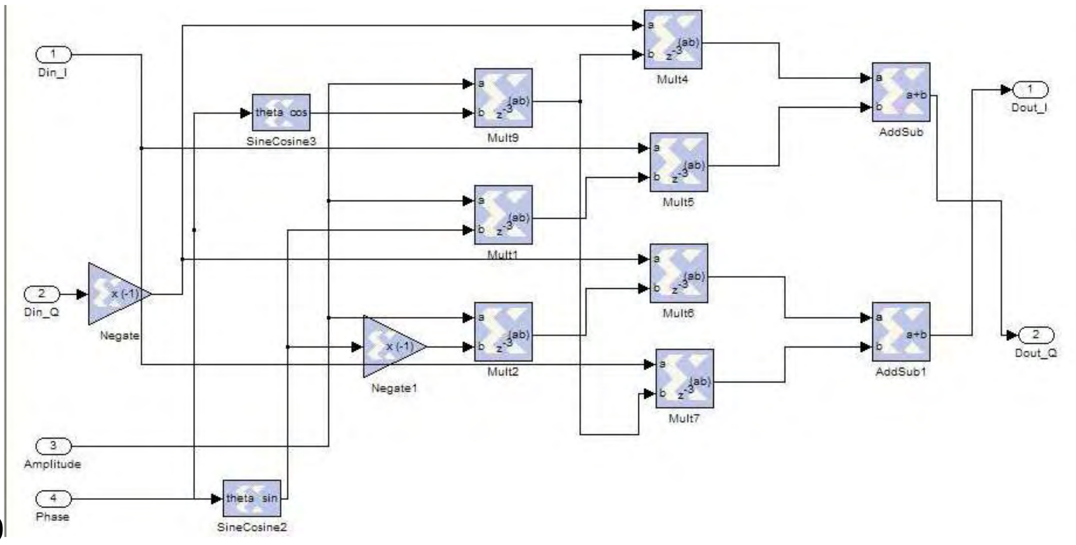

Figure 3.2 Diagram of simulated DDC (3.2a) and CWM (3.2b) stage in DBF receiver

TABLE 3.2 Parameters of the DBF receiver’s components

Parameter	Value
Multiplier’s bit resolution	18 bits -16 bit decimal precision
Adder’s bit resolution	14 bits – 12 bit decimal precision
DDS Operating Frequency	f_{DDS} = 3 MHz
ADC Sample Frequency	f_{ADC} = 200 MHz
ADC bit resolution	14 bits – 12 bit decimal precision
DDC Sample Frequency	f_{DDC} = 200 MHz
CIC Filter Stages	N_{CIC} = 8
CIC Differential Filter	M = 2
CIC Rate Change Factor	R = 4
CIC bit resolution	18 bits – 16 bit decimal precision
CWM Sample Frequency	f_{CWM} = 50 MHz
Weight Coefficient – Amplitude bit resolution	16 bits – 14 bit decimal precision
Weight Coefficient – Phase bit resolution	8 bits with no decimal precision
Sine/Cosine Look-Up Table input bit resolution	8 bits – 7 bit decimal precision
DBF Output Signal bit resolution	14 bits – 12 bit decimal precision

The DBF receiver simulations consist in applying sinusoidal signals with the same intermediate carrier frequency and a variable phase shift between each signal. The initial phase shift between each element gives an equivalent space signal coming from endfire (direction parallel to the array's axis) at the left side of the array. As the simulation iterates, the relative phase difference between each element changes until it reaches to a phase shift equivalent to a signal coming from endfire at the right side of the array. Since the weight coefficients of each DBF channel is held constant, the output in-phase and quadrature channel of the DBF receiver will experience changes on each signal's amplitude as the simulation time progresses. In the post-processing phase of the PAA, the two quadrature output signals are use to calculate the resulting beam pattern's amplitude and phase. The resulting beam pattern of each DBF receiver simulation shown in this chapter will be compared with the theorical beam pattern calculated using Eq. 2.6.

3.1.1 First Spatial Filter Example: Beam pattern with Uniform Amplitude Weight Function pointing to θ_{MRA} = 45º

The first spatial filter example used in the DBF receiver for a 4-element linear PAA produces a beam pattern with an MRA pointing at an angular position of 45º with respect to endfire on the right side of the array. If the desired beam pattern of a PAA has only one MRA, the weigh coefficients for each channel can be derived using the Narrowband Beamformer model discussed in Section 2.1.3:

$$w*_n = \frac{1}{N} e^{j \overline{k^T(\theta_{MRA,}\phi_{MRA})} \cdot \overline{p_n}}, \qquad \textbf{3.1}$$

where the wavenumber *k* and the position vector *p* are:

$$k\left(\theta_{MRA,}\varphi_{MRA}\right)=2\pi\!\!\diagup\!\!\lambda\begin{bmatrix}\sin\theta_{MRA}\cos\phi_{MRA}\\ \sin\theta_{MRA}\sin\phi_{MRA}\\ \cos\theta_{MRA}\end{bmatrix},\qquad \overline{p}=\begin{bmatrix}p_x\\ p_y\\ p_z\end{bmatrix}. \qquad \mathbf{3.2}$$

For a linear array, the position vector's p_x and p_y value is equal to zero reducing the calculation of the weight coefficient for each channel n into:

$$w*_n=\frac{1}{N}e^{j\left(2\pi\!\diagup\!\lambda\right)p_z\cos\left(\theta_{MRA}\right)}. \qquad \mathbf{3.3}$$

Table 3.3 shows the resulting weight coefficients for a uniform 4-element linear PAA with an inter-element spacing of $\lambda/2$. It can be seen that the amplitude of each weight coefficient has a value of $1/N$, which is equivalent to applying a uniform spectral window

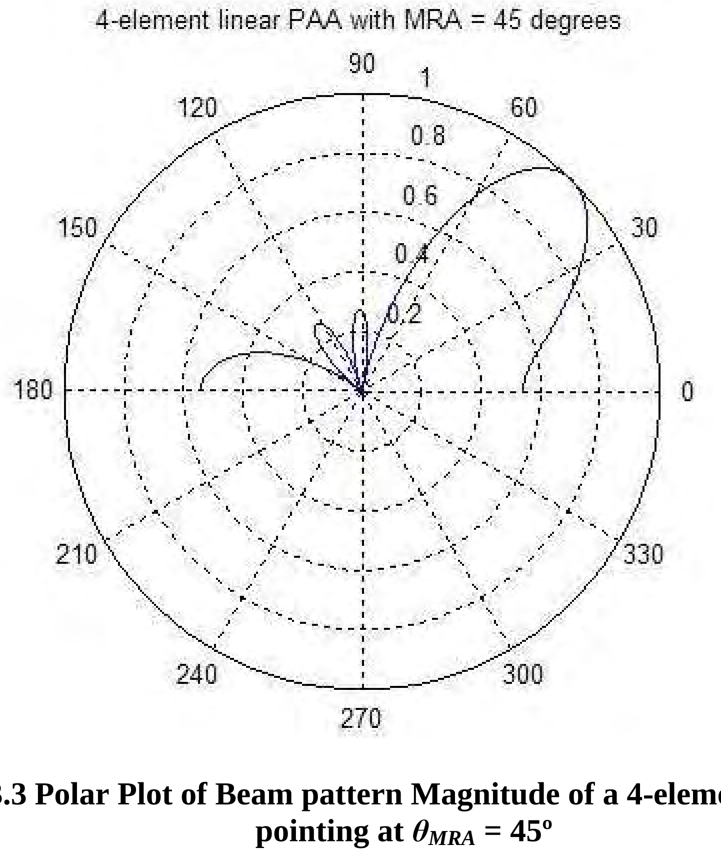

Figure 3.3 Polar Plot of Beam pattern Magnitude of a 4-element linear DBF pointing at θ_{MRA} = 45º

into the weight coefficients. A MATLAB program named “linear_steering_array.m” (which is shown in Appendix A) was prepared in order to calculate the theoretical beam pattern, the directivity and the beamwidth of the PAA for a one-MRA spatial filter design for a linear PAA. Figure 3.3 shows a polar graph of the theoretical beam pattern’s amplitude with the weight coefficients shown in Table 3.3. Figure 3.4 shows a rectangular plot of the beam pattern’s amplitude in dB units. These plots show the maximum value of the beam pattern’s amplitude at a signal’s angle-of-arrival of 45º with a directivity of 6.02 dB. The beamwidth of the MRA beam for the theoretical beam pattern is 40.5º.

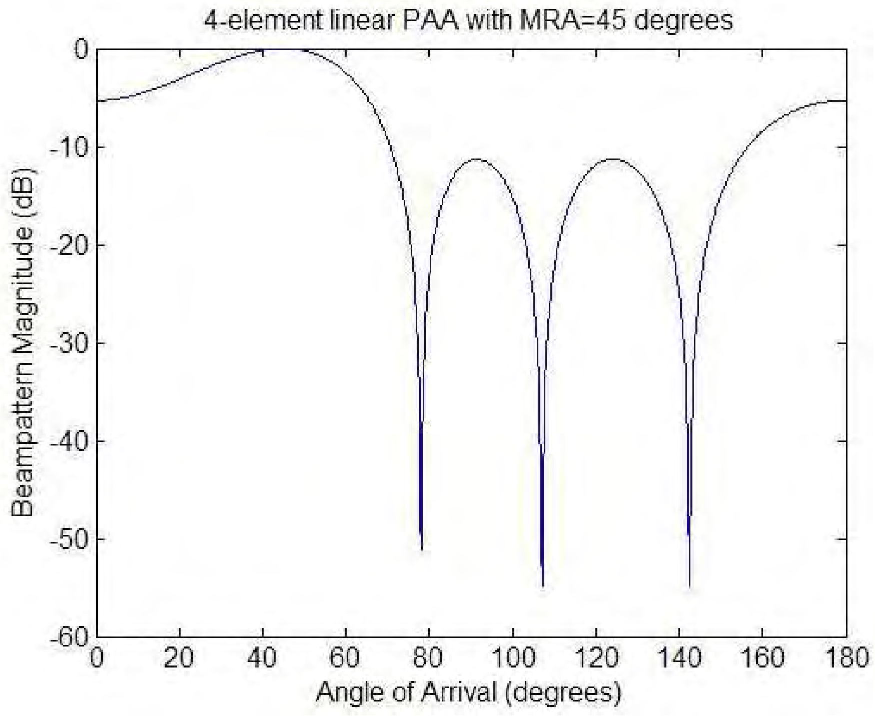

Figure 3.4 Rectangular plot of Beam pattern Magnitude of a 4-element linear DBF pointing at θ_{MRA} = 45º

TABLE 3.3 First Spatial Filter Weight Coefficients – Theoretical Weights

Element	Weight
1	$w_1 = 0.25 \angle 169.0812^o$
2	$w_2 = 0.25 \angle -63.6396^o$
3	$w_3 = 0.25 \angle 63.6396^o$
4	$w_1 = 0.25 \angle -169.0812^o$

After the weight coefficients have been calculated, the next step in the simulation preparation is the transformation of these coefficients into a form suitable for the DBF receiver to use. A MATLAB program named “linear_DBFreceiver_parameters.m” (included in the Appendix A) was prepared to quantize and transform the weight coefficients for each channel and set all the necessary DBF receiver parameters (shown in Table 3.2) needed to perform the DBF receiver simulation. The total simulation time used for this DBF receiver was 2 x 10^{-5} seconds, which is equivalent to 60 periods of the intermediate carrier frequency. The weight coefficients obtained after quantization of the weight values into the fixed-point representation used in the DBF receiver simulation are shown in Table 3.4. The results of the DBF receiver for the first spatial filter showing the behavior of the in-phase output signal, quadrature output signal and the amplitude and phase signals obtained in the post-processing phase of the PAA are shown in Figure 3.5 and Figure 3.6. Figure 3.5 and Figure 3.6 shows the time plots for plane wave signals with the angle of arrival changing from 90º to 0º and 90º to 180º, respectively, with respect to right-side endfire. The change in amplitude experienced in the in-phase and quadrature output signals as time progresses illustrates the spatial filter’s response characteristics with respect to signals with different angle-of-arrival directions. These characteristics can be seen clearer in the amplitude and phase plots shown at the bottom of each figure, which where generated in the post-processing phase (not part of the DBF receiver) using the in-phase and quadrature output signals.

TABLE 3.4 First Spatial Filter Weight Coefficients – FPGA Weights

Element	Weight
1	w_1 = 0.25 ∟168.75º
2	w_2 = 0.25 ∟-63.2813º
3	w_3 = 0.25 ∟63.2813º
4	w_1 = 0.25 ∟-168.75º

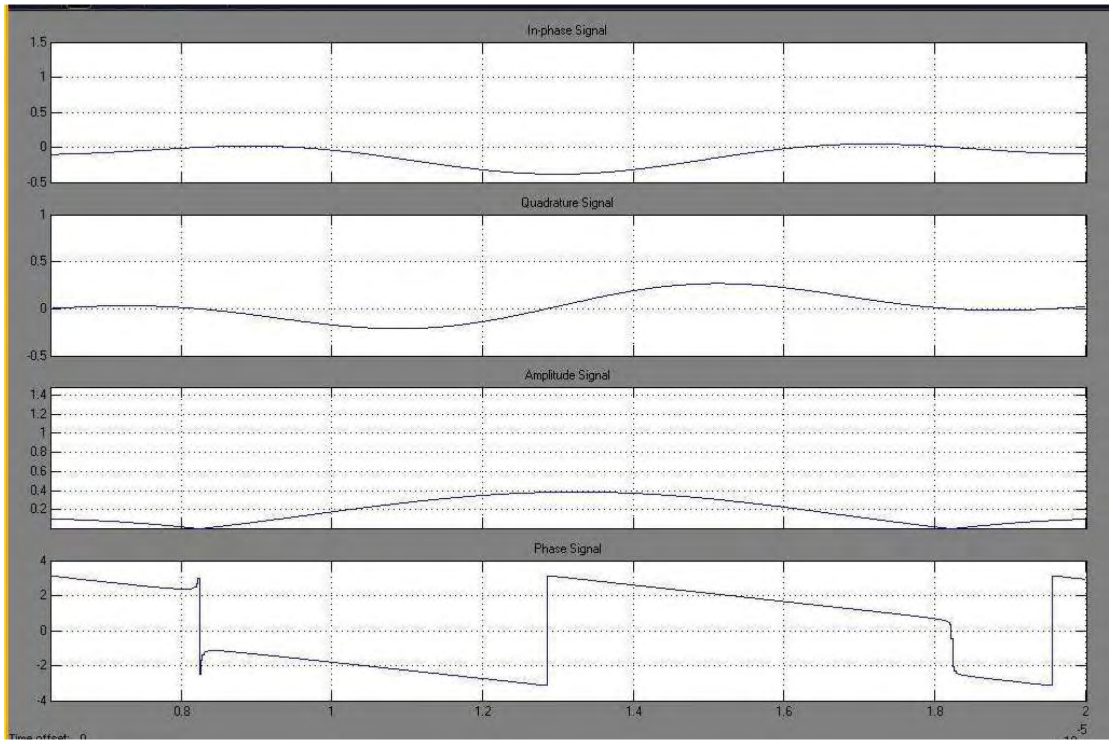

Figure 3.5 Time plots for plane wave signals with the angle of arrival changing from 90º to 0º for first spatial filter on 4-element linear DBF

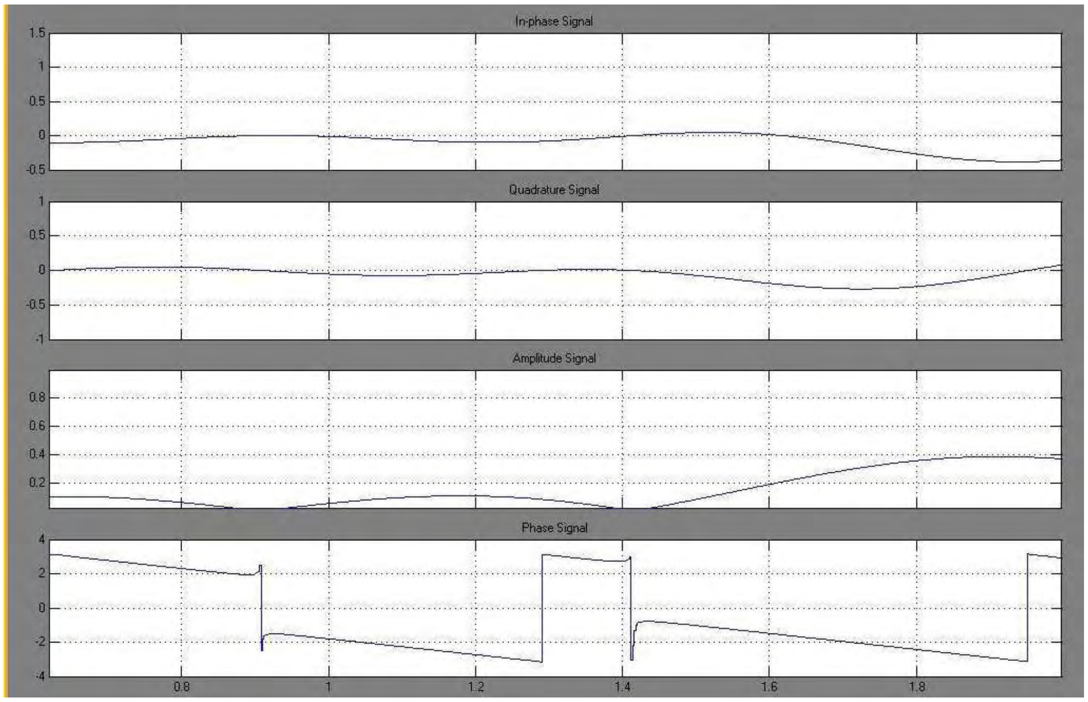

Figure 3.6 Time plots for plane wave signals with the angle of arrival changing from 90º to 180º for first spatial filter on 4-element linear DBF

To analyze the data results obtained in the DBF receiver simulation, each output signal generated was stored in a .mat files. A MATLAB program named "linear_DBFreceiver_results.m" was created to retrieve the simulation results stored in the .mat files and condition this output data in order to achieve proper viewing of the results. Figure 3.7 shows a polar graph of the simulation beam pattern's amplitude with the weight coefficients and Figure 3.8 shows a rectangular plot of the simulation beam pattern's amplitude in dB units. These plots show the maximum value of the beam pattern's amplitude at a signal's angle-of-arrival of 44.9º with a directivity of 6.03 dB. The beamwidth of the MRA beam for the simulated beam pattern is 40.49º. Table 3.5

shows the results obtained from the DBF receiver simulation with the results obtained in the theoretical beam pattern calculation.

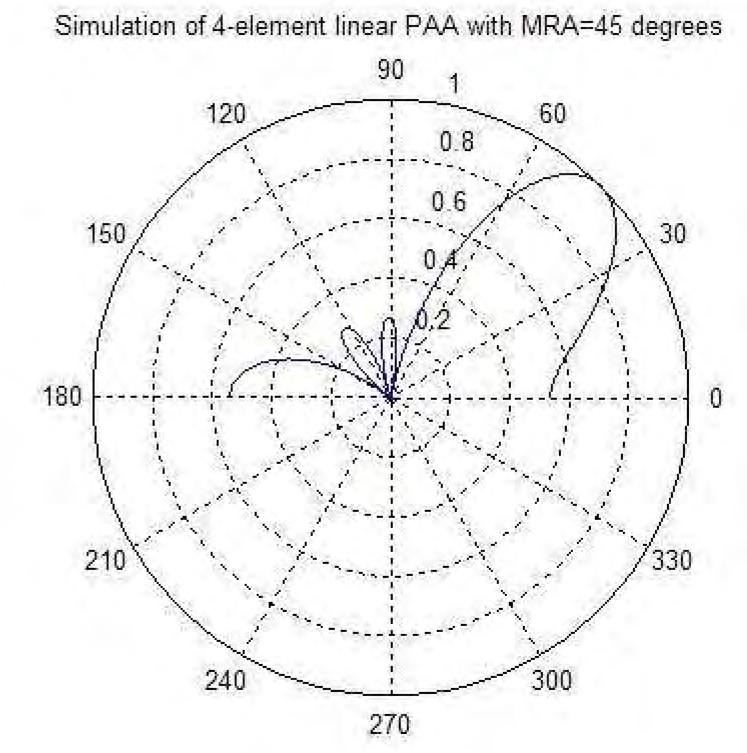

Figure 3.7 Polar Plot of Beam pattern Magnitude of a 4-element linear DBF Simulation pointing at θ_{MRA} = 45º

TABLE 3.5 First Spatial Filter Beam pattern Characteristics for a 4-element linear PAA

Beam pattern Characteristic	Theoretical Result	Simulation Result
MRA angle-of-arrival	Θ_{MRA} = 45º	Θ_{MRA} = 45.09º
Half-power Beamwidth	Θ_{BW} = 40.47º	Θ_{BW} = 40.28º
Directivity	D_{dB} = 6.02 dB	D_{dB} = 6.03 dB
Sidelobe level	SLL_{dB} = -11.30 dB	SLL_{dB} = -11.43 dB

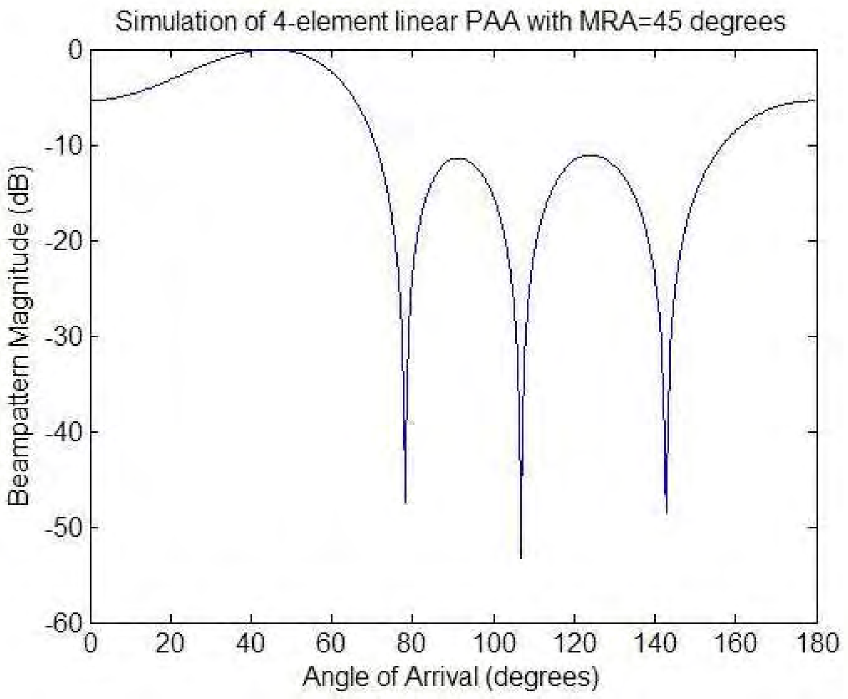

Figure 3.8 Rectangular plot of Beam pattern Magnitude of a 4-element linear DBF pointing at θ_{MRA} = 45º

3.1.2 Second Spatial Filter Example: Synthesized Beam pattern using Schlkunoff polynomial null-placement method

The second spatial filter example used in the DBF receiver for a 4-element linear PAA produces a beam pattern with 3 nulls positioned at different angular positions: 30º, 60º, and 100º from right-side endfire. The calculation of the weight coefficients was performed using the Schelkunoff polynomial null-placement method, which can position a maximum of *N*-1 nulls for an *N*-element PAA. A MATLAB file named “linear_DBFreceiver_nullplacer.m” (shown in the Appendix A) was created to calculate the weight coefficients for a linear PAA with null-placement specifications on its beam pattern. The calculation of the weight coefficients involves the solution of a linear system which contains information of the position of the nulls and null depth (which can be controlled by means of null multiplicity). Table 3.6 shows the resulting weight coefficients for the specified beam pattern parameters. In this case, the amplitude of each weight coefficient is different from one implying the necessity for amplitude weight control on a DBF receiver where null-placement characteristics are required. Figure 3.9 shows a polar graph of the theoretical beam pattern's amplitude with the weight coefficients shown in Table 3.6. Figure 3.10 shows a rectangular plot of the beam pattern's amplitude in dB units, which shows nulls placed at angles-of-arrival 30.06º, 59.94º, and 100.08º from right-side endfire with a null depth of -60.22 dB, -56.64 dB, and -47.73 dB respectively.

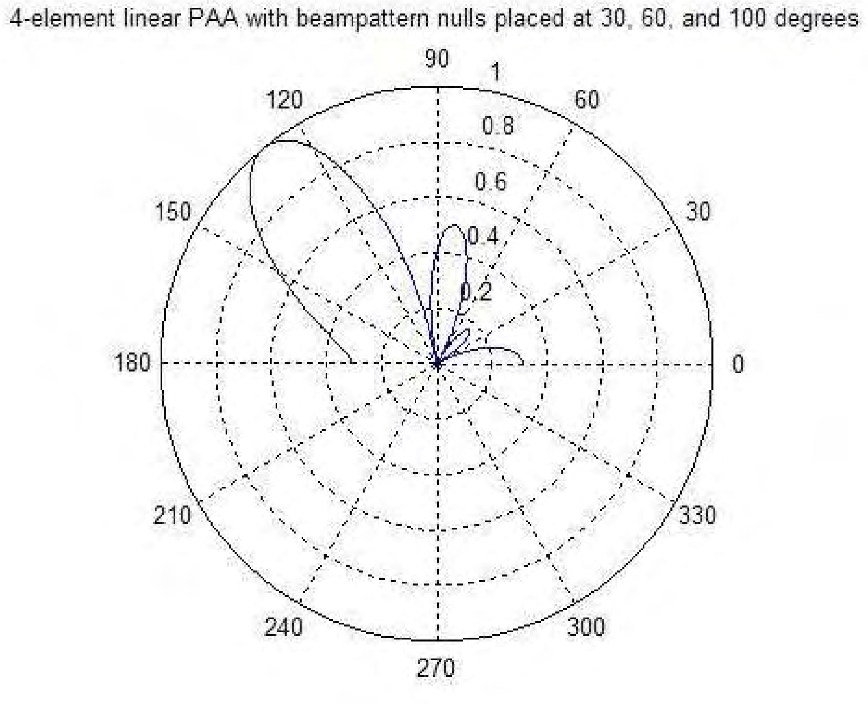

Figure 3.9 Polar Plot of Beam pattern Magnitude of a 4-element linear DBF with beam pattern nulls placed at 30º, 60º, and 100º

TABLE 3.6 Second Spatial Filter Weight Coefficients – Theoretical Weights

Element	Weight
1	W_1 = 0.8787 ∟-17.3140º
2	W_2 = 0.7835 ∟-103.5923º
3	W_3 = 0.7835 ∟103.5923º
4	W_1 = 0.8787 ∟-17.3140º

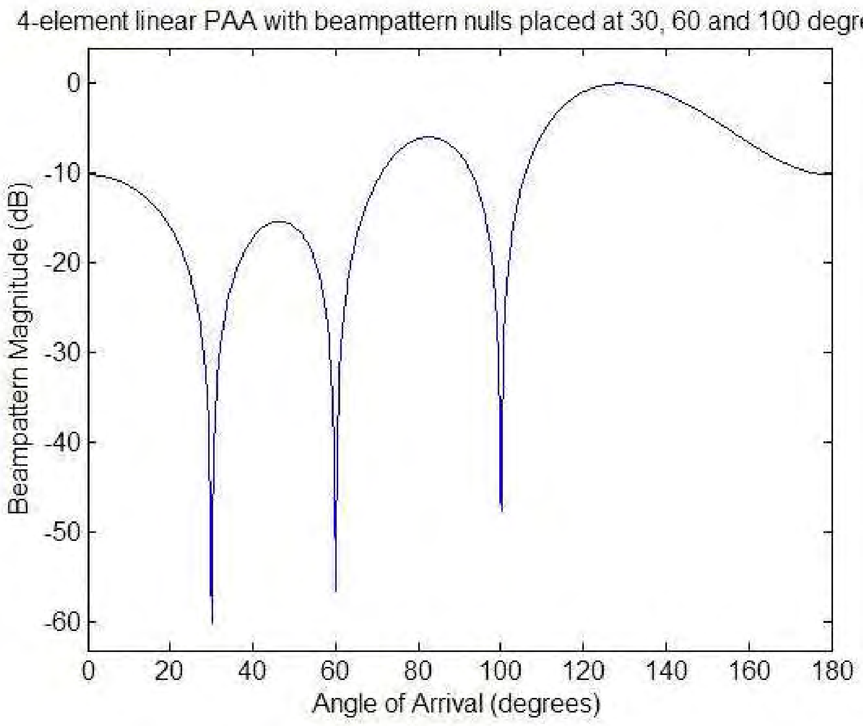

Figure 3.10 Rectangular Plot of Beam pattern Magnitude of a 4-element linear DBF with beam pattern nulls placed at 30º, 60º, and 100º

The MATLAB file “linear_DBFreceiver_parameters.m” was also used in the second filter example to transform the weight coefficient values obtained and set the DBF receiver parameters. The resulting weight coefficients, which are used in the simulation of the DBF receiver, are shown in Table 3.7. The simulation parameters used for this spatial filter example are the same parameters used for the first spatial filter example. Figure 3.11 and Figure 3.12 shows the time plots for plane wave signals with the angle of arrival changing from 90º to 0º and 90º to 180º, respectively, with respect to right-side endfire using the weight coefficients derived in the second spatial filter example.

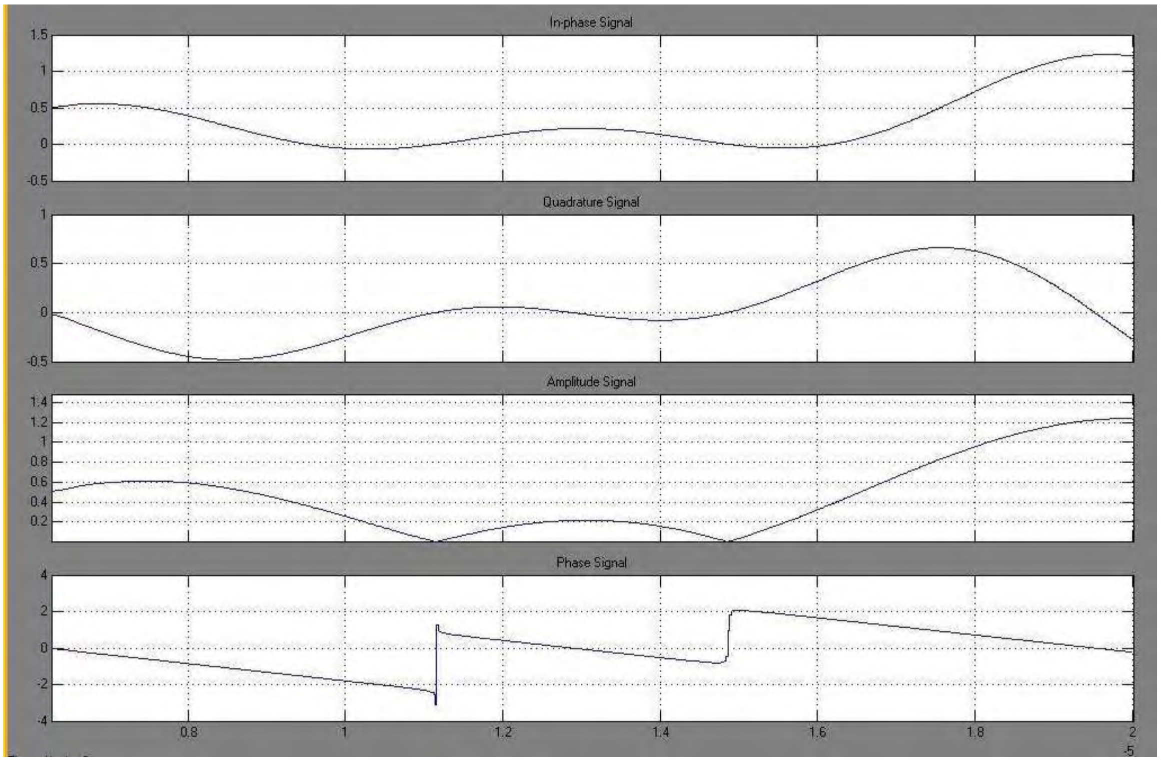

Figure 3.11 Time plots for plane wave signals with the angle of arrival changing from 90º to 0º for second spatial filter on 4-element linear DBF

TABLE 3.7 Second Spatial Filter Weight Coefficients – FPGA Weights

Element	Weight

1	$w_1 = 0.878723 \angle -16.875^{\circ}$
2	$w_2 = 0.783447 \angle -104.0625^{\circ}$
3	$w_3 = 0.783447 \angle 104.0625^{\circ}$
4	$w_1 = 0.878723 \angle -17.3140^{\circ}$

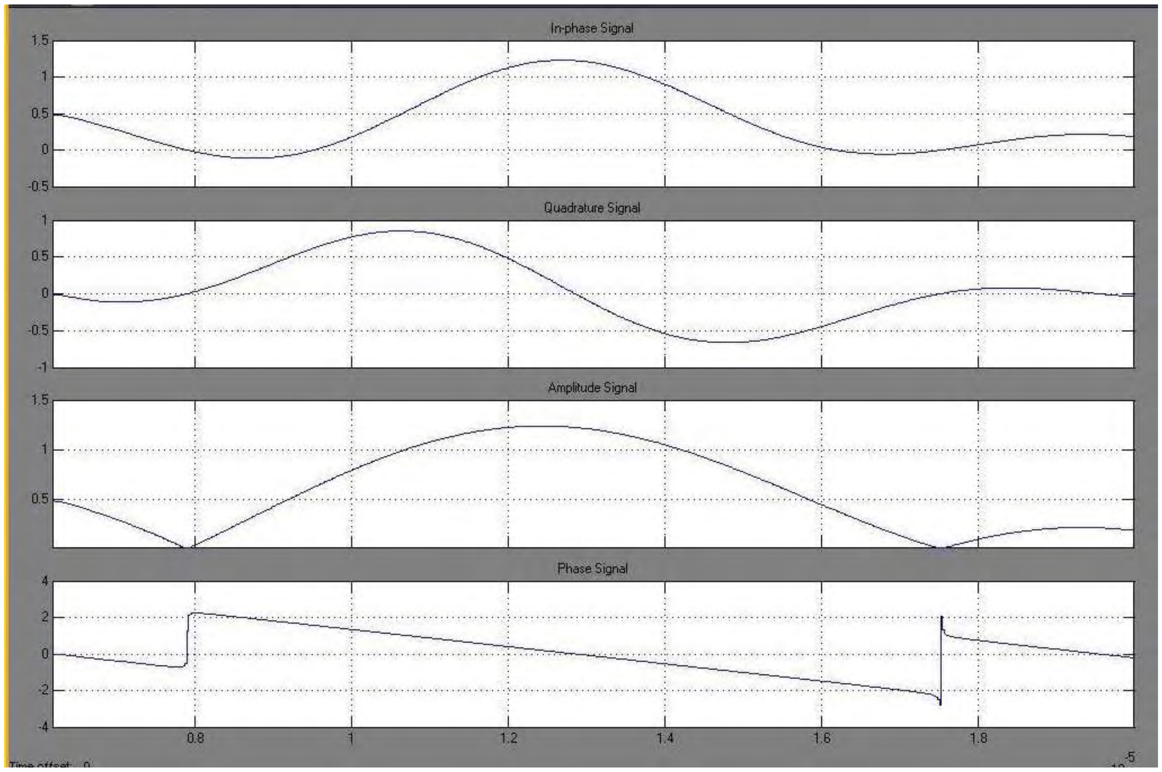

Figure 3.12 Time plots for plane wave signals with the angle of arrival changing from 90º to 180º for second spatial filter on 4-element linear DBF

The MATLAB program "linear_DBFreceiver_results.m" was also used to retrieve and analyze the data results for the second spatial filter example. Figure 3.13 shows a polar graph of the simulation beam pattern's amplitude with the second spatial filter's weight coefficients and Figure 3.14 shows a rectangular plot of the simulation beam pattern's amplitude in dB units. These plots show the beam pattern nulls placed at angles-of-arrival 29.77º, 60.26º, and 99.91º from right-side endfire with a null depth of -55.56 dB, -56.43 dB, and -55.3 dB respectively. Table 3.8 shows the beam pattern characteristics of the theoretical results and the simulation results for the second spatial filter example.

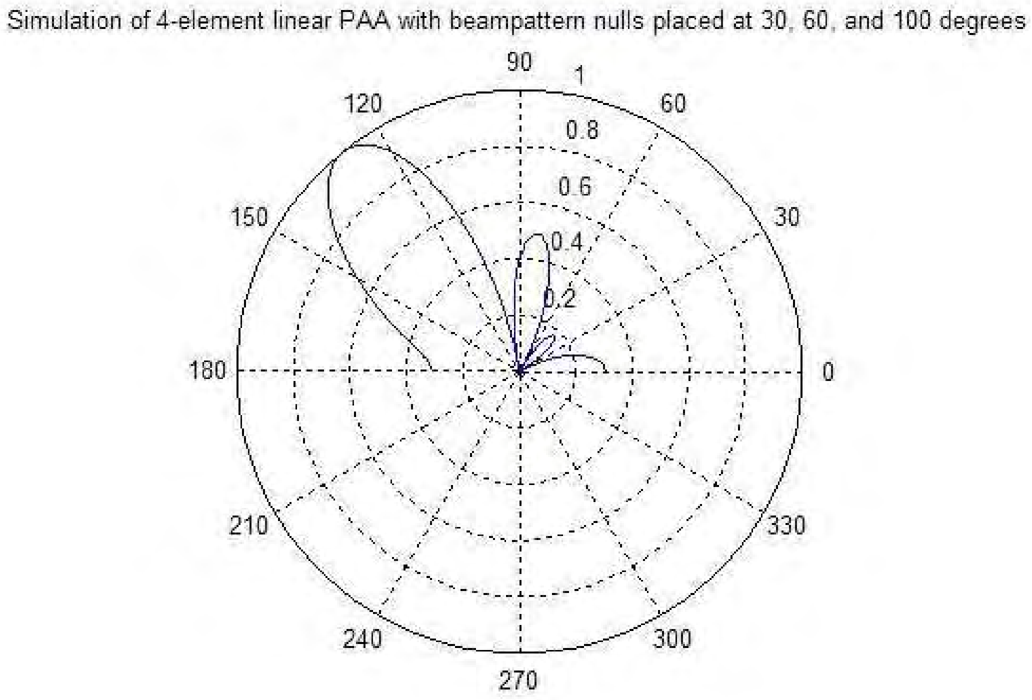

Figure 3.13 Polar Plot of Beam pattern Magnitude of a simulated 4-element linear DBF with beam pattern nulls placed at 30º, 60º, and 100º

TABLE 3.8 Second Spatial Filter Beam pattern Characteristics for a 4-element linear PAA

Beam pattern Characteristic	Theoretical Result	Simulation Result
Null #1: Angle of Arrival = 30º	Θ_{N1} = 30.06º	Θ_{N1} = 29.77º
Null-depth of Null #1	$\lvert B(\Theta_{N1})\rvert_{dB}$ = -60.22 dB	$\lvert B(\Theta_{N1})\rvert_{dB}$ = -55.56 dB

Null #2: Angle of Arrival = 60º	Θ_{N2} = 59.94º	Θ_{N2} = 60.26º
Null-depth of Null #2	$\vert B(\Theta_{N1})\vert_{dB}$ = -56.64 dB	$\vert B(\Theta_{N1})\vert_{dB}$ = -56.43 dB
Null #3: Angle of Arrival = 100º	Θ_{N3} = 100.08º	Θ_{N3} = 99.91º
Null-depth of Null #3	$\vert B(\Theta_{N1})\vert_{dB}$ = -47.73 dB	$\vert B(\Theta_{N1})\vert_{dB}$ = -55.3 dB
MRA angle-of-arrival	Θ_{MRA} = 128.7º	Θ_{MRA} = 128.6º
Half-power Beamwidth	Θ_{BW} = 33.82º	Θ_{BW} = 33.86º
Directivity	D_{dB} = 5.73 dB	D_{dB} = 5.74 dB
Sidelobe level	SLL_{dB} = -5.95 dB	SLL_{dB} = -6.12 dB

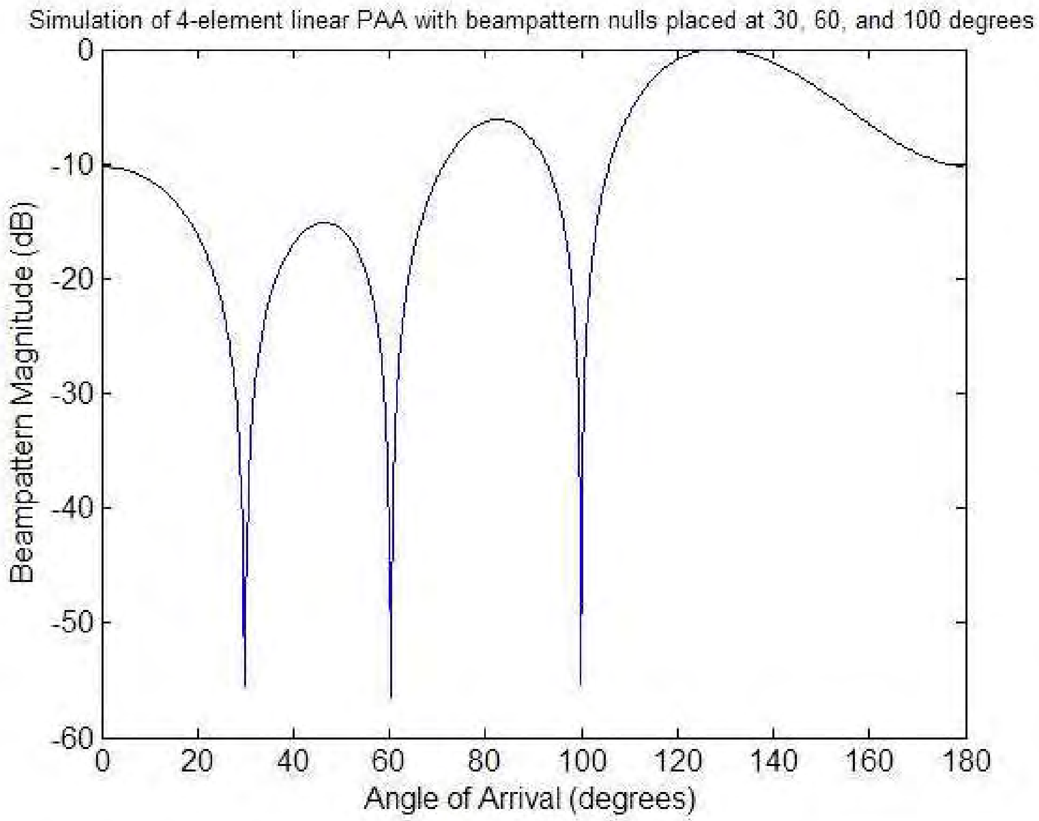

Figure 3.14 Rectangular Plot of Beam pattern Magnitude of a simulated 4-element linear DBF with beam pattern nulls placed at 30º, 60º, and 100º

3.1.3 Beam pattern Granularity for 4-element linear PAA

Granularity is defined as “the finest realizable increment between adjacent beam positions. [*Hatcher*, 1968]” The beam pattern granularity is controlled by the bit resolution of the weight coefficient’s phase parameter since the MRA’s angle-of-arrival of a beam pattern is controlled by the relative phase found between the signals of the elements in the PAA. For a linear array, the beam pattern granularity can be described by the following mathematical equation:

$$BG\left(\theta_{MRA1},\theta_{MRA2}\right)=\theta\,|_{\max\left(\left|B(\theta_{MRA2})\right|\right)}-\theta\,|_{\max\left(\left|B(\theta_{MRA1})\right|\right)} \qquad \textbf{3.4}$$

Ideally, $\theta\,|_{\max\left(\left|B(\theta_{MRA2})\right|\right)}$ would be equal to θ_{MRA2} and $\theta\,|_{\max\left(\left|B(\theta_{MRA1})\right|\right)}$ would be equal to θ_{MRA1} making $BG(\theta_{MRA1},\theta_{MRA2}) = \theta_{MRA2} - \theta_{MRA1}$. For DBF receivers with low bit resolution on the weight coefficient’s phase parameter, one may find that the MRA’s angle-of-arrival is not exactly θ_{MRA}, but an angular value close to θ_{MRA}. The relationship between the MRA’s angle-of-arrival and the weight coefficient’s phase parameter includes sine and cosine functions (not linear), making the beam pattern granularity dependent on the MRAs’ angular values, not just its angular difference. Figure 3.15 shows a plot of the beam pattern granularity as a function of the MRA’s angle-of-arrival when the weight coefficient’s phase parameter has a bit resolution of 8 bits with no decimal precision for the 4-element linear PAA. The beam pattern granularity plot has been constructed using a constant MRA angle difference (θ_{MRA2} - θ_{MRA1}) of one degree along each angle-of-arrival value. It can be seen how the granularity value is larger on beam patterns with MRAs pointing towards endfire of the array (leftside and rightside) with a value of approximately 5 degrees from beam patterns with MRAs pointing near broadside where the beam pattern granularity has a value close to one degree, which is the desired MRA angle difference. Figure 3.16 and Figure 3.17 shows beam pattern granularity for weight coefficient's phase parameters with bit resolutions of 4 bits with no decimal precision and 16 bits with no decimal precision, respectively. In these figures, it can be seen how low bit resolution results into poor beam pattern granularity restricting the MRA's permissible angular value whereas high bit resolution results into good beam pattern graunularity where the resulting MRA's angle difference is very close the proposed angular difference.

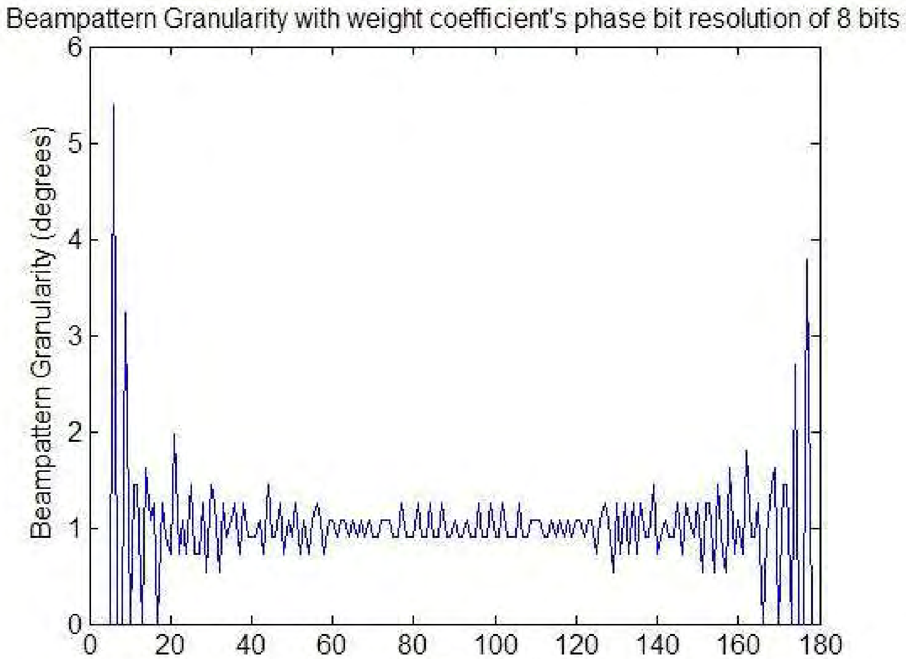

Figure 3.15 Beam pattern Granularity Plot for a 4-element linear DBF with 8 bits of resolution on the weight coefficient's phase

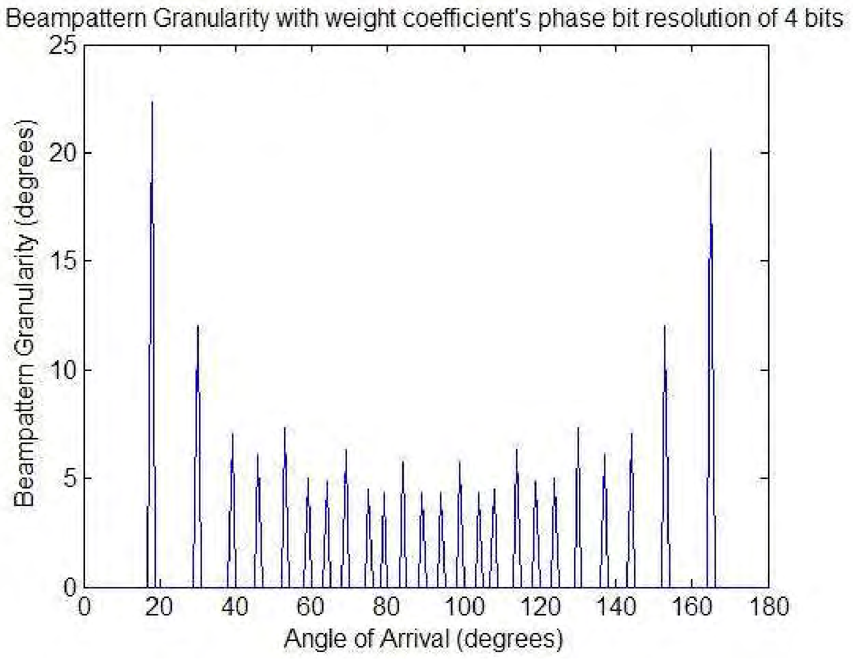

Figure 3.16 Beam pattern Granularity Plot for a 4-element linear DBF with 4 bits of resolution on the weight coefficient's phase

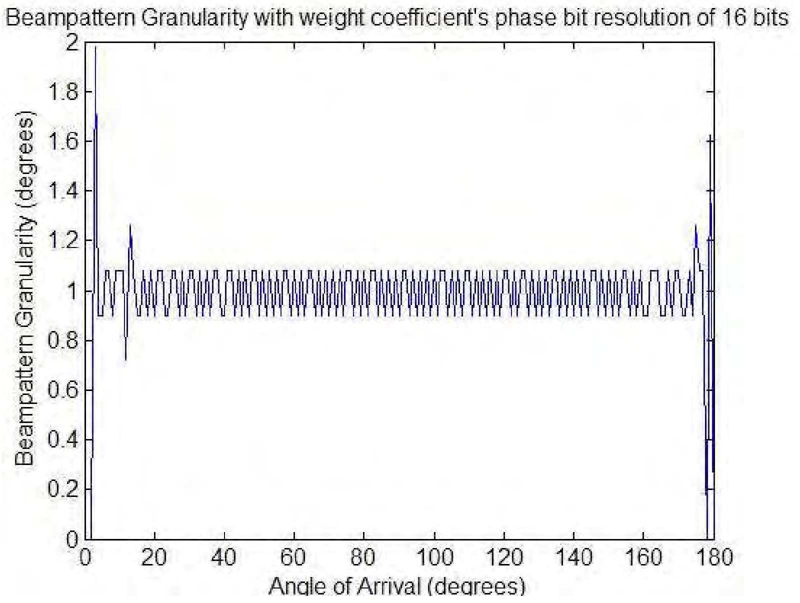

Figure 3.17 Beam pattern Granularity Plot for a 4-element linear DBF with 16 bits of resolution on the weight coefficient's phase

3.2 16-element linear PAA Transmitter Prototype

The 16-element linear PAA Transmitter Prototype consists of 16 isotropic radiating antennas arranged in a linear distribution and uniformly spaced by half-wavelength. Some PAA parameters, such as signal bandwidth, RF carrier frequency, IF frequency and inter-element spacing, are the same parameters used in the 4-element linear PAA receiver prototype. Since this PAA has a different number of elements, the Narrowband Factor needs to be recalculated to assure proper array performance based on narrowband beamformer model implementation. Table 3.9 shows the PAA parameters for this 16-element linear array. In this case, the Narrowband Factor ($B_S \cdot \Delta T_{max}$) is extremely small compared to one thus, the narrowband beamformer can be used to control the beam pattern of this 16-element PAA.

TABLE 3.9 16-element linear PAA parameters

Parameter	**Value**
RF Carrier Frequency	f_{RF} = 5.85 GHz
IF Frequency	f_{IF} = 3 MHz
Signal Bandwidth	B_S = 2 MHz
Number of Elements	N = 16
Inter-element Spacing	$\Delta z = \lambda_c/2$
Maximum Travel Time	$\Delta T_{max} = 15/2f_{RF}$
Narrowband Factor	$B_S \cdot \Delta T_{max}$ = 0.0026

The implementation of this DBF transmitter is based on the design described in Section 2.4.2. Figure 3.18 shows a diagram of the DBF transmitter implementation for a 16-element linear PAA using MATLAB's Simulink and Xilinx's System Generator Blockset. Each of the sixteen white blocks in the middle of the figure arranged in 4 x 4 matrix represent a DBF transmitter channel. The blue blocks at the left side of each DBF transmitter channel are the amplitude and phase of the weight coefficient of that particular channel. A single DDS Block has been used as the local digital oscillator for the 16 DBF channels. The DDS outputs a sinusoidal signal and its 90º phase-shifted version at a frequency of 3 MHz, where each sample has a sample frequency of 100 MHz. The yellow blocks at the right side of the each DBF transmitter channel represent the DACs of the DBF, which transform the digital signal into the analog domain at a sample

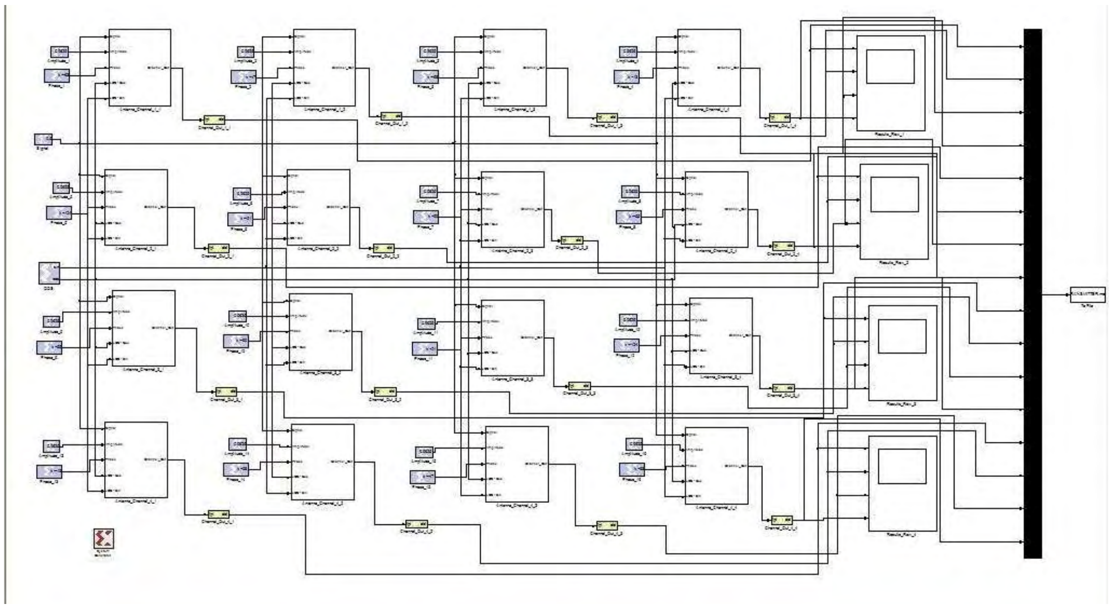

Figure 3.18 Diagram of the simulated 16-element linear DBF transmitter

rate of 100 MHz per channel at a resolution of 14 bits with 12 bits of decimal precision. At the left side of the figure, the white figures and black figures are Simulink blocks used to display and store as a .mat file the 16 generated IF signals.

Figure 3.19 shows diagrams of the DUC and the CWM phase components, which are inside of each DBF transmitter channel. The CWM (Figure 3.19a) operates at a sampling frequency of 10 MHz, which is the sampling frequency at the input of the CIC interpolation filter. The resolution of the weight coefficient's amplitude is 16 bits with 14 bits of decimal precision and the weight coefficient's phase is 8 bits with no decimal precision. The output of the sine/cosine table in the CWM gives a bit resolution of 8 bits with 7 bits of decimal precision. The mathematical operations in the DBF transmitter channel (addition and multiplication) have the same bit resolution used in the 4-element linear PAA receiver. The DUC (right side of Figure 3.19b) operates at the sampling frequency of the DAC, which is 100 MHz. Each DUC contains two CIC filters (one for each quadrature channel) with 2 stages (N = 2), a differential delay of 1 samples (M = 1), a rate change factor of 10 (R = 10) and a latency of 2 clock cycles. The two other blue blocks at the right of the CIC filter ("force" block and "cast" block) quantizes the output of the filter to samples with a bit resolution of 18 bits with 16 bits of decimal precision. The two scale blocks located at the output of the register, which are part of the CIC filter implementation, are used to condition the output of the CIC filter and prevent overflow in the multiplication stages. As for the output of DBF transmitter, each output channel has a bit resolution of a resolution of 14 bits at a sampling frequency of 100 MHz. Table 3.10 summarizes the parameters of the DBF receiver's components.

a)

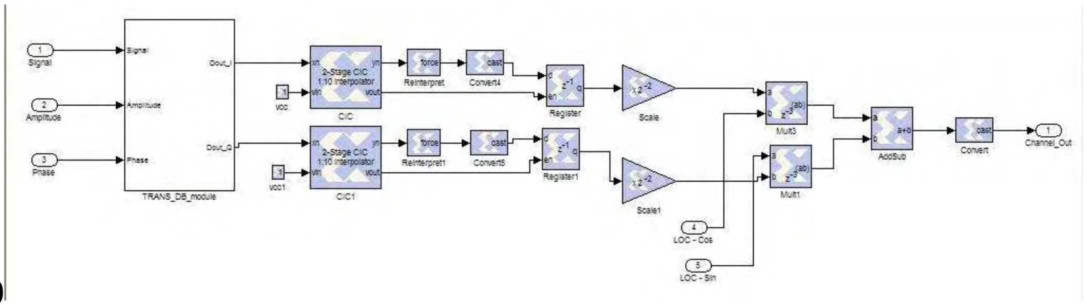

b)

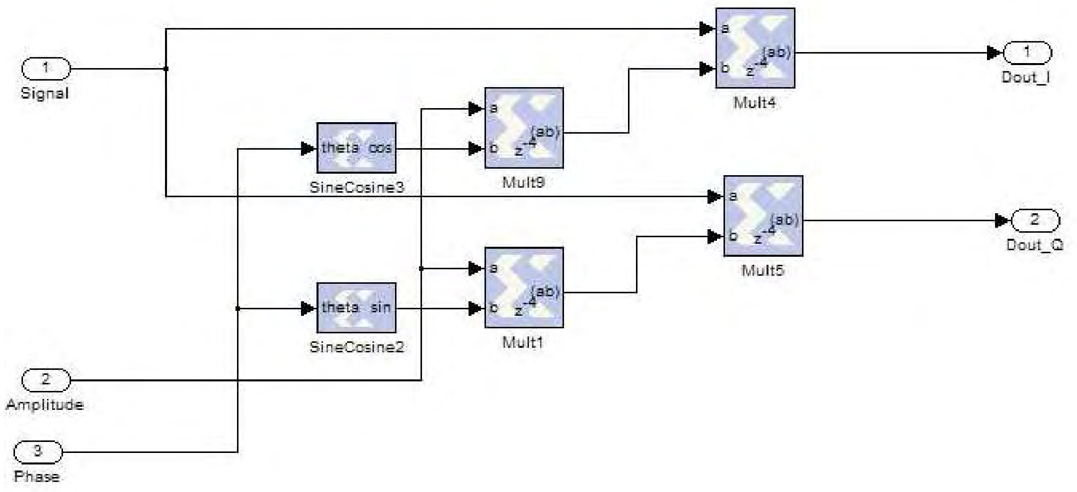

Figure 3.19 Diagram of the DUC (3.19a) and CWM (3.19b) of the simulated DBF transmitter

TABLE 3.10 Parameters of the DBF transmitter's components

Parameter	Value
Multiplier's bit resolution	18 bits -16 bit decimal precision
Adder's bit resolution	14 bits – 12 bit decimal precision

DDS Operating Frequency	f_{DDS} = 3 MHz
DAC Sample Frequency	f_{DAC} = 100 MHz
DAC bit resolution	14 bits – 12 bit decimal precision
DUC Sample Frequency	f_{DUC} = 100 MHz
CIC Filter Stages	N_{CIC} = 2
CIC Differential Filter	M = 1
CIC Rate Change Factor	R = 10
CIC bit resolution	18 bits – 16 bit decimal precision
CWM Sample Frequency	f_{CWM} = 10 MHz
Weight Coefficient – Amplitude bit resolution	16 bits – 14 bit decimal precision
Weight Coefficient – Phase bit resolution	8 bits with no decimal precision
Sine/Cosine Look-Up Table input bit resolution	8 bits – 7 bit decimal precision
DBF Output Signal bit resolution	14 bits – 12 bit decimal precision

The DBF transmitter simulations consist in generating a single data signal in the FPGA code for all the 16 DBF transmitter channels. At the output of the DBF transmitter simulation, 16 IF signals are generated, each with a relative phase shit associated with the channel's weight coefficients. Four signal scopes are placed at the right side of each row channel to display the output of each DBF channel and make a visual comparison of the amplitude and relative phase difference between each signal. As for a post-processing phase for the PAA transmitter, the 16 IF signals are stored on a .mat file as a matrix variable where, later, they will be analyzed to observe the beam pattern formed based on the spatial combination of all the output signals.

3.2.1 *First Spatial Filter Example: Beam pattern with Taylor Amplitude Weight Function pointing to θ_{MRA} = 60º*

The first spatial filter example used in the DBF transmitter for a 16-element linear PAA produces a beam pattern with an MRA pointing at an angular position of 60º (respect to right-side endfire) with a Taylor distribution amplitude-weighting function. As mentioned in Section 2.1.4, the Taylor distribution method generates the amplitude of weight coefficients to minimize the MRA's beamwidth based on sidelobe level specifications. This beam pattern synthesis technique gives constant inner sidelobe levels by moving the inner zeros of the beam pattern into new locations in the unit circle and decaying outer sidelobes by leaving the outer zeros in the same location as the uniform weight distribution [*Van Trees*, 2002]. The method requires two design parameters: maximum sidelobe height and number of inner zeros in the beam pattern. The position of the nulls in ψ-space for Taylor weight distribution can be described in the following mathematical form:

$$\psi_n = \frac{2\pi}{N}\left\{ \bar{n}\left[\frac{A^2 + \left(n - \frac{1}{2}\right)^2}{A^2 + \left(\bar{n} - \frac{1}{2}\right)^2} \right]^{\frac{1}{2}} \right\} \qquad \textbf{3.5}$$

where $\bar{n}$ is the number of inner zeros in the beam pattern and A is related to the maximum sidelobe height R by the following equation:

$$\cosh\left(\pi A\right) = R \qquad \textbf{3.6}$$

A MATLAB file named “linear_DBFtransmitter_taylor.m” (shown in the Appendix A) was created to compute the weight coefficients for the first spatial filter example of the linear 16-element PAA. The code uses the Schelkunoff polynomial null-placement method, where the null positions are given by Eq. 3.5, to calculate amplitude of the weight and Eq. 3.1 to calculate the phase of the weight coefficient. The Taylor distribution specification for this filter is a maximum sidelobe level of -30 dB with a number of inner zeros equal to 6. Table 3.11 shows the resulting weight coefficients for the specified beam pattern parameters. Figure 3.20 shows a polar graph of the theoretical beam pattern’s amplitude with the weight coefficients shown in Table 3.11. Figure 3.21 shows a rectangular plot of the beam pattern’s amplitude in dB units. These plots show the maximum value of the beam pattern’s amplitude at a signal’s angle-of-transmission of 59.94º with a directivity of 11.34 dB. The beamwidth of the MRA beam for the theoretical beam pattern is 9.34º with a maximum sidelobe level of -30.11 dB.

TABLE 3.11 First Spatial Filter Weight Coefficients – Theoretical Weights

Element	**Weight**
1	$w_1 = 0.0076 \angle 45^\circ$
2	$w_2 = 0.0102 \angle 135^\circ$
3	$w_3 = 0.0134 \angle -135^\circ$
4	$w_4 = 0.0185 \angle -45^\circ$
5	$w_5 = 0.0226 \angle 45^\circ$
6	$w_6 = 0.0266 \angle 135^\circ$

7	w_7 = 0.0293 ∟-135º
8	w_8 = 0.0309 ∟-45º
9	w_9 = 0.0309 ∟45º
10	w_{10} = 0.0293 ∟135º
11	w_{11} = 0.0266 ∟-135º
12	w_{12} = 0.0226 ∟-45º
13	w_{13} = 0.0185 ∟45º
14	w_{14} = 0.0134 ∟135º
15	w_{15} = 0.0102 ∟-135º
16	w_{16} = 0.0076 ∟-45º

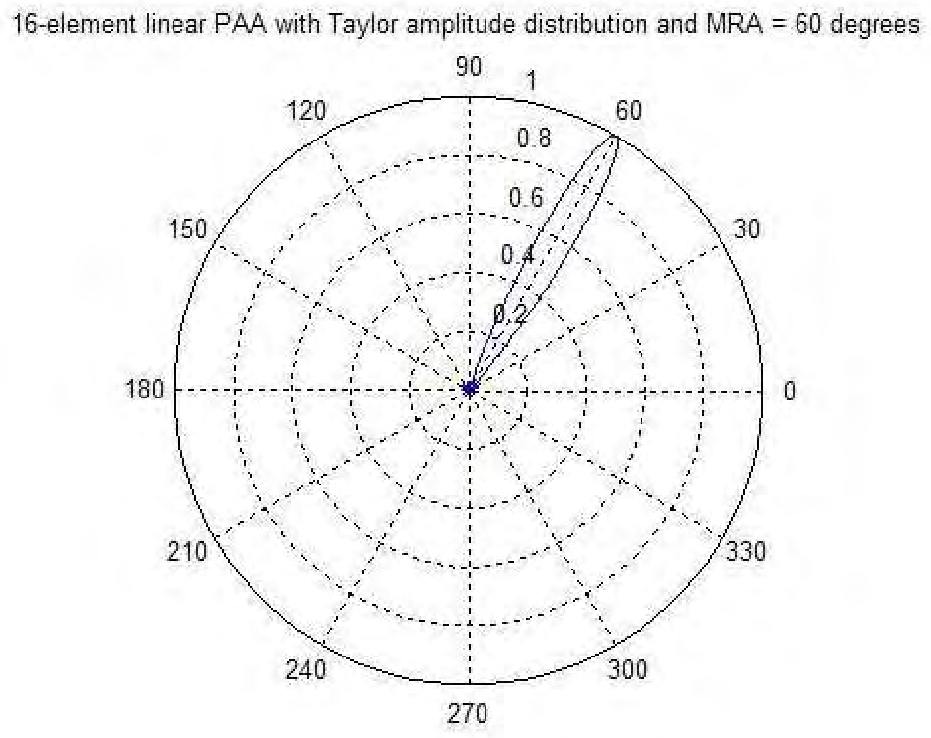

Figure 3.20 Polar Plot of Beam pattern Magnitude of a 4-element linear DBF with Taylor Amplitude Distribution pointing at θ_{MRA} = 60º.

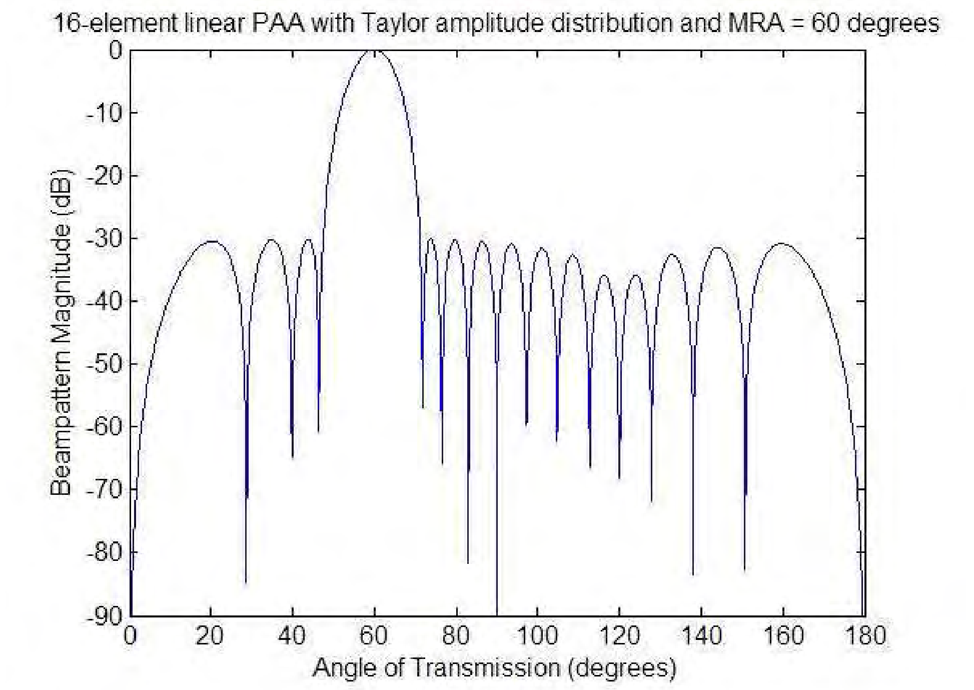

Figure 3.21 Rectangular Plot of Beam pattern Magnitude of a 4-element linear DBF with Taylor Amplitude Distribution pointing at θ_{MRA} = 60º

The next step before proceeding with the simulations of the DBF transmitter consist in the transformation of the weight coefficients into constant encoded in the FPGA code simulator. A MATLAB program named "linear_DBFtrasnmitter_parameters.m" (included in the Appendix A) was prepared to change the weight coefficients into its fixed-point format values and set all the necessary DBF transmitter parameters (shown in Table 3.10) needed to perform the DBF transmitter simulation. The total simulation time used for this DBF transmitter was 2 x 10^{-5} seconds. The weight coefficients obtained after quantization of the weight values into the fixed-point representation used in the DBF receiver simulation are shown in

Table 3.12. Figure 3.22 shows 4 time plots of the first 4 elements in the 16-element DBF transmitter (elements 1 through 4). This figure shows the amplitude and phase difference found in the output IF signals, which is necessary in order to acquire proper spatial combination of the signals and achieve a desirable beam pattern.

TABLE 3.12 First Spatial Filter Weight Coefficients – FPGA Weights

Element	**Weight**
1	w_1 = 0.00757 ∟45º
2	w_2 = 0.01025 ∟135º
3	w_3 = 0.01337 ∟-135º
4	w_4 = 0.01849 ∟-45º
5	w_5 = 0.02258 ∟45º
6	w_6 = 0.02661 ∟135º
7	w_7 = 0.02936 ∟-135º
8	w_8 = 0.03088 ∟-45º
9	w_9 = 0.03088 ∟45º
10	w_{10} = 0.02936 ∟135º
11	w_{11} = 0.02661 ∟-135º
12	w_{12} = 0.02258 ∟-45º
13	w_{13} = 0.01849 ∟45º
14	W_{14} = 0.01337 ∟135º
15	w_{15} = 0.01025 ∟-135º
16	W_{16} = 0.00757 ∟-45º

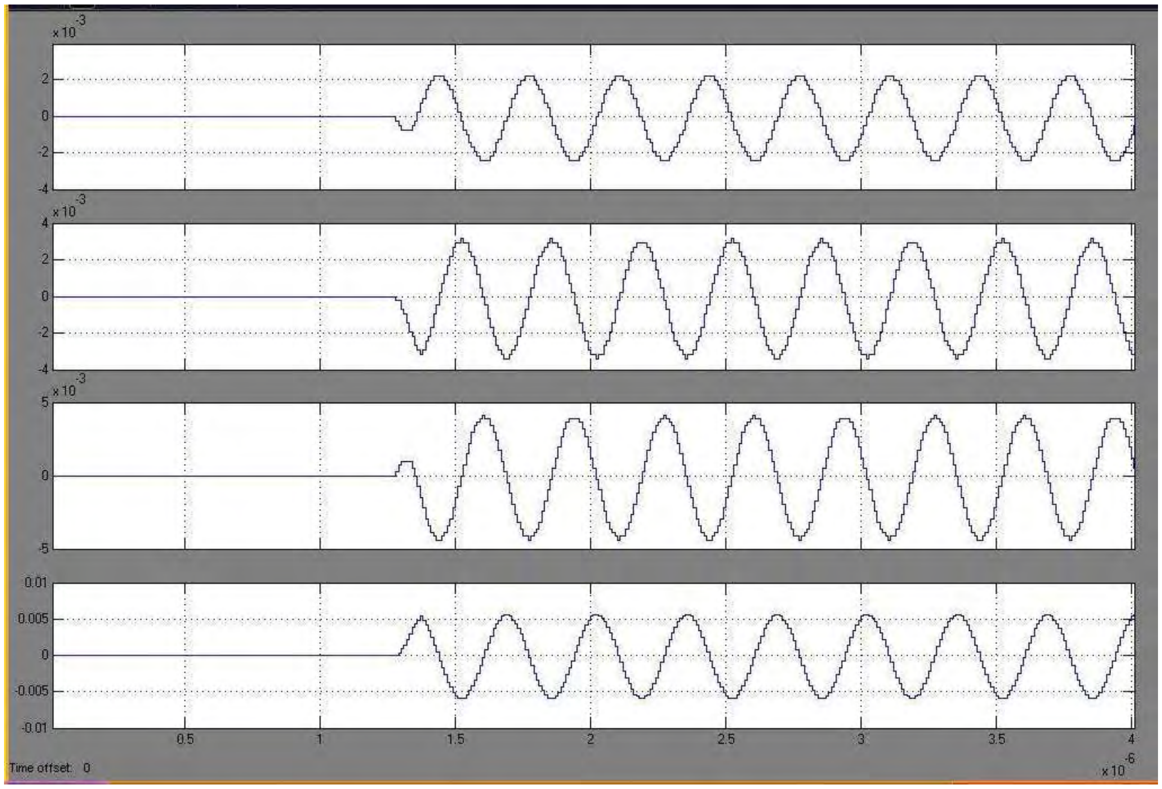

Figure 3.22 Signal Plots of 4 of the 16-elements in the linear DBF transmitter for first spatial filter simulation

To analyze the data results obtained in the DBF transmitter simulation, each output signal generated was stored in a .mat files. A MATLAB program named "linear_DBFtransmitter_results.m" was created to retrieve the simulation results stored in the .mat files and calculate the beam pattern from the spatial combination of the IF output signals. The code calculates the Discrete Fourier Transform (DFT) of each of the 16 output signals, retrieves the amplitude and phase difference value for the IF carrier frequency (in these case f_{IF} = 3MHz), and computes the beam pattern based on the weight coefficients derived from the each signal's amplitude and phase difference. Figure 3.23 shows a polar graph of the simulation beam pattern's amplitude with the weight coefficients derived from DFT analysis and Figure 3.24 shows a rectangular plot of the simulation beam pattern's amplitude in dB units. These plots show the maximum value of the beam pattern's amplitude at a signal's angle-of-transmission of 59.94º with a directivity of 11.34 dB. The beamwidth of the MRA beam for the theoretical beam pattern is 9.34º with a maximum sidelobe level of -30.08 dB. Table 3.13 shows the results obtained from the DBF transmitter simulation with the results obtained in the theoretical beam pattern calculation. The results of each DBF (theoretical and simulated DBF) are similar in terms of beam pattern characteristics which makes the simulated DBF a good implementation of its theoretical counterpart.

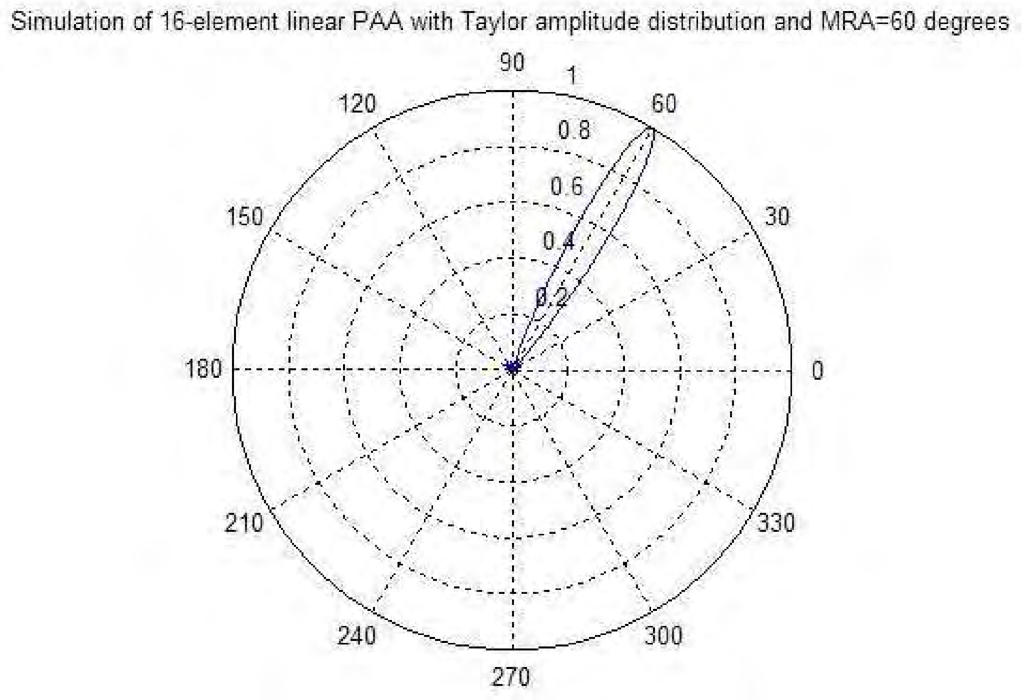

Figure 3.23 Polar Plot of Beam pattern Magnitude of a simulated 4-element linear DBF with Taylor Amplitude Distribution pointing at θ_{MRA} = 60º

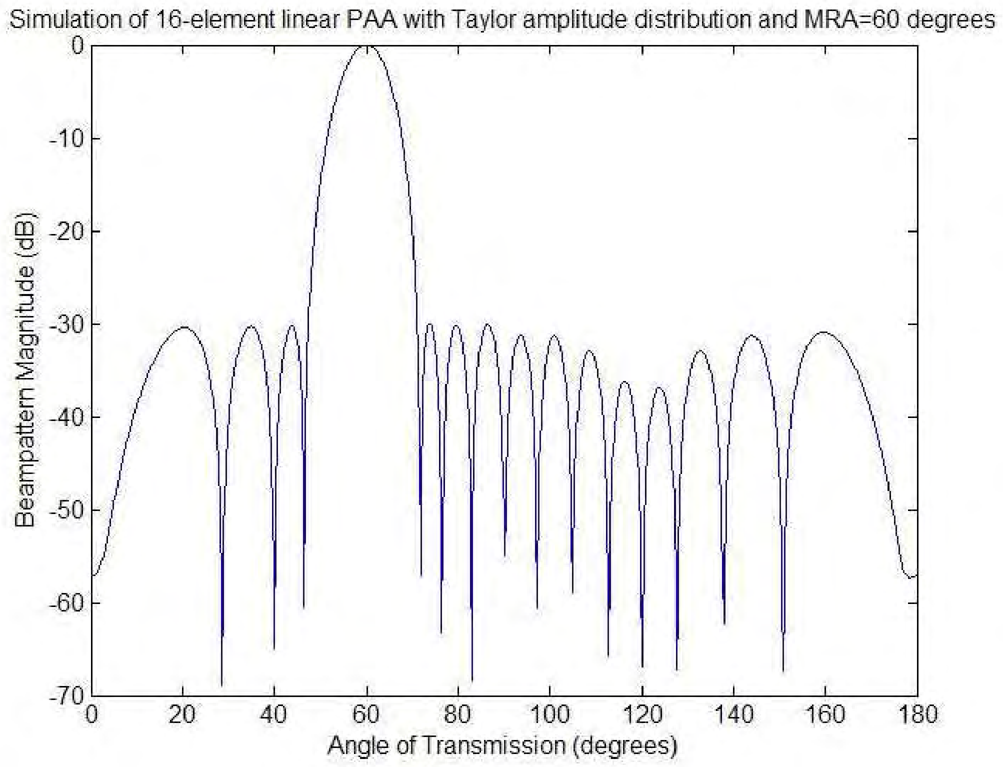

Figure 3.24 Rectangular Plot of Beam pattern Magnitude of a simulated 4-element linear DBF with Taylor Amplitude Distribution pointing at θ_{MRA} = 60º

TABLE 3.13 First Spatial Filter Beam pattern Characteristics for a 16-element linear PAA

Beam pattern Characteristic	**Theoretical Result**	**Simulation Result**
MRA angle-of-arrival	Θ_{MRA} = 59.94º	Θ_{MRA} = 59.94º
Half-power Beamwidth	Θ_{BW} = 9.34º	Θ_{BW} = 9.34º
Directivity	D_{dB} = 11.34 dB	D_{dB} = 11.34 dB
Sidelobe level	SLL_{dB} = -30.11 dB	SLL_{dB} = -30.08 dB

3.2.2 *Second Spatial Filter Example: Beam pattern with Blackman-Harris Amplitude Weight Function pointing to θ_{MRA} = 82º*

The second spatial filter example used in the DBF transmitter for a 16-element linear PAA produces a beam pattern with an MRA pointing at an angular position of 82º (respect to right-side endfire) with a Blackman-Harris window amplitude-weighting function. The Blackman-Harris window is one of the Spectral Windows used to control the beam pattern behavior of a PAA, as mentioned in Section 2.1.4. It contains all the characterisitics associated with a Spectral Window where the beam pattern characteristics such as beamwidth, sidelobe behavior and directivity are fixed by the number of elements in the PAA. The amplitude weight coefficients for each DBF element can be obtained using the mathematical equation [*Van Trees,* 2001] associated with this Spectral Window:

$$w(n) = 0.42 + 0.5\cos\left(\frac{2\pi n}{N}\right) + 0.08\cos\left(\frac{4\pi n}{N}\right), \quad -\frac{N-1}{2} \le n \le \frac{N-1}{2}. \qquad \textbf{3.7}$$

The beam pattern characteristics of an *N*-element PAA with a Blackman-harris spectral window can be calculated using the following mathematical equations:

$$\Theta_{BW} = 1.65\frac{2}{N}, \qquad \textbf{3.8}$$

$$SLL_{dB} = -56.6\ dB, \qquad \textbf{3.9}$$

$$D_{dB} = 10 \cdot \log_{10}\left(N \cdot 0.577\right). \qquad \textbf{3.10}$$

A MATLAB file named “linear_DBFtransmitter_blackmannharris.m” (shown in the Appendix A) was created to compute the weight coefficients for the second spatial filter example of the linear 16-element PAA. The code uses the Blackman-Harris amplitude function (Eq. 3.7) to generate the amplitude of the weights and Eq. 3.1 to calculate the phase of the weight coefficients. Table 3.14 shows the resulting weight coefficients for the specified beam pattern parameters. Figure 3.25 shows a polar graph of the theoretical beam pattern's amplitude with the weight coefficients shown in Table 3.14. Figure 3.26 shows a rectangular plot of the beam pattern's amplitude in dB units. These plots show the maximum value of the beam pattern's amplitude at a signal's angle-of-transmission of 82.08º with a directivity of 9.67 dB. The beamwidth of the MRA beam for the theoretical beam pattern is 11.89º with a maximum sidelobe level of -57.79 dB.

TABLE 3.14 Second Spatial Filter Weight Coefficients – Theoretical Weights

Element	Weight
1	$w_1 = 0.0035 \angle 172.12^\circ$
2	$w_2 = 0.0349 \angle -162.83^\circ$
3	$w_3 = 0.1116 \angle -137.78^\circ$
4	$w_4 = 0.2485 \angle -112.73^\circ$
5	$w_5 = 0.4436 \angle -87.68^\circ$
6	$w_6 = 0.6672 \angle -62.63^\circ$
7	$w_7 = 0.8663 \angle -37.58^\circ$
8	$w_8 = 0.9843 \angle -12.53^\circ$
9	$w_9 = 0.9843 \angle 12.53^\circ$
10	$w_{10} = 0.8663 \angle 37.58^\circ$
11	$w_{11} = 0.6672 \angle 62.63^\circ$
12	$w_{12} = 0.4436 \angle 87.68^\circ$
13	$w_{13} = 0.2485 \angle 112.73^\circ$

14	w_{14} = 0.1116 ∟137.78º
15	w_{15} = 0.0349 ∟162.83º
16	w_{16} = 0.0035 ∟-172.12º

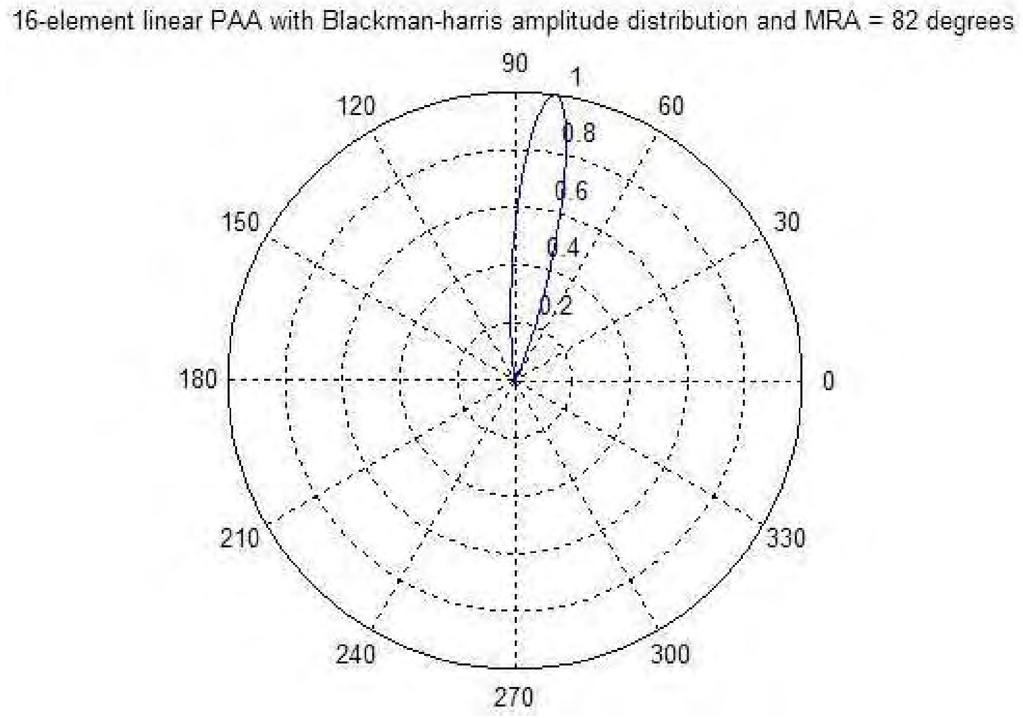

Figure 3.25 Polar Plot of Beam pattern Magnitude of a 4-element linear DBF with Blackmann-Harris Amplitude Distribution pointing at θ_{MRA} = 82º

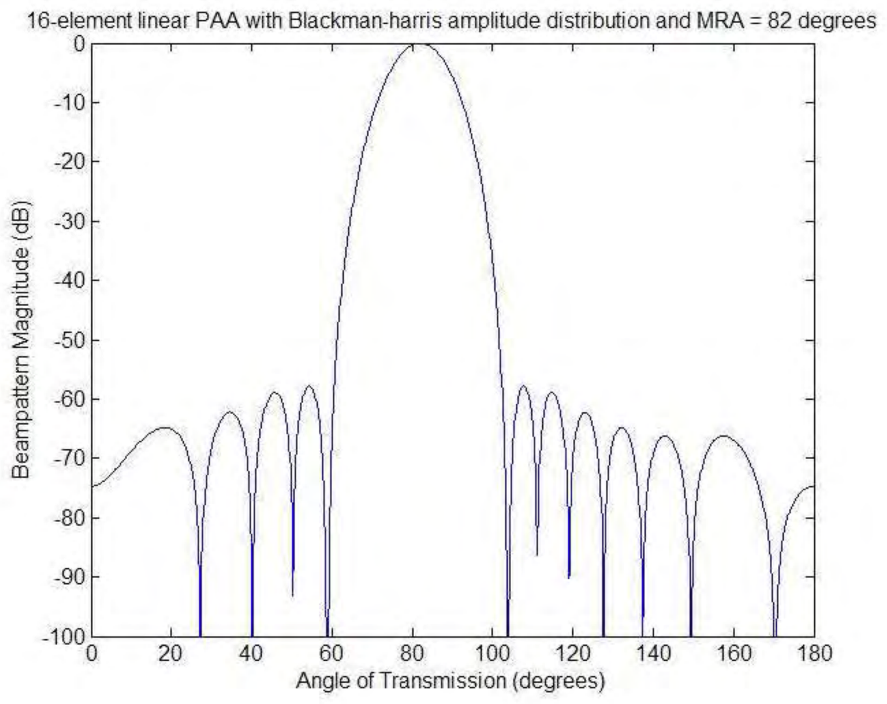

Figure 3.26 Rectangular Plot of Beam pattern Magnitude of a 4-element linear DBF with Blackmann-Harris Amplitude Distribution pointing at θ_{MRA} = 82º

The MATLAB file "linear_DBFtransmitter_parameters.m" was also used in the second filter example to transform the weight coefficient values obtained and set the DBF transmitter parameters. The resulting weight coefficients, which are used in the simulation of the DBF transmitter, are shown in Table 3.15. The simulation parameters used for this spatial filter example are the same parameters used for the first spatial filter example for the 16-element DBF. Figure 3.27 shows 4 time plots of the first 4 elements in the 16-element DBF transmitter (elements 1 through 4). Each signal shown in Figure 3.27 exhibits a distinct amplitude and phase difference where the contribution of each signal forms the specified beam pattern.

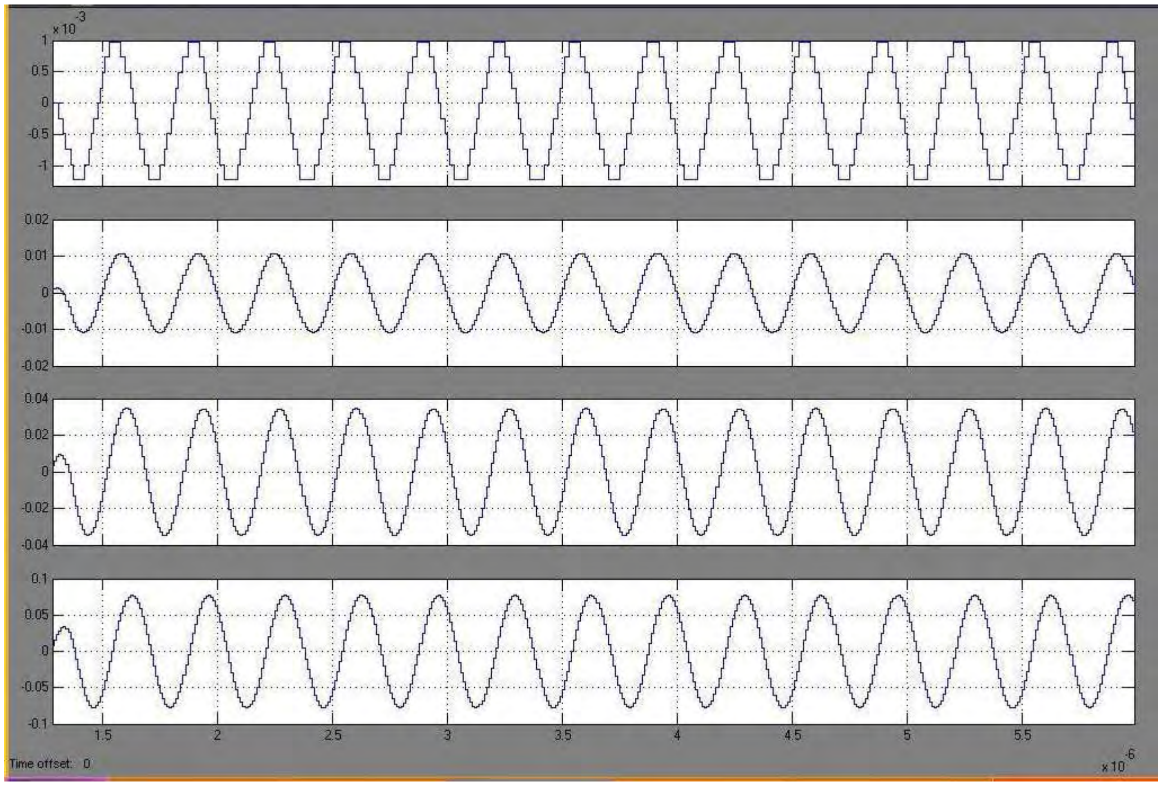

Figure 3.27 Signal Plots of 4 of the 16-elements in the linear DBF transmitter for second spatial filter simulation

TABLE 3.15 Second Spatial Filter Weight Coefficients – FPGA Weights

Element	Weight
1	w_1 = 0.0035 ∟171.56º
2	w_2 = 0.0349 ∟-163.13º
3	w_3 = 0.1116 ∟-137.81º
4	w_4 = 0.2485 ∟-112.50º
5	w_5 = 0.4437 ∟-87.19º
6	w_6 = 0.6672 ∟-63.28º
7	w_7 = 0.8663 ∟-37.97º
8	w_8 = 0.9843 ∟-12.66º

9	w_9 = 0.9843 ∟12.53º
10	w_{10} = 0.8663 ∟37.97º
11	w_{11} = 0.6672 ∟63.28º
12	w_{12} = 0.4436 ∟87.19º
13	w_{13} = 0.2485 ∟112.50º
14	w_{14} = 0.1116 ∟137.81º
15	w_{15} = 0.0349 ∟162.13º
16	w_{16} = 0.0035 ∟-171.56º

The analysis of the results obtained in the simulation of the second spatial filter for the 16-element linear DBF is performed using the MATLAB program "linear_DBFtransmitter_results.m" also. Figure 3.28 shows a polar graph of the simulation beam pattern's amplitude with the weight coefficients derived from DFT analysis and Figure 3.29 shows a rectangular plot of the simulation beam pattern's amplitude in dB units. The maximum value of the beam pattern's amplitude is found at a signal's angle-of-transmission of 82.08º with a directivity of 9.68 dB. Its beamwidth is 11.89º with a maximum sidelobe level of -44.60 dB. Table 3.16 shows the results obtained from the DBF transmitter simulation with the results obtained in the theoretical beam pattern calculation. The beam pattern characteristics of the simulated DBF are similar to the results obtained from the theoretical DBF with a notable difference in the sidelobe level of the beam pattern. This difference of more than 10 dB may be found do to the low sidelobe level specification, which has nearly the same beam pattern magnitude as a first order null for a typical DBF system.

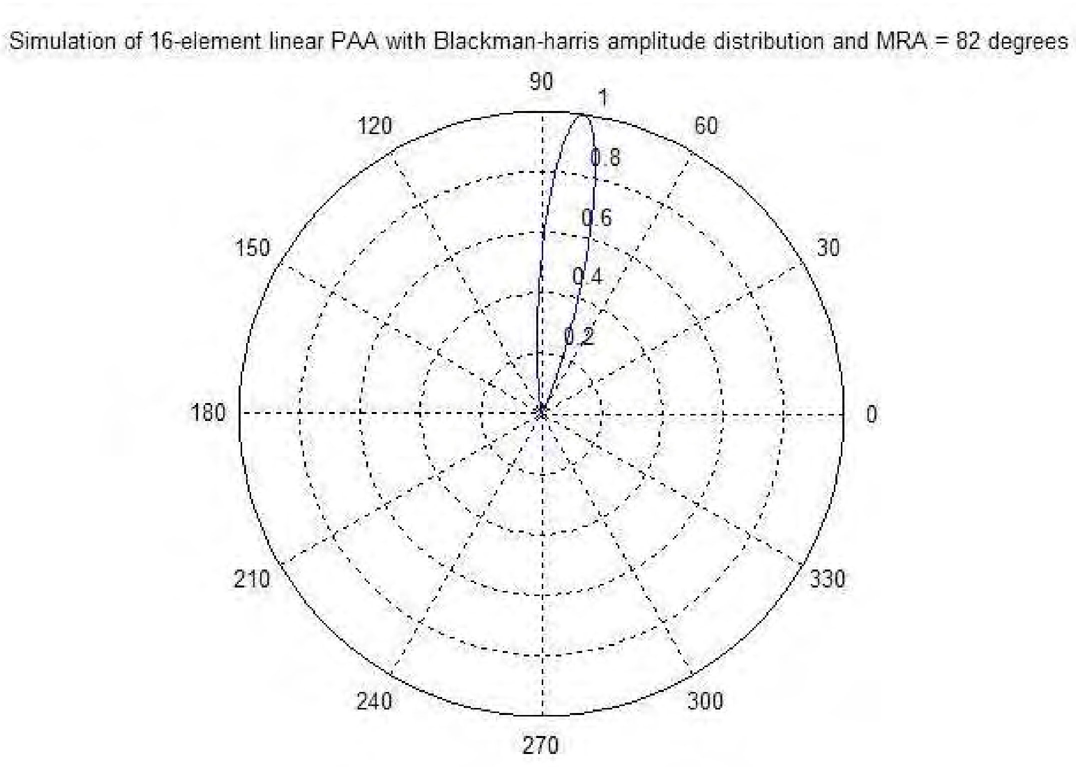

Figure 3.28 Polar Plot of Beam pattern Magnitude of simulated 4-element linear DBF with Blackmann-Harris Amplitude Distribution pointing at θ_{MRA} = 82º

TABLE 3.16 Second Spatial Filter Beam pattern Characteristics for a 16-element linear PAA

Beam pattern Characteristic	Theoretical Result	Simulation Result
MRA angle-of-arrival	Θ_{MRA} = 82.08º	Θ_{MRA} = 82.08º
Half-power Beamwidth	Θ_{BW} = 11.89º	Θ_{BW} = 11.89º
Directivity	D_{dB} = 9.67 dB	D_{dB} = 9.68 dB
Sidelobe level	SLL_{dB} = -57.79 dB	SLL_{dB} = -44.60 dB

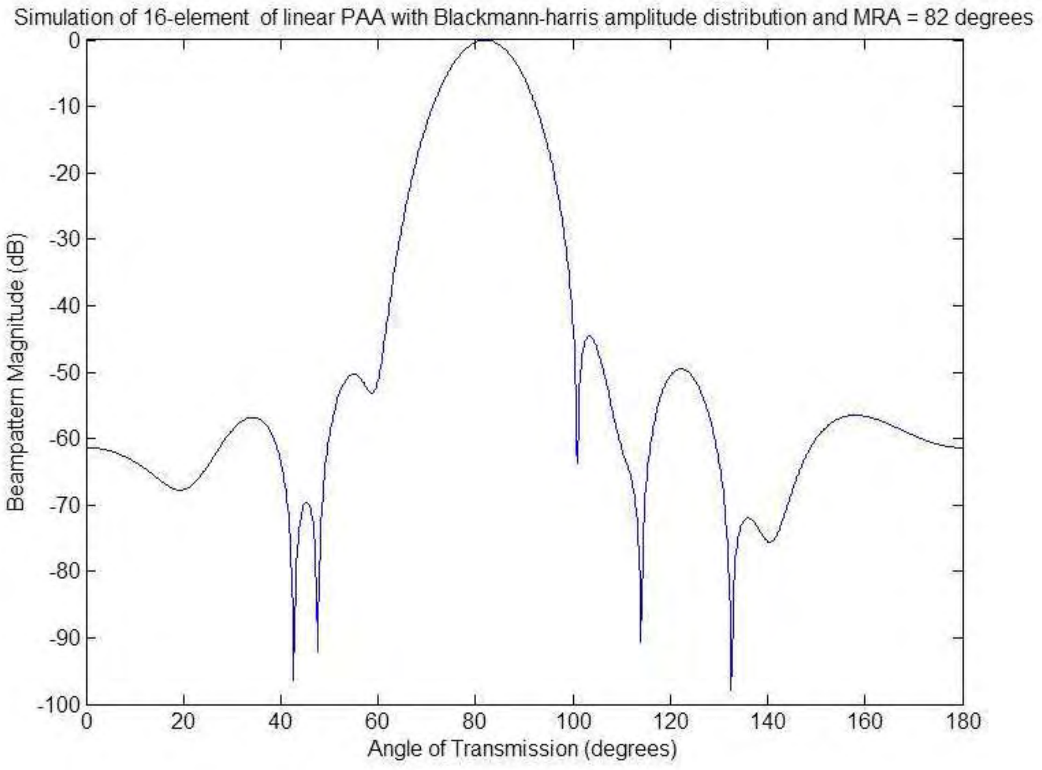

Figure 3.29 Rectangular Plot of Beam pattern Magnitude of simulated 4-element linear DBF with Blackmann-Harris Amplitude Distribution pointing at θ_{MRA} = 82°

3.2.3 Beam pattern Granularity for 16-element linear PAA

The beam pattern granularity, which was introduced as an important parameter in Section 3.1.3, is also affected by the number of elements in the PAA. Figure 3.30 shows a plot of the beam pattern granularity as a function of the MRA's angle-of-arrival when the weight coefficient's phase parameter has a bit resolution of 8 bits with no decimal precision for the 16-element linear PAA. Eq. 3.4 was also used to calculate the beam pattern granularity of this linear array. As in the case of the 4-element linear PAA, the granularity value is larger on beam patterns with MRAs pointing towards endfire of the array (leftside and rightside) with a value of approximately 5 degrees from beam patterns with MRAs pointing near broadside where the beam pattern granularity has a value close to one degree, which is the desired MRA angle difference. Figure 3.31 and Figure 3.33 shows beam pattern granularity for weight coefficient's phase parameters with bit resolutions of 4 bits with no decimal precision and 16 bits with no decimal precision for the 16-element linear PAA, respectively. If these beam pattern granularity plots are compared with the ones shown in Section 3.1.3, it can be seen that for the same bit resolution a linear array with more elements exhibits a better beam pattern granularity in terms of an obtained degree difference closer to the real degree difference found between the two MRAs.

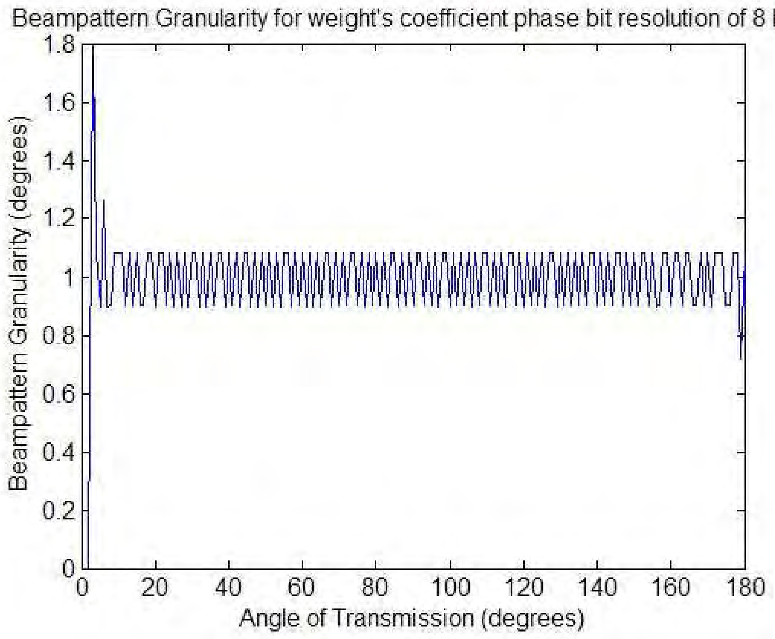

Figure 3.30 Beam pattern Granularity Plot for a 16-element linear DBF with 8 bits of resolution on the weight coefficient's phase

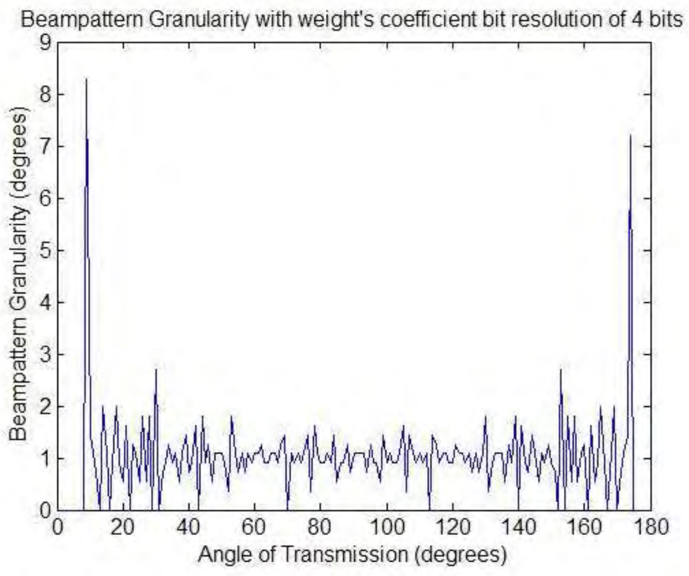

Figure 3.31 Beam pattern Granularity Plot for a 16-element linear DBF with 4 bits of resolution on the weight coefficient's phase

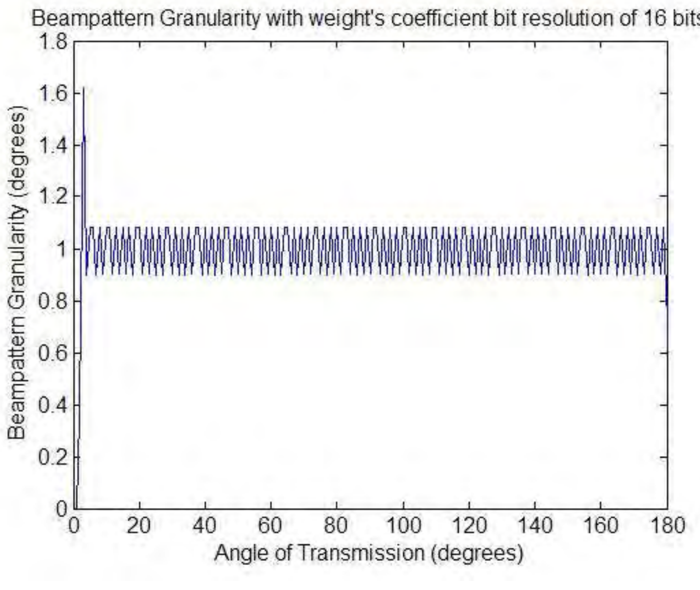

Figure 3.32 Beam pattern Granularity Plot for a 16-element linear DBF with 16 bits of resolution on the weight coefficient's phase

3.3 16-element rectangular PAA Transmitter Prototype

The 16-element rectangular PAA Transmitter Prototype consists of 16 isotropic radiating antennas arranged in a rectangular distribution and uniformly spaced in each axis by half-wavelength. Most of the parameters of this PAA, such as signal bandwidth, RF carrier frequency, IF frequency and inter-element spacing, are the same parameters used in the 16-element linear PAA transmitter prototype. Table 3.17 shows the PAA parameters for this 16-element rectangular array. The 16-element rectangular PAA has the same number of elements as the PAA studied in Section 3.2 but since its geometrical distribution is different, a recalculation of the Narrowband Factor is necessary. In this case, the Maximum Travel Time (ΔT_{max}) is the time taken for a planar wave to travel in endfire direction from the first element in the first row to the last element in the last row of the planar array. The Narrowband Factor for this PAA ($B_S \cdot \Delta T_{max}$) is extremely small compared to one thus, the narrowband beamformer can be used to control this PAA's beam pattern.

TABLE 3.17 16-element rectangular PAA parameters

Parameter	**Value**
RF Carrier Frequency	f_{RF} = 5.85 GHz
IF Frequency	f_{IF} = 3 MHz
Signal Bandwidth	B_S = 2 MHz
Number of Elements	N = 16
Inter-element Spacing	$\Delta x = \lambda_c/2$, $\Delta y = \lambda_c/2$

Maximum Travel Time	$\Delta T_{max} = \sqrt{2} * 3/2f_{RF}$
Narrowband Factor	$B_S \cdot \Delta T_{max} = 0.000725$

The implementation of this DBF transmitter is based on the design described in Section 2.4.2. The DBF architecture provides design flexibility where a DBF with a particular number of channels can be used with any PAA with the same amount of antennas, not taking into account the geometrical distribution of the array. Since the 16-element rectangular PAA has the same amount of channels as its linear counterpart studied in Section 3.2, the architecture, design parameters, and simulation process of the DBF are the same as the one explained in Section 3.2. The architecture design of the DBF transmitter for this PAA can be reviewed in Figures 3.18 and 3.19 and its DBF design parameters are shown in Table 3.10.

3.3.1 First Spatial Filter Example: Beam pattern with Uniform Amplitude Weight Function pointing to $\varphi_{MRA} = 0^o$ and $\theta_{MRA} = 30^o$

The first spatial filter example used in the DBF transmitter for a 16-element rectangular PAA produces a beam pattern with an MRA pointing at angular positions of $\varphi = 0^o$ (angle formed in the planar axis) and $\theta = 30^o$ (angle formed in the axis perpendicular to the planar array) with a uniform distribution amplitude-weighting function. In Section 3.1, Eq. 1 showed the calculation of the weight coefficients for a general PAA with one MRA beam specification. For a rectangular array, the position vector's p_z value is equal to zero reducing the calculation of the weight coefficient for each channel *n* into:

$$w*_n = \frac{1}{N} e^{j\left(2\pi/\lambda\right)\sin(\theta_{MRA})\left[p_x\cos(\phi_{MRA}) + p_y\sin(\phi_{MRA})\right]}. \qquad \textbf{3.11}$$

The phase value found in each weight coefficient can be viewed as the sum of the phase differences between neighboring elements in the same *x* axis value and phase difference between neighboring elements in the same *y* axis of the rectangular array. This relationship can be seen by restructuring Eq. 3.11 into the following mathematical form:

$$w*_n = \frac{1}{N} e^{j\left(\Delta\psi_x + \Delta\psi_y\right)}, \qquad \textbf{3.12}$$

where:

$$\Delta\psi_x = \left(2\pi/\lambda\right) p_x \sin\left(\theta_{MRA}\right)\cos\left(\phi_{MRA}\right), \qquad \textbf{3.13}$$

$$\Delta\psi_y = \left(2\pi/\lambda\right) p_y \sin\left(\theta_{MRA}\right)\sin\left(\phi_{MRA}\right). \qquad \textbf{3.14}$$

Table 3.18 shows the resulting weight coefficients for a uniform 16-element rectangular PAA with an inter-element spacing of *λ/2* in *x* and *y* axis, which are the axis parallel to the planar array. A MATLAB program named "rectangular_DBFtransmitter_steering.m" (which is shown in Appendix A) was prepared in order to calculate the theoretical beam pattern, the directivity and the beamwidth of the PAA for a one-MRA spatial filter design for a rectangular PAA. Figure 3.33 shows a top view polar graph of the theoretical beam pattern's amplitude with the weight coefficients shown in Table 3.18. The top view polar graph was generated using MATLAB function *polar3D()* provided by Dr. Sébastien

Rondineau, Research Professor at the University of Colorado at Boulder. Figure 3.34 shows rectangular plots of the beam pattern's amplitude in dB units for beam pattern cuts of φ = 0º and φ = 45º. These plots show the maximum value of the beam pattern's amplitude at a signal's angle-of-transmission of φ = 0º and θ = 30º with a directivity of 12.80 dB. The beamwidth of the MRA beam (shown in Figure 3.34a) for the theoretical beam pattern is 30.68º with a sidelobe of -7.40 dB (shown in Figure 3.34b). Figure 3.35 shows a 3D surf plot of the beam pattern's amplitude for this spatial filter design.

TABLE 3.18 First Spatial Filter Weight Coefficients for 16-element rectangular PAA – Theoretical Weights

Element	Weight
1, 1	$w_{1,1}$ = 0.0625 ∟-135º
1, 2	$w_{1,2}$ = 0.0625 ∟-135º
1, 3	$w_{1,3}$ = 0.0625 ∟-135º
1, 4	$w_{1,4}$ = 0.0625 ∟-135º
2, 1	$w_{2,1}$ = 0.0625 ∟-45º
2, 2	$w_{2,2}$ = 0.0625 ∟-45º
2, 3	$w_{2,3}$ = 0.0625 ∟-45º
2, 4	$w_{2,4}$ = 0.0625 ∟-45º
3, 1	$w_{3,1}$ = 0.0625 ∟45º
3, 2	$w_{3,2}$ = 0.0625 ∟45º
3, 3	$w_{3,3}$ = 0.0625 ∟45º
3, 4	$w_{3,4}$ = 0.0625 ∟45º
4, 1	$w_{4,1}$ = 0.0625 ∟135º
4, 2	$w_{4,2}$ = 0.0625 ∟135º

4, 3	$w_{4,3}$ = 0.0625 ∟135º
4, 4	$w_{4,4}$ = 0.0625 ∟135º

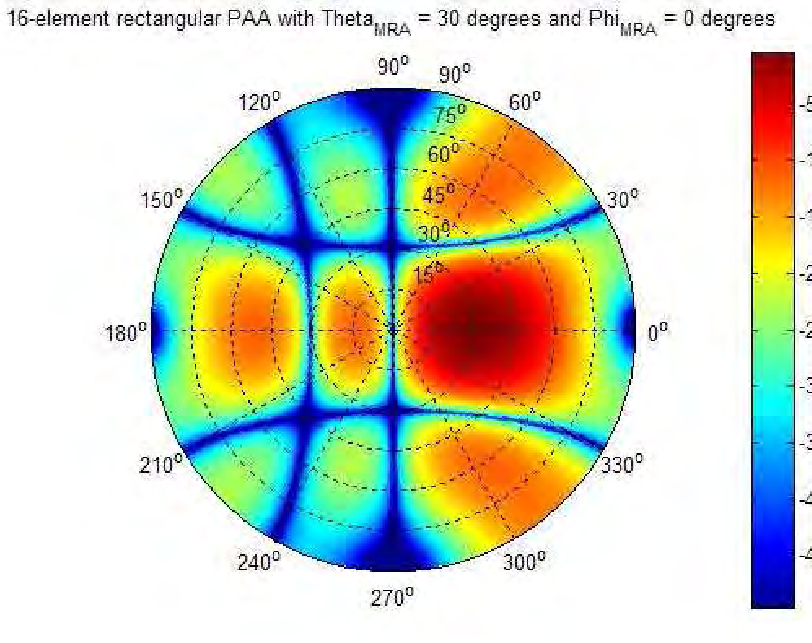

Figure 3.33 Top View Polar Plot of Beam pattern Magnitude of 16-element rectangular DBF with Uniform Amplitude Distribution pointing at φ_{MRA} = 0º and θ_{MRA} = 30º

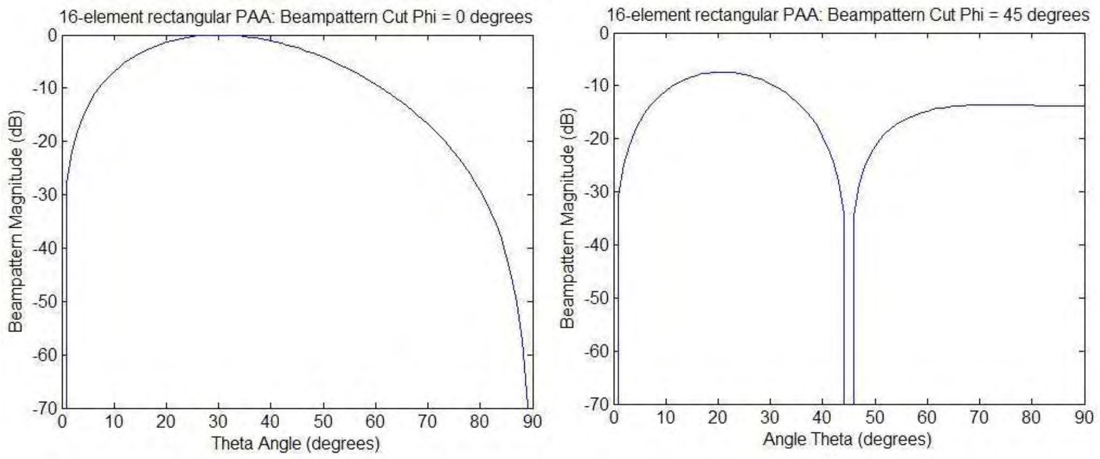

Figure 3.34 Rectangular Plots of Beam pattern Magnitude of 16-element rectangular DBF with Uniform Amplitude Distribution pointing at φ_{MRA} = 82º and θ_{MRA} = 0º for Plane cut on φ = 0º and φ = 45º

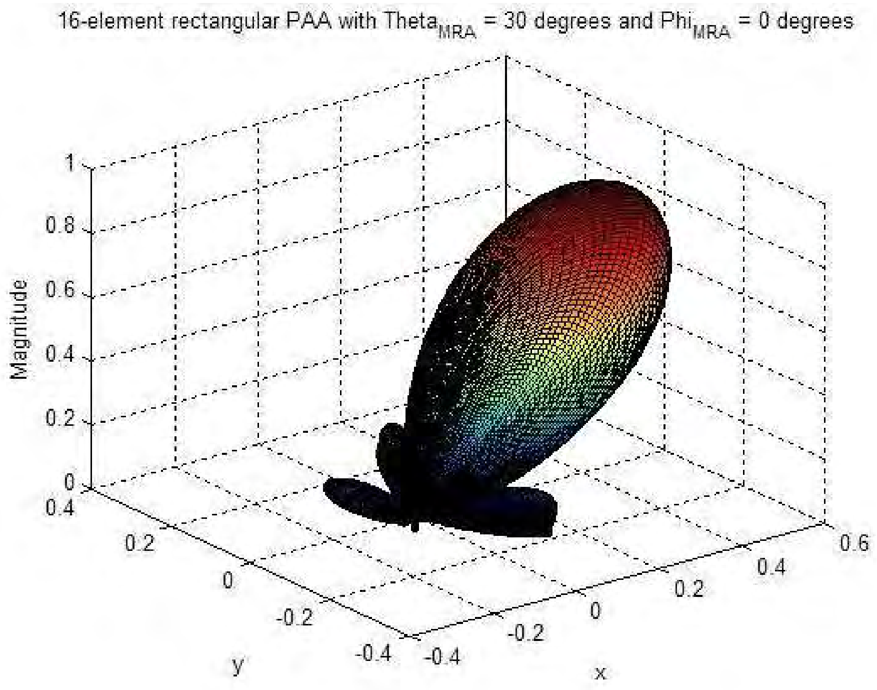

Figure 3.35 Surf Plot of Beam pattern Magnitude of 16-element rectangular DBF with Uniform Amplitude Distribution pointing at φ_{MRA} = 0º and θ_{MRA} = 30º

Before a simulation of the rectangular PAA is performed, transformation of the weight coefficients into constant encoded in the FPGA code simulator is required. A MATLAB program named “rectangular_DBFtransmitter_parameters.m” (included in the Appendix A) was prepared to change the weight coefficients into its fixed-point format values and set all the necessary DBF transmitter parameters. This MATLAB file is similar to the file created to set DBF parameters and condition weight coefficients values for a 16-element linear PAA. The difference strives in the way the file reads the weight coefficient; weights in a linear array are stored in vector form whereas weights in a rectangular array are stored in matrix form. The total simulation time used for this DBF transmitter was 2 x 10^{-5} seconds. Table 3.19 shows the weight coefficients used by the DBF to perform the spatial signal processing. Figure 3.36 shows 4 time plots of the 4 elements of the first row associated with the 16-element rectangular PAA. Since each weigh coefficient has the same weight amplitude, the signals shown in Figure 3.36 show only a difference in their relative phase.

TABLE 3.19 First Spatial Filter Weight Coefficients for 16-element rectangular PAA – FPGA Weights

Element	Weight
1, 1	$w_{1,1}$ = 0.0625 ∟-135º
1, 2	$w_{1,2}$ = 0.0625 ∟-45º
1, 3	$w_{1,3}$ = 0.0625 ∟45º
1, 4	$w_{1,4}$ = 0.0625 ∟135º
2, 1	$w_{2,1}$ = 0.0625 ∟-135º
2, 2	$w_{2,2}$ = 0.0625 ∟-45º
2, 3	$w_{2,3}$ = 0.0625 ∟45º
2, 4	$w_{2,4}$ = 0.0625 ∟135º
3, 1	$w_{3,1}$ = 0.0625 ∟-135º
3, 2	$w_{3,2}$ = 0.0625 ∟-45º
3, 3	$w_{3,3}$ = 0.0625 ∟45º
3, 4	$w_{3,4}$ = 0.0625 ∟135º
4, 1	$w_{4,1}$ = 0.0625 ∟-135º
4, 2	$w_{4,2}$ = 0.0625 ∟-45º
4, 3	$w_{4,3}$ = 0.0625 ∟45º
4, 4	$w_{4,4}$ = 0.0625 ∟135º

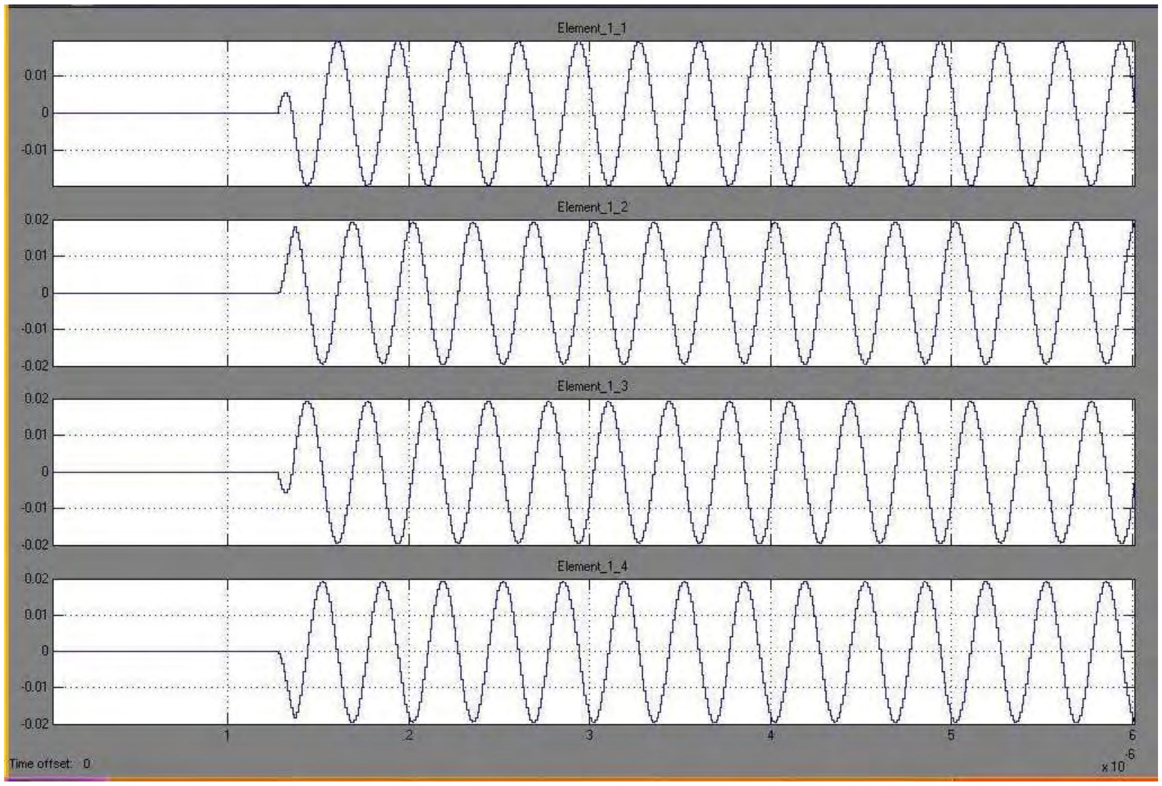

Figure 3.36 Signal Plots of 4 of the 16-elements in the rectangular DBF transmitter for first spatial filter simulation

The next step in the simulation process involves analyzing the data obtained in the DBF transmitter simulation results which were stored in a .mat files. A MATLAB program named “rectangular_DBFtransmitter_results.m” was created to retrieve the simulation results stored in the .mat files and calculate the beam pattern from the spatial combination of the IF output signals for a planar array. The code uses the Discrete Fourier Transform (DFT) to retrieves the amplitude and phase difference value for the IF carrier frequency (in these case f_{IF} = 3MHz) like the file used in Section 3.2 to retrieve beam pattern results from a linear transmitter array. The difference, in this case, is that the weight coefficient's phase value for each element is calculated using Eq. 3.12, where the relative phase difference considers phase difference between neighboring elements in *x* and phase difference between neighboring elements in the *y* axis. Figure 3.37 shows a top view polar graph of the simulation beam pattern's amplitude with the weight coefficients derived from DFT analysis. Figure 3.38 shows rectangular plots of the simulation beam pattern's amplitude in dB units for beam pattern cuts of φ = 0º and φ = 45º. These plots show the maximum value of the beam pattern's amplitude at a signal's angle-of-transmission of φ = 0º and θ = 30º with a directivity of 12.80 dB. The beamwidth of the MRA beam (shown in Figure 3.38a) for the theoretical beam pattern is 30.81º with a sidelobe of -7.37 dB (shown in Figure 3.38b). Figure 3.39 shows a 3D surf plot of the beam pattern's amplitude for this spatial filter design. Table 3.20 shows the results obtained from the DBF transmitter simulation with the results obtained in the theoretical beam pattern calculation.

TABLE 3.20 First Spatial Filter Beam pattern Characteristics for a 16-element rectangular PAA

Beam pattern Characteristic	Theoretical Result	Simulation Result
MRA angle-of-arrival	φ_{MRA} = 0º, Θ_{MRA} = 30º	φ_{MRA} = 0º, Θ_{MRA} = 30º
Half-power Beamwidth	Θ_{BW} = 30.68º @ φ_{MRA} = 0º	Θ_{BW} = 30.80º @ φ_{MRA} = 0º
Directivity	D_{dB} = 12.80 dB	D_{dB} = 12.80 dB
Sidelobe level	SLL_{dB} = -7.40 dB @ φ_{MRA} = 45º	SLL_{dB} = -7.37 dB @ φ_{MRA} = 45º

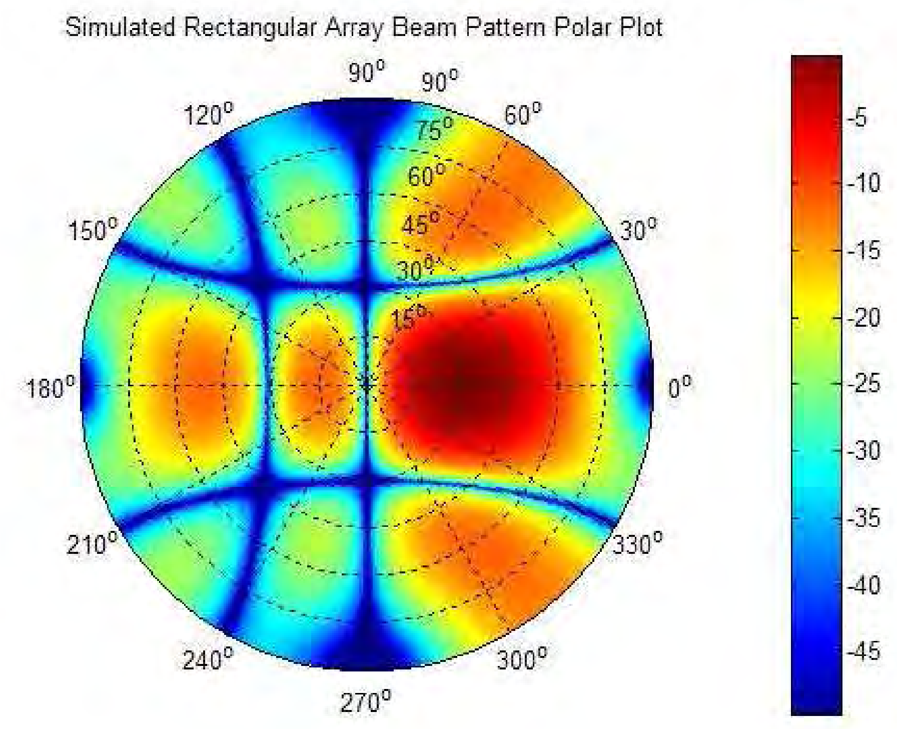

Figure 3.37 Top View Polar Plot of Beam pattern Magnitude of simulated 16-element rectangular DBF with Uniform Amplitude Distribution pointing at φ_{MRA} = 0° and θ_{MRA} = 30°

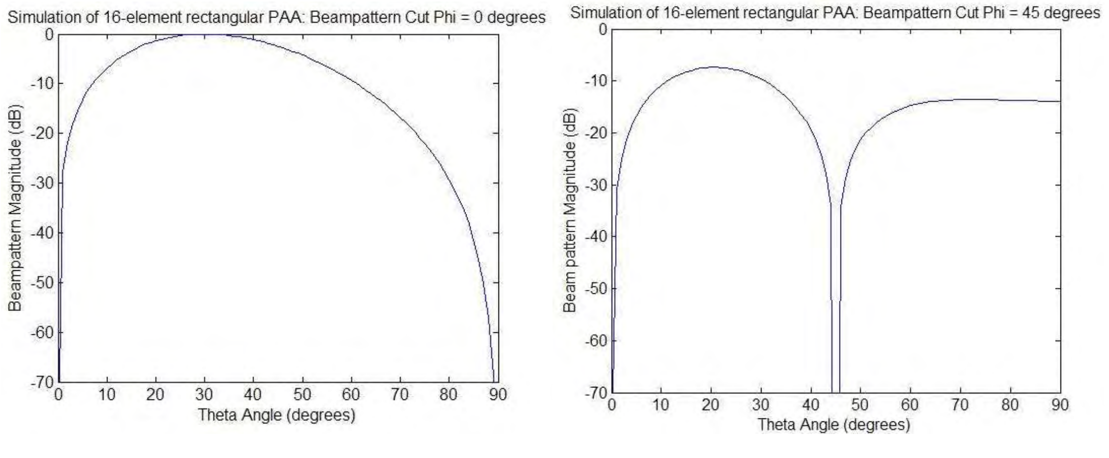

Figure 3.38 Rectangular Plots of Beam pattern Magnitude of simulated 16-element rectangular DBF with Uniform Amplitude Distribution pointing at φ_{MRA} = 0° and θ_{MRA} = 30° for Plane cut on φ = 0° and φ = 45°

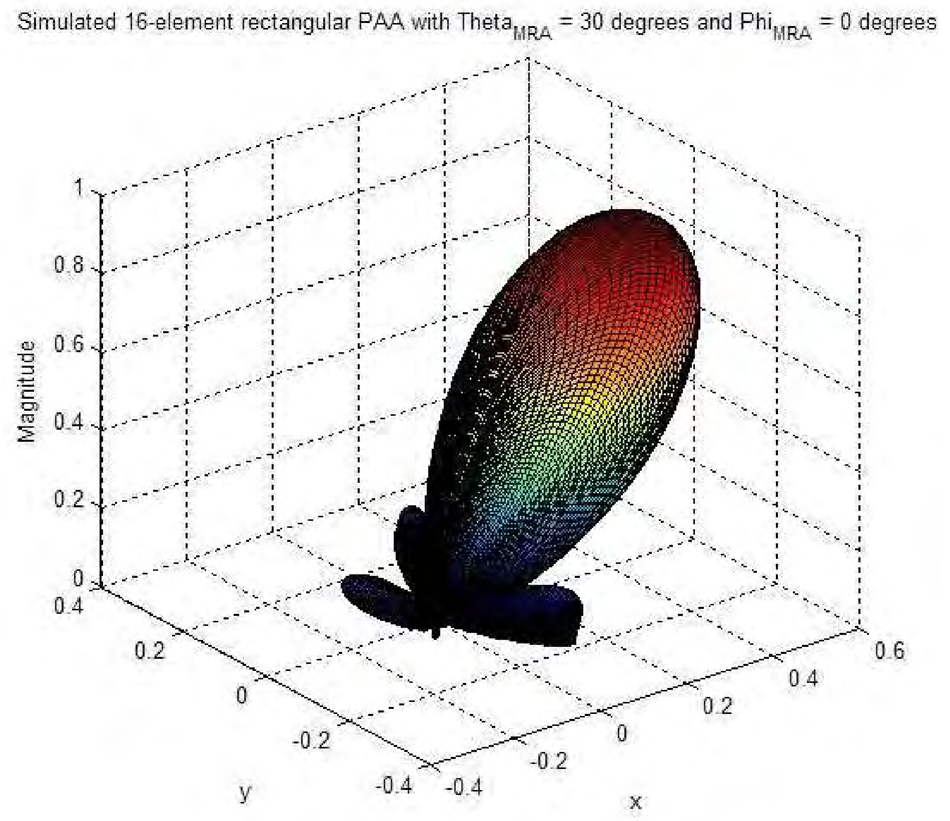

Figure 3.39 Surf Plot of Beam pattern Magnitude of simulated 16-element rectangular DBF with Uniform Amplitude Distribution pointing at φ_{MRA} = 0º and θ_{MRA} = 30º

3.3.2 *Second Spatial Filter Example: Beam pattern with Dolph-Chebyshev Amplitude Weight Function pointing to φ_{MRA} = 122º and θ_{MRA} = 16º*

The second spatial filter example used in the DBF transmitter for a 16-element rectangular PAA produces a beam pattern with an MRA pointing at angular positions of φ = 122º (angle formed in the planar axis) and θ = 16º (angle formed in the axis perpendicular to the planar array) with a Dolph-Chebyshev distribution amplitude-weighting function. As mentioned in Section 2.1.4, the Dolph-Chebyshev distribution method generates the amplitude of weight coefficients to minimize the MRA's beamwidth based on constant sidelobe level specifications. In this method, the properties of the Chebyshev polynomials are used to control the ratio R_{DCV} of the MRA's magnitude to the sidelobe level where the value of the magnitude of the MRA lobe corresponds to the value of the *m*-th degree Chebyshev polynomial $T_m(x_0)$ and the magnitude of the sidelobe is unity [*Van Trees*, 2002]. The relationship between the value x_0 and the ratio $\mathrm{R_{DCV}}$ is shown in the following equation:

$$x_0 = \cosh\left(\frac{\cosh^{-1}(R_{DCV})}{L-1}\right), \qquad \textbf{3.15}$$

where *L* is the number of elements along one of the axis of the rectangular array. After the parameter R_{DCV} has been specified, the amplitude of the weight coefficients can be calculated using the beam pattern sampling in the wavenumber space. The beam pattern of a rectangular array with *L* elements in the x-axis and *M* elements in the y-axis using Dolph-Chebyshev weight distribution can be expressed in the following form:

$$B_\psi(\psi_x, \psi_y) = T_{L-1}\left(x_0 \cos\left(\frac{\psi_x}{2}\right)\cos\left(\frac{\psi_y}{2}\right)\right), \qquad \textbf{3.16}$$

where ψ_x and ψ_y are:

$$\psi_x = \frac{2\pi d_x}{\lambda}(\sin\theta\cos\varphi), \qquad \textbf{3.17}$$

$$\psi_y = \frac{2\pi d_y}{\lambda}(\sin\theta\sin\varphi). \qquad \textbf{3.18}$$

The *m*-th degree Chebyshev polynomial $T_m(x)$ is defined:

$$T_m(x) = \begin{cases} \cos\left(m\cos^{-1}(x)\right), & |x| \le 1, \\ \cosh\left(m\cosh^{-1}(x)\right), & x > 1, \\ (-1)^m \cosh\left(m\cosh^{-1}(x)\right), & x < -1. \end{cases} \qquad \textbf{3.19}$$

In many beam pattern synthesis applications, the Inverse Discrete Fourier Transform (IDFT) algorithm is used to obtain the weights of a pattern sampled in the wavenumber space. In this algorithm, a function $B(k_1, k_2)$ is calculated using the beam pattern function $B_\psi(\psi_x, \psi_y)$:

$$B(k_1,k_2) = e^{-j\left(\frac{L-1}{2}\psi_{xk_1} + \frac{M-1}{2}\psi_{yk_2}\right)} T_{L-1}\left(x_0 \cos\left(\frac{\psi_{xk_1}}{2}\right)\cos\left(\frac{\psi_{yk_2}}{2}\right)\right) R^{-1}, \qquad \textbf{3.20}$$

where ψ_{xk1} and ψ_{yk2} are:

$$\psi_{xk_1} = \left(k_1 - \frac{L-1}{2}\right)\frac{2\pi}{L}, \quad k_1 = 0,1,\ldots,L-1, \qquad \textbf{3.21}$$

$$\psi_{yk_2} = \left(k_2 - \frac{M-1}{2}\right)\frac{2\pi}{M}, \quad k_2 = 0,1,\ldots,M-1. \qquad \textbf{3.22}$$

Applying the 2-D IDFT on the function $B(k_1,k_2)$ gives a function $b(l,m)$, which is related to the weight distribution function $w(l,m)$. The final step in the algorithm involves the calculation of the weight coefficient of each antenna in the array using the following equation:

$$w(l,m) = b(l,m)\, e^{-j\left(l\pi\left(\frac{L-1}{L}\right) + m\pi\left(\frac{M-1}{M}\right)\right)}, \qquad \textbf{3.23}$$

where the variables l and m represent the index position of the antenna in the array along the x-axis and y-axis respectively. A MATLAB file named "rectangular_DBFtransmitter_dolphchebyshev.m" (shown in the Appendix A) was created to compute the weight coefficients for the second spatial filter example of the rectangular 16-element PAA. The code uses the Dolph-Chebyshev polynomials to calculate the amplitude of the weight coefficients and Eq. 3.11 to calculate the phase of the weight coefficients. Table 3.21 shows the resulting weight coefficients for the specified beam pattern parameters. Figure 3.40 shows a top view polar graph of the theoretical beam pattern's amplitude with the weight coefficients shown in Table 3.21. Figure 3.41 shows rectangular plots of the beam pattern's amplitude in dB units for beam pattern cuts of $\varphi = 122^o$ and $\varphi = 302^o$. These plots show the maximum value of the beam pattern's amplitude at a signal's angle-of-transmission of $\varphi = 122^o$ and $\theta = 16^o$ with a directivity of 12.58 dB. The beamwidth of the MRA beam (shown in Figure 3.41a) for the theoretical beam pattern is 33.1^o with a sidelobe of -25.00 dB (shown in Figure 3.41b). Figure 3.42 shows a 3D surf plot of the beam pattern's amplitude for this spatial filter design.

TABLE 3.21 Second Spatial Filter Weight Coefficients for 16-element rectangular PAA – Theoretical Weights

Element	Weight
1, 1	$w_{1,1} = 0.0204 \angle -23.68^o$
1, 2	$w_{1,2} = 0.0611 \angle -49.97^o$
1, 3	$w_{1,3} = 0.0611 \angle -76.26^o$
1, 4	$w_{1,4} = 0.0204 \angle -102.55^o$
2, 1	$w_{2,1} = 0.0611 \angle 18.40^o$
2, 2	$w_{2,2} = 0.1075 \angle -7.89^o$

2, 3	$w_{2,3}$ = 0.1075 ∟-34.18º
2, 4	$w_{2,4}$ = 0.0611 ∟-60.48º
3, 1	$w_{3,1}$ = 0.0611 ∟60.48º
3, 2	$w_{3,2}$ = 0.1075 ∟34.18º
3, 3	$w_{3,3}$ = 0.1075 ∟7.89º
3, 4	$w_{3,4}$ = 0.0611 ∟-18.49º
4, 1	$w_{4,1}$ = 0.0204 ∟102.55º
4, 2	$w_{4,2}$ = 0.0611 ∟76.26º
4, 3	$w_{4,3}$ = 0.0611 ∟49.97º
4, 4	$w_{4,4}$ = 0.0204 ∟23.68º

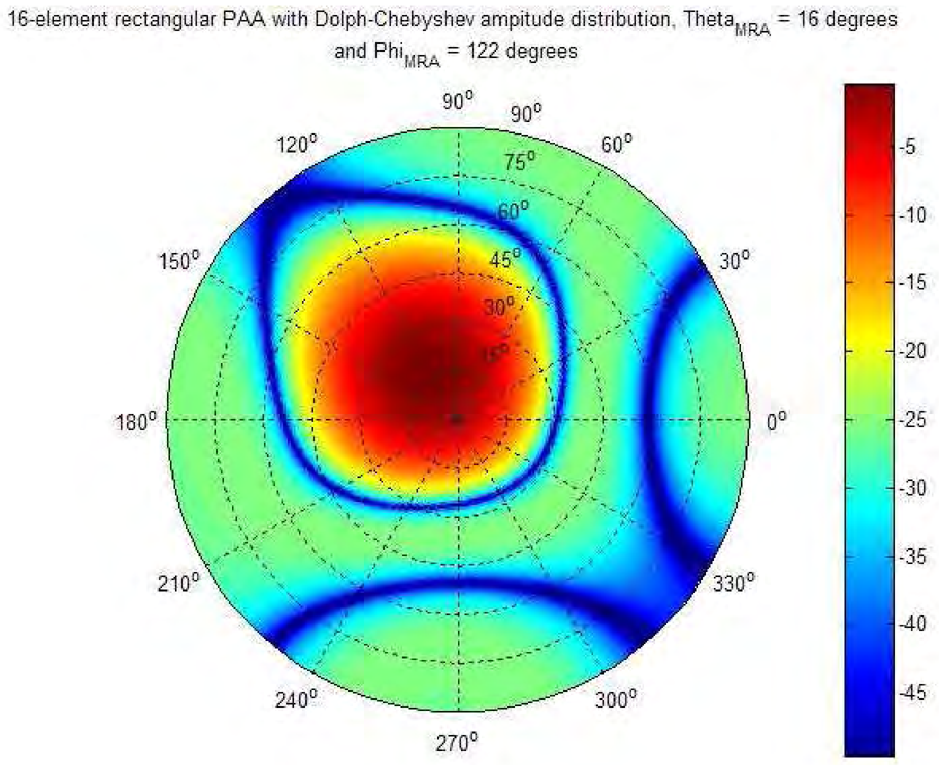

Figure 3.40 Top View Polar Plot of Beam pattern Magnitude of 16-element rectangular DBF with Dolph-Chebyshev Amplitude Distribution pointing at φ_{MRA} = 122º and θ_{MRA} = 16º

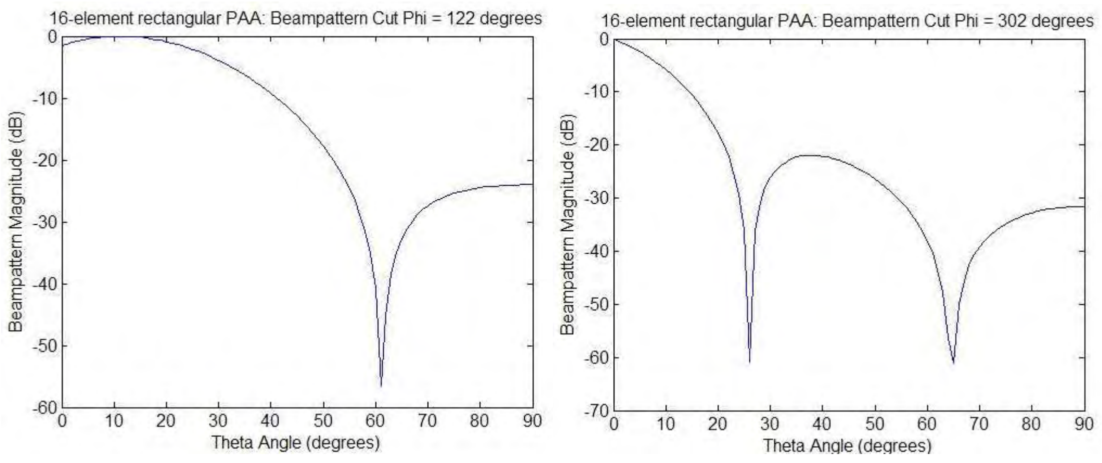

Figure 3.41 Rectangular Plots of Beam pattern Magnitude of 16-element rectangular DBF with Dolph-Chebyshev Amplitude Distribution pointing at φ_{MRA} = 122º and θ_{MRA} = 16º for Plane cut on φ = 122º and φ = 302º

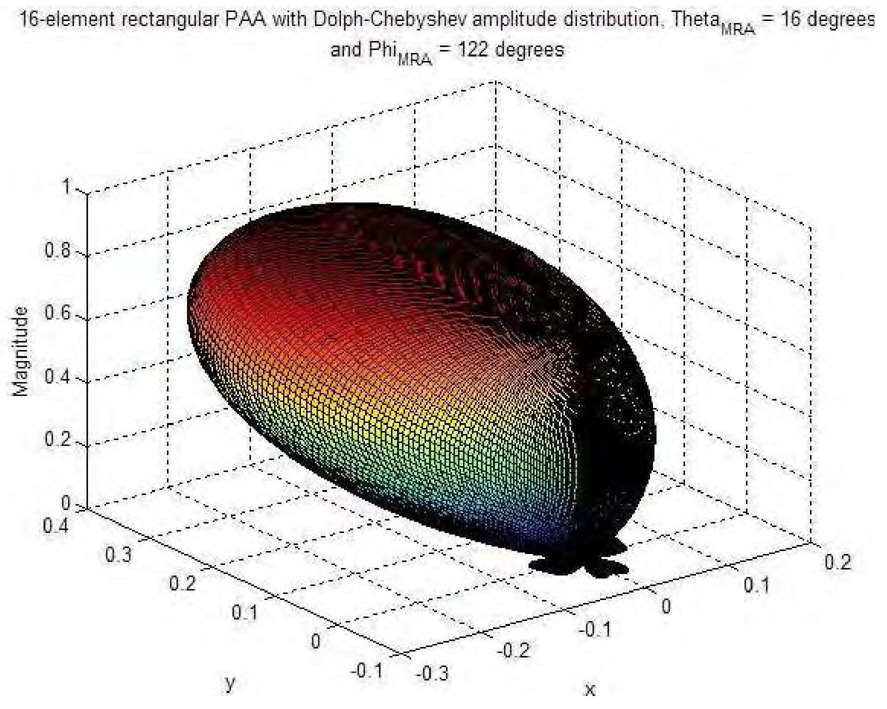

Figure 3.42 Surf Plot of Beam pattern Magnitude of 16-element rectangular DBF with Dolph-Chebyshev Amplitude Distribution pointing at φ_{MRA} = 122º and θ_{MRA} = 16º

The MATLAB file “rectangular_DBFtransmitter_parameters.m” was also used to set DBF parameters and condition weight coefficients values for the second spatial filter simulation for the 16-element rectangular PAA. Table 3.22 shows the weight coefficients used by the DBF to perform the second spatial filter on the FPGA simulation. Figure 3.40 shows 4 time plots of the 4 elements of the first row associated with the 16-element rectangular PAA. The difference in the amplitude of each signal shown in Figure 3.43 is related to the Dolph-Chebyshev amplitude-distribution function, which assigns the magnitude of the weights to each antenna element in the array.

TABLE 3.22 Second Spatial Filter Weight Coefficients for 16-element rectangular PAA – FPGA Weights

Element	Weight
1, 1	$w_{1,1}$ = 0.0204 ∟-23.91º
1, 2	$w_{1,2}$ = 0.0611 ∟-50.63º
1, 3	$w_{1,3}$ = 0.0611 ∟-75.94º
1, 4	$w_{1,4}$ = 0.0204 ∟-102.66º
2, 1	$w_{2,1}$ = 0.0611 ∟18.28º
2, 2	$w_{2,2}$ = 0.1075 ∟-8.44º
2, 3	$w_{2,3}$ = 0.1075 ∟-33.75º
2, 4	$w_{2,4}$ = 0.0611 ∟-60.47º
3, 1	$w_{3,1}$ = 0.0611 ∟60.47º
3, 2	$w_{3,2}$ = 0.1075 ∟33.75º
3, 3	$w_{3,3}$ = 0.1075 ∟8.44º
3, 4	$w_{3,4}$ = 0.0611 ∟-18.28º
4, 1	$w_{4,1}$ = 0.0204 ∟102.66º

4, 2	$w_{4,2}$ = 0.0611 ∟75.94º
4, 3	$w_{4,3}$ = 0.0611 ∟50.63º
4, 4	$w_{4,4}$ = 0.0204 ∟23.91º

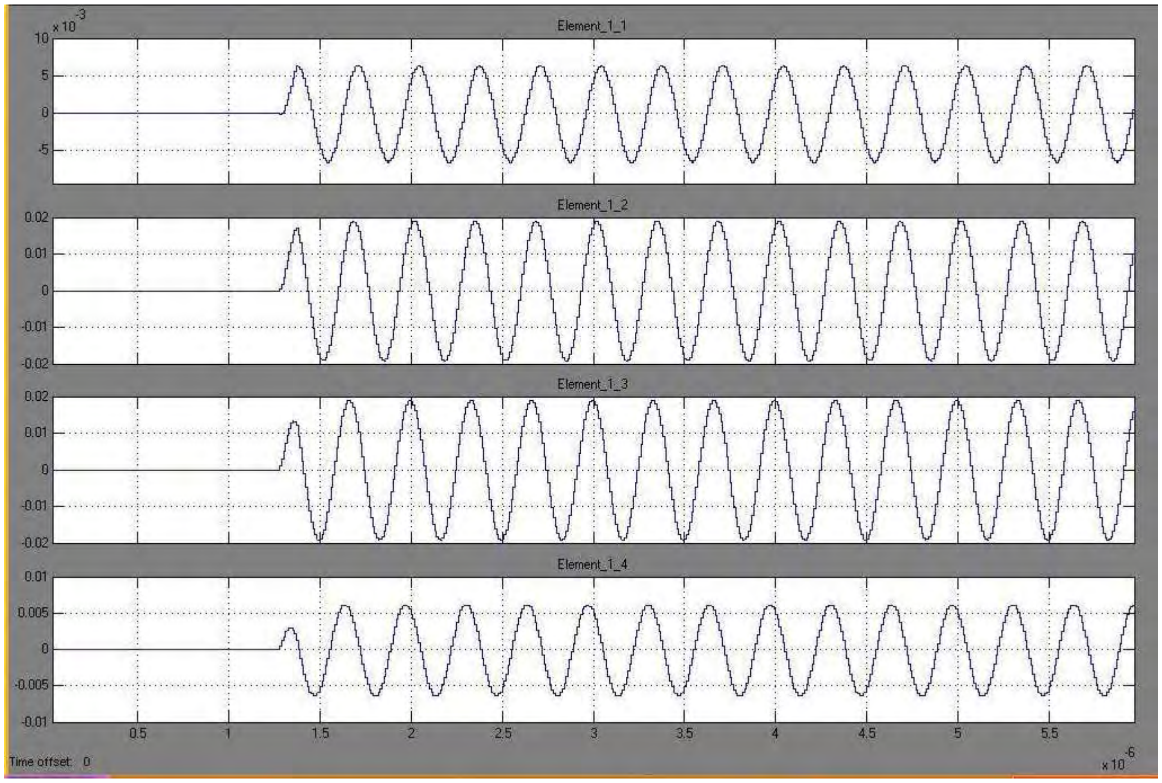

Figure 3.43 Signal Plots of 4 of the 16-elements in the rectangular DBF transmitter for second spatial filter simulation

After storing the results obtained in the simulation of the second spatial filter, the data is analyzed by means of the DFT, exactly like the first spatial filter example. The MATLAB program “rectangular_DBFtransmitter_results.m” was used to retrieve the results obtained in the simulation and analyze the data of each DBF channel. Figure 3.44 shows a top view polar graph of the simulation beam pattern’s amplitude with the weight coefficients derived from DFT analysis. Figure 3.45 shows rectangular plots of the simulation beam pattern's amplitude in dB units for beam pattern cuts of φ = 122º and φ = 302º. These plots show the maximum value of the beam pattern's amplitude at a signal's angle-of-transmission of φ = 122º and θ = 16º with a directivity of 12.60 dB. The beamwidth of the MRA beam (shown in Figure 3.45a) for the theoretical beam pattern is 33.01º with a sidelobe of -25.00 dB (shown in Figure 3.45b). Figure 3.46 shows a 3D surf plot of the beam pattern's amplitude for this spatial filter design. Table 3.23 shows the results obtained from the DBF transmitter simulation with the results obtained in the theoretical beam pattern calculation.

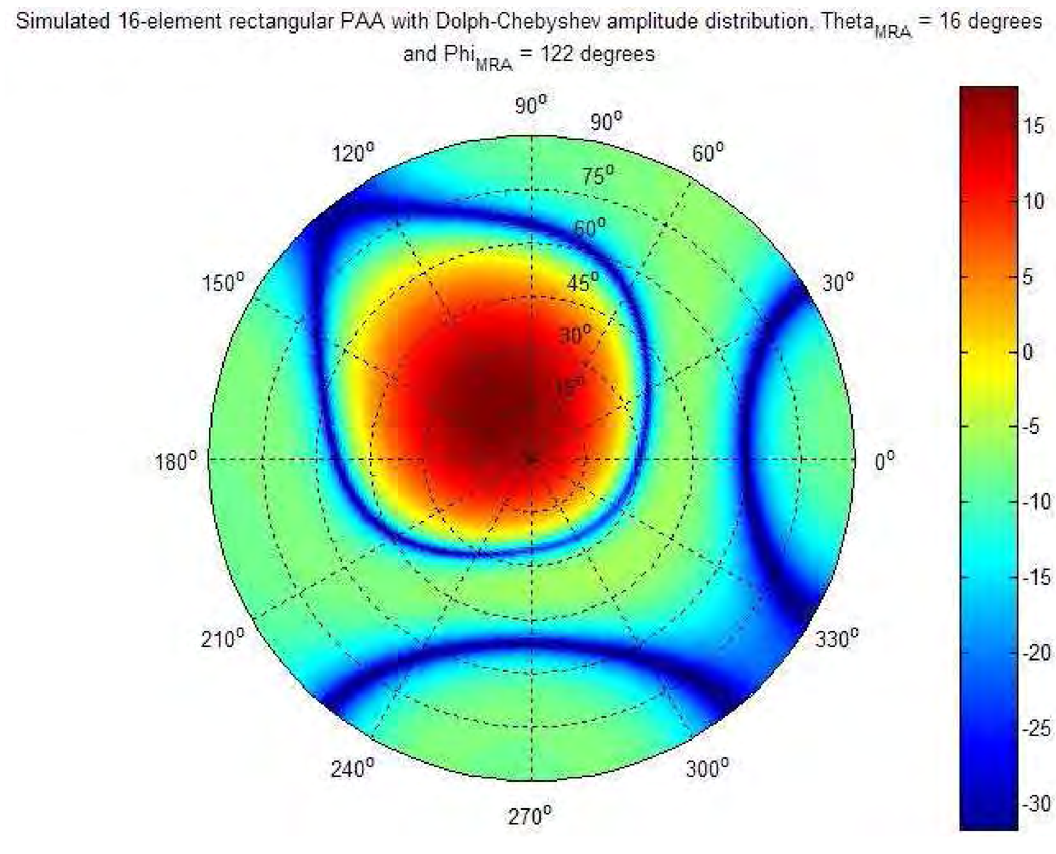

Figure 3.44 Top View Polar Plot of Beam pattern Magnitude of simulated 16-element rectangular DBF with Dolph-Chebyshev Amplitude Distribution pointing at φ_{MRA} = 122º and θ_{MRA} = 16º

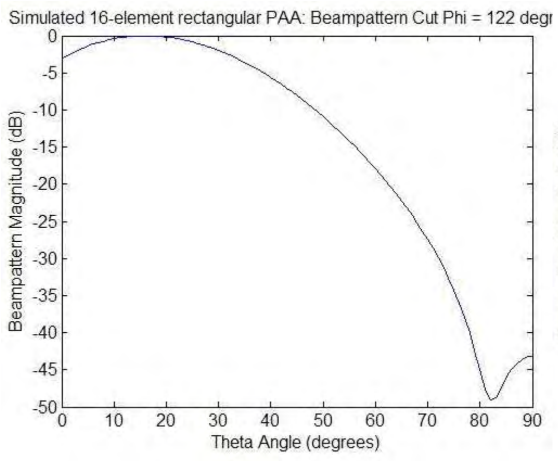

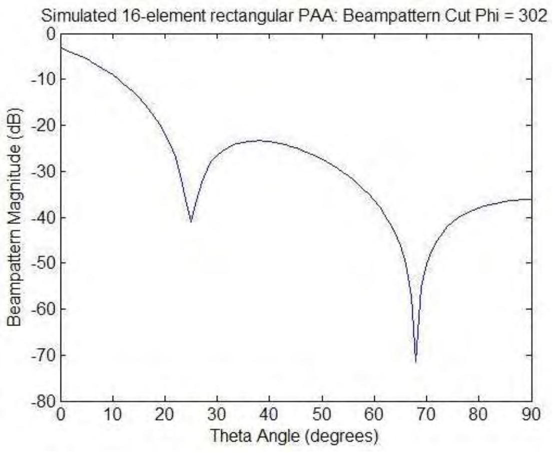

Figure 3.45 Rectangular Plots of Beam pattern Magnitude of simulated 16-element rectangular DBF with Dolph-Chebyshev Amplitude Distribution pointing at φ_{MRA} = 122º and θ_{MRA} = 16º for Plane cut on φ = 122º and φ = 302º

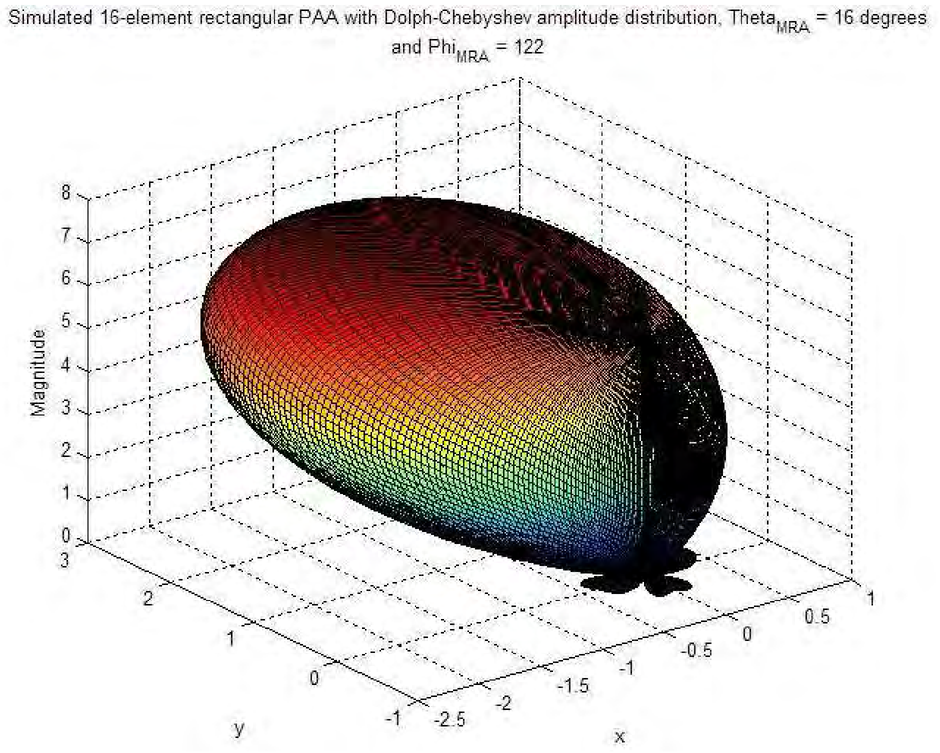

Figure 3.46 Surf Plot of Beam pattern Magnitude of simulated 16-element rectangular DBF with Dolph-Chebyshev Amplitude Distribution pointing at φ_{MRA} = 122º and θ_{MRA} = 16º

TABLE 3.23 Second Spatial Filter Beam pattern Characteristics for a 16-element rectangular PAA

Beam pattern Characteristic	Theoretical Result	Simulation Result
MRA angle-of-arrival	φ_{MRA} = 122º, Θ_{MRA} = 16º	φ_{MRA} = 122º, Θ_{MRA} = 16º
Half-power Beamwidth	Θ_{BW} = 33.1º @ φ_{MRA} = 122º	Θ_{BW} = 33.01º @ φ_{MRA} = 122º
Directivity	D_{dB} = 12.58 dB	D_{dB} = 12.60 dB
Sidelobe level	SLL_{dB} = -25.00 dB @ φ_{MRA} = 302º	SLL_{dB} = -23.39 dB @ φ_{MRA} = 302º

3.3.3 Beam pattern Granularity for 16-element rectangular PAA

As all beam pattern characteristics, the beam pattern granularity is affected by the geometrical distribution of the antenna array. In the case of the rectangular array, the beam pattern granularity can be expressed in the following form:

$$BG\left(\theta_{MRA1},\theta_{MRA2},\phi_{MRA}\right)=\theta\,|_{\max\left(\left|B(\theta_{MRA2},\phi_{MRA})\right|\right)}-\theta\,|_{\max\left(\left|B(\theta_{MRA1},\phi_{MRA})\right|\right)}\ . \qquad \textbf{3.24}$$

Eq. 3.24 is equivalent to applying Eq. 3.4 to a beam pattern cut in the φ-plane determined by the angle φ_{MRA}. Figure 3.47 shows a surf plot of the beam pattern granularity as a function of the MRA's direction-of-arrival in terms of angle φ and angle θ when the weight coefficient's phase parameter has a bit resolution of 8 bits with no decimal precision for the 16-element rectangular PAA. Similar to the beam pattern granularity plots for the linear arrays, the beam pattern granularity surf plot has been constructed using a constant MRA angle difference (θ_{MRA2} - θ_{MRA1}) of one degree along each direction-of-arrival value for each φ-plane beam pattern cut. The maximum beam pattern granularity value is shown at an angle-of-incidence φ = 38º, θ = 88º with a value of 3.6º, which illustrates the increase in error in terms of MRA beam position for scan angles near endfire of the array. Figure 3.48 illustrates this maximum beam pattern granularity value in a beam pattern cut on φ = 38º and φ = 208º.

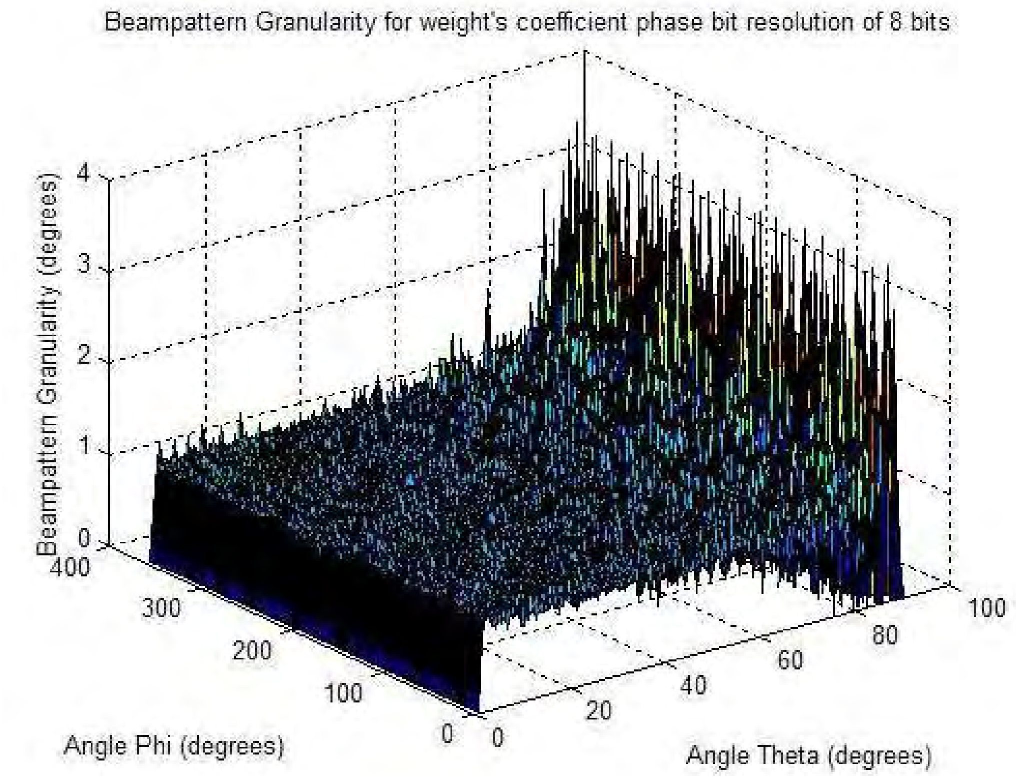

Figure 3.47 Beam pattern Granularity Surf Plot for a 16-element rectangular DBF with 8 bits of resolution on the weight coefficient's phase

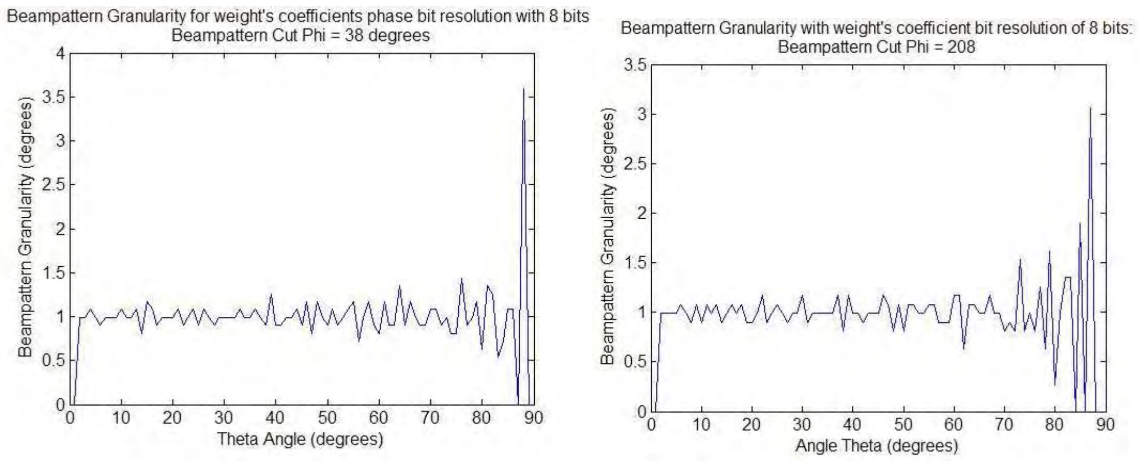

Figure 3.48 Beam pattern Granularity Rectangular Plots for a 16-element rectangular DBF with 8 bits of resolution on the weight coefficient's phase for Plane cut on φ = 38º and φ = 208º

3.4 16-element rectangular PAA Transmitter

The 16-element rectangular PAA transmitter is the transmitter containing the DBF transmitter discussed in Section 3.3. The antenna array consists of 16 patch antennas arranged in a rectangular distribution and uniformly spaced in each axis by half-wavelength. The array and signal parameters in the PAA transmitter are equal to parameters of the DBF transmitter (shown in Table 3.17), thus satisfying the narrowband characteristic requirement necessary for a narrowband beamformer implementation as a means to control the beam pattern of the array. The PAA transmitter contains 3 stages: the DBF transmitter, the RF up-conversion stage, and the patch antenna array. The DBF transmitter receives the information signal, digitally modulates the signal into IF and applies the appropriate weight to each channel. It uses the design proposed in Section 2.3 and it is implemented using the Lyrtech VHS-DAC High-Speed Multichannel

Development Platform. The RF up-conversion stage distributes the Local Oscillator signal into each antenna channel, mixes the IF information signal with the LO signal, and amplifies the resulting signal prior transmission of the signal by means of power amplification. The final stage of the microwave transmitter consists in the transmission of the signal using a 16-element rectangular patch antenna array. The S-Parameter simulations of all the RF circuits in the RF up-conversion stage and the Electromagnetic simulations of the rectangular patch antenna array were performed using Ansoft Designer V2. Table 3.24 shows the ideal system requirements for each stage of the PAA transmitter.

TABLE 3.24 Ideal System Requirements for PAA transmitter

Requirement	Value
Wilkinson Power Dividers (WPD)	
VSWR at input port of each circuit	Less than 2
Gain of each output port	5 dB
Relative amplitude difference between output port	0 dB
Relative phase difference between output port	0º
Mixer/Amplifier Stage	
Relative amplitude difference between output port	0 dB
Relative phase difference between output port	0º
Rectangular Patch Array	

VSWR at input port of each antenna	Less than 2
Polarization Type	Linear Polarization

3.4.1 *DBF Transmitter*

The Lyrtech VHS-DAC High-Speed Multichannel Development Platform is the physical device which implements the DBF Transmitter. The VHS-DAC module contains a Xilinx XC2V6000 FPGA, 16 DAC channels with a bit resolution 14-bits and a sampling frequency of 125 mega-samples per second (MSPS) per channel, a programmable clock up to 125 MHz with a resolution of 10 kHz, and SD-RAM of 128 MB. The data transmission module can interface with other digital devices by using the Front Panel Data Port (FPDP), which can communicate with an external processing board or a data acquisition module, additional input signal ports for external clock and manual trigger, and a GPIO connector, which provides connection to certain pins of the FPGA included inside the board. The VHS-DAC board also includes four read/write custom registers accessible to the user through VHS Control Utility software, which provides a real-time interface between the user and the computational equipment. The VHS-DAC is installed in a Compact PCI Card Cage, which includes a computer board with a 1.7 GHz Mobile Pentium 4 CPU, 512 MB of SDRAM and a 20 GB Hard Drive. A program named SMCCE allows the computer to monitor the status of the VHS-DAC module. Lyrtech Signal Processing, which is the company that manufactures the data transmission module, provides a software package which includes low-level drivers for programming the board on a VHDL environment, and FPGALink, which is a blockset providing Lyrtech's hardware integration with Simulink. Figure 3.49 shows a picture of the VHS-DAC module.

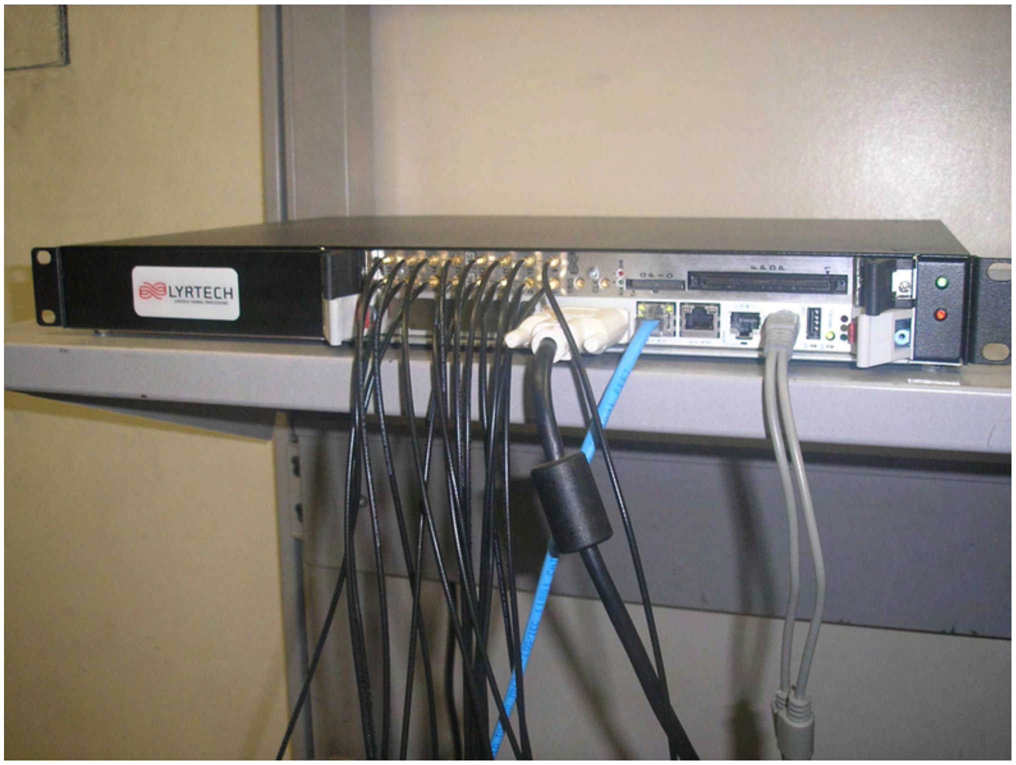

Figure 3.49 Picture of VHS-DAC High-Speed Multichannel Development Platform

Using Xilinx System Generator for DSP, the simulation code for the DBF transmitter created on MATLAB's Simulink discussed in Section 3.3 was translated into VHDL code. This VHDL code was downloaded into the FPGA inside the VHS-DAC module, which provides a physical realization of the simulation performed on Simulink. Table 3.10 in Section 3.2 shows the parameters used in the implementation of the DBF transmitter for the PAA. An additional hardware module was designed to interface the control unit with the DBF transmitter. This hardware module, which was programmed in the FPGA through Simulink software, controls the assignation of amplitude and phase weight coefficients for each of the DBF channels. Figure 3.50 shows the Simulink diagram of the Control Interface Module (CIM). Figure 3.51 shows a diagram of the input and one of the channels of the CIM. Initially, the CIM was constructed to interface with the memory of the VHS-DAC, which is a typical communication topology in digital control systems. This initial design provided the flexibility of separating the DBF transmitter with the algorithm generating the weight coefficients, where the system memory would be used the link to interchange data between the two system components. Unfortunatly, a problem with the memory and its block module in the Simulink environment prevented it from functioning properly under real-time operation. Inactivity

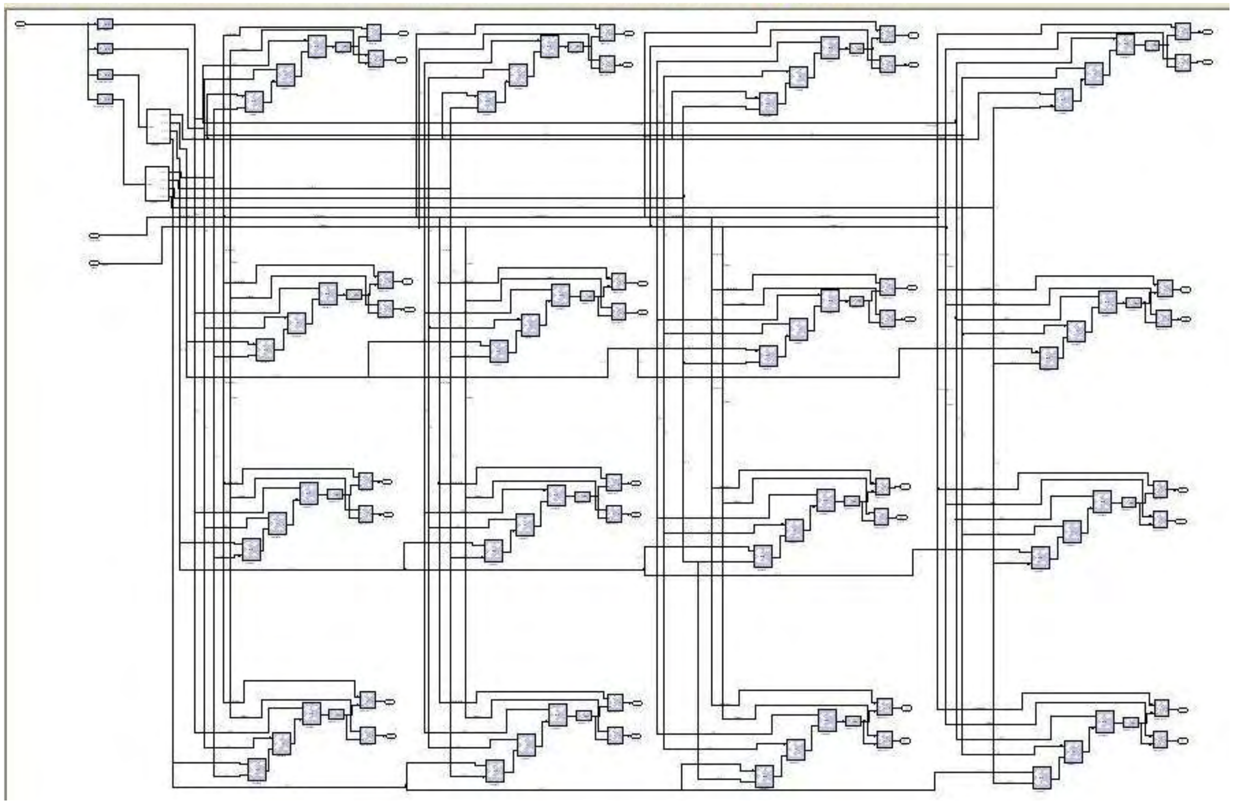

Figure 3.50 Simulink Diagram of CIM

of the memory's "request signal" and "ready signal" in the block module was the main problem found in the system memory's performance. During the debugging process, Lyrtech Signal Processing was notified of the errors in the performance in the memory, only to find out that its lack of performance under certain conditions is a known issue, which is currently being attended.

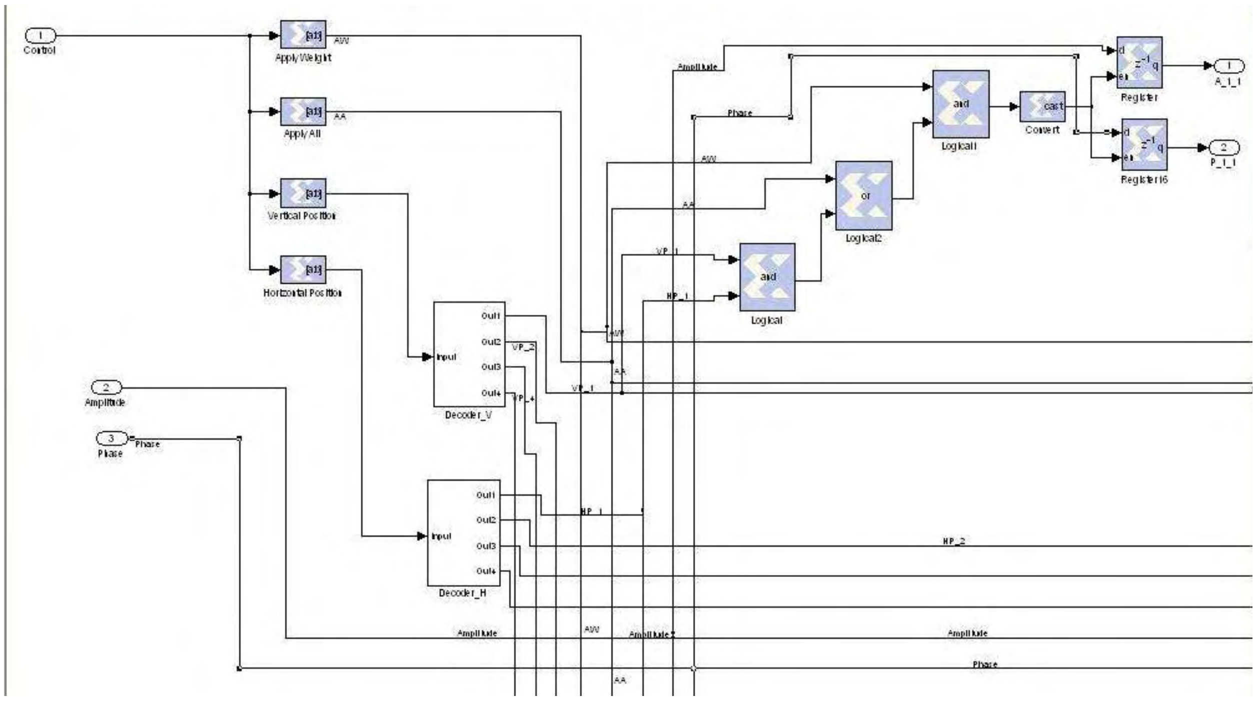

Figure 3.51 Diagram of input ports and one of the 16 channels in the CIM

The memory's task in the CIM was substituted with the use of the custom register in the VHS-DAC as a means to input the weight coefficients of each DBF channel. Table 3.25 shows the information of the relationship between the bit structure of each custom registers and the parameters of the CIM. The bit description of the registers is given starting from the Least Significant Bit (LSB). Three of the four custom register were used to store the weight coefficient information used in the DBF transmitter. The first register, which is the control register, contains the vertical and horizontal position of the DBF channel and gives the triggering signal to DBF transmitter communicating that the weight coefficients are ready. The second register and third register store the amplitude and phase coefficient of the DBF channel, respectively. The bit resolution of the amplitude and phase coefficients in the registers are determined by the MATLAB file *.m, which was used earlier to program the DBF transmitter simulations. A MATLAB code named *.m reads a MAT file containing the weight coefficient of each DBF channel in the PAA and translates the information into 3 vectors representing the 3 custom registers where the value of the control register is related to the value of the amplitude and phase register for each index.

TABLE 3.25 Relationship between bit structure of custom register and DBF transmitter weight parameters

Custom Register	Bit Structure	DBF Parameter
Control Register	Unsigned 6-bit value	1st – 2nd bit: Horizontal position of DBF channel 3rd – 4th bit : Vertical position of DBF channel 5th bit: Trigger application of weight to current DBF channel 6th bit: Trigger application of weight to all channels
Weight Amplitude Register	Signed 2's complement value	Amplitude of weight coefficient
Weight Phase Register	Signed 2's complement value	Phase of weight coefficient

After the VHDL code has been generated and the values of the custom registers for each DBF channel has been calculated, the next step involves downloading the synthesized code in the FPGA and programming the real-time parameters of the VHS-DAC. As mentioned earlier in the section, the VHS Control Utility provides the means to program each VHS-DAC component. The process of programming the VHS-DAC module involves programming the FPGA, the programmable on-board clock, the system memory, the channel gains, and the custom register's content. The user is encouraged to read the user manual of the VHS-DAC [*Lyrtech*, 2004] to find details on the procedure of programming each device. The file generated by Xilinx System's Generator and the vectors generated in the MATLAB code *.m are used to program the FPGA and assign the values of the custom registers, respectively.

3.4.2 RF Up-Conversion Stage

The RF up-conversion stage of the microwave system contains three important sub-stages: the power divider network of the LO, the mixer stage, and power amplification of the RF carrier signal. The power divider network receives the signal of the LO and distributes the LO signal into each element of the PAA. The output signals of this stage must have the necessary power to assure proper operation of the mixer stage, since a minimum power requirement is expected at the input port of the LO of the mixers. The PAA controls the beam pattern of the array by means of progressive phase shift between each antenna element, thus the relative phase difference between each output signal in the power divider network must be very small. The mixer stage modulates the IF signal into the RF signal with the use of the LO received from the power divider network. The final stage of the RF up-conversion stage is the power amplification stage, where the RF signal received from the mixer stage is amplified in order to be transmitted by the antenna array. Two microwave circuits were designed to implement the RF up-conversion stage of the microwave transmitter. The first designed circuit was a 1-to-4 power divider circuit. The power divider network uses 5 of this circuits to distribute the LO signal into the 16 antenna channels in the PAA. The second circuit contains four transmitter channels, where the mixer stage and the amplification stage are combined. The PAA uses 4 of this circuits to mix the LO signal with the IF signal and amplify the modulated RF signal in order to be transmitted by the antenna array.

A diagram of the first designed circuit is shown in Figure 3.52. The first stage of the circuit is composed of 3 Wilkinson Power Dividers which splits the power of the input equally into 4 output ports. Since the system impedance is 50 Ω, Each Wilkinson Power Divider contains a 100 Ω necessary to provide impedance matching at its output ports. The next stage of the circuit includes a linear amplifier in each output of the Wilkinson Power Dividers, which increases the power of the each signal. The Hittite HMC315 Darlington Amplifier is the RF amplifier component used to amplify the signals prior the output ports. The amplifier provides a typical gain of 4 dB for a frequency range of DC to 7 GHz with a single positive supply voltage of +5 V. The circuit also contains other RF passive components necessary to assure proper operation of the amplifiers. The amplifiers need a DC-bias resistance R_{bias} in order to receive the desired collector voltage *Vcc* voltage at its output port. Using a power supply voltage *Vs* = 8 V and a R_{bias} = 100 Ω, the transistors in the amplifier can received a required collector current *Icc* = 30 mA and the *Vcc* = 5 V.

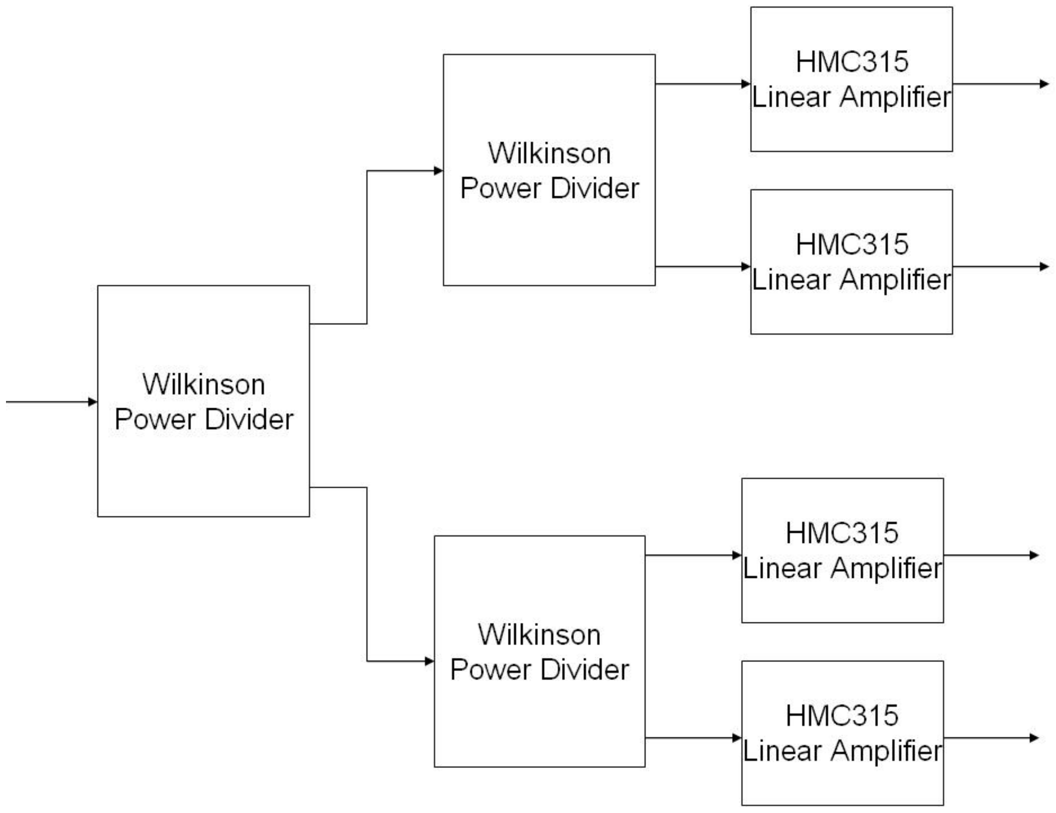

Figure 3.52 Diagram of Power Divider Network Circuit

An RF-choke circuit was designed at the output of the amplifier in order to protect the DC power supply from the RF output signal. The requirements for the two-port circuit included good impedance match at a frequency of 5.85 GHz, which is the frequency of the LO, and low transmission losses. The layout diagram of the RF-shoke circuit is shown in Figure 3.53. The circuit is based on the Bias-T model and contains the 100 Ω bias resistor and 2 chip capacitors with a capacitance of 220 pF. A simulation of the RF-choke circuit was performed in order to calculate its S-Parameters. The Scattering Parameters (S-Parameters) of a circuit relates the voltage waves incident on the ports to those reflected from the ports [*Pozar*, 1998]. Figure 3.54 shows rectangular plots of the magnitude of the S-Parameters *S(1,1)* and S*(2,1)* for a frequency range of 4.5 GHz to 6.5 GHz. Since the structure exhibits symmetry, *S(1,2)* and *S(2,2)* parameters exhibit the same behavior as *S(2,1)* and *S(1,1)* respectively. The magnitude of *S(1,1)* is -27.49 dB and the magnitude of *S(2,1)* is -0.11 , which satisfies with the requirements of a good RF-shoke network at 5.85 GHz. At the input port of the amplifier and at the output port of the RF-shoke are 2 DC block capacitors with a capacitance of 0.1 μF with the purpose of protecting the RF signal source and the RF output sink from DC power.

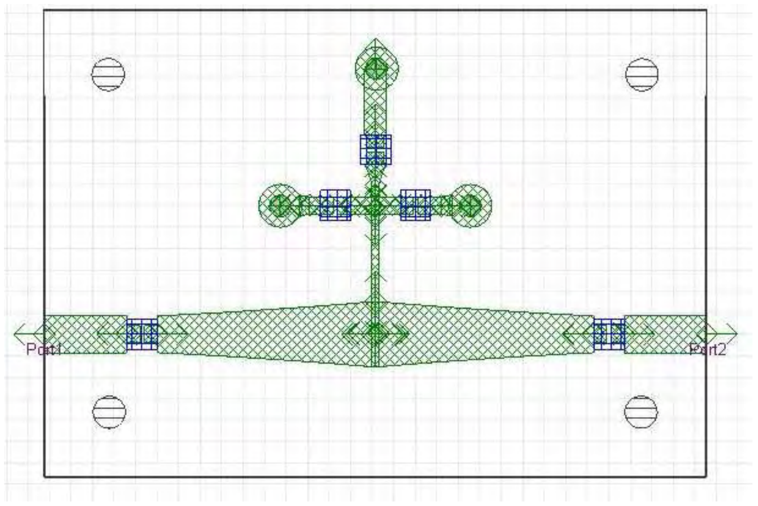

Figure 3.53 Layout of RF-Choke Circuit

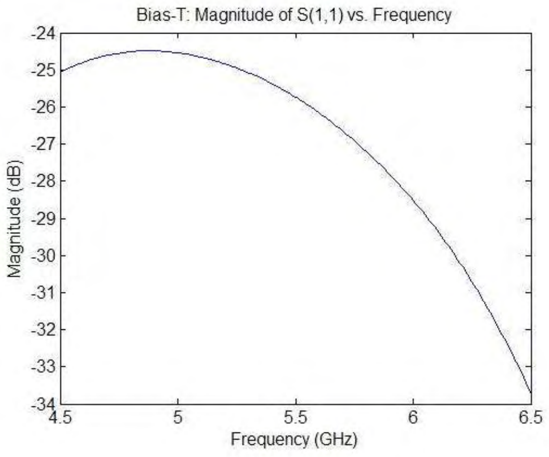

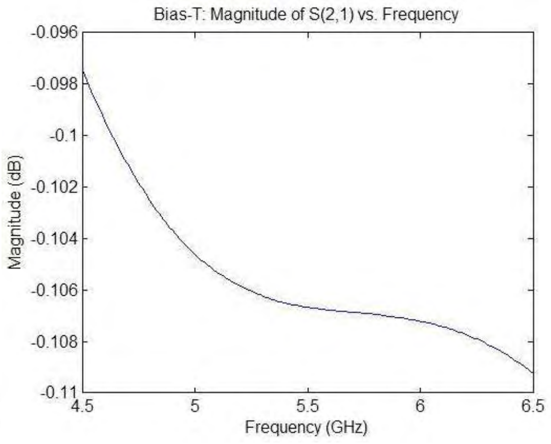

Figure 3.54 Magnitude of S-Parameters *S(1,1)* and *S(2,1)* for Simulated Bias-T Circuit

A simulation of the power divider network circuit with Bias-T was performed to test the performance of the circuit and compare the results with the required system parameters. Figure 3.55 shows 4 rectangular plots of the magnitude of the S-Parameters for all the 5 ports of the circuit. The magnitude of *S(1,1)* is -10.27 dB for a frequency of 5.85 GHz, which satisfies the requirement of VSWR lower than 2. In the case of the input-output port relationship, the magnitude of *S(2,1)*, *S(3,1)*, *S(4,1)*, and *S(5,1)* shows a circuit gain of 10 dB, which also fulfills the condition of at least 5 dB gain needed to deliver a considerable amount of power signal into the LO input port of the mixers. The magnitude of *S(2,2)*, *S(3,3)*, *S(4,4)* and *S(5,5)* is -16.12 dB but since the magnitudes of *S(1,2)*, *S(1,3)*, *S(1,4)*, and *S(1,5)* are very small (around -28 dB), the reflections at the output ports have very little effect on the return loss of the circuit. Another important circuit requirement is guaranteeing zero phase error between the output ports of the circuit, since phase coherency is a very crucial characteristic in the implementation of a PAA. Figure 3.56 shows a rectangular plot of the phase of *S(2,1)*, *S(3,1)*, *S(4,1)*, and *S(5,1)* as a function of frequency. The phase plot is equal for *S(2,1)*, *S(3,1)*, *S(4,1)*, and *S(5,1)* over all the frequency range of 4.5 GHz to 6.5 GHz, which assures phase coherency between the output ports. The phase value for the transmission S-Parameters at a frequency of 5.85 GHz is 172.15º.

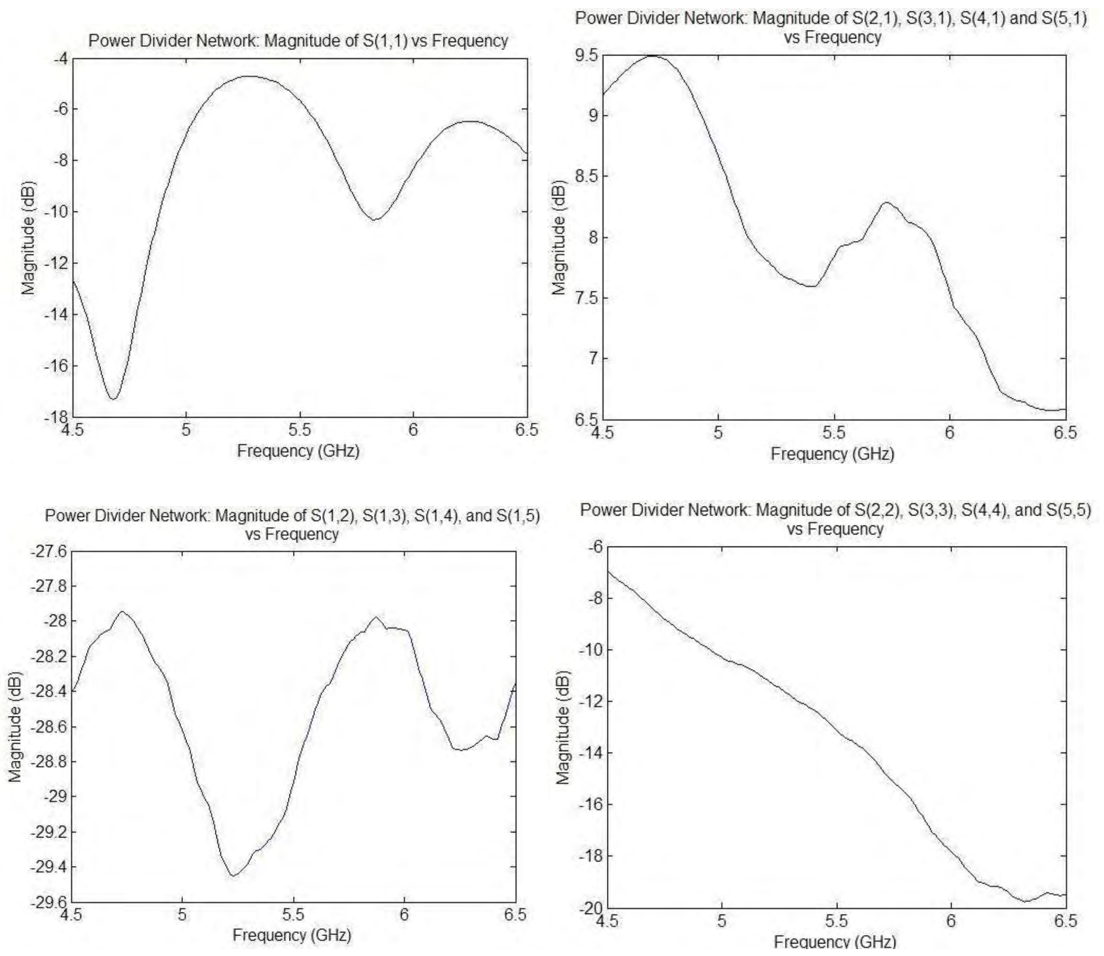

Figure 3.55 Magnitude of S-Parameters for Simulated Power Divider Network

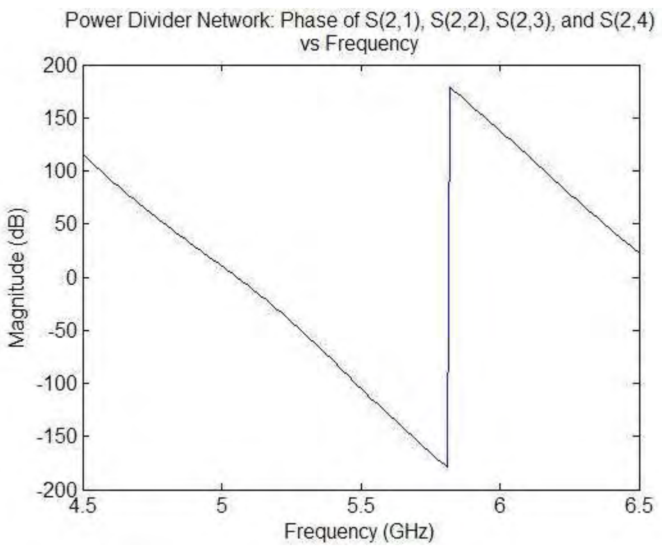

Figure 3.56 Phase of S-Parameters *S(2,1)*, *S(3,1)*, *S(4,1)*, and *S(5,1)* for Simulated Wilkinson Power Divider

After performing the simulations of the power divider network and confirming a fulfillment of the system requirements, the next step in the development of the RF up-conversion stage was the construction of the circuit. Figure 3.57 shows the circuit layout of the power divider network. With the help of Ansoft Designer's export utility, the *.dxf layout file was generated containing all the information necessary to construct a physical representation of the developed design. This *.dxf file is imported to Circuit CAM Software, which calculates the trajectory path of the router's drills in order to make the construction of the microwave circuit possible and stores this information into a *.cam file. The LPKF H-100 router was used to construct all the microwave circuits, including the antenna array. A router is a machine used to construct a PCB based on a layout file containing the PCB design. The BoardMaster software controls the operation of the HP1000 router using the file generated by Circuit CAM software. Figure 3.58 shows a picture of the constructed power divider network circuit. The printed circuit board (PCB) has rectangular dimensions of 116 mm x 90 mm. The distance between each output port of the Power Divider circuits is 26.6 mm, which is the inter-element distance between each antenna in the rectangular patch antenna array. Table 3.26 contains information of the components and the physical dimensions of the transmission lines in the Power Divider Network. An additional BNC connector was incorporated to provide the DC power supply port for the amplifiers in the circuit.

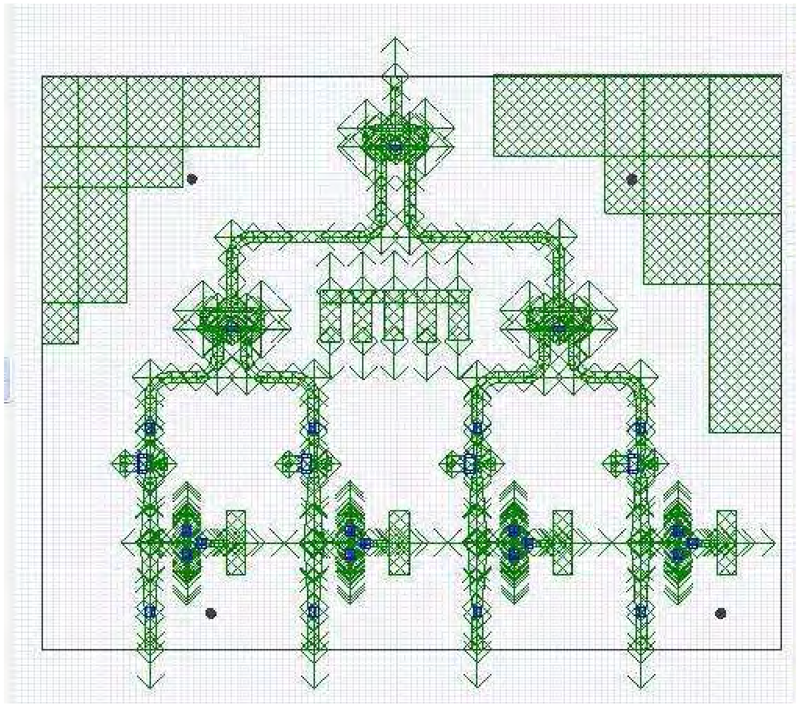

Figure 3.57 Layout of Power Divider circuit

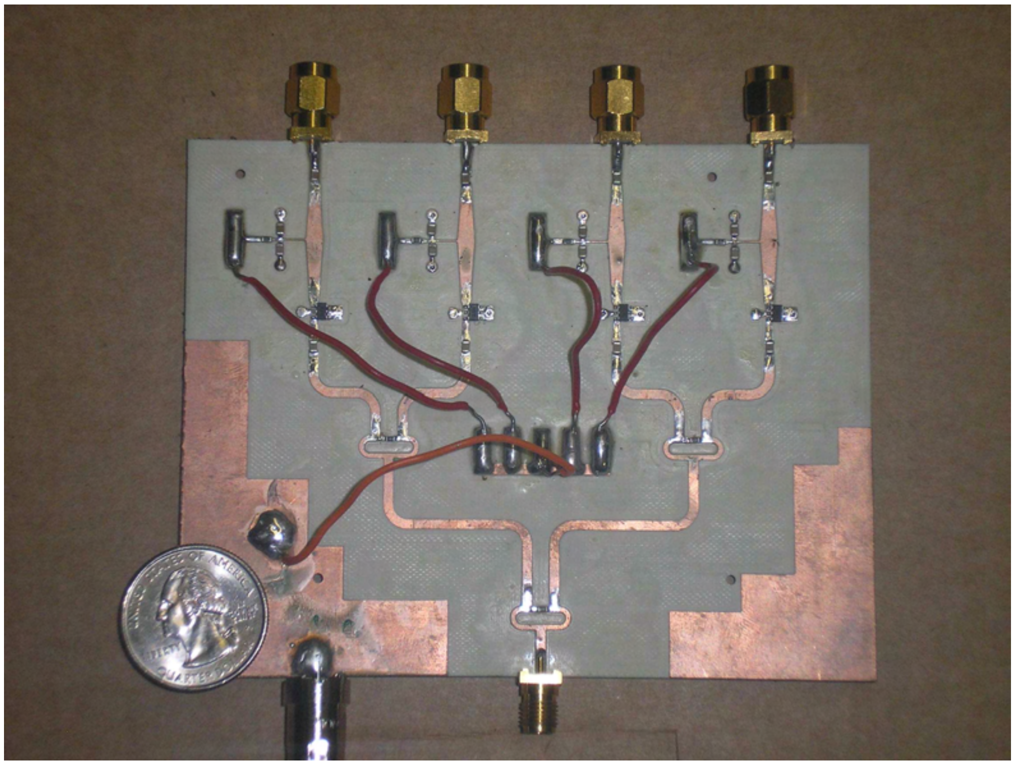

Figure 3.58 Picture of the Power Divider circuit

TABLE 3.26 Parameters of the Power Divider circuit

Parameter	**Value**
Wilkinson Power Dividers (WPD)	
Width of 50 transmission lines	1.7316 mm
Width of 50*√2 transmission lines	0.9444 mm
Length of $\lambda/4$ lines	7.8711 mm
Length of transmission lines interconnecting 1st WPD with 2nd WPD	42.5232 mm
Length of transmission lines interconnecting 2nd WPD with amplifiers	19.291 mm
Resistance of WPD resistor	100 Ω
Amplifier Stage	
Capacitance of DC Block Capacitors	0.1 µF

Capacitance of Bypass Capacitors	220 pF
Width of $\lambda/4$ High Impendance Transmission Lines in Bias-T	0.3171 mm
Length of $\lambda/4$ High Impedance Transmission Lines in Bias-T	4.0865 mm
Width of Low Impendance Line Section of Bias-T	3.03491 mm
Resistance of Bias Resistor	100 Ω
Power Supply Voltage	8 V

After constructing the 5 Power Divider Network circuits, the S-Parameters for each cricuit were measured to verify them with the results obtained in Ansoft Designer V2. The S-Paremeters of the circuits were tested using the Agilent 8510C Network Analyzer. The frequency range used to test the antennas was form 4.5 GHz to 6.5 GHz with a resolution of 201 frequency points. The test results were stored in citifile format files. A MATLAB file function named *sp_read(datafile,matfile)* (shown in Appendix A) was created to read the *datafile* file, retrieve the S-Parameter data, and store the data in a *matfile*.mat file. Figure 3.59 shows a rectangular plot of the S-Parameter *S(1,1)* for the 5 Power Divider Network circuits. The circuit with the highest *S(1,1)* magnitude at 5.85 GHz is Circuit 5 with -12.69 dB, which ensures that all the Power Divider Network circuits satisfy the requirement of VSWR lower than 2. Figure 3.60 shows a rectangular plot of the S-Parameters *S(2,1)*, *S(3,1)*, *S(4,1)* and *S(5,1)* for 5 Power Divider Network circuits. The plot uses the same legend as the plot in Figure 3.53. The average value of the gain of each output channel of the circuits is 4.78 dB for 5.85 GHz. Even though the gain is not 5 dB for every channel, gain compensation can be performed by the DBF at the mixer stage. Finally, Figure 3.61 shows a rectangular plot of the phase of S-Parameters *S(2,1)*, *S(3,1)*, *S(4,1)* and *S(5,1)* as a function of frequency. The average value of the phase of each output channel of the circuits is -97.56 for 5.85 GHz. The larges phase error between two output of any of the output channels is 80º. Still, this relative phase error can be compensated by the DBF at the mixer stage of the RF up-converter. Table 3.27 shows important S-Parameters values of Power Divider Circuit for 5.85 GHz.

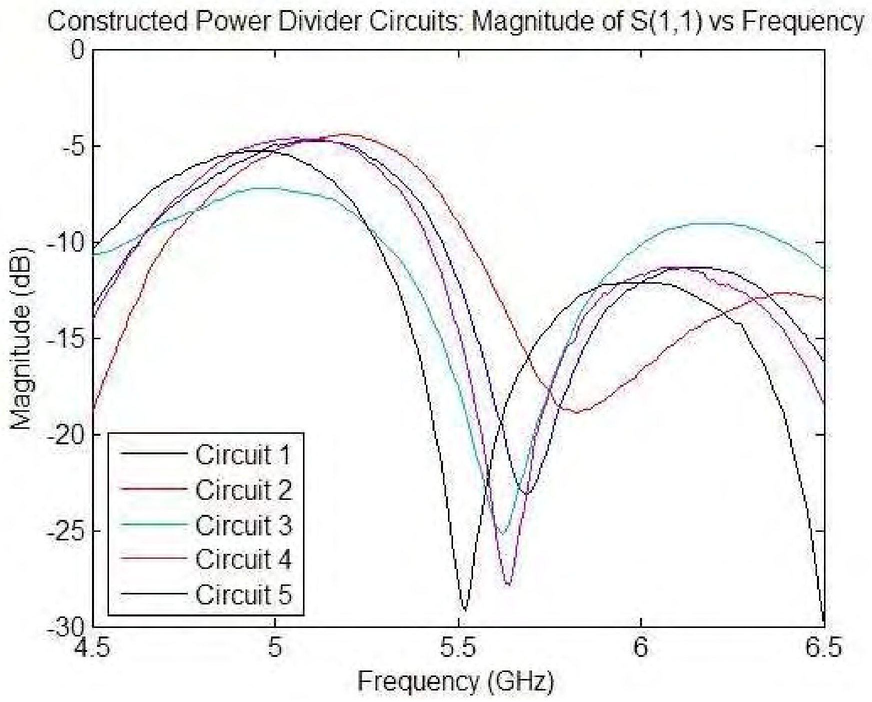

Figure 3.59 Magnitude of *S(1,1)* for all constructed Power Divider circuits

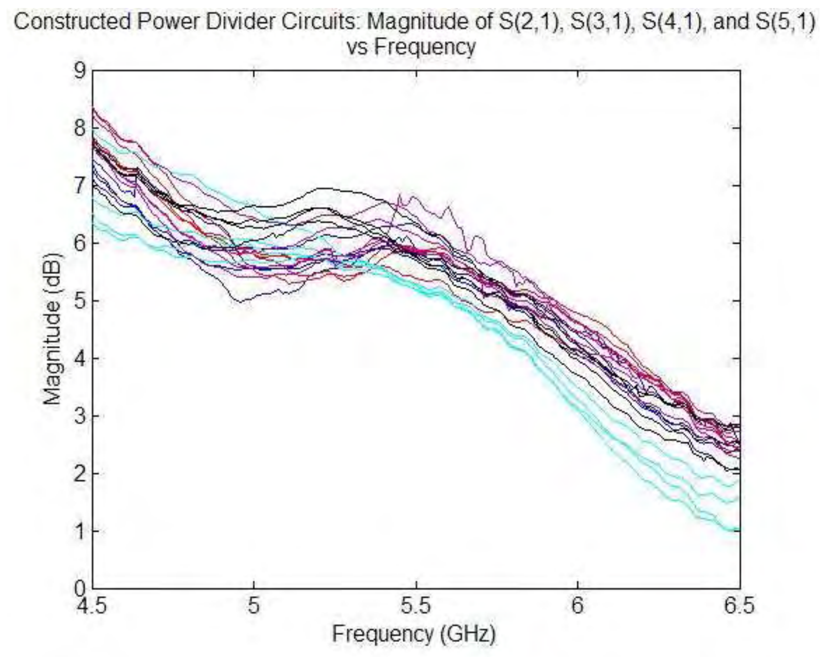

Figure 3.60 Magnitude of *S(2,1)*, *S(3,1)*, *S(4,1)*, and *S(5,1)* for all constructed Power Divider circuits

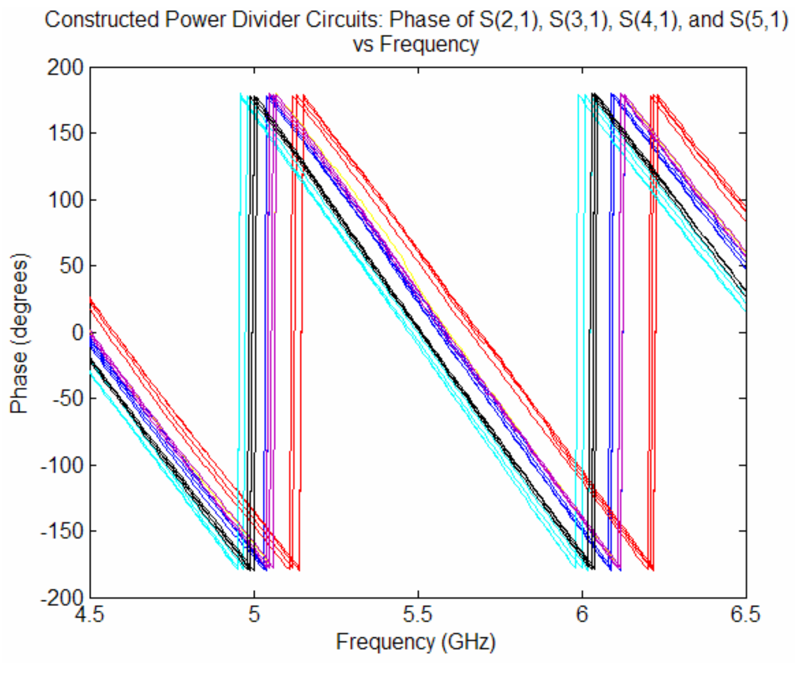

Figure 3.61 Phase of S(2,1), S(3,1), S(4,1), and S(5,1) for all constructed Power Divider circuits

TABLE 3.27 S-Parameters for Constructed Power Divider Network Circuits at 5.85 GHz

S-Parameter	Circuit 1	Circuit 2	Circuit 3	Circuit 4	Circuit 5
Magnitude of S(1,1)	-15.37 dB	-18.75 dB	-13.33 dB	-13.83 dB	-12.69 dB
Magnitude of S(2,1)	4.72 dB	4.61 dB	4.30 dB	5.33 dB	4.42 dB
Magnitude of S(3,1)	4.83 dB	4.86 dB	4.23 dB	5.36 dB	4.78 dB
Magnitude of S(4,1)	5.04 dB	5.09 dB	4.05 dB	4.96 dB	5.04 dB
Magnitude of S(5,1)	5.07 dB	5.17 dB	4.04 dB	4.86 dB	4.80 dB
Phase of S(2,1)	-99.06º	-63.02º	-121.95º	-91.18º	-116.42º
Phase of S(3,1)	-90.37º	-53.64º	-133.12º	-88.26º	-119.24º
Phase of S(4,1)	-98.23º	-55.30º	-128.02º	-89.55º	-119.16º
Phase of S(5,1)	-94.53º	-53.35º	-133.00º	-88.26º	-115.43º

The second circuit designed for the RF up-conversion stage combines the mixer stage and the power amplification stage into a single PCB. Each circuit contains 4 channels meaning that a total of 4 circuits are needed to implement the PAA with the 16-element rectangular patch antenna array. The mixer stage was implemented the Hittite HMC488MS8G Mixer. This IC mixer comes with an integrated amplifier to improve the gain of the LO signal prior mixing the two incoming signals. The mixer operates with an LO signal with a frequency range of 5.0 GHz to 6.0 GHz and an IF signal from DC to 2.5 GHz. The conversion loss of the mixer, which is the power ratio between the RF output signal and the IF input, is typically 8 dB. The mixer requires an external 10 nF bypass capacitor at the power supply terminal. The power amplification stage is implemented using the Hittite HMC407MS8G Power Amplifier. This power amplifier operates at a frequency range of 5.0 GHz to 7.0 GHz, with a gain of 15 dB, and a saturated power of +29 dBm. The power amplifier has an integrated power down capability pin, which can be used to power down the amplifier when transmission is not required reducing the consumption of the 230mA of supply current. The amplifier has a thermal paddle at the bottom, which needs to be connected to the ground of the circuit in order to improve the heat dissipation of the component. Three 220 pF bypass capacitors and a 2.2 μF Tantalum capacitor are needed at the voltage supply terminals to assure proper operation.

The mixer, which is the first stage in the second circuit, is a nonlinear device. Thus, the S-Parameter simulation, which is a linear operation calculating voltage ratio between circuit ports, cannot be performed. Still, the Ansoft Designer V2 software was used to construct the layout diagram. Transmission lines between the mixers and the power amplifiers were designed to satisfy the requirement of good 50Ω-impedance match at 5.85 GHz. Figure 3.62 shows the layout diagram of the second circuit. The circuit was constructed using the Circuit CAM software, the BoardMaster software and the H-100 router. Figure 3.63 shows the constructed circuit. Two signal generators and a spectrum analyzer were used to test the performance of the 4 constructed circuits. An IF signal of 0 dBm at 3 MHz and a LO signal of 0 dBm at 5.85 GHz were used as input to the circuit. Table 3.28 shows the power obtained at the output of each channel in the 4 circuits. Even though the relative power difference between each circuit is not zero, the IF signal coming from the DBF stage can be used to compensate for gain differences between the channels of the PAA.

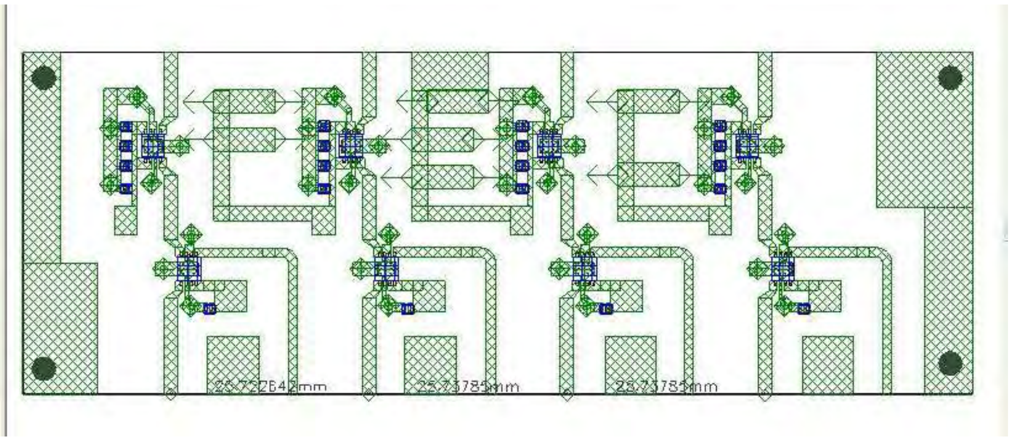

Figure 3.62 Layout of Mixer and Power Amplifier Circuit

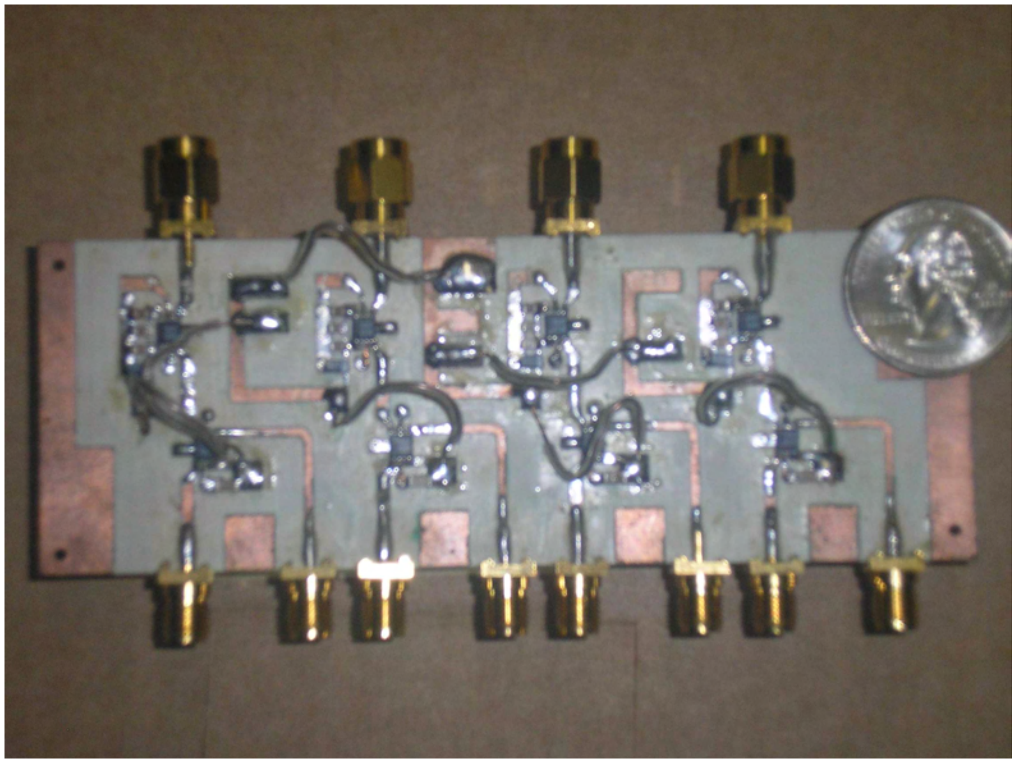

Figure 3.63 Picture of Mixer and Power Amplifier Circuit

TABLE 3.28 Power Gain of each PAA channel in the second circuit

Channel	Gain Circuit 1	Gain Circuit 2	Gain Circuit 3	Gain Circuit 4
Output Channel 1	1.33 dB	0 dB	-0.5 dB	0.5 dB
Output Channel 2	0.83 dB	1.8 dB	-1.5 dB	-1.5 dB
Output Channel 3	0.83 dB	-1.3 dB	-0.4 dB	-1.5 dB
Output Channel 4	0.5 dB	1 dB	-1.5 dB	-1.5 dB

3.4.3 Rectangular Patch Antenna Array

The rectangular patch antenna array used in the PAA transmitter consists of 4 x 4 array of microstrip patch antennas spaced in each axis by half-wavelength. Each patch antenna element has square dimensions of half-wavelength by half-wavelength. The antenna resonates at a frequency of 5.85 GHz with linear polarization. The antennas are fed by a coaxial probe feed connected through the PCB and attached to the ground plane of the array. The position of the inner conductor of the coaxial cable was placed at with respect to one of the edges to match the impedance of the antenna with the impedance of the system, which is $Z_0 = 50\ \Omega$. The antenna array was designed by Prof. Rafael Rodriguez-Solis. The parameters of the antenna array are summarized in Table 3.29.

TABLE 3.29 Parameters of the Rectangular Patch Array

Parameter	Value
Length of Patch Antenna	16.5 mm
Width of Patch Antenna	16.5 mm

Inter-element spacing in x-axis and y-axis	25.6 mm
Distance of probe feed in the x-axis	8.3 mm
Distance of probe feed in the y-axis	10.77 mm

The simulation of the antenna array was performed using Ansoft Designer V2, which calculates the S-Parameters and the current distribution of the antennas using the method of moments. The S-Parameters for the antenna port, which for a one-port network is *S(1,1)*, determines the amount of power loss as a result of impedance mismatch between the RF Up-conversion stage and the antenna. The current distribution in the antenna determines the type of polarization exhibited in the waves radiated or received by the antenna. Also, the Fourier Transform relates the current distribution along the antenna to its far-field pattern. The simulation was performed in a frequency range of 4.5 GHz to 6.5 GHz. Figure 3.64 shows the magnitude of the S-Parameter *S(1,1)* for all the antenna's in the rectangular array. The magnitude of *S(1,1)* -32.19 dB for a frequency of 5.85 GHz, thus satisfying the requirement for a *S(1,1)* magnitude lower than -10 dB, which is a Voltage Standing Wave Ratio (VSWR) smaller than 2. The Electric Field (E-Field) pattern of the array, shown in Figure 3.65, has a beamwidth of 24.5º with sidelobe levels of -13.8dB. The E-Field magnitude in the x-direction (E_x) and the E-Field magnitude in the y-direction (E_y) plots are show in Figure 3.66 for a field φ-plane cut of 0º. Since the magnitude of E_y is *20 dB lower than the magnitude of E_x, the antenna array exhibits linear polarization in the direction of E_x. Figure 3.67 shows the layout of the patch antenna array.

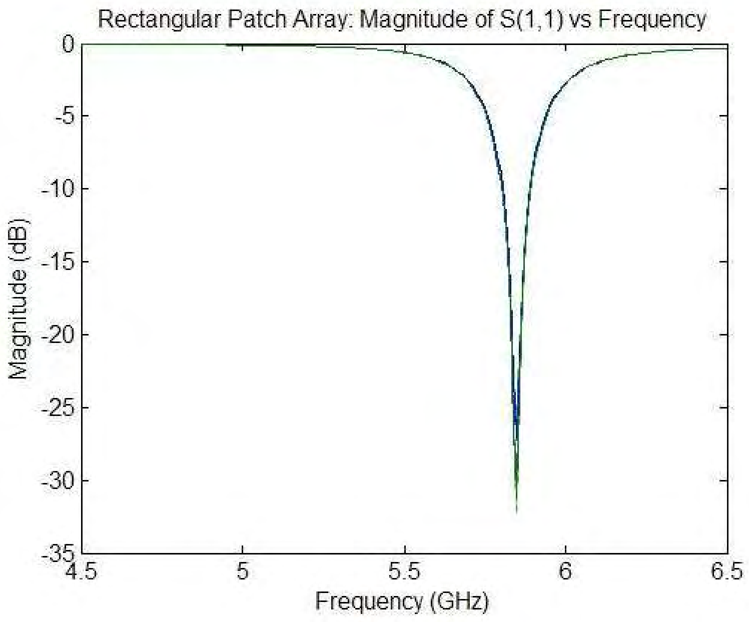

Figure 3.64 Magnitude of *S(1,1)* for antennas in Rectangular Patch Array

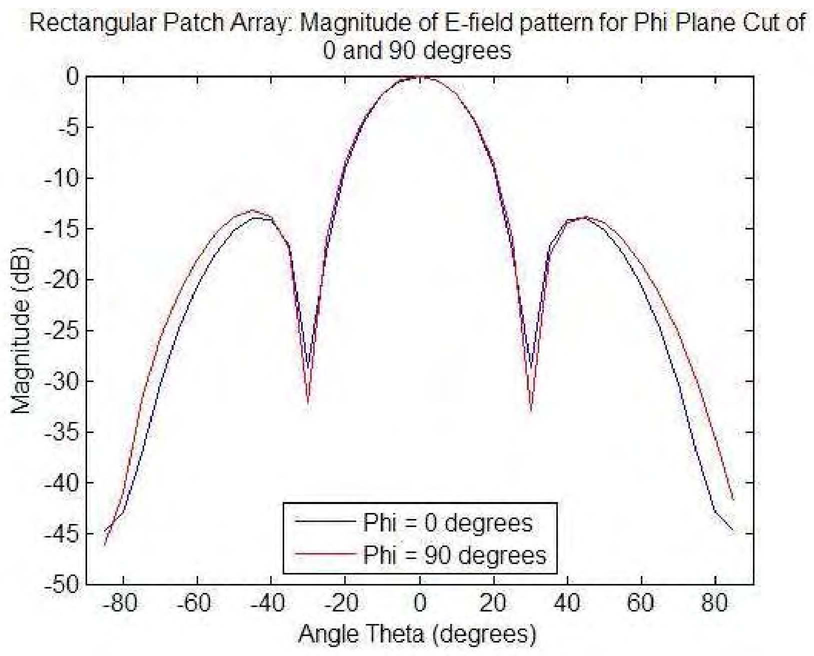

Figure 3.65 Magnitude of E-Field for antennas in Rectangular Patch Array on Plane Cut of φ = 0º and φ = 90º

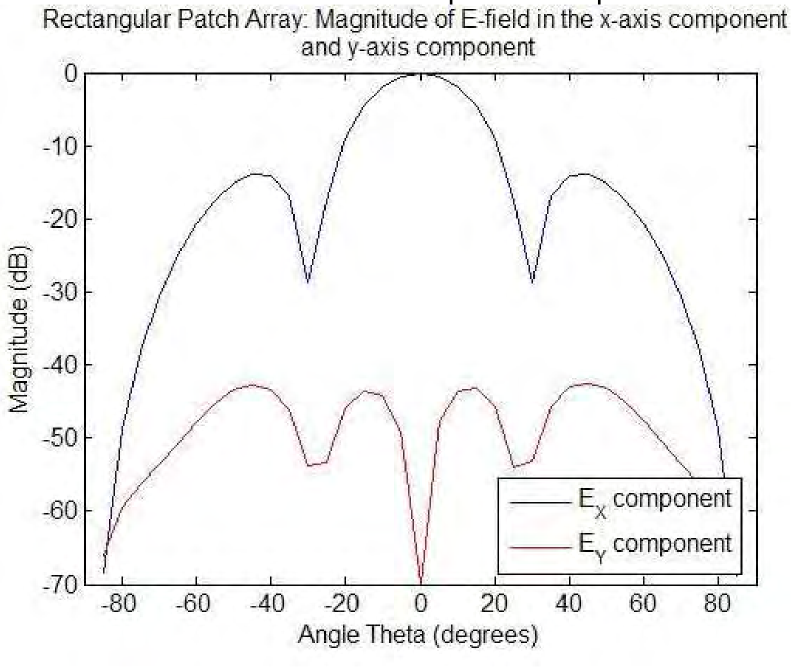

Figure 3.66 Magnitude of E-Field Components E_x and E_y

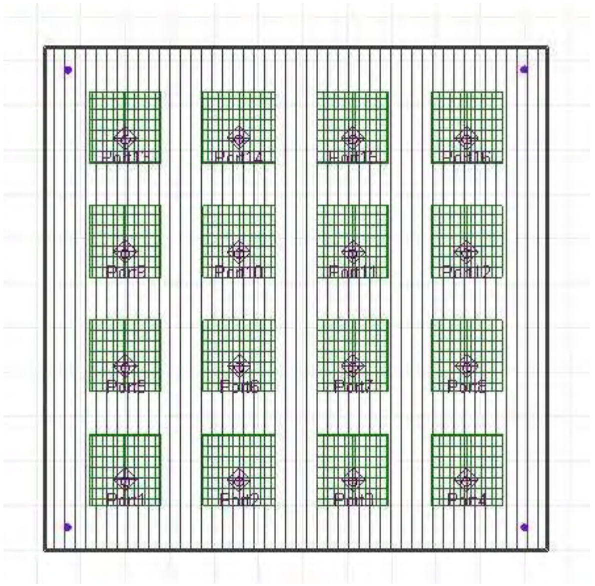

Figure 3.67 Layout of Rectangular Patch Antenna Array

Since the antenna array simulations results satisfied the specified requirements in terms of bandwidth and beam pattern characteristics, the next step in the process of implementing the PAA was the construction of the rectangular patch antenna array. Figure 3.68 shows a picture of the constructed rectangular patch array antenna. The S-Parameters for each antenna port in the constructed array was measured to verify the reflection coefficient of the antennas and compare them with the simulation results obtained in Ansoft Designer V2. The S-Paremeters of the antennas were tested using the Agilent 8510C Network Analyzer. The frequency range used to test the antennas was form 4.5 GHz to 6.5 GHz with a resolution of 201 frequency points. The test results for each antenna were stored in citifile format files. A MATLAB file function named *sp_read(datafile,matfile)* (shown in Appendix A) was created to read the *datafile* file, retrieve the S-Parameter data, and store the data in a *matfile*.mat file. Figure 3.69 shows a rectangular plot of the S-Parameter *S(1,1)* for all the antennas in the rectangular array. The Return Loss for a frequency of 5.85 GHz, which is the RF carrier frequency used in the microwave transmitter, is larger than 10 dB satisfying the system requirement of an antenna array with a VSWR smaller than 2.

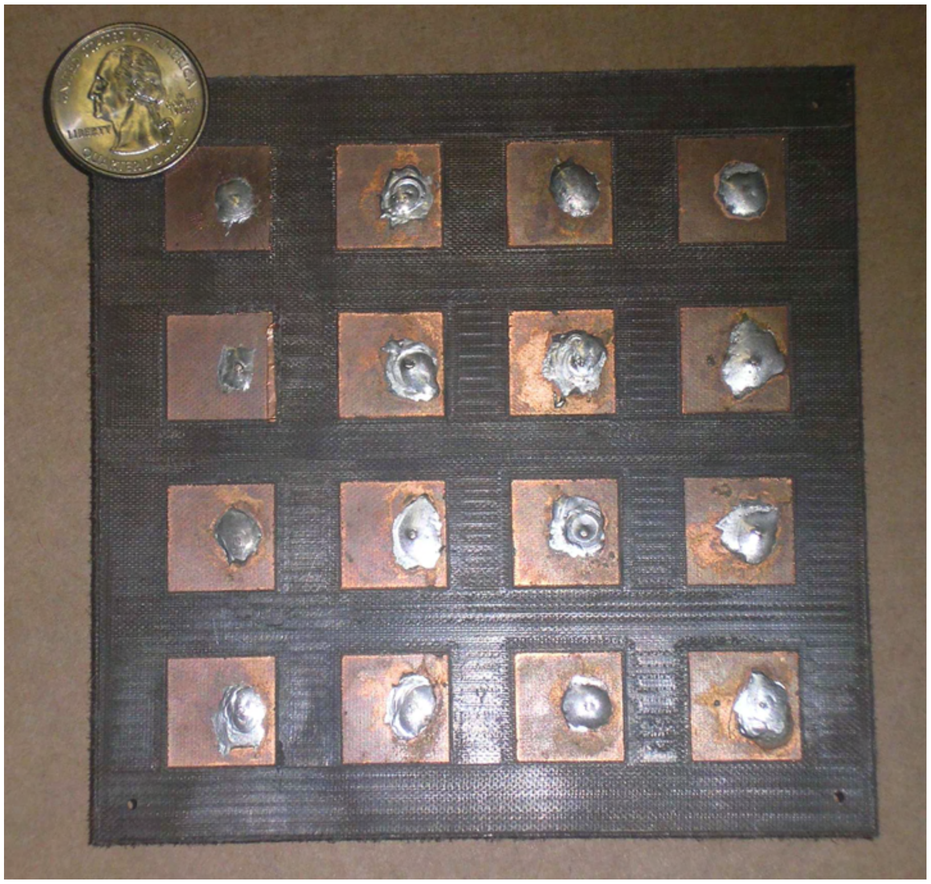

Figure 3.68 Picture of Rectangular Patch Antenna Array

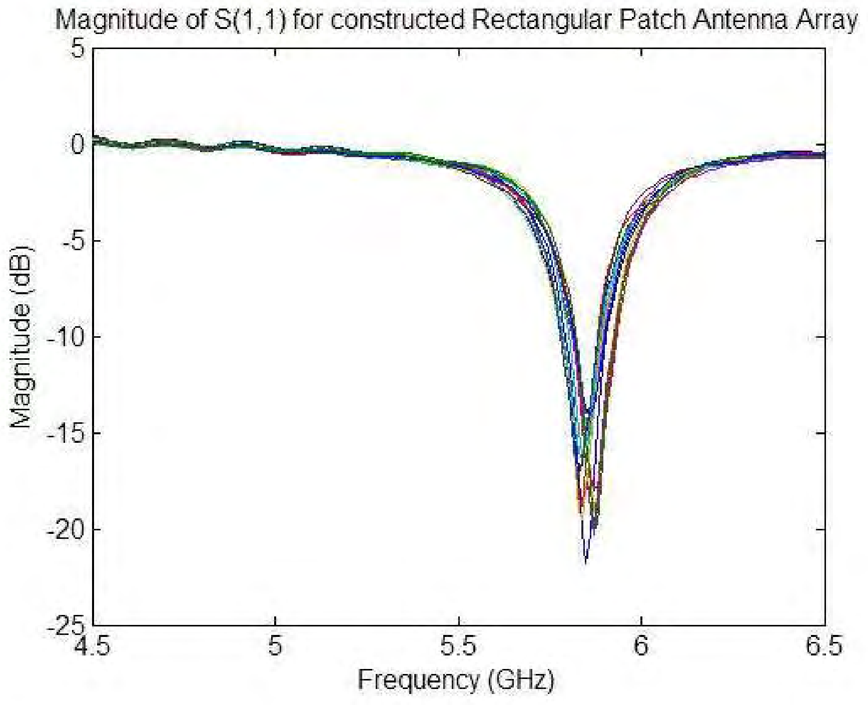

Figure 3.69 Magnitude of *S(1,1)* for antennas in constructed Rectangular Patch Antenna Array

3.4.4 PAA Measurement Results

After each PAA component was tested and fulfilled the specified system requirements, the last stage of this thesis project involved the measurement of the PAA transmitter's radiation pattern. The radiation pattern measurement was performed using the NSI spherical near-field measurement system located in an anechoic chamber on the Radiation Laboratory in Stefani Building Room 120. The measurement data was extracted using the NSI 2000 Software and processed using MATLAB program called *pattern_read()* (shown in Appendix A). The first measurement was performed on an antenna array composed of the LO Feed Network connected to the 16-element patch antenna array. The simulated top-view radiation pattern plot of this antenna array is shown in Figure 3.70. The beam pattern plot calculation considers changes in the antenna's current distribution produced by the relative gain and phase difference experimented by the LO feed network circuits. Figure 3.80 shows the measured top-view beam pattern plot, where the drift experimented in the main beam's angular position is approximately two degrees from broadside.

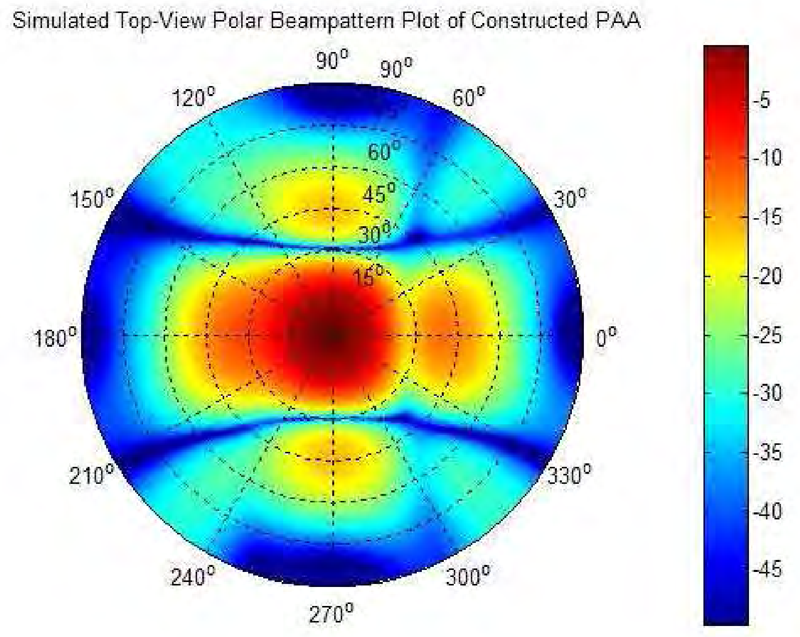

Figure 3.70 Simulated Top-View Polar Beam pattern Plot of the 16-element patch rectangular array with the LO Feed Network

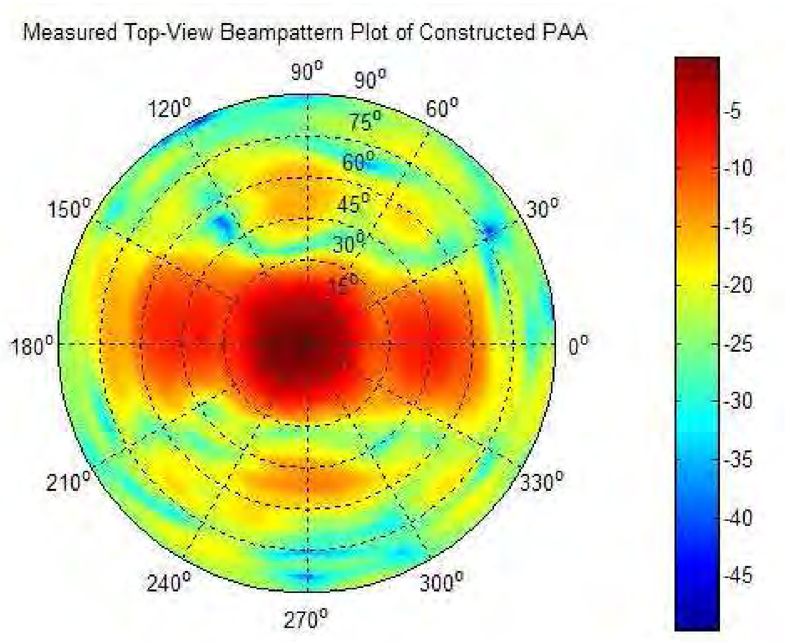

Figure 3.71 Measured Top-View Polar Beam pattern Plot of the 16-element patch rectangular array with the LO Feed Network

The second measurement was performed on the PAA transmitter, which is composed of the DBF Transmitter, LO Feed Network, the Mixer/Power Amplification Stage, and the 16-element rectangular patch array. A picture of the PAA transmitter (without DBF Transmitter) is shown in Figure 3.72. Figures 3.73 and 3.74 show the simulated and measured beam pattern plot of the PAA transmitter, respectively. The drift in the main beam's angular position is still approximately two degrees from broadside. An increase in sidelobe power levels was found in the measured beam pattern plot. Since these increase was not experienced in the first measurement, the gain and phase changes in the antenna element's current distribution is being significantly affected by the mixer/power amplification stage. To correct this problem, each channel of the PAA transmitter must be properly calibrated.

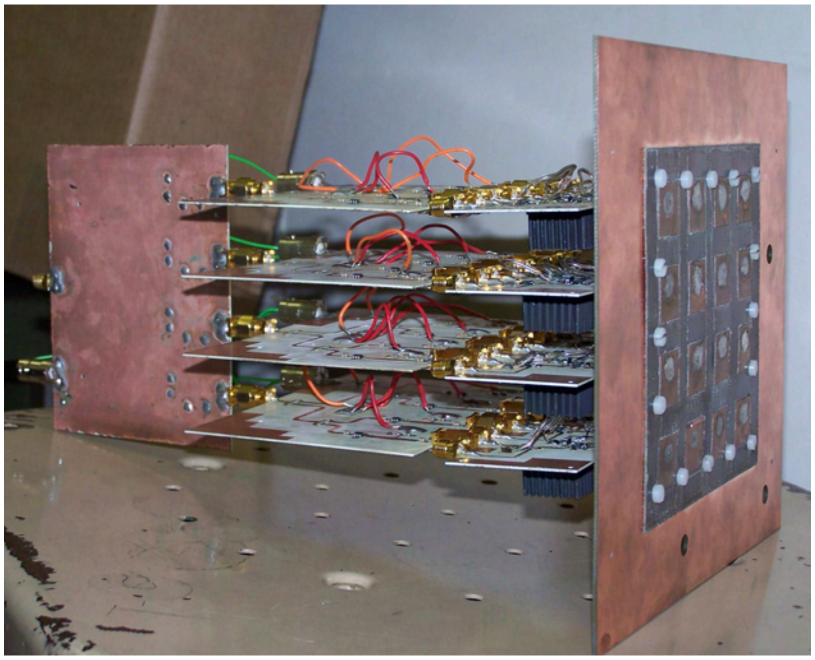

Figure 3.72 Picture of the PAA Transmitter

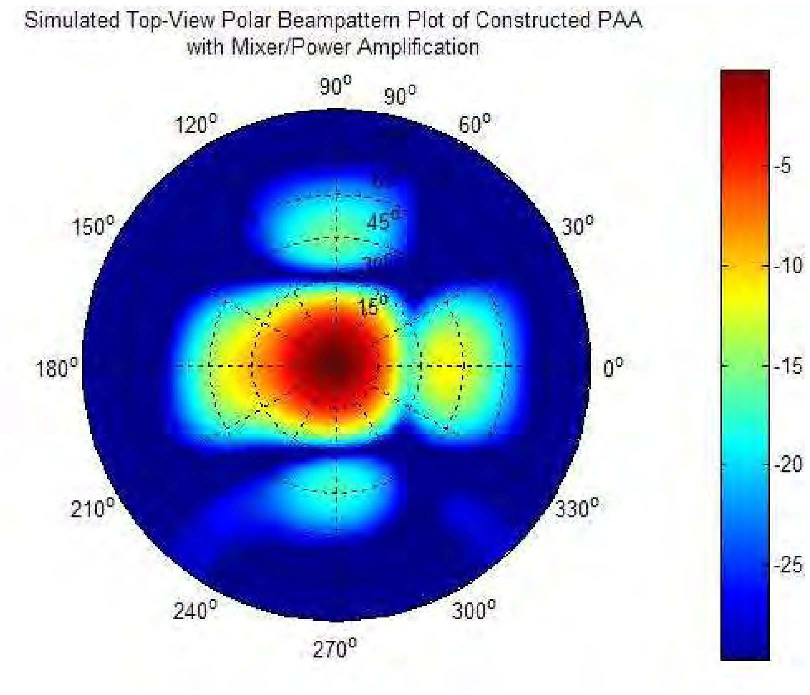

Figure 3.73 Simulated Top-View Polar Beam pattern Plot of Constructed PAA Transmitter

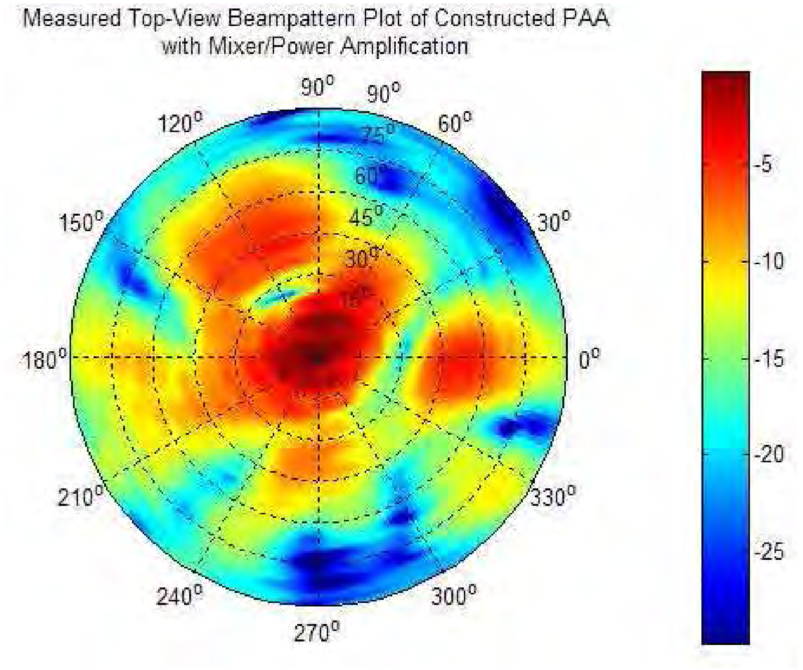

Figure 3.74 Measured Top-View Beam pattern Plot of Constructed PAA Transmitter

The last measurement was performed on the PAA Transmitter, where the DBF Transmitter implements the spatial filter discussed in Section 3.3.1. The spatial filter was constructed based on a uniform amplitude distribution with the MRA angle-of-transmission of φ = 0º and θ = 30º. Figure 3.75 shows the simulated top-view beam pattern plot of the PAA with the DBF Transmitter implementing the spatial filter. Differences between this beam pattern plot and the beam pattern plot shown in the simulation results on Figure 3.37 can be found, which result from using a non-isotropic element (patch antenna) as the sensor array and gain/phase changes introduced by the linear amplifiers in the LO feed network and the Mixer/Amplification Stage. The measured beam pattern plot in the anechoic chamber is shown in Figure 3.76. The MRA angle-of-transmission of the resulting beam pattern points at φ = 5.4° and θ = 35.1°, which represents an error of approximately 5 degrees in each angular direction. The measured results still show an increase in sidelobe levels, which is produced from gain/phase changes introduced by the rf components in the RF Conversion Stage. Figure 3.77 and Figure 3.78 show surf plots of the simulated and measured PAA Transmitter beam pattern magnitude, respectively.

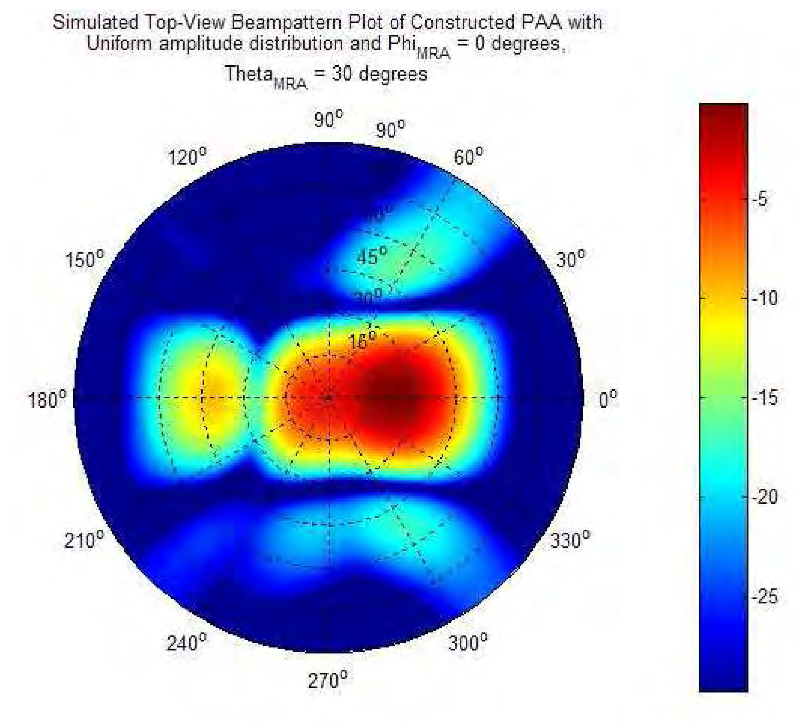

Figure 3.75 Simulated Top-View Beam pattern Plot of PAA Transmitter with Uniform Amplitude Distribution pointing at φ_{MRA} = 0° and θ_{MRA} = 30°

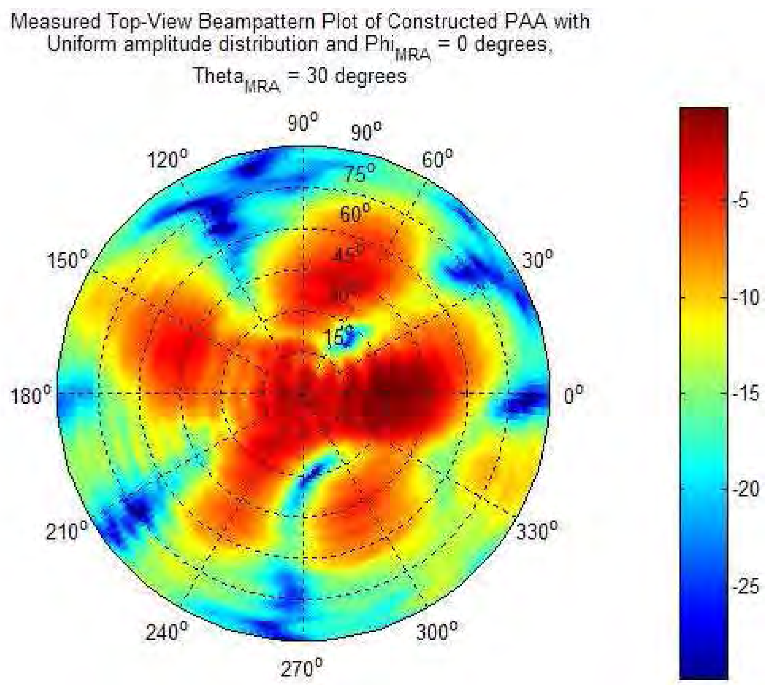

Figure 3.76 Measured Top-View Beam pattern Plot of PAA Transmitter with Uniform Amplitude Distribution pointing at φ_{MRA} = 0° and θ_{MRA} = 30°

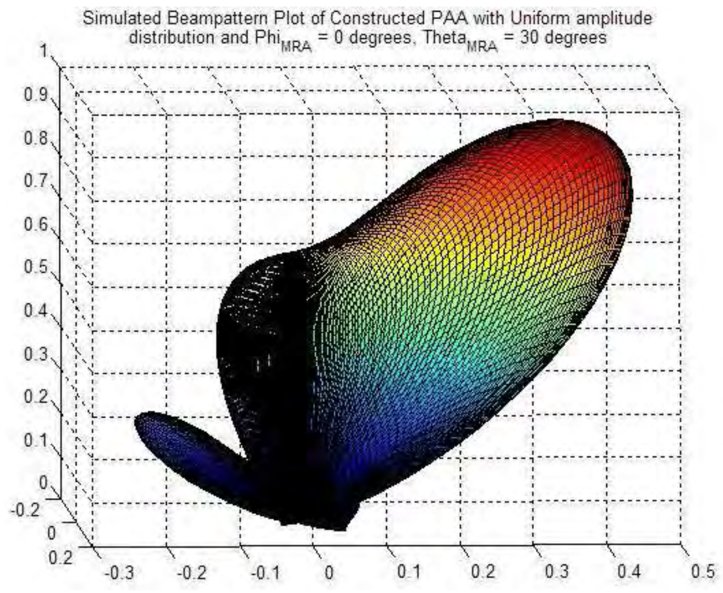

Figure 3.77 Simulated Surf Plot of Beam pattern Magnitude for a PAA Transmitter with Uniform Amplitude Distribution pointing at φ_{MRA} = 0° and θ_{MRA} = 30°

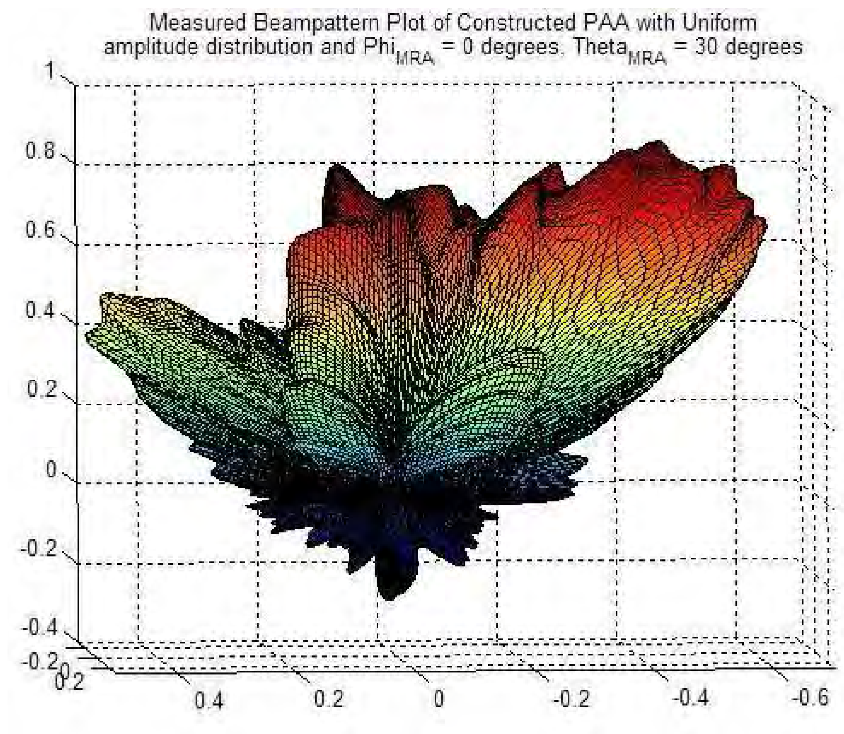

Figure 3.78 Measured Surf Plot of Beam pattern Magnitude for a PAA Transmitter with Uniform Amplitude Distribution pointing at φ_{MRA} = 0º and θ_{MRA} = 30º

4 CONCLUSIONS AND FUTURE WORK

4.1 Conclusions

After comparing the beam pattern results obtained for the theoretical, simulated and measured data, it can be seen that the Digital Beamformer has proven to be a versatile option as a controller for a Phased Array Antenna. The PAA measured results obtained showed an increase in sidelobe level due to the gain/phase changes in the linear amplifiers, mixers, and power amplifiers. This can be corrected by calibrating each channel of the PAA, where the error introduced by the RF components in the current distribution on the antennas of the array is considered in the calculation of the complex weight of each DBF channel. Thus, the digital implementation of the control architecture in the PAA provides flexibility in the design of each stage, making it suitable for applications where controlling special requirements in the beam pattern of a sensor array is necessary. The DBF transmitter and receiver design model can be derived from the mathematical model describing a far-field plane wave intersecting an array of sensors. If the bandwidth of the signal is small compared to the maximum travel time of the plane wave across the antenna array, the narrowband beamformer model can be employed in the implementation of a PAA.

Compared to the Delay-and-Sum Beamformer model, which uses time delays in each channel as a means of creating the beam pattern, the Narrowband Beamformer model can be expressed as a Finite Impulse Response (FIR) spatial filter with complex coefficients operating on a space-time signal. In the case of the antenna array, the weight coefficients control the amplitude and relative phase of the current in the antennas. Since the current distribution is related to the beam pattern of an antenna by the Fourier Transform, a synthesized beam pattern can be implemented by carefully choosing the coefficients of each antenna channel in the array. The resulting spatial filter, thus, can be used in the DBF receiver or transmitter to create a beam pattern based on the geometrical distribution of the antennas in the array. The results obtained in each simulation prove the versatility of the DBF in implementing the control of a PAA. Different spatial filters were tested, where each one represented particular beam pattern characteristics. The simulations, which were performed in MATLAB's Simulink using software code representing FPGA hardware based on Xilinx's System Generator for DSP Blockset, gave results closely matching the results obtained from a theoretical DBF. After obtaining successful simulations results, the System Generator for DSP tool was used to transform the DBF transmitter design into VHDL code. The resulting code was used to program the FPGA in the digital processing board.

Another advantage offered by the DBF is its independence on the geometrical distribution of the array. A DBF with an *N*-channel capacity is able to operate on a PAA with *N*-elements, not mattering if the *N* elements are distributed linearly, rectangularly, cubically, etc. The calculation of the weight coefficients of the spatial filter is the operation which considers the geometrical distribution of the array. As for the physical implementation of the PAA, the RF up-conversion stage and the antenna array were designed and constructed based on the system requirements of a microwave transmitter operating in the C band frequency. The RF up-conversion stage was implemented using two microwave circuits: a power divider circuit which distributed the LO signal into each antenna channel and a mixer/power amplification signal which performed the RF modulation and amplification of the RF signal before the antenna array stage. The simulations and the testing results of both circuits satisfied most of the system requirements of the PAA microwave transmitter. The relative amplitude and phase errors found between antenna channels may be corrected in the DBF transmitter stage. The rectangular antenna array also fulfilled the system requirements, providing a good return loss at the RF carrier frequency for a system impedance of 50Ω.

4.2 Future Work

Even though the design of the DBF receiver and transmitter was greatly simplified, future work should be addressed on improving the DBF design in terms of component reduction. The presented DBF model is a scalable model, capable of being implemented for any array size, as long as the spatial filter weight coefficient calculation has considered the number of elements and the geometrical distribution of the antenna array. Still, a large PAA with very strict beam pattern requirements might prove to be costly and complex in terms of system integration. Alternative PAA designs must be considered, where reducing the complexity of the design should lie on how rigorous the system requirements of the application containing the PAA are. For example, if the system requires a beam pattern with a single MRA beam and MRA steering control, the progressive phase shift nature found in the currents of the antenna array can be exploited to reduce the complexity of the PAA system. Figure 4.1 shows a diagram of a simplified PAA implementation for a single MRA-beam beam pattern known as row-column phasing architecture [*Corey*, 1996]. The PAA uses a phase-shifted LO signal and a phase-shifted IF signal to generate the progressive phase shift necessary to steer the beam into a desired direction. If the LO signal is mixed twice, where one mixing stage adds the relative phase shift in the x-axis and the second mixing stage adds the relative phase shift in the y-axis (Eq. 3.12), theoretically an $L*M$ antenna array can be controlled by processing $L+M$ IF signals in the DBF stage. Still, the condition of a fixed amplitude value in the input of the mixers might limit the dynamic range of the weight coefficient's amplitude in the DBF transmitter.

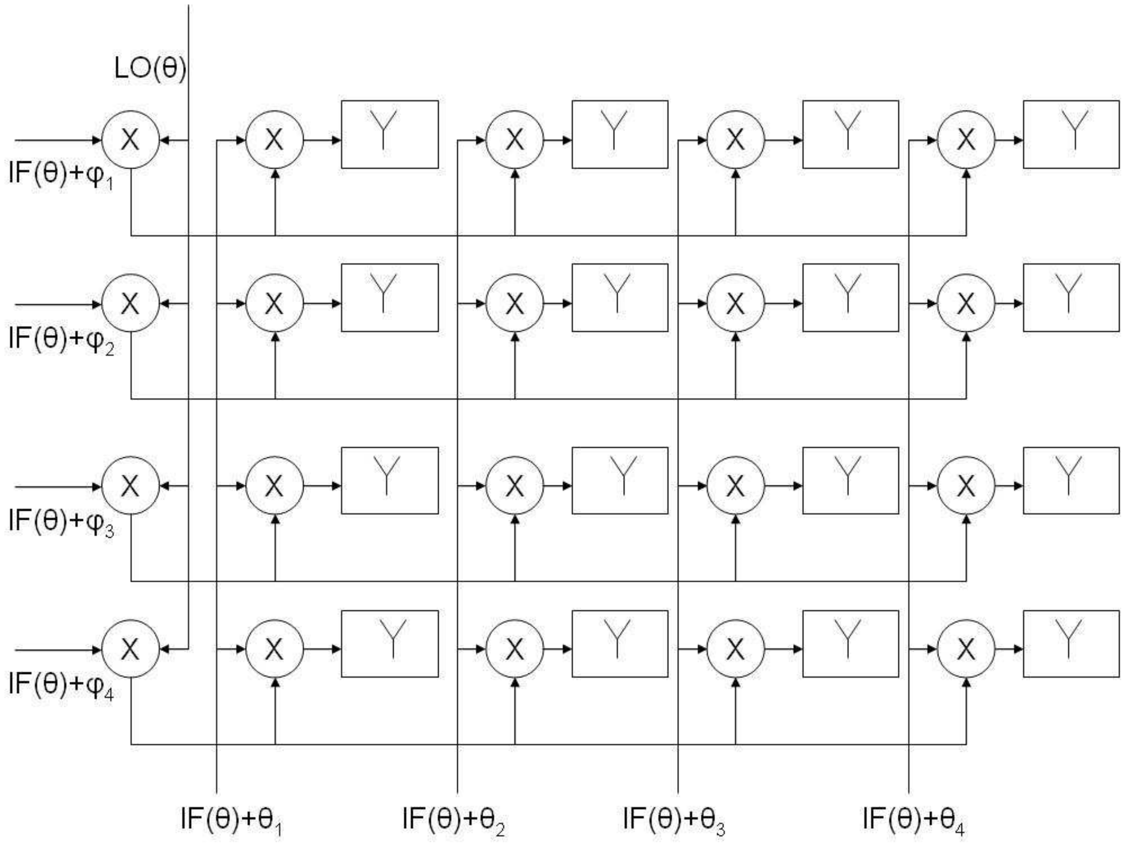

Figure 4.1 Diagram of PAA with single MRA beam and steering capability

Also, future work should be concentrated on the scalability of the DBF receiver and DBF transmitter. Although the FPGA provided flexibility in the creation of the DBF design, a system topology where ICs are used in certain substages of the DBF might reduce the cost of implementing a PAA. For example, semiconductor companies such as TI and Analog Devices provide ICs such as GC5016 (TI) and AD6654 (Analog Devices) which perform the Digital Down-conversion and Digital Up-conversion at high speeds. Some ICs may even have an integrated ADC/DAC and provide the two conversion modes into a single chip. Still, an FPGA would be very useful in performing the necessary “gluelogic” in order to interconnect the different digital devices in the DBF receiver/transmitter. The FPGA’s use as an interconnection component versus a signal processing component might increase its capacity in terms of number of DBF channels interconnected by a single FPGA. If low sampling frequencies can be obtained on the signal processing stage in the DBF, a DSP can be used to perform weight coefficient calculation.

Finally, the use of an analog pre-processor might improve the performance of a PAA with strict system requirements. RF Discrete Lens Antenna Arrays (DLAA) might be used to transform the signals from an element-space domain into a beamspace signal domain, were each signal in the DBF receiver or transmitter represents beams that are separated by space instead of being signals separated by distance. In this approach, a spatial filter with real coefficients might satisfy the beam pattern characteristics of the PAA. However, the use of a DLAA requires a change in the way signals are processed inside the DBF [*Torres*, 2005]. Algorithms which only considers power incidence at the antennas on the focal surface of the DLAA are suitable for this type of systems.

REFERENCES

Alliot S., "**THEA Adaptive Weight Estimation, implemented on a DSP**"; Tech. Report, ASTRON, Dwingeloo, March 2000.

Alliot S., Cazamier W., "**Beamforming Interpolation for THEA**"; Research Report-THEA-00024, Astron: October 2000.

Balanis C.A., **Antenna Theory: Analysis and Design**, Second Edition, John Wiley & Sons, New York, 1997.

Chang, D.C.D.; Klimczak, W.N.; Busche, G.C. **"An Experimental Digital Beamforming Array"**; Antennas and Propagation Society International Symposium, 1988. AP-S. Digest, 6-10 June 1988; Pages: 1300 - 1303 vol.3.

Corey, L **"A Survey of Russian Low Cost Phased-Array Technology"**; Antennas and Propagation Society International Symposium, 1988. AP-S. Digest, 6-10 June 1988; Pages: 1300 - 1303 vol.3.

Dreher, A.; Hekmat, T.; Niklasch, N.E.; Lieke, M.; Klefenz, F.; Schroth, A. "**Planar Digital-Beamforming Antenna for Satellite Navigation**"; Microwave Symposium Digest, 1999 IEEE MTT-S International , Volume: 2 , 13-19; June 1999 Pages:647 - 650 vol.2

Dreher, A.; Niklasch, N.; Klefenz, F.; Schroth, A. "**Antenna and Receiver System with Digital Beamforming for Satellite Navigation and Communication**"; Microwave Theory and Techniques, IEEE Transactions on , Volume: 51 , Issue: 7 , July 2003; Pages:1815 - 1821

Franks L. E., **Signal Theory**, Prentice-Hall, Englewood Cliffs, N.J., 1969.

Garret P. H., **Analog I/O Design: Acquisiton: Conversion: Recovery**, Reston Publishing Company, Reston, 1981

Harris F. J. "**Multirate FIR Filters for Interpolating and Desampling**", Handbook of Digital Signal Processing: Engineering Applications, Academic Press, San Diego, 1987

Hatcher, B. R. "**Granularity of Beam Positions in Digital Phased Arrays**"; Proceedings of the IEEE, Volume: 56, Issue: 11, November 1968; Pages:1795 - 1800

Haynes T., "**A Primer on Digital Beamforming**"; Spectrum Signal Processing.

Hiemstra L., "**Real-Time Digital Signal Processing implemented on a Multi-Processor System**"; Tech. Report., NFRA, Dwingeloo, July 2000.

Hogenauer E., "**An Economical Class of Digital Filters for Decimation and Interpolation**", *Acoustics, Speech, and Signal Processing,* IEEE Transactions on Volume 29, Issue 2, Apr 1981, Pages:155-162.

Kajala, M.; Hamalainen, M. "**Filter-and-Sum Beamformer with Adjustable Filter Characteristics**"; Acoustics, Speech, and Signal Processing, 2001. Proceedings. (ICASSP '01). 2001 IEEE International Conference on, Volume: 5, 7-11; May 2001 Pages:2917 - 2920 vol.5.

Kajala, M.; Hamaldinen, M. "**Broadband Beamforming Optimization for Speech Enhancement in Noisy Environments**"; Applications of Signal Processing to Audio and Acoustics, 1999 IEEE Workshop on , 17-20; Oct. 1999 Pages:19 – 22.

Lyrtech Processing Company, **SM-VHS-DAC User's Manual**, November 2004

Manassewitch V., **Frequency Synthesizers: Theory and Design**, Second Edition. John Wiley & Sons, New York, 1980.

Miura, R.; Tanaka, T.; Chiba, I.; Horie, A.; Karasawa, Y. "**Beamforming Experiment with a DBF Multibeam Antenna in a Mobile Satellite Environment**" ; Antennas and Propagation, IEEE Transactions on , Volume: 45 , Issue: 4 , April 1997; Pages:707 – 714

Mucci R., "**A Comparison of Efficient Beamforming Algorithms"**, Acoustics, Speech, and Signal Processing [see also IEEE Transactions on Signal Processing], IEEE Transactions on Volume 32, Issue 3, Jun 1984 Page(s):548 - 558

Pozar D. M., **Microwave Engineering**, Second Edition. John Wiley & Sons, New York, 1998.

Simonangeli L. J., Agrawal A., "**A C-Band Digital Beamforming Array"**, Antennas and Propagation Society International Symposium, 1988. AP-S. Digest 6-10 June 1988 Page(s):1385 - 1388 vol.3

Steyskal, H., **"Digital Beamforming – An Emerging Approach";** Military Communications Conference, 1988. MILCOM 88, Conference record. '21st Century Military Communications - What's Possible?' 1988 IEEE, 23-26 Oct. 1988; Pages: 399 - 403 vol.2.

Torres-Rosario J. A., Rodríguez-Solís R., Hunt S., Popovic Z., "**Adaptive Discrete Lens Antenna Array for Direction of Arrival Detection**", Antennas and Propagation Society International Symposium, 2005. AP-S. Digest, 6-10 June 2005.

Van Trees, Harry L. **Optimum Array Processing: Detection, Estimation, and Modulation Theory, Part IV**. Wiley Interscience, New York, 2002

APPENDIX A. MATLAB CODE FILES

```
%% File: linear_steering_array.m

clear;
clc;

% Number of Elements
N = 4;

% Antenna Array Vector
n = 0:(N-1);

% MRA Angle Theta
theta_d = 45;
sai_d = pi*cos(theta_d*pi/180);

% Weight Coefficients
w = (1/N)*exp(j*(n.'-(N-1)/2)*sai_d);

% Parameters prior sampling of the Beampattern
sample = 1000;
theta = 0:(180/sample):180;
sai = pi*cos(theta*pi/180);

% Calculation of the Beampattern
SA = 0;
BSA_max = 0;
for k=1:length(theta)

   v = exp(j*(n - (N-1)/2)*sai(k));
   v_sai(:,k) = v.';

   B(k) = w'*v_sai(:,k);

   SA = SA + 0.5*abs(B(k)).^2*sin(theta(k)*pi/180)*(180/sample)*(pi/180);

   if(abs(B(k))>BSA_max)
      BSA_max = abs(B(k));
   end

end

% Calculation of Directivity
D = 10*log10(BSA_max.^2/SA);

B_max = max(B);
Bl_max = 20*log10(B_max);
B_min = min(B);
Bl_min = 20*log10(B_min);
```

```
% Calculation of Beamwidth
B_3dB = B_max/2;
theta_beam = theta([abs(B)]>=B_3dB);
Beamwidth_theta = theta(610)-theta(1);

% Result Figures
figure(1)
polar(theta*pi/180,abs(B));

figure(2)
plot(theta,20*log10(abs(B)));

%% File: linear_DBFreceiver_parameters.m

% Information Signal
fis = 0;
sig_ts = 1e-9;
samp_period = 100;

% Carrier Signal
fif = 3e6;
i_phase = pi/2-2*pi*(fif)*(3/200e6);

% ADC Parameters
adc_ts = 1/200e6;
adc_bit_res = 14;
adc_point_res = 12;

% Operation Precision Parameters
% Adder Block Parameters
add_bit_width = 14;
add_point_width = 12;
% Multiply Block Parameters
mult_bit_width = 18;
mult_point_width = 16;
mult_latency = 3;
% Operator Parameters
prec_bit_width = 18;
prec_point_width = 16;

% Antenna Weights and Digital Beamformer
w_amp = abs(w);
phase_res = 8;
w_phase_d = angle(w)*180/pi;
w_phase_r = angle(w);
bit_phase = w_phase_r*2^phase_res/(2*pi);
db_ts = 1/50e6;
wamp_bit_res = 16;
wamp_point_res = 14;
wphase_bit_res = phase_res;
wphase_point_res = 0;
```

```
% Max Time Delay
plane_wave_angle = 0;
ant_spacing = 0.5;
fant = 8.2e9;
maxt = ant_spacing/fif;
sim_t = 1e-5;
slope_t = maxt/sim_t;

% DDS Parameters
output_width = 32;
flo = fif;
ddc_ts = adc_ts;
npi = flo*ddc_ts;

% Scope Parameters
scope_ts = 1e-11;
scope_sig = 1e-11;

% Latency Repair
lat_n = 12;
lat_time = lat_n*100e-9;
total_time = lat_time+sim_t;

% CIC Specs
d_sample = db_ts/adc_ts;
n_stages = 8;
cic_lat = 8;
diff_delay = 2;
force_bit_width = 45;
scale_factor = 0;

% Butterworth Analog Filter for post-processing
[Nb,Wnb]=buttord(3e6*db_ts,4e6*db_ts,3,25);
[Bb,Ab]=butter(Nb,Wnb);

% Gain of IF Signal prior Time Delay
K2 = 0.99;
K1 = 1;

%% File: linear_DBFreceiver_results.m

clear all;
clear;

% load MAT Files
load signal_out_0;
load signal_out_1;
load signal_out_2;
load signal_out_3;
load signal_out_4;
load signal_out_5;
```

```
% Simulation Parameters
total_time = 1e-5;
db_ts = 1/50e6;
delta_index = total_time/db_ts;
angle_low_index = 251;
angle_high_index = angle_low_index+delta_index;
mag_low_index = 310;
mag_high_index = mag_low_index+delta_index;
phase_low_index = 310;
phase_high_index = phase_low_index+delta_index;

% Retrieving Beampattern Results
angle = [fliplr(angle_0_90(2,angle_low_index:angle_high_index))
angle_90_180(2,(angle_low_index+1):angle_high_index)];
mag = [fliplr(mag_0_90(2,mag_low_index:mag_high_index))
mag_90_180(2,(mag_low_index+1):mag_high_index)];
mag = mag/max(mag);
phase = [fliplr(phase_0_90(2,phase_low_index:phase_high_index))
phase_90_180(2,(phase_low_index+1):phase_high_index)];

% Calculation of Directivity in Beampattern
SA = 0;
BSA_max = 0;
for k=1:(length(angle)-1)

   SA = SA + 0.5*mag(k).^2*sin(angle(k)*pi/180)*(angle(k+1)-angle(k))*(pi/180);

   if(mag(k)>BSA_max)
      BSA_max = mag(k);
   end

end
D = 10*log10(BSA_max.^2/SA);

% Result Figures
figure(1)
polar(angle*pi/180,mag);

figure(2)
plot(angle,20*log10(mag));

%% File: linear_DBFreceiver_nullplacer.m

clear;
clc;

% Number of Antennas
N = 4;

% Generation of Antenna Array Vector
n = 0:(N-1);
```

```
% Calculation of Weight Coefficients based on Null Placement parameters
Bd = [1 zeros(1,N-1)];
MRA = 0;
Nulls = [30 60 100];
theta_d = [MRA Nulls];
sai_d = pi*cos(theta_d*pi/180);

for k=1:length(theta_d)

   v = exp(j*(n - (N-1)/2)*sai_d(k));
   v_sai_d(:,k) = v.';

end

w = (inv(v_sai_d))'*Bd';


% Parameters prior sampling of the Beampatter
sample = 1000;
theta = 0:(180/sample):180;
sai = pi*cos(theta*pi/180);

% Calculation of the Beampattern
SA = 0;
BSA_max = 0;
for k=1:length(theta)

   v = exp(j*(n - (N-1)/2)*sai(k));
   v_sai(:,k) = v.';

   B(k) = w'*v_sai(:,k);

   SA = SA + 0.5*abs(B(k)).^2*sin(theta(k)*pi/180)*(180/sample)*(pi/180);

   if(abs(B(k))>BSA_max)
      BSA_max = abs(B(k));
   end

end


% Calculation of the Directivity
D = 10*log10(BSA_max.^2/SA);


B = B/max(B);

B_max = abs(max(B));
Bl_max = 20*log10(B_max);
B_min = abs(min(B));
Bl_min = 20*log10(B_min);
```

```
% Result Figures
figure(1);
plot(theta,20*log10(abs(B)));
axis([0 180 Bl_min-3 Bl_max+4]);

figure(2);
polar(theta*pi/180,abs(B));

%% File: linear_DBFtransmitter_taylor.m

clear;
clc;

% Number of Antennas
N = 16;

% Inter-element Spacing (in lambda terms)
d = 0.5;

% Generation of Array Vector
n = 0:(N-1);

% Parameters of Taylor Amplitude Function
R_l = 20;
R = 10^(R_l/20);

A = acosh(R)/pi;
n_l = 4;


% Calculation of Taylor Amplitude Function based on Null-placement Method
Nulls = [];
if (round(N/2)-N/2)==0.5

   for k=1:(N-1)/2

      Nulls(k)=2*pi/N*(n_l*sqrt((A^2+(k-0.5)^2)/(A^2+(n_l-0.5)^2)));

   end

   Nulls = [Nulls -1*Nulls];

   % MRA Broadside
   MRA = pi*cos(90*pi/180);

   sai_d = [MRA Nulls];

   Bd = [1 zeros(1,N-1)];

else

   theta_d = [89.9 90.1];
```

```
    u_d = cos(theta_d*pi/180);

    Bd = sin(N*d*u_d)./(pi*N*d*u_d);

    for k=1:(N-1)/2

        Nulls(k)=2*pi/N*(n_l*sqrt((A^2+(k-0.5)^2)/(A^2+(n_l-0.5)^2)));

    end

    Nulls = [Nulls -1*Nulls];

    sai_d = [pi*u_d Nulls];

    Bd = [Bd zeros(1,N-2)];

end


for k=1:length(sai_d)

    v = exp(j*(n - (N-1)/2)*sai_d(k));
    v_sai_d(:,k) = v.';

end

w_t = (inv(v_sai_d))'*Bd';

% Calculation of MRA Beam Direction
theta_d = 82;
sai_d = pi*cos(theta_d*pi/180);

w = w_t.*exp(j*(n.'-(N-1)/2)*sai_d);

% Parameters prior sampling of the Beampattern
sample = 1000;
theta = 0:(180/sample):180;
sai = pi*cos(theta*pi/180);

% Calculation of Beampattern
SA = 0;
BSA_max = 0;
for k=1:length(theta)

    v = exp(j*(n - (N-1)/2)*sai(k));
    v_sai(:,k) = v.';

    B(k) = w'*v_sai(:,k);

    SA = SA + 0.5*abs(B(k)).^2*sin(theta(k)*pi/180)*(180/sample)*(pi/180);
    if(abs(B(k))>BSA_max)
        BSA_max = abs(B(k));
    end

end

% Calculation of Directivity
D = 10*log10(BSA_max.^2/SA);


% Result Figures
figure(1)
polar(theta*pi/180,abs(B));

figure(2)
plot(theta,20*log10(abs(B)));


% File: linear_DBFtransmitter_parameters.m

% Information Signal
sig_ts = 1e-8;

% Information Signal
output_width = 16;
fis = 1e6;
db_ts = 1/10e6;
npi = fis*db_ts;

% Antenna Weights and Digital Beamformer
phase_res = 8;
w_amp = abs(w);
w_phase_d = angle(w)*180/pi;
w_phase_r = angle(w);
bit_phase = w_phase_r*2^phase_res/(2*pi);
wamp_bit_res = 16;
wamp_point_res = 14;
wphase_bit_res = 8;
wphase_point_res = 0;
w_phase_d_corr = round(bit_phase)*2*pi/(2^phase_res)*180/pi;

% DAC
dac_ts = 1/100e6;
dac_bit_res = 14;
dac_point_res = 12;

% System Frequencies
fc = 8.2e9;
fif = 3e6;
error_index = 0;
i_phase = pi/2-(2*pi*fif)*(1e-8)*error_index;
```

```
% DDS Parameters
output_width = 16;
flo = fif;
duc_ts = dac_ts;
npd = flo*duc_ts;

% Max Time Delay
plane_wave_angle = 0;
ant_spacing = 0.5;
maxt = (fc/fif)*ant_spacing/fc;
sim_t = 1e-5;
slope_t = maxt/sim_t;

% DUC Filter Specs
filter_order = 30;
factor = 10;
u_sample = db_ts/dac_ts;
hp = u_sample*fir1(filter_order,1/(factor*u_sample));
filter_lat = 15;

% CIC Specs
n_stages = 2;
cic_lat = 2;
diff_delay = 2;
force_bit_width = 18;
scale_factor = -2;

% Scope Parameters
scope_ts = 1e-8;
scope_sig = 1e-8;

% Latency Repair
lat_duc_n = 3 + filter_lat;
lat_db_n = 8;
lat_time = (lat_duc_n+filter_order)*duc_ts+lat_db_n*db_ts;
total_time = lat_time+sim_t;

% Operation Precision
add_bit_width = 14;
add_point_width = 12;
mult_bit_width = 18;
mult_point_width = 16;
prec_bit_width = 16;
prec_point_width = 14;

% Transforming Weight Matrix into vector form
w_amp = reshape(w_amp,sqrt(N),sqrt(N)).';
bit_phase = reshape(bit_phase,sqrt(N),sqrt(N)).';

%% File: linear_DBFtransmitter_results.m

clear;
```

```
clc;

% Load MAT FILE
load TRANSMITTER;

% Removing Transient State of Transmission Signal
total_time = 2e-5;
sim_time = 1e-5;
sim_period = 1e-8;
extra_samples = (total_time-sim_time)/sim_period;
[r_trans_signal,c_trans_signal] = size(trans_signal);
trans_signal = trans_signal(:,(c_trans_signal-extra_samples):c_trans_signal);
[r_trans_signal,c_trans_signal] = size(trans_signal);

% Calculate FFT of each antenna signal
fft_size = 2^16;

spectral_signal = [];

for k=1:r_trans_signal-1

    spectral_signal(k,:) = fft(trans_signal(k+1,:),fft_size);

end

f_range = 0:1/(fft_size*sim_period):1/sim_period-1/(fft_size*sim_period);
index_range = 1:length(f_range);

% Frequencies and index where information signal is present
center_f = 3e6;
delta_f = 1/(2*fft_size*sim_period);

center_f_index = [f_range>=center_f-delta_f & f_range<=center_f+delta_f]*index_range.';

% Rectangular Array Size
N = 1;
M = 16;
w_phase_x = [];
w_phase_x(:,1) = zeros(N,1);

% Calculation of Weight Coefficient's Phase
for k=2:M
    center_phase = -1*(angle(spectral_signal(k,center_f_index))-angle(spectral_signal(1,center_f_index)));
    if (center_phase>=180)
        center_phase = center_phase-360;
    end
    w_phase_x(k)=center_phase;
end

% Calculation of Weight Coefficient's Magnitude
for k=1:M
```

```
    w_abs(k) = abs(spectral_signal(k,center_f_index))/2;

end

% Number of Antennas
N = 16;

% Generation of Array Vector
n = 0:(N-1);

% Calculation of Array Weight
w = (w_abs.*exp(j*w_phase_x)).';

save WEIGHT_INFO w;

% Parameters prior sampling of the Beampattern
sample = 1000;
theta = 0:(180/sample):180;
sai = pi*cos(theta*pi/180);


% Calculation of the Beampattern
SA = 0;
BSA_max = 0;
for k=1:length(theta)

    v = exp(j*(n - (N-1)/2)*sai(k));
    v_sai(:,k) = v.';

    B(k) = w'*v_sai(:,k);

    SA = SA + 0.5*abs(B(k)).^2*sin(theta(k)*pi/180)*(180/sample)*(pi/180);

    if(abs(B(k))>BSA_max)
        BSA_max = abs(B(k));
    end

end


% Calculation of the Directivity
D = 10*log10(BSA_max.^2/SA);

% Result Figures
figure(1)
polar(theta*pi/180,abs(B));

figure(2)
plot(theta,20*log10(abs(B)));

% File: linear_DBFtransmitter_blackmannharris.m
```

```
clear;
clc;

% Number of Antennas
N = 16;

% Generation of Array Vector
n = 0:(N-1);

% Calculation of MRA Beam Direction
theta_d = 82;
sai_d = pi*cos(theta_d*pi/180);

% Calculation of Weight's Amplitude based on Blackmann-harris Spectral
% Window function
w_abs = (0.42+0.5*cos(2*pi*(n-(N-1)/2)/N)+0.08*cos(4*pi*(n-(N-1)/2)/N)).';

% Calculation of Weight Coefficients
w = w_abs.*exp(j*(n.'-(N-1)/2)*sai_d);

% Paramaters prior sampling of the Beampatter
sample = 1000;
theta = 0:(180/sample):180;
sai = pi*cos(theta*pi/180);

% Calculation of Beampattern
SA = 0;
BSA_max = 0;
for k=1:length(theta)

   v = exp(j*(n - (N-1)/2)*sai(k));
   v_sai(:,k) = v.';

   B(k) = w'*v_sai(:,k);

   SA = SA + 0.5*abs(B(k)).^2*sin(theta(k)*pi/180)*(180/sample)*(pi/180);

   if(abs(B(k))>BSA_max)
      BSA_max = abs(B(k));
   end

end

% Calculation  of Directivity
D = 10*log10(BSA_max.^2/SA);


% Result Figures
figure(1)
polar(theta*pi/180,abs(B));

figure(2)
```

```
plot(theta,20*log10(abs(B)));


%% File: rectangular_DBFtransmitter_steering.m

clear;
clc;

% Rectangular Array Size
N = 4;
M = 4;
[n,m] = meshgrid(-1*(N-1)/2:(N-1)/2,-1*(M-1)/2:(M-1)/2);

% Inter-element spacing in lambda terms
dx = 0.5;
dy = 0.5;

% Weight function
theta_d = 30;
phi_d = 0;

sai_x_d = 2*pi*dx*sin(theta_d*pi/180)*cos(phi_d*pi/180);
sai_y_d = 2*pi*dy*sin(theta_d*pi/180)*sin(phi_d*pi/180);

W = (1/(M*N))*exp(j*(n*sai_x_d + m*sai_y_d));
w = reshape(W,N*M,1);


save TRAINING -append W;

% Creating U and Sai Space
sample_u_x = 100;
sample_u_y = 100;
u_x = -1:1/(sample_u_x*2):1;
u_y = -1:1/(sample_u_y*2):1;
sai_x = 2*pi*dx*u_x;
sai_y = 2*pi*dy*u_y;


% 2-D Beampattern Calculation
for k=1:length(sai_x)

   for h=1:length(sai_y)

      V = exp(j*(n*sai_x(k) + m*sai_y(h)));
      v = reshape(V,N*M,1);

      B(k,h) = w'*v;


   end
```

```
end

% 2-D Beampattern Calculation in Angle Space
phi_coor_real = 0:360;
theta_coor_real = 0:90;
theta_coor_extra = 0:180;
V = [];
v = [];
SA = 0;
for k=1:length(phi_coor_real)

  for h=1:length(theta_coor_extra)



    sai_x_now = 2*pi*dx*sin(theta_coor_extra(h)*pi/180)*cos(phi_coor_real(k)*pi/180);
    sai_y_now = 2*pi*dx*sin(theta_coor_extra(h)*pi/180)*sin(phi_coor_real(k)*pi/180);

    V = exp(j*(n*sai_x_now + m*sai_y_now));
    v = reshape(V,N*M,1);

    if theta_coor_extra(h) <= 90

      B_sph(k,h) = w'*v;

      phi_coor_real_sph(k,h) = phi_coor_real(k);
      theta_coor_real_sph(k,h) = theta_coor_real(h);

      if (phi_coor_real(k)~=360)

        SA = SA + (abs(B_sph(k,h)))^2*sin(theta_coor_real(h)*pi/180)*(pi/180)^2;

      end

    else

      B_SA = w'*v;

      if (phi_coor_real(k)~=360 && theta_coor_extra(h)~=180 )

        SA = SA + (abs(B_SA))^2*sin(theta_coor_extra(h)*pi/180)*(pi/180)^2;

      end

    end

  end

end

SA = SA/(4*pi);
```

```
% Calculation of Directivity

D = abs(B_sph(phi_d+1,theta_d+1))^2/SA;
D_dB = 10*log10(D);

B_max = max(max(abs(B_sph)));

B_sph = B_sph/max(max(abs(B_sph)));

[x_B,y_B,z_B] = sph2cart(phi_coor_real_sph*pi/180, (-(theta_coor_real_sph-90)*pi/180), abs(B_sph));


% Phi = 0 & Phi = MRA_phi Cut Beampattern Calculation
phi_1 = 0;
phi_2 = phi_d;
phi_3 = phi_d + 45;

theta = 0:1:90;
for k=1:length(theta)

   u_x_1 = sin(theta(k)*pi/180)*cos(phi_1*pi/180);
   u_y_1 = sin(theta(k)*pi/180)*sin(phi_1*pi/180);

   u_x_2 = sin(theta(k)*pi/180)*cos(phi_2*pi/180);
   u_y_2 = sin(theta(k)*pi/180)*sin(phi_2*pi/180);

   u_x_3 = sin(theta(k)*pi/180)*cos(phi_3*pi/180);
   u_y_3 = sin(theta(k)*pi/180)*sin(phi_3*pi/180);

   sai_x_1 = 2*pi*dx*u_x_1;
   sai_y_1 = 2*pi*dy*u_y_1;

   sai_x_2 = 2*pi*dx*u_x_2;
   sai_y_2 = 2*pi*dy*u_y_2;

   sai_x_3 = 2*pi*dx*u_x_3;
   sai_y_3 = 2*pi*dy*u_y_3;

   V_1 = exp(j*(n*sai_x_1 + m*sai_y_1));
   v_1 = reshape(V_1,N*M,1);

   Bt_1(k) = w'*v_1;

   V_2 = exp(j*(n*sai_x_2 + m*sai_y_2));
   v_2 = reshape(V_2,N*M,1);

   Bt_2(k) = w'*v_2;

   V_3 = exp(j*(n*sai_x_3 + m*sai_y_3));
   v_3 = reshape(V_3,N*M,1);

   Bt_3(k) = w'*v_3;
```

```
end

if (phi_2<180)
   Bt_s = [fliplr(Bt_2) Bt_3];
else
   Bt_s = [fliplr(Bt_3) Bt_2];
end

% Calculation of Beamwidth in Phi Plane Cut
Bt_s = Bt_s([1:92 94:182]);
theta_m = 0:180;
Bt_s_max = max(abs(Bt_s));
Bt_s_3dB = Bt_s_max/2;
theta_beam = theta_m([abs(Bt_s)]>=Bt_s_3dB);
Beamwidth_theta = max(theta_beam)-min(theta_beam);

figure('Name','Beam Pattern of Standard Rectangular Array');
surf(x_B,y_B,z_B);
title('Magnitude in dB of Rectangular Array Beam Pattern');
xlabel('x');
ylabel('y');
zlabel('Magnitude (dB)');

polar3D(theta_coor_real,phi_coor_real,(20*log10(abs(B_sph)))',50,3,'Rectangular Array Beam Pattern
Polar Plot');


function hpol = polar3D(theta,phi,z,graph_dynamic,fig_nb,title_fig)
%POLAR3D  3D Polar coordinate plot.
%   polar3D(THETA,PHI,Z,GRAPH_DYNAMIC,FIG_NB,TITLE_FIG) makes a plot using polar
coordinates of
%   the angles THETA and PHI, in degrees, versus the 3rd dimension Z.
%   GRAPH_DYNAMIC allows to display the dynamic range from the maximum value of Z.
%   FIG_NB indicates the figure number in which the graph has to be displayed.
%   TITLE_FIG is a string containing the figure's title.
%
%   Copyright Sebastien and Marcelo, The Dream-Team, Nov. 21, 2003.

% get hold state
figure(fig_nb)
cax = newplot;
next = lower(get(cax,'NextPlot'));
hold_state = ishold;

% get x-axis text color so grid is in same color
tc = get(cax,'xcolor');
ls = get(cax,'gridlinestyle');

% Hold on to current Text defaults, reset them to the
% Axes' font attributes so tick marks use them.
```

```
fAngle  = get(cax, 'DefaultTextFontAngle');
fName   = get(cax, 'DefaultTextFontName');
fSize   = get(cax, 'DefaultTextFontSize');
fWeight = get(cax, 'DefaultTextFontWeight');
fUnits  = get(cax, 'DefaultTextUnits');
set(cax, 'DefaultTextFontAngle',  get(cax, 'FontAngle'), ...
    'DefaultTextFontName',   get(cax, 'FontName'), ...
    'DefaultTextFontSize',   get(cax, 'FontSize'), ...
    'DefaultTextFontWeight', get(cax, 'FontWeight'), ...
    'DefaultTextUnits','data')


% transform data to Cartesian coordinates.
xx=theta.'*cos(pi*phi/180);
yy=theta.'*sin(pi*phi/180);
pcolor(xx,yy,z), shading interp;
if (graph_dynamic~=0)
    caxis([(max(max(z))-graph_dynamic) max(max(z))]);
end
axis square;
colorbar;
title(title_fig)

% plot gird on top of data

% make a radial grid
    hold on;
    max_theta = max( max(abs(theta)));
    hhh=plot([-max_theta -max_theta max_theta max_theta],[-max_theta max_theta max_theta -max_theta]);
    set(gca,'dataaspectratio',[1 1 1],'plotboxaspectratiomode','auto')
    v = [get(cax,'xlim') get(cax,'ylim')];
    ticks = 7;
    delete(hhh);
% check radial limits and ticks
    rmin = 0; rmax = 90; rticks = max(ticks-1,2);

% define a circle
    th = 0:pi/50:2*pi;
    xunit = cos(th);
    yunit = sin(th);
% now really force points on x/y axes to lie on them exactly
    inds = 1:(length(th)-1)/4:length(th);
    xunit(inds(2:2:4)) = zeros(2,1);
    yunit(inds(1:2:5)) = zeros(3,1);

% draw radial circles
    c82 = cos(82*pi/180);
    s82 = sin(82*pi/180);
    rinc = (rmax-rmin)/rticks;
    for i=(rmin+rinc):rinc:rmax
        hhh = plot(xunit*i,yunit*i,ls,'color',tc,'linewidth',1,...
                'handlevisibility','off');
        text((i+rinc/20)*c82,(i+rinc/20)*s82, ...
            ['  ' num2str(i) '^o'],'verticalalignment','bottom',...
            'handlevisibility','off')
   end
     set(hhh,'linestyle','-') % Make outer circle solid

% plot spokes
    th = (1:6)*2*pi/12;
    cst = cos(th); snt = sin(th);
    cs = [-cst; cst];
    sn = [-snt; snt];
    plot(rmax*cs,rmax*sn,ls,'color',tc,'linewidth',1,...
         'handlevisibility','off')

% annotate spokes in degrees
    rt = 1.1*rmax;
    for i = 1:length(th)
        text(rt*cst(i),rt*snt(i),[int2str(i*30) '^o'],...
             'horizontalalignment','center',...
             'handlevisibility','off');
        if i == length(th)
            loc = int2str(0);
        else
            loc = int2str(180+i*30);
        end
        text(-rt*cst(i),-rt*snt(i),[loc '^o'],'horizontalalignment','center',...
             'handlevisibility','off')
    end

% set view to 2-D
    view(2);
% set axis limits
     axis(rmax*[-1 1 -1.15 1.15]);

% Reset defaults.
set(cax, 'DefaultTextFontAngle', fAngle , ...
    'DefaultTextFontName',   fName , ...
    'DefaultTextFontSize',   fSize, ...
    'DefaultTextFontWeight', fWeight, ...
    'DefaultTextUnits',fUnits );

hold off;

if nargout > 0
    hpol = q;
end
if ~hold_state
    set(gca,'dataaspectratio',[1 1 1]), axis off; set(cax,'NextPlot',next);
end
set(get(gca,'xlabel'),'visible','on')
set(get(gca,'ylabel'),'visible','on')
```

```
hold off;


% File: rectangular_DBFtransmitter_parameters.m

% Information Signal
sig_ts = 1e-8;

% Information Signal
output_width = 16;
fis = 1e6;
db_ts = 1/10e6;
npi = fis*db_ts;

% Antenna Weights and Digital Beamformer
phase_res = 8;
w_amp = abs(W)/sum(sum(abs(W)));
w_phase_d = angle(W)*180/pi;
w_phase_r = angle(W);
bit_phase = w_phase_r*2^phase_res/(2*pi);
wamp_bit_res = 16;
wamp_point_res = 14;
wphase_bit_res = phase_res;
wphase_point_res = 0;
w_phase_d_corr = round(bit_phase)*2*pi/(2^phase_res)*180/pi;

% DAC
dac_ts = 1/100e6;
dac_bit_res = 14;
dac_point_res = 12;

% System Frequencies
fc = 8.2e9;
fif = 3e6;
error_index = 0;
i_phase = pi/2-(2*pi*fif)*(1e-8)*error_index;

% DDS Parameters
output_width = 16;
flo = fif;
duc_ts = dac_ts;
npd = flo*duc_ts;

% Max Time Delay
plane_wave_angle = 0;
ant_spacing = 0.5;
maxt = (fc/fif)*ant_spacing/fc;
sim_t = 1e-5;
slope_t = maxt/sim_t;

% DUC Filter Specs
filter_order = 30;
```

```
factor = 10;
u_sample = db_ts/dac_ts;
hp = u_sample*fir1(filter_order,1/(factor*u_sample));
filter_lat = 15;

% CIC Specs
n_stages = 2;
cic_lat = 2;
diff_delay = 2;
force_bit_width = 18;
scale_factor = -2;

% Scope Parameters
scope_ts = 1e-8;
scope_sig = 1e-8;

% Latency Repair
lat_duc_n = 3 + filter_lat;
lat_db_n = 8;
lat_time = (lat_duc_n+filter_order)*duc_ts+lat_db_n*db_ts;
total_time = lat_time+sim_t;

% Operation Precision
add_bit_width = 14;
add_point_width = 12;
mult_bit_width = 18;
mult_point_width = 16;
prec_bit_width = 16;
prec_point_width = 14;

load TRAINING;

save WEIGHT_INFO w_amp w_phase_r w_phase_d_corr;


%% File: rectangular_DBFtransmitter_results.m

clear;
clc;

% Load MAT FILE
load TRANSMITTER;

% Removing Transient State of Transmission Signal
total_time = 1.1e-5;
sim_time = 1e-5;
sim_period = 1e-8;
extra_samples = (total_time-sim_time)/sim_period;
[r_trans_signal,c_trans_signal] = size(trans_signal);
trans_signal = trans_signal(:,(c_trans_signal-extra_samples):c_trans_signal);
[r_trans_signal,c_trans_signal] = size(trans_signal);
```

```
% Calculate FFT of each antenna signal
fft_size = 2^16;
spectral_signal = [];
for k=1:r_trans_signal-1

    spectral_signal(k,:) = fft(trans_signal(k+1,:),fft_size);

end

f_range = 0:1/(fft_size*sim_period):1/sim_period-1/(fft_size*sim_period);
index_range = 1:length(f_range);

% Frequencies and index where information signal is present
center_f = 3e6;
delta_f = 1/(2*fft_size*sim_period);

center_f_index = [f_range>=center_f-delta_f & f_range<=center_f+delta_f]*index_range.';

% Rectangular Array Size
N = 4;
M = 4;
w_phase_x = [];
w_phase_x(:,1) = zeros(N,1);


% Calculation of Weight Coefficients' Phase
for k=1:N

    for h=2:M
        center_phase = -1*(angle(spectral_signal(h+(k-1)*N,center_f_index))-angle(spectral_signal(1+(k-
1)*N,center_f_index)));
        if (center_phase>=180)
            center_phase = center_phase-360;
        end
        w_phase_x(k,h)=center_phase;
    end
end

w_phase_y = [];
w_phase_y(1,:) = zeros(1,M);

for k=2:N

    for h=1:M
        center_phase = -1*(angle(spectral_signal(h+(k-1)*N,center_f_index))-
angle(spectral_signal(h,center_f_index)));
        if (center_phase>=180)
            center_phase = center_phase-360;
        end
        w_phase_y(k,h)=center_phase;
    end
end
```

```
% Calculation of Weight Coefficients' Magnitude
for k=1:N
    for h=1:M
        w_abs(k,h) = abs(spectral_signal(h+(k-1)*N,center_f_index))/2;
    end
end

% Rectangular Array Size
N = 4;
M = 4;
[n,m] = meshgrid(-1*(N-1)/2:(N-1)/2,-1*(M-1)/2:(M-1)/2);

% Inter-element spacing in lambda terms
dx = 0.5;
dy = 0.5;

% Weight function
theta_d = 16;
phi_d = 122;

sai_x_d = 2*pi*dx*sin(theta_d*pi/180)*cos(phi_d*pi/180);
sai_y_d = 2*pi*dy*sin(theta_d*pi/180)*sin(phi_d*pi/180);

W = w_abs.*exp(j*(w_phase_x + w_phase_y));
w = reshape(W,N*M,1);

save WEIGHT_INFO W -append;

% Creating U and Sai Space
sample_u_x = 100;
sample_u_y = 100;
u_x = -1:1/(sample_u_x*2):1;
u_y = -1:1/(sample_u_y*2):1;
sai_x = 2*pi*dx*u_x;
sai_y = 2*pi*dy*u_y;

% [u_x,u_y] = meshgrid(2*pi*dx*(-1:1/(sample_u_x*2):1),2*pi*dy*(-1:1/(sample_u_y*2):1));

% 2-D Beampattern Calculation
for k=1:length(sai_x)

    for h=1:length(sai_y)

        V = exp(j*(n*sai_x(k) + m*sai_y(h)));
        v = reshape(V,N*M,1);

        B(k,h) = w'*v;


    end
```

```
end

% 2-D Beampattern Calculation in Angle Space
phi_coor_real = 0:360;
theta_coor_real = 0:90;
theta_coor_extra = 0:180;
V = [];
v = [];
SA = 0;
for k=1:length(phi_coor_real)

   for h=1:length(theta_coor_extra)



      sai_x_now = 2*pi*dx*sin(theta_coor_extra(h)*pi/180)*cos(phi_coor_real(k)*pi/180);
      sai_y_now = 2*pi*dx*sin(theta_coor_extra(h)*pi/180)*sin(phi_coor_real(k)*pi/180);

      V = exp(j*(n*sai_x_now + m*sai_y_now));
      v = reshape(V,N*M,1);

      if theta_coor_extra(h) <= 90

         B_sph(k,h) = w'*v;

         phi_coor_real_sph(k,h) = phi_coor_real(k);
         theta_coor_real_sph(k,h) = theta_coor_real(h);

         if (phi_coor_real(k)~=360)

            SA = SA + (abs(B_sph(k,h)))^2*sin(theta_coor_real(h)*pi/180)*(pi/180)^2;

         end

      else

         B_SA = w'*v;

         if (phi_coor_real(k)~=360 && theta_coor_extra(h)~=180 )

            SA = SA + (abs(B_SA))^2*sin(theta_coor_extra(h)*pi/180)*(pi/180)^2;

         end

      end

   end

end

SA = SA/(4*pi);
```

```
D = abs(B_sph(phi_d+1,theta_d+1))^2/SA;
D_dB = 10*log10(D);

B_max = max(max(abs(B_sph)));

[x_B,y_B,z_B] = sph2cart(phi_coor_real_sph*pi/180, (-(theta_coor_real_sph-90)*pi/180), abs(B_sph));


% Phi = 0 & Phi = MRA_phi Cut Beampattern Calculation

phi_1 = 0;
phi_2 = phi_d;
phi_3 = phi_d + 180;

theta = 0:1:90;
for k=1:length(theta)

   u_x_1 = sin(theta(k)*pi/180)*cos(phi_1*pi/180);
   u_y_1 = sin(theta(k)*pi/180)*sin(phi_1*pi/180);

   u_x_2 = sin(theta(k)*pi/180)*cos(phi_2*pi/180);
   u_y_2 = sin(theta(k)*pi/180)*sin(phi_2*pi/180);

   u_x_3 = sin(theta(k)*pi/180)*cos(phi_3*pi/180);
   u_y_3 = sin(theta(k)*pi/180)*sin(phi_3*pi/180);

   sai_x_1 = 2*pi*dx*u_x_1;
   sai_y_1 = 2*pi*dy*u_y_1;

   sai_x_2 = 2*pi*dx*u_x_2;
   sai_y_2 = 2*pi*dy*u_y_2;

   sai_x_3 = 2*pi*dx*u_x_3;
   sai_y_3 = 2*pi*dy*u_y_3;

   V_1 = exp(j*(n*sai_x_1 + m*sai_y_1));
   v_1 = reshape(V_1,N*M,1);

   Bt_1(k) = w'*v_1;

   V_2 = exp(j*(n*sai_x_2 + m*sai_y_2));
   v_2 = reshape(V_2,N*M,1);

   Bt_2(k) = w'*v_2;

   V_3 = exp(j*(n*sai_x_3 + m*sai_y_3));
   v_3 = reshape(V_3,N*M,1);

   Bt_3(k) = w'*v_3;


end
```

```
if (phi_2<180)
    Bt_s = [fliplr(Bt_2) Bt_3];
else
    Bt_s = [fliplr(Bt_3) Bt_2];
end

% Calculation of Beamwidth in Phi Cut Plane
Bt_s = Bt_s([1:92 94:182]);
theta_m = 0:180;
Bt_s_max = max(abs(Bt_s));
Bt_s_3dB = Bt_s_max/2;
theta_beam = theta_m([abs(Bt_s)]>=Bt_s_3dB);
Beamwidth_theta = max(theta_beam)-min(theta_beam);

% Theta = MRA_theta Cut Pattern

theta_1 = theta_d;
phi = 0:360;

for k=1:length(phi)

    u_x_p = sin(theta_1*pi/180)*cos(phi(k)*pi/180);
    u_y_p = sin(theta_1*pi/180)*sin(phi(k)*pi/180);

    sai_x_p = 2*pi*dx*u_x_p;
    sai_y_p = 2*pi*dy*u_y_p;

    V_p = exp(j*(n*sai_x_p + m*sai_y_p));
    v_p = reshape(V_p,N*M,1);

    B_p(k) = w'*v_p;

end

% Result Figures
figure('Name','Simulated Beam Pattern of Standard Rectangular Array');
surf(x_B,y_B,z_B);
title('Magnitude in dB of Rectangular Array Beam Pattern');
xlabel('x');
ylabel('y');
zlabel('Magnitude (dB)');

polar3D(theta_coor_real,phi_coor_real,(20*log10(abs(B_sph)))',50,6,'Simulated Rectangular Array Beam
Pattern Polar Plot');

%% File: rectangular_DBFtransmitter_dolphchebyshev.m

clear;
clc;

% Rectangular Array Size
```

```
N = 4;
M = 4;
[n,m] = meshgrid(-1*(N-1)/2:(N-1)/2,-1*(M-1)/2:(M-1)/2);

% Inter-element spacing in lambda terms
dx = 0.5;
dy = 0.5;

% Calculation of Weight Coefficients
theta_d = 16;
phi_d = 122;

sai_x_d = 2*pi*dx*sin(theta_d*pi/180)*cos(phi_d*pi/180);
sai_y_d = 2*pi*dy*sin(theta_d*pi/180)*sin(phi_d*pi/180);

W = (1/M*N)*exp(j*(n*sai_x_d + m*sai_y_d));
w = reshape(W,N*M,1);

R_l = 25;
R = 10^(R_l/20);
x0=cosh(acosh(R)/(N-1));

for k1=0:N-1
   for k2=0:M-1

      saix_k1 = (k1-(N-1)/2)*2*pi/N;
      saiy_k2 = (k2-(M-1)/2)*2*pi/M;
      ev(k1+1,k2+1) = x0*cos(saix_k1/2)*cos(saiy_k2/2);

      if abs(ev(k1+1,k2+1)) <= 1
         B_n(k1+1,k2+1) = exp(-j*((N-1)/2*saix_k1+(M-1)/2*saiy_k2))*cos((N-
1)*acos(ev(k1+1,k2+1)))/R;
      elseif ev(k1+1,k2+1) > 1
         B_n(k1+1,k2+1) = exp(-j*((N-1)/2*saix_k1+(M-1)/2*saiy_k2))*cosh((N-
1)*acosh(ev(k1+1,k2+1)))/R;
      else
         B_n(k1+1,k2+1) = exp(-j*((N-1)/2*saix_k1+(M-1)/2*saiy_k2))*(-1)^(N-1)*cosh((N-
1)*acosh(ev(k1+1,k2+1)))/R;
      end


   end
end

b_n = ifft2(B_n,N,M);

for a_i=0:N-1
   for b_i=0:M-1

      E_m(a_i+1,b_i+1) = exp(j*(a_i*pi*(N-1)/N+b_i*pi*(M-1)/M));

   end
```

```
end

W_dc = b_n./E_m;
w_dc = reshape(W_dc,N*M,1);

w = w.*w_dc;
W = reshape(w,N,M);

save TRAINING -append W;

% Creating U and Sai Space
sample_u_x = 100;
sample_u_y = 100;
u_x = -1:1/(sample_u_x*2):1;
u_y = -1:1/(sample_u_y*2):1;
sai_x = 2*pi*dx*u_x;
sai_y = 2*pi*dy*u_y;

% 2-D Beampattern Calculation
for k=1:length(sai_x)

    for h=1:length(sai_y)

        V = exp(j*(n*sai_x(k) + m*sai_y(h)));
        v = reshape(V,N*M,1);

        B(k,h) = w'*v;


    end

end

% 2-D Beampattern Calculation in Angle Space
phi_coor_real = 0:360;
theta_coor_real = 0:90;
theta_coor_extra = 0:180;
V = [];
v = [];
SA = 0;
for k=1:length(phi_coor_real)

    for h=1:length(theta_coor_extra)



        sai_x_now = 2*pi*dx*sin(theta_coor_extra(h)*pi/180)*cos(phi_coor_real(k)*pi/180);
        sai_y_now = 2*pi*dx*sin(theta_coor_extra(h)*pi/180)*sin(phi_coor_real(k)*pi/180);

        V = exp(j*(n*sai_x_now + m*sai_y_now));
        v = reshape(V,N*M,1);
        if theta_coor_extra(h) <= 90

            B_sph(k,h) = w'*v;

            phi_coor_real_sph(k,h) = phi_coor_real(k);
            theta_coor_real_sph(k,h) = theta_coor_real(h);

            if (phi_coor_real(k)~=360)

                SA = SA + (abs(B_sph(k,h)))^2*sin(theta_coor_real(h)*pi/180)*(pi/180)^2;

            end

        else

            B_SA = w'*v;

            if (phi_coor_real(k)~=360 && theta_coor_extra(h)~=180 )

                SA = SA + (abs(B_SA))^2*sin(theta_coor_extra(h)*pi/180)*(pi/180)^2;

            end

        end

    end

end

SA = SA/(4*pi);

% Calculation of Directivity
D = abs(B_sph(phi_d+1,theta_d+1))^2/SA;
D_dB = 10*log10(D);

B_max = max(max(abs(B_sph)));

B_sph = B_sph/max(max(abs(B_sph)));

[x_B,y_B,z_B] = sph2cart(phi_coor_real_sph*pi/180, (-(theta_coor_real_sph-90)*pi/180), abs(B_sph));


% Phi = 0 & Phi = MRA_phi Cut Beampattern Calculation

phi_1 = phi_d;
phi_2 = phi_d-45;
phi_3 = phi_d+45;
phi_4 = phi_d+180;

% sample_theta = 100;
theta = 0:1:90;
```

```
for k=1:length(theta)

    u_x_1 = sin(theta(k)*pi/180)*cos(phi_1*pi/180);
    u_y_1 = sin(theta(k)*pi/180)*sin(phi_1*pi/180);

    u_x_2 = sin(theta(k)*pi/180)*cos(phi_2*pi/180);
    u_y_2 = sin(theta(k)*pi/180)*sin(phi_2*pi/180);

    u_x_3 = sin(theta(k)*pi/180)*cos(phi_3*pi/180);
    u_y_3 = sin(theta(k)*pi/180)*sin(phi_3*pi/180);

    u_x_4 = sin(theta(k)*pi/180)*cos(phi_4*pi/180);
    u_y_4 = sin(theta(k)*pi/180)*sin(phi_4*pi/180);

    sai_x_1 = 2*pi*dx*u_x_1;
    sai_y_1 = 2*pi*dy*u_y_1;

    sai_x_2 = 2*pi*dx*u_x_2;
    sai_y_2 = 2*pi*dy*u_y_2;

    sai_x_3 = 2*pi*dx*u_x_3;
    sai_y_3 = 2*pi*dy*u_y_3;

    sai_x_4 = 2*pi*dx*u_x_4;
    sai_y_4 = 2*pi*dy*u_y_4;

    V_1 = exp(j*(n*sai_x_1 + m*sai_y_1));
    v_1 = reshape(V_1,N*M,1);

    Bt_1(k) = w'*v_1;

    V_2 = exp(j*(n*sai_x_2 + m*sai_y_2));
    v_2 = reshape(V_2,N*M,1);

    Bt_2(k) = w'*v_2;

    V_3 = exp(j*(n*sai_x_3 + m*sai_y_3));
    v_3 = reshape(V_3,N*M,1);

    Bt_3(k) = w'*v_3;

    V_4 = exp(j*(n*sai_x_4 + m*sai_y_4));
    v_4 = reshape(V_4,N*M,1);

    Bt_4(k) = w'*v_4;


end

if (phi_2<180)
    Bt_s = [fliplr(Bt_2) Bt_3];
else
```

```
    Bt_s = [fliplr(Bt_3) Bt_2];
end

% Calculation of Beamwidth in Phi Cut Plane
Bt_s = Bt_s([1:92 94:182]);
theta_m = 0:180;
Bt_s_max = max(abs(Bt_s));
Bt_s_3dB = Bt_s_max/2;
theta_beam = theta_m([abs(Bt_s)]>=Bt_s_3dB);
Beamwidth_theta = max(theta_beam)-min(theta_beam);

% Theta = MRA_theta Cut Pattern

theta_1 = theta_d;
phi = 0:360;

for k=1:length(phi)

    u_x_p = sin(theta_1*pi/180)*cos(phi(k)*pi/180);
    u_y_p = sin(theta_1*pi/180)*sin(phi(k)*pi/180);

    sai_x_p = 2*pi*dx*u_x_p;
    sai_y_p = 2*pi*dy*u_y_p;

    V_p = exp(j*(n*sai_x_p + m*sai_y_p));
    v_p = reshape(V_p,N*M,1);

    B_p(k) = w'*v_p;

end

B_p_max = max(abs(B_p));
B_p_3dB = B_p_max/2;
phi_beam = phi([abs(B_p)]>=B_p_3dB);
Beamwidth_phi = max(phi_beam)-min(phi_beam);

% Result Figures
figure('Name','Beam Pattern of Standard Rectangular Array');
surf(x_B,y_B,z_B);
title('Magnitude in dB of 2-D Beam Pattern');
xlabel('x');
ylabel('y');
zlabel('Magnitude (dB)');

polar3D(theta_coor_real,phi_coor_real,(20*log10(abs(B_sph)))',50,4,'Polar Color Plot');


function status = sp_read(data_filename,mat_filename)
% SP_read S-Parameter File Reader (Citiype file)
%    SP_read(data_filename,mat_filename) retrieves S-Parameter data stored
%    in cititype format named data_filename and stores the S-Parameter
%    values in .MAT format on a file named mat_filename.mat. SP_read()
%    stores the frequency vector 'freq', the name of the S-Parameter
%    'SP_Name' and the S-Parameter value 'SP' where each row of the matrix
%    represents an S-Parameter at frequencies specified by the frequency
%    vector.
%   Author: Juan A. Torres-Rosario

fid = fopen(data_filename,'r');

% Read the filetype name
ftype = fgetl(fid);

% Read Network Analyzer Version
NAversion = fgetl(fid);

% Read citifile type
cftype = fgetl(fid);

% Read register value
register_value = fgetl(fid);

% Read comment
comment_var = fgetl(fid);

% Read Number of S-Parameters in File
k = 0;
l = 1;

SP_Name(l,:)=fread(fid,14,'uint8=>char').';
fread(fid,2,'uint8=>char');

next = fread(fid,4,'uint8=>char').';

if next~='DATA'
      k = 1;
end

l = l+1;

while k==0

   SP_Name(l,:)=[next fread(fid,10,'uint8=>char').'];
   fread(fid,2,'uint8=>char');

   next = fread(fid,4,'uint8=>char').';

   if next~='DATA'
       k = 1;
   end

   l = l+1;

end
```

```
% Read Segment Begin Label
begin_label = [next fread(fid,10,'uint8=>char').'];
fread(fid,2,'uint8=>char');

% Read Number of Frequency Points in S-Parameter File
% Note: Only works when 3 digits are used to express number of
%       frequency points

freq_label = fgetl(fid);

freq_min = str2num(freq_label(5:14));
freq_max = str2num(freq_label(16:25));
freq_points = str2num(freq_label(27:29))-1;

freq_delta = (freq_max-freq_min)/freq_points;

freq = freq_min:freq_delta:freq_max;

% Read Segment End Label
end_label = fgetl(fid);

% Read Comment Information (Time,Date,Year)
comment_label = fgetl(fid);
comment_info = fgetl(fid);

%% Use space later for file information

% Begin process of reading S-Parameters
SP = [];
for j=1:size(SP_Name,1)

   begin_splabel = fgetl(fid);

   for k=1:length(freq)

      SP_line = fgetl(fid);
      SP_value = str2num(SP_line);

      if SP_Name(j,13:14)=='RI'

         SP(j,k) = complex(SP_value(1),SP_value(2));

      end

   end

   end_splabel = fgetl(fid);


end
```

```
save(mat_filename,'SP_Name','SP','freq','-mat');

status = 1;

fclose(fid);


function status = sp_show(mat_filename);
% SP_SHOW S-Parameter Plotter
%       sp_show(mat_filename) reads the specified mat_filename and plots
%       the magnitude (in dB) and phase (in degrees) of the S-Parameters
%       specified in the file
%   Author: Juan A. Torres-Rosario


load(mat_filename);

figure('Name','S-Parameter Magnitude Plots');
subplot(221),plot(freq,20*log10(abs(SP(1,:))));
grid on;
title(['S-Parameter ',SP_Name(1,6:11)]);
xlabel('Frequency (Hz)');
ylabel('Magnitude (dB)');
subplot(222),plot(freq,20*log10(abs(SP(2,:))));
grid on;
title(['S-Parameter ',SP_Name(2,6:11)]);
xlabel('Frequency (Hz)');
ylabel('Magnitude (dB)');
subplot(223),plot(freq,20*log10(abs(SP(3,:))));
grid on;
title(['S-Parameter ',SP_Name(3,6:11)]);
xlabel('Frequency (Hz)');
ylabel('Magnitude (dB)');
subplot(224),plot(freq,20*log10(abs(SP(4,:))));
grid on;
title(['S-Parameter ',SP_Name(4,6:11)]);
xlabel('Frequency (Hz)');
ylabel('Magnitude (dB)');

figure('Name','S-Parameter Phase Plots');
subplot(221),plot(freq,angle(SP(1,:))*180/pi);
grid on;
title(['S-Parameter ',SP_Name(1,6:11)]);
xlabel('Frequency (Hz)');
ylabel('Phase (degrees)');
subplot(222),plot(freq,angle(SP(2,:))*180/pi);
grid on;
title(['S-Parameter ',SP_Name(2,6:11)]);
xlabel('Frequency (Hz)');
ylabel('Phase (degrees)');
subplot(223),plot(freq,angle(SP(3,:))*180/pi);
grid on;
```

```
title(['S-Parameter ',SP_Name(3,6:11)]);
xlabel('Frequency (Hz)');
ylabel('Phase (degrees)');
subplot(224),plot(freq,angle(SP(4,:))*180/pi);
grid on;
title(['S-Parameter ',SP_Name(4,6:11)]);
xlabel('Frequency (Hz)');
ylabel('Phase (degrees)');

function status = pattern_read(data_filename,mat_filename)
% pattern_read Antenna Pattern File Reader
%    pattern_read(data_filename,mat_filename) retreives antenna
%    measurement data stored in data_filename from the NSI 2000 software
%    and stores the file information and measurement
%    electric field pattern data into the mat_filename.
%    Note: The content in the description field of the file must not exceed
%    one line.
%   Author: Juan A. Torres-Rosario

fid = fopen(data_filename,'r');

% Read line
line = fgetl(fid);
k = 1;

while line(k)~=',',
   k = k+1;
end

% Polarization Cut
k = k+2;
polarization = [];
while line(k)~=':',
   polarization = [polarization line(k)];
   k = k+1;
end

% Polarization Type
k = k+2;
pol_type = [];
while line(k)~=',',
   pol_type = [pol_type line(k)];
   k = k+1;
end

% Tau: Polarization Tilt
tau = [];
while line(k)~='='
   k = k+1;
end
k = k+2;
while line(k)~=' '
```

```
    tau = [tau line(k)];
    k = k+1;
end

% Read line
line = fgetl(fid);
k = 1;

% Gain Parameter
gain = [];
while line(k)~='='
    k = k+1;
end
k = k+2;
while line(k)~=' '
    gain = [gain line(k)];
    k = k+1;
end

% Max Far-Field (Global) in dB
max_global = [];
while line(k)~='='
    k = k+1;
end
k = k+2;
while line(k)~=' '
    max_global = [max_global line(k)];
    k = k+1;
end

% Max Far-Field (Plot) in dB
max_plot = [];
while line(k)~='='
    k = k+1;
end
k = k+2;
while line(k)~=' '
    max_plot = [max_plot line(k)];
    k = k+1;
end

% Read line
line = fgetl(fid);
k = 1;

% Normalization
normalization = [];
while line(k)~=':'
    k = k+1;
end
k = k+2;
while line(k)~=','
```

```
    normalization = [normalization line(k)];
    k = k+1;
end

% Network Offset
network_offset = [];
while line(k)~='='
    k = k+1;
end
k = k+2;
while line(k)~=' '
    network_offset = [network_offset line(k)];
    k = k+1;
end

% Read line
line = fgetl(fid);
k = 1;

% Hpeak
hpeak = [];
while line(k)~=':'
    k = k+1;
end
k = k+2;
while line(k)~=' '
    hpeak = [hpeak line(k)];
    k = k+1;
end

% Vpeak
vpeak = [];
while line(k)~=':'
    k = k+1;
end
k = k+2;
while line(k)~=' '
    vpeak = [vpeak line(k)];
    k = k+1;
end

status = 1;

% Read line
line = fgetl(fid);
k = 1;

% Plot Centering
plot_centering = [];
while line(k)~=':'
    k = k+1;
end
```

```
k = k+2;
while k<=length(line)
    plot_centering = [plot_centering line(k)];
    k = k+1;
end


% Read line
line = fgetl(fid);
k = 1;

% Directivity
directivity = [];
while line(k)~='='
    k = k+1;
end
k = k+2;
while line(k)~=' '
    directivity = [directivity line(k)];
    k = k+1;
end

% FF Amplitude Info Structure
FF_amplitude_info = struct('Eprincipal',pol_type,'Tau',str2num(tau),'Gain',str2num(gain),...
    'Global_Max_Farfield',str2num(max_global),'Plot_Max_Farfield',str2num(max_plot),...
    'Normalization',normalization,'Network_Offset',str2num(network_offset),'Hpeak',str2num(hpeak),...
    'Vpeak',str2num(vpeak),'Plot_Centering',plot_centering,'Directivity',str2num(directivity));

% Read line
line = fgetl(fid);
k = 1;

% Read line
line = fgetl(fid);
k = 1;

% Read line
line = fgetl(fid);
k = 1;

% Description
Description = line;

% Read line
line = fgetl(fid);
k = 1;

% Read line
line = fgetl(fid);
k = 1;

% Read line
```

```
line = fgetl(fid);
k = 1;

% Program Version
prog_version = [];
while line(k)~=','
    prog_version = [prog_version line(k)];
    k = k+1;
end

% Filename
filename = [];
while line(k)~=':'
    k = k+1;
end
k = k+1;
while k<=length(line)
    filename = [filename line(k)];
    k = k+1;
end

% Read line
line = fgetl(fid);
k = 1;

% Measurement Date/Time
measurement_date = [];
while line(k)~=':'
    k = k+1;
end
k = k+2;
while line(k)~=' '
    measurement_date = [measurement_date line(k)];
    k = k+1;
end
k = k+1;
measurement_time = [];
while line(k)~=','
    measurement_time = [measurement_time line(k)];
    k = k+1;
end

% Filetype
filetype = [];
while line(k)~=':'
    k = k+1;
end
k = k+2;
while k<=length(line)
    filetype = [filetype line(k)];
    k = k+1;
end
```

```
% File Info Structure
File_info =
struct('Program_Version',prog_version,'Filename',filename,'Measurement_date',measurement_date,...
    'Measurement_Time',measurement_time,'Filetype',filetype);

%% Far-Field Display Setup
% Read line
line = fgetl(fid);
k = 1;

% Read line
line = fgetl(fid);
k = 1;

% Read line
line = fgetl(fid);
k = 1;

% Theta_Info
theta_span = [];
theta_center = [];
theta_points = [];
while line(k)~='='
    k = k+1;
end
k = k+2;
while line(k)~=' '
    theta_span = [theta_span line(k)];
    k = k+1;
end
while line(k)~='='
    k = k+1;
end
k = k+2;
while line(k)~=' '
    theta_center = [theta_center line(k)];
    k = k+1;
end
while line(k)~='='
    k = k+1;
end
k = k+2;
while line(k)~=' '
    theta_points = [theta_points line(k)];
    k = k+1;
end

% Read line
line = fgetl(fid);
k = 1;
```

```
theta_start = [];
theta_stop = [];
theta_delta = [];
while line(k)~='='
    k = k+1;
end
k = k+2;
while line(k)~=' '
    theta_start = [theta_start line(k)];
    k = k+1;
end
while line(k)~='='
    k = k+1;
end
k = k+2;
while line(k)~=' '
    theta_stop = [theta_stop line(k)];
    k = k+1;
end
while line(k)~='='
    k = k+1;
end
k = k+2;
while line(k)~=' '
    theta_delta = [theta_delta line(k)];
    k = k+1;
end

% Read line
line = fgetl(fid);
k = 1;

% Read line
line = fgetl(fid);
k = 1;

% Phi_Info
phi_span = [];
phi_center = [];
phi_points = [];
while line(k)~='='
    k = k+1;
end
k = k+2;
while line(k)~=' '
    phi_span = [phi_span line(k)];
    k = k+1;
end
while line(k)~='='
    k = k+1;
end
k = k+2;
```

```
while line(k)~=' '
   phi_center = [phi_center line(k)];
   k = k+1;
end
while line(k)~='='
   k = k+1;
end
k = k+2;
while line(k)~=' '
   phi_points = [phi_points line(k)];
   k = k+1;
end

% Read line
line = fgetl(fid);
k = 1;

phi_start = [];
phi_stop = [];
phi_delta = [];
while line(k)~='='
   k = k+1;
end
k = k+2;
while line(k)~=' '
   phi_start = [phi_start line(k)];
   k = k+1;
end
while line(k)~='='
   k = k+1;
end
k = k+2;
while line(k)~=' '
   phi_stop = [phi_stop line(k)];
   k = k+1;
end
while line(k)~='='
   k = k+1;
end
k = k+2;
while line(k)~=' '
   phi_delta = [phi_delta line(k)];
   k = k+1;
end

% Read Line
line = fgetl(fid);
k = 1;

% Plot Rotation
plot_rotation = [];
while line(k)~='='
```

```
    k = k+1;
end
k = k+2;
while line(k)~=' '
    plot_rotation = [plot_rotation line(k)];
    k = k+1;
end

% Read Line
line = fgetl(fid);
k = 1;

% Interpolation
interpolation = [];
while line(k)~=':'
    k = k+1;
end
k = k+2;
while k<=length(line)
    interpolation = [interpolation line(k)];
    k = k+1;
end

% Read Line
line = fgetl(fid);
k = 1;

% Coordinate System
coordinate_system = [];
while line(k)~=':'
    k = k+1;
end
k = k+2;
while line(k)~=';'
    coordinate_system = [coordinate_system line(k)];
    k = k+1;
end

% Far-Field Display Polarization
display_polarization = [];
while line(k)~=':'
    k = k+1;
end
k = k+2;
while k<=length(line)
    display_polarization = [display_polarization line(k)];
    k = k+1;
end

% FF Display Setup Info Structure
FF_display_setup_info = struct('Theta_Span',str2num(theta_span),'Theta_Center',str2num(theta_center),...
'Theta_Points',str2num(theta_points),'Theta_Start',str2num(theta_start),'Theta_Stop',str2num(theta_stop),...
    'Theta_Delta',str2num(theta_delta),'Phi_Span',str2num(phi_span),'Phi_Center',str2num(phi_center),...
    'Phi_Points',str2num(phi_points),'Phi_Start',str2num(phi_start),'Phi_Stop',str2num(phi_stop),...
    'Phi_Delta',str2num(phi_delta),'Plot_Rotation',str2num(plot_rotation),'Interpolation',interpolation,...
    'Coordinate_System',coordinate_system,'Display_Polarization',display_polarization);


%% Far-Field Transform
% Read Line
line = fgetl(fid);
k = 1;

% Read Line
line = fgetl(fid);
k = 1;

% FFT Size
fft_size = [];
while line(k)~=':'
    k = k+1;
end
k = k+3;
while k<=length(line)
    fft_size = [fft_size line(k)];
    k = k+1;
end

% Read Line
line = fgetl(fid);
k = 1;

% Far-Field Display Polarization
filter_mode = [];
while line(k)~=':'
    k = k+1;
end
k = k+2;
while line(k)~=','
    filter_mode = [filter_mode line(k)];
    k = k+1;
end

zoom = [];
while line(k)~=':'
    k = k+1;
end
k = k+2;
while k<=length(line)
    zoom = [zoom line(k)];
    k = k+1;
end
```

```
% Read Line
line = fgetl(fid);
k = 1;

% Probe Setup
probe_setup = [];
while line(k)~=':'
   k = k+1;
end
k = k+2;
while k<=length(line)
   probe_setup = [probe_setup line(k)];
   k = k+1;
end

% Read Line
line = fgetl(fid);
k = 1;

% Probe Model
probe_model = [];
while line(k)~=':'
   k = k+1;
end
k = k+2;
while k<=length(line)
   probe_model = [probe_model line(k)];
   k = k+1;
end

% FF Transform Setup Info Structure
FF_transform_setup_info = struct('FFT_Size',fft_size,'Filter_Mode',filter_mode,...
   'Zoom',zoom,'Probe_Setup',probe_setup,'Probe_Model',probe_model);

%% Beam Information (Code valid only for one beam)

% Read Line
line = fgetl(fid);
k = 1;

% Read Line
line = fgetl(fid);
k = 1;

% Read Line
line = fgetl(fid);
k = 1;

% Read Line
line = fgetl(fid);
k = 1;
```

```
% Beam - Future work involves rearranging the information
beam_info = line;

%% Near-field setup

% Read Line
line = fgetl(fid);
k = 1;

% Read Line
line = fgetl(fid);
k = 1;

% Read Line
line = fgetl(fid);
k = 1;

% Near-field data
near_field_data = [];
while line(k)~='-'
   k = k+1;
end
k = k+2;
while k<=length(line)
   near_field_data = [near_field_data line(k)];
   k = k+1;
end

% Read Line
line = fgetl(fid);
k = 1;

% Truncation
truncation = [];
while line(k)~=':'
   k = k+1;
end
k = k+2;
while k<=length(line)
   truncation = [truncation line(k)];
   k = k+1;
end

% Read Line
line = fgetl(fid);
k = 1;

% Amplitude Tapering
amplitude_tapering = [];
while line(k)~=':'
   k = k+1;
```

```
end
k = k+2;
while k<=length(line)
    amplitude_tapering = [amplitude_tapering line(k)];
    k = k+1;
end

% Read Line
line = fgetl(fid);
k = 1;

% Network Correction
network_correction = [];
while line(k)~=':'
    k = k+1;
end
k = k+2;
while k<=length(line)
    network_correction = [network_correction line(k)];
    k = k+1;
end

% Read Line
line = fgetl(fid);
k = 1;

% Phase Correction
phase_correction = [];
while line(k)~=':'
    k = k+1;
end
k = k+2;
while k<=length(line)
    phase_correction = [phase_correction line(k)];
    k = k+1;
end

% NF Setup Info Structure
NF_setup_info =
struct('Data',near_field_data,'Truncation',truncation,'Amplitude_Tapering',amplitude_tapering,...
    'Network_Correction',network_correction,'Position_Phase_Correction',phase_correction);


%% Measured Data

% Read Line
line = fgetl(fid);
k = 1;

% Read Line
line = fgetl(fid);
k = 1;
```

```
% Read Line
line = fgetl(fid);
k = 1;

% Measured Theta_Info
mtheta_span = [];
mtheta_center = [];
mtheta_points = [];
while line(k)~='='
    k = k+1;
end
k = k+2;
while line(k)~=' '
    mtheta_span = [mtheta_span line(k)];
    k = k+1;
end
while line(k)~='='
    k = k+1;
end
k = k+2;
while line(k)~=' '
    mtheta_center = [mtheta_center line(k)];
    k = k+1;
end
while line(k)~='='
    k = k+1;
end
k = k+2;
while line(k)~=' '
    mtheta_points = [mtheta_points line(k)];
    k = k+1;
end

% Read line
line = fgetl(fid);
k = 1;

mtheta_start = [];
mtheta_stop = [];
mtheta_delta = [];
while line(k)~='='
    k = k+1;
end
k = k+2;
while line(k)~=' '
    mtheta_start = [mtheta_start line(k)];
    k = k+1;
end
while line(k)~='='
    k = k+1;
end
```

```
k = k+2;
while line(k)~=' '
    mtheta_stop = [mtheta_stop line(k)];
    k = k+1;
end
while line(k)~='='
    k = k+1;
end
k = k+2;
while line(k)~=' '
    mtheta_delta = [mtheta_delta line(k)];
    k = k+1;
end

% Read line
line = fgetl(fid);
k = 1;

% Read line
line = fgetl(fid);
k = 1;

% Phi_Info
mphi_span = [];
mphi_center = [];
mphi_points = [];
while line(k)~='='
    k = k+1;
end
k = k+2;
while line(k)~=' '
    mphi_span = [mphi_span line(k)];
    k = k+1;
end
while line(k)~='='
    k = k+1;
end
k = k+2;
while line(k)~=' '
    mphi_center = [mphi_center line(k)];
    k = k+1;
end
while line(k)~='='
    k = k+1;
end
k = k+2;
while line(k)~=' '
    mphi_points = [mphi_points line(k)];
    k = k+1;
end

% Read line
```

```
line = fgetl(fid);
k = 1;

mphi_start = [];
mphi_stop = [];
mphi_delta = [];
while line(k)~='='
    k = k+1;
end
k = k+2;
while line(k)~=' '
    mphi_start = [mphi_start line(k)];
    k = k+1;
end
while line(k)~='='
    k = k+1;
end
k = k+2;
while line(k)~=' '
    mphi_stop = [mphi_stop line(k)];
    k = k+1;
end
while line(k)~='='
    k = k+1;
end
k = k+2;
while line(k)~=' '
    mphi_delta = [mphi_delta line(k)];
    k = k+1;
end

% Read Line
line = fgetl(fid);
k = 1;

% AUT Dimensions
aut_height = [];
aut_width = [];
while line(k)~=':'
    k = k+1;
end
k = k+2;
while line(k)~=' '
    aut_width = [aut_width line(k)];
    k = k+1;
end
while line(k)~=','
    k = k+1;
end
k = k+2;
while line(k)~=' '
    aut_height = [aut_height line(k)];
    k = k+1;
end

% Read Line
line = fgetl(fid);
k = 1;

% H/V Max Far-field Angles
h_max_angle = [];
v_max_angle = [];
while line(k)~=':'
    k = k+1;
end
k = k+2;
while line(k)~=' '
    h_max_angle = [h_max_angle line(k)];
    k = k+1;
end
while line(k)~=','
    k = k+1;
end
k = k+2;
while line(k)~=' '
    v_max_angle = [v_max_angle line(k)];
    k = k+1;
end

% Read Line
line = fgetl(fid);
k = 1;

% Measurement Radius
measure_radius = [];
while line(k)~=':'
    k = k+1;
end
k = k+2;
while line(k)~=' '
    measure_radius = [measure_radius line(k)];
    k = k+1;
end

% Read Line
line = fgetl(fid);
k = 1;

% MRE
mre = [];
while line(k)~=':'
    k = k+1;
end
k = k+2;
```

```
while line(k)~=' '
   mre = [mre line(k)];
   k = k+1;
end

% Read Line
line = fgetl(fid);
k = 1;

% Read Line
line = fgetl(fid);
k = 1;

% Measured Data Info Structure
Measured_data_info =
struct('Measured_Theta_Span',str2num(mtheta_span),'Measured_Theta_Center',str2num(mtheta_center),...

'Measured_Theta_Points',str2num(mtheta_points),'Measured_Theta_Start',str2num(mtheta_start),'Measured
_Theta_Stop',str2num(mtheta_stop),...

'Measured_Theta_Delta',str2num(mtheta_delta),'Measured_Phi_Span',str2num(mphi_span),'Measured_Phi
_Center',str2num(mphi_center),...

'Measured_Phi_Points',str2num(mphi_points),'Measured_Phi_Start',str2num(mphi_start),'Measured_Phi_St
op',str2num(mphi_stop),...

'Measured_Phi_Delta',str2num(mphi_delta),'AUT_Width',str2num(aut_width),'AUT_Height',str2num(aut_
height),'H_Max_Farfield_Angle',str2num(h_max_angle),...

'V_Max_Farfield_Angle',str2num(v_max_angle),'Measurement_Radius',str2num(measure_radius),'MRE',st
r2num(mre));

% Measurement Type
measure_type = [];
while line(k)~=':'
   k = k+1;
end
k = k+2;
while k<=length(line)
   measure_type = [measure_type line(k)];
   k = k+1;
end

% Read Line
line = fgetl(fid);
k = 1;

% Scan Options
scan_options = [];
while line(k)~=':'
   k = k+1;
end
```

```
k = k+2;
while k<=length(line)
   scan_options = [scan_options line(k)];
   k = k+1;
end

% Read Line
line = fgetl(fid);
k = 1;

% Beamset Smear
beamset_smear = [];
while line(k)~=':'
   k = k+1;
end
k = k+2;
while line(k)~=' '
   beamset_smear = [beamset_smear line(k)];
   k = k+1;
end

%% Probe setup as acquired
% Read Line
line = fgetl(fid);
k = 1;

% Read Line
line = fgetl(fid);
k = 1;

% Beamset Smear
mprobe_model = [];
while line(k)~=':'
   k = k+1;
end
k = k+2;
while k<=length(line)
   mprobe_model = [mprobe_model line(k)];
   k = k+1;
end

% Read Line
line = fgetl(fid);
k = 1;

% Probe 1
probe_1 = [];
while line(k)~=':'
   k = k+1;
end
k = k+2;
while line(k)~=','
```

```
    probe_1 = [probe_1 line(k)];
    k = k+1;
end

% Probe 2
probe_2 = [];
while line(k)~=':'
    k = k+1;
end
k = k+1;
while k<=length(line)
    probe_2 = [probe_2 line(k)];
    k = k+1;
end

% Measurement Info Structure
Measurement_info = struct('Measure_Type',measure_type,'Scan_Options',scan_options,...
    'Beamset_Smear',str2num(beamset_smear),'Probe_Setup','as Acquired','Probe_Model',mprobe_model,...
    'Probe_1',probe_1,'Probe_2',probe_2);


%% RF System

% Read Line
line = fgetl(fid);
k = 1;

% Read Line
line = fgetl(fid);
k = 1;

% Read Line
line = fgetl(fid);
k = 1;

% Integration Time
integration_time = [];
while line(k)~=':'
    k = k+1;
end
k = k+2;
while line(k)~=' '
    integration_time = [integration_time line(k)];
    k = k+1;
end

% Read Line
line = fgetl(fid);
k = 1;

% Scan Speed
scan_speed = [];
```

```
while line(k)~=':'
    k = k+1;
end
k = k+2;
while line(k)~=' '
    scan_speed = [scan_speed line(k)];
    k = k+1;
end

% Read Line
line = fgetl(fid);
k = 1;

% Scan Info
scan_info = line;

% Read Line
line = fgetl(fid);
k = 1;

% Amp/Phase Initial
amp_initial = [];
phase_initial = [];
while line(k)~='='
    k = k+1;
end
k = k+3;
while line(k)~=' '
    amp_initial = [amp_initial line(k)];
    k = k+1;
end
while line(k)~=','
    k = k+1;
end
k = k+3;
while line(k)~=' '
    phase_initial = [phase_initial line(k)];
    k = k+1;
end

% Read Line
line = fgetl(fid);
k = 1;

% Amp/Phase Drift
amp_drift = [];
phase_drift = [];
while line(k)~='='
    k = k+1;
end
k = k+3;
while line(k)~=' '
```

```
    amp_drift = [amp_drift line(k)];
    k = k+1;
end
while line(k)~=','
    k = k+1;
end
k = k+3;
while line(k)~=' '
    phase_drift = [phase_drift line(k)];
    k = k+1;
end

% RF System Info Structure
RF_system_info =
struct('Integration_Time',str2num(integration_time),'Scan_Speed',str2num(scan_speed),...

'Amp_Initial',str2num(amp_initial),'Phase_Initial',str2num(phase_initial),'Amp_Drift',str2num(amp_drift),...
    'Phase_Drift',str2num(phase_drift));


%% Measurement Data

% Read Line
line = fgetl(fid);
k = 1;

% Read Line
line = fgetl(fid);
k = 1;

for p=1:FF_display_setup_info.Phi_Points

    for q=1:FF_display_setup_info.Theta_Points

        % Read Line
        line = fgetl(fid);
        k = 1;

        % Change String Format into Numerical Format
        nline = str2num(line);

        % Spherical Coordinates
        theta_coor(p,q) = nline(1);
        phi_coor(p,q) = nline(2);

        % E-field Pattern
        E_field(p,q) = 10^(nline(3)/20).*exp(j*nline(4)*pi/180);

    end

end
```

```
save(mat_filename,'FF_amplitude_info','File_info','FF_display_setup_info','FF_transform_setup_info',...
    'NF_setup_info','Measured_data_info','Measurement_info','RF_system_info','theta_coor','phi_coor',...
    'E_field','-mat');

fclose(fid);

function status = pattern_calc(Ephi_filename,Etheta_filename,Efield_filename)
% pattern_calc Antenna Pattern Calculator
%    pattern_calc(Ephi_filename,Etheta_filename,Efield_filename) retrieves
%    Electric Field measurement data from Ephi_filename and
%    Etheta_filename MAT files, calculates the Magnitude of the Electric Field, and
%    stores the result in the Efield_filename mat file.
%    Note: Linear antenna is placed along Azimuth plane
%   Author: Juan A. Torres-Rosario


% Load Ephi Component
load(Ephi_filename);
E_phi = E_field;

% Load Etheta Component
load(Etheta_filename);
E_theta = E_field;

% Calculate Electric Field Radiation Pattern
E_field = sqrt(abs(E_theta).^2+abs(E_phi).^2);
[E_x,E_y,E_z] = sph2cart(phi_coor*pi/180, (-(theta_coor)*pi/180), abs(E_field));
theta_coor = theta_coor+90;

% Calculate Efield for Polar Plot View
E_polar = E_field(:,1:101);

% Calculate Theta vector
theta_vector = [-1*fliplr(theta_coor(151,2:201)) theta_coor(51,1:201)];

% Calculate Elevation Cut
El_cut = [fliplr(E_field(151,2:201)) E_field(51,1:201)];

% Calculate Azimuth Cut
Az_cut = [fliplr(E_field(101,2:201)) E_field(1,1:201)];

save(Efield_filename,'E_field','theta_coor','phi_coor','theta_vector','E_x','E_y','E_z','Az_cut','El_cut',...
    'E_phi','E_theta','E_polar');
```